

**Investigations on the Behaviour and Properties of
Different Types of Unilamellar Vesicles**

Dissertation

zur Erlangung des Doktorgrades

der Fakultät Biologie, Chemie und Geowissenschaften

der Universität Bayreuth

vorgelegt von

Md. Ekramun Nabi

aus Bangladesch

Oktober 2005

Vollständiger Abdruck der vom Fachbereich Biologie, Chemie und Geowissenschaften der Universität Bayreuth genehmigten Dissertation zur Erlangung des akademischen Grades eines Doktors der Naturwissenschaften

Abgabe der Arbeit 27. Oktober 2005

Wissenschaftliches Kolloquium: 30. März 2006

Prüfungsausschuss:

Prof. Dr. J. Senker (Vorsitzender)

Prof. Dr. M. Gradzielski (Erstgutachter)

Prof. Dr. G. Platz (Zweitgutachter)

Prof. Dr. C. Unverzagt

Acknowledgements

It is my great pleasure to express cordial thanks and deep gratitude to my supervisor Prof. Dr. Michael Gradzielski for providing me an interesting theme for my PhD work and for his valuable guidance. Really he gave me much support from the first day I came here in Bayreuth. I have much to say to my supervisor Prof. Gradzielski, but I can't crystallize it in just abstract words.

I take this opportunity to express my thanks with gratitude to Prof. Dr. em. H. Hoffmann for permitting me in using the equipments in his laboratory and helping me in scientific discussion.

I am very grateful to Dr. Markus Drechsler for cryo-TEM measurements and useful discussion in their interpretation. I am thankful to Markus Burkhardt and Harald Becker for their immense help in DLS measurements and some scientific discussions. My thanks are also due to Dr Li Li for her help in SAXS measurement and its data analysis.

I would like to express my thanks to Karlheinz Lauterbach not only for his technical support in the laboratory work, but also for his friendly behaviour outside of the campus. His wife Mrs Friedel Lauterbach is also greatly acknowledged for giving a similar feeling of my second family here in Germany.

I would like to express my cordial thanks to our working group members here in BZKG especially Christian Wolf and Claudia Oppel for their friendly and cooperative behaviour in the laboratory.

My thanks are due to Awal Noor, Haif Alshammari and Saleh A Khan for their encouragement, reading and correcting the manuscript. For you, I would like to say, "Jazakallahu khairan fiddarain".

At last I would like to express my deepest sense of gratitude to my family members in Bangladesh for their constant moral support during the course of my studying here in Germany.

The financial support provided by the German Research Foundation (DFG) is greatly acknowledged.

Contents

Chapter 1: Introduction.....	1
1.1 General	1
1.2 Out line.....	2
1.3 Aim of the present work.....	6
Chapter 2: Theory	9
2.1 General	9
2.2 Micellization.....	9
2.3 Kraft Temperature	12
2.4 Colloidal forces	13
2.4.1 Van der Waals force.....	13
2.4.2 Electric double layer force	16
2.4.3 DLVO Theory	18
2.4.4 Hydration force	20
2.5 Vesicle formation	21
2.5.1 Shear induced vesicle formation	22
2.5.2 Spontaneous vesicle formation.....	23
2.6 Phase transition	24
2.6.1 Concentration-induced phase transition	24
2.6.2 Effect of additives	25
2.6.3 Temperature-induced phase transition	27
2.6.4 Shear-induced phase transition.....	29
Chapter 3: Experimental	32
3.1 Chemicals	32
3.1.1 Surfactants.....	32
3.1.2 Co-surfactants.....	34
3.1.3 Other chemicals.....	34

3.2 Phase study	35
3.2.1 Single phases	35
3.2.2 Phase rule and tie line.....	36
3.3 Rheology	37
3.3.1 Newtonian fluid.....	38
3.3.2 Non-Newtonian fluid.....	38
3.3.3 Viscoelastic fluid.....	40
3.3.4 Equipments.....	43
3.4. Dynamic light scattering	44
3.4.1 Principle of dynamic light scattering	44
3.4.2 Correlation function	45
3.4.3 Method of cumulants.....	46
3.4.4 Equipments.....	48
3.5 Small angle X-ran scattering	48
3.5.1 Data treatment	49
3.5.2 Power law.....	50
3.5.3 Equipments.....	51
3.6 Surface tension	52
3.6.1 Gibbs adsorption isotherm	52
3.6.2 Equipments.....	53
3.7 UV-visible spectrophotometry	53
3.7.1 Turbidity measurements.....	53
3.7.2 Equipments.....	54
3.8 Transmission electron microscopy.....	54
3.8.1 Cryogenic preparation.....	55
3.8.2 Equipments.....	55

3.9 Conductometry	56
3.9.1 Equipments	57
3.10 pH-measurements	57
Chapter 4: Results and Discussion	58
4.1 Surfactant with co-surfactants	58
4.1.1 Phase behaviour.....	58
4.1.2 Hydrodynamic radii and polydispersity	62
4.1.3 Microscopic observation	65
4.1.4 Conductivity and pH measurements	70
4.1.5 Rheological properties.....	73
4.1.6 Kinetics of vesicle formation	81
4.1.7 Effects of electrolytes on vesicular gel	86
4.2 Templating anionic vesicles by mean of Ti(OBu) ₄	92
4.2.1 Viscoelastic behaviour	92
4.2.2 Non-linear behaviour.....	96
4.2.3 Cox-Merz rule	97
4.2.4 Yield stress	98
4.2.5 SAXS analysis.....	99
4.2.6 Kinetic measurements	100
4.3 Oleic acid/ C ₁₀ TAB System	105
4.3.1 Phase behaviour	105
4.3.2 Surface tension and Gibbs molecular area	107
4.3.3 Turbidity measurements	110
4.3.4 Conductivity and pH	111
4.3.5 Microscopic observation	113
4.3.6 Dynamic light scattering measurements	118
4.3.7 SANS analysis.....	122

4.4 Catanionic System.....	124
4.4.1 Phase behaviour.....	124
4.4.2 Conductivity measurements	128
4.4.3 Rheological measurements.....	130
4.4.4 Dynamic light scattering	133
4.5 Thermodynamic behaviour of mixed vesicular system.....	136
4.5.1 Phase behaviour.....	136
4.5.2 Electrical conductivity.....	138
4.5.3 Dynamic light scattering	139
4.5.4 Microscopic observation	143
4.5.5 Shear viscosity.....	146
4.5.6 Synergism.....	150
4.5.7 SANS analysis.....	151
Chapter 5: Summary	153
Chapter 6: Zusammenfassung	157
Chapter 7: References.....	162

Chapter 1: Introduction

1.1 General

Surfactant is a single word for surface active agent, which literally means the substance which is active at a surface. In other words, a surfactant is characterized by its tendency to be adsorbed at the surface and interface. The driving force for a surfactant to be adsorbed at an interface is to lower the free energy of that phase boundary. This force originates from the chemical structure of surfactant molecules that consist of incompatible functional groups of the identical molecule. These molecules contain at least one polar or ionic hydrophilic part and one hydrophobic unit. These molecules may also be called amphiphilic or tensioactive. The coexistence of two opposite types of behaviour (hydrophilic and hydrophobic) inside the same molecule is the origin of local constraints which lead to spontaneous aggregation into microscopic labile structures observed with surfactants in solution, in oil or water¹⁻⁵. The driving force of this aggregation process is the tendency of the hydrophobic part to minimise the contact with water, an effect called the *hydrophobic effect* and that is mainly due to the entropic gain of water structure by not being in contact with the hydrophobic part⁶.

These supermolecular aggregates, at thermodynamic equilibrium, give surprising macroscopic properties to the solution. They could be explained in terms of microscopic structure. Knowledge of these structures, their equilibrium, formation and growing conditions is important for detergent manufacture, cosmetic industries, mineral flotation and the understanding of chemistry in heterogeneous media. Micellar aggregation is a primitive and easily controllable model for transformation into other type of aggregation by proper treatment. Therefore, these structures have been studied intensively in last many years.

The name colloid is derived from the Greek word “Kolla” meaning glue as it was considered that all colloids are more or less like glue^{7, 8}. The first notional classification of colloids was proposed by Von Weimar and Ostwald⁷. The notion of a dispersed system was introduced and the particle size was taken as the major factor in the classification and characterisation of colloids. Thus, colloids are substances consisting of a homogeneous medium and of particles

dispersed therein. So the part of science which deals with homogeneous dispersion of nano- to micro- scale was termed colloid science⁹. Surfactant solutions fall in this region because of their self-association feature. The self-associate mechanism has been well explored and defined theoretically and experimentally. However, differing from “hard matter” such as inorganic materials, the aggregate consisting of molecules is easily deformable and in many cases rearrangeable by changing physical and chemical factors and therefore, we need to correct further information in order to establish these “soft matter”.

In our daily life we often use surfactants for versatile purposes, for instance, emulsification, detergency, lubrication, wetting and so on. In the scientific fields, moreover, it is well-known that amphiphilic materials are useful as a template of mesoporous material¹⁰, emulsion polymerization¹¹ and drug delivery¹². One can imagine that these properties are applicable for numerous life-products. Besides the industrial materials, it is noteworthy that surfactant would be a potential working area in the field of nano-technologies.

1.2 Outline

Thermodynamic properties of amphiphiles in solution are controlled by the tendency of the hydrophobic parts of the molecule to minimize contact with water, which is termed the *hydrophobic effect*⁶. This leads to the association of molecules into micelles, which has spherical or elongated structure in which the hydrophobic inner core is shielded from water by the surrounding corona formed from the hydrophilic head group of the molecules. These aggregates are formed by spontaneous self-assembly at sufficiently high concentrations of amphiphiles, above a *critical micelle concentration (CMC)*. The formation of micelles is predominantly an entropic effect, as deduced from the comparisons of the contributions of enthalpy and entropy to the Gibbs free energy of micellization. The enthalpy contribution results partly from the energetically favourable enhancement of interactions between the hydrocarbon chains. The entropic contribution arises from the local structuring of water due to hydrogen bonding. Isolated hydrocarbon chains break up the hydrogen bonds between water molecules and impose a locally more ordered structure that is entropically unfavourable. Because of this reduction in disruption of water structure when micelles are formed, they are entropically favoured compared to unassociated molecules.

Colloidal assemblies are stabilized or destabilized by numerous interactions, which can be classified into two interactive forces, repulsive force and attractive force. Interaction between dispersions is determined in terms of the balance of van der Waals force (attractive potential energy) and electrostatic force (repulsive potential energy). This is well-known as *Derjaguin-Landau-Verwey-Overbeek (DLVO) theory*^{13, 14}. DLVO theory, in general, applies for considerably low surfactant concentration, especially for ionic surfactants which have the strong electric hindrance on coagulation. For the solution with higher surfactant concentration, micelles are obliged to approach each other because of the decrease in bulk phase volume which is energetically disfavoured. However, if a micellar structure reconstructs into a long cylindrical micelle, the assemblies can have enough space to be segregated from one another.

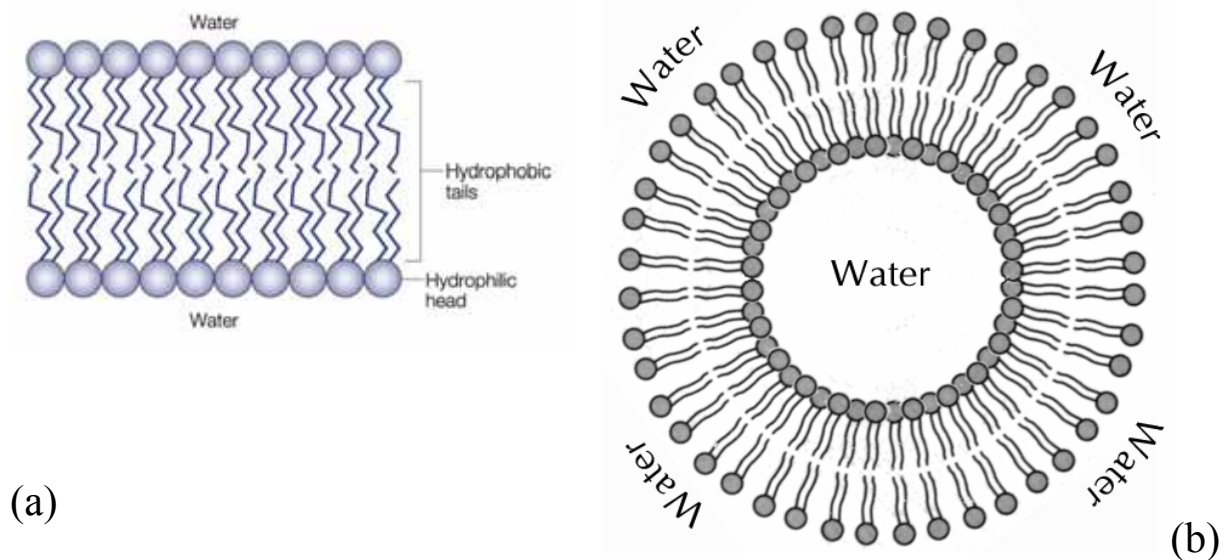


Figure 1.1: A schematic drawing of an amphiphilic bilayer (a) and a vesicle (b)

[From Ref. 15]

Another aggregation possibility for higher surfactant concentration, amphiphiles can be self-assembled into *lyotropic liquid crystalline phase*. “Lyotropic phase” refers to the fact that such phases are built up by amphiphilic aggregation as a function of concentration. Lyotropic phases with one dimensional translational order consisting of bilayers of amphiphiles separated by solvent are called lamellar phase. A two dimensional structure is formed by rod-like micelles packed in the hexagonal arrays. Cubic phases are formed by packing micelles into body-centered cubic or face-centered cubic arrays. The bicontinuous cubic phases are more complex structures, where space is separated into two continuous labyrinths.

The actual form assumed by an aggregate depends on the molecular construction of the amphiphile and can be explained by simple geometric consideration. In a first-order approximation, geometry of an amphiphile is described by the packing parameter p of the amphiphile, which is defined as the ratio of the hydrophobic volume (v) to the product of the head-group area (a) and chain length (l)¹⁶:

$$p = al / v \tag{1.1}$$

The packing parameter p determines the preferred curvature of the aggregates formed. In forming space filling aggregates, for $p \geq 0.33$ spherical objects, for $0.33 < p \leq 0.5$ rod-like particles and for $0.5 < p \leq 1$ disc-like or bilayer structures are expected, while for the value of $p < 1$, reverse structures should be formed. In general this simple scheme works well for the explanation of experimentally observed amphiphilic structures. The general sequence of the surfactant aggregates with increasing concentration – spheres, rods and discs or bilayers respectively – is always valid, but this does not mean that all of these forms have to be present for each amphiphilic compounds. Systems are known which form spherical micelles up to high concentrations where a cubic phase appears¹⁷; other systems form rod-like micelles¹⁸ or bilayers¹⁹ as first aggregation.

Accordingly, one very common way of self-assembly is the formation of amphiphilic bilayers, in which the hydrophilic polar head groups of the amphiphile face the aqueous surroundings and the hydrophobic parts of the amphiphiles constitute the interior of the bilayers (see Figure 1a). In the simplest arrangement, these bilayers just form planar structures. However, it is also possible that the bilayers can enclose keeping some continuous medium inside, thereby forming closed and spherical objects which are called vesicles (see Figure 1b). Vesicles are not always static in nature, but typically in a dynamic system where shape fluctuations may be pronounced.

On the basis of their size and structure, vesicles can be subdivided into various groups. They may be classified as single bilayer known as unilamellar vesicles or multilamellar vesicles. Further classification brings the small unilamellar vesicles (SUV; $R_h = 5 - 40$ nm) and large unilamellar vesicles (LUV; $R_h = 50$ nm – 10 μ m) where this distinction may be drawn on the basis of whether a molecule in the bilayer still experiences the fact that it is a curved bilayer (SUV) or where on a molecular basis bilayer is effectively planar (LUV)¹⁵. Accordingly LUV is defined by $cL \ll 1$, where c is the curvature of the vesicle, i.e., the inverse of the radius, and L is the maximum dimension of the amphiphilic molecule.

In addition to the unilamellar vesicles there exists also the possibility to form multilamellar vesicles (MLV)²⁰ (for the case of phospholipids, often called liposomes^{21, 22}) where one has concentric shells of vesicles i.e., a structure similar to that of an onion – that is why this phase sometimes called “onion phase”²³. As a general tendency, one finds that unilamellar vesicles are more likely to be observed for dilute systems while MLV are frequently found in more concentrated surfactant systems. Typically for bilayer forming amphiphilic systems, one observes that with increasing concentration there exists a structural progression according to;

Unilamellar vesicles \rightarrow multilamellar vesicles \rightarrow planar bilayers¹⁵

In such an inter-lamellar or bilayer transformation, typically no macroscopic phase separation is observed for the transition from unilamellar vesicles to multilamellar vesicles or from multilamellar vesicles to bilayers²⁴. Instead, extended structurally biphasic, but macroscopically homogeneous regions are observed that contains different morphological structures in equilibrium. In general they are relatively turbid.

To form vesicles, the amphiphiles should have a propensity for the formation of bilayers. According to the geometric model, the formation of bilayers is to be expected if the packing parameter p is more than 0.5, but less than or equal to 1^{15, 25}. However such a relatively large packing parameter requires amphiphiles with small head groups and bulky hydrophobic parts. Typically this situation arises for double chain hydrocarbon amphiphiles, or perfluoro-surfactants (as a $-\text{CF}_2-$ unit is much more space demanding than $-\text{CH}_2-$ unit), or non-ionic single-chain surfactants with small hydrophilic groups²⁶. Another way to increase packing parameter of a surfactant system is by admixing a co-surfactant or oppositely charged surfactants. For many ionic surfactants such an admixture leads to the formation of bilayer structure^{1, 5}.

Planar bilayers as in lamellar phases or even isotropic sponge phases²⁷⁻³² can also be formed instead of vesicles. According to the packing considerations, planar bilayers should be formed if the packing parameter $p = 1$. However, for smaller values of p but not less than 0.5, vesicle formation may be preferred, as this reduces the energetically unfavourable edges of finite planar bilayers. Accordingly one may expect vesicle formation for p values not too close to 1^{15, 25, 33}. Another important quantity is the bending elasticity of the bilayer. The bending properties are described by two elastic moduli, the mean bending modulus κ and the Gaussian modulus (or saddle-splay modulus) $\bar{\kappa}$. The bending free energy of a bilayer system can be calculated by integration over the total surface of the bilayers according to Helfrich³⁴ model:

$$F_b = \int \left[\frac{\kappa}{2} (c_1 + c_2 - 2c_0)^2 + \bar{\kappa} c_1 c_2 \right] dA \quad (1.2)$$

Where c_1 and c_2 are the principal curvatures and c_0 is the spontaneous curvature of the bilayer. This integration can be performed straightforwardly in a simplified way for the various bilayer structures for the case of a vanishing spontaneous curvature ($c_0 = 0$).

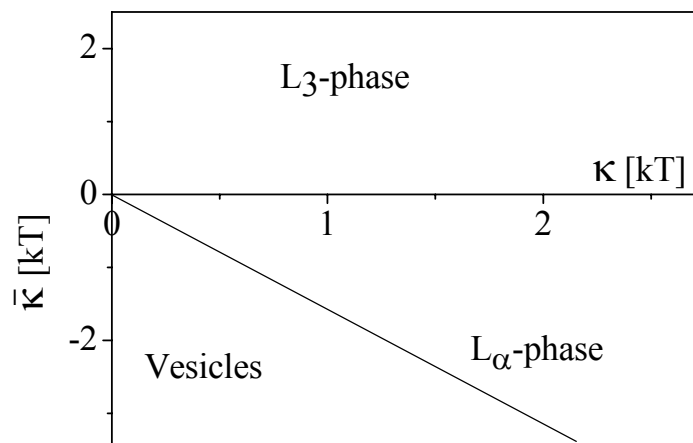


Figure 1.2: A schematic phase diagram for the different bilayer-morphologies as a function of mean bending modulus κ and saddle-splay modulus $\bar{\kappa}$ for a system with a spontaneous curvature $c_0 = 0$ [according to ref. 15, 35]

By comparison of the calculated energies one can construct a simple phase diagram (see Figure 2) where the energetically favourable structure depends on the two moduli κ and $\bar{\kappa}$. For positive value of $\bar{\kappa}$, the isotopic sponge phase (L_3 phase) is the most stable, while the negative value of $\bar{\kappa}$, planar lamellae become more stable. In addition, one finds that if the Gaussian modulus $\bar{\kappa}$ becomes negative enough a transition from planar bilayer to vesicles is to be expected even for a symmetric bilayer, i.e. one that has a spontaneous curvature of $c_0 = 0$ ³⁵.

1.3 Aim of the present work

Amphiphilic molecules spontaneously self-assemble in solution to form a variety of aggregates. The understanding of the equilibrium properties of these aggregates, such as their shape and size, has made significant progress. However, only limited information is available on the formation and kinetics of the structural transitions from micellar to vesicular systems

with oleic acid or its Na-salt. Aqueous mixtures of oleate with some co-surfactants are very interesting model-systems which exhibit a spontaneous transition from polymer-like mixed micelles to vesicles upon homogeneous mixing. Vesicles are of interest not only from a fundamental point of view, as they are one of the principal structures in which amphiphiles can self-assemble, but also due to their high potential for applications. Such close bilayers are model systems for cell membranes³⁶ and can be used to study the physical properties of amphiphilic bilayers³⁷. Furthermore, vesicles are able to encapsulate active molecules and therefore can be used as drug delivery system^{38, 39}. A particular application of this sort that has attracted a lot of attention is the use of liposomes as non-viral carriers in gene therapy^{40, 41}. Accordingly they may be applied in a large variety of pharmaceutical and cosmetic applications^{42, 43}. On the light of these observations the present work has undertaken as a prime objective to characterise and describe some vesicular transformations in terms of their micro and macro structural properties.

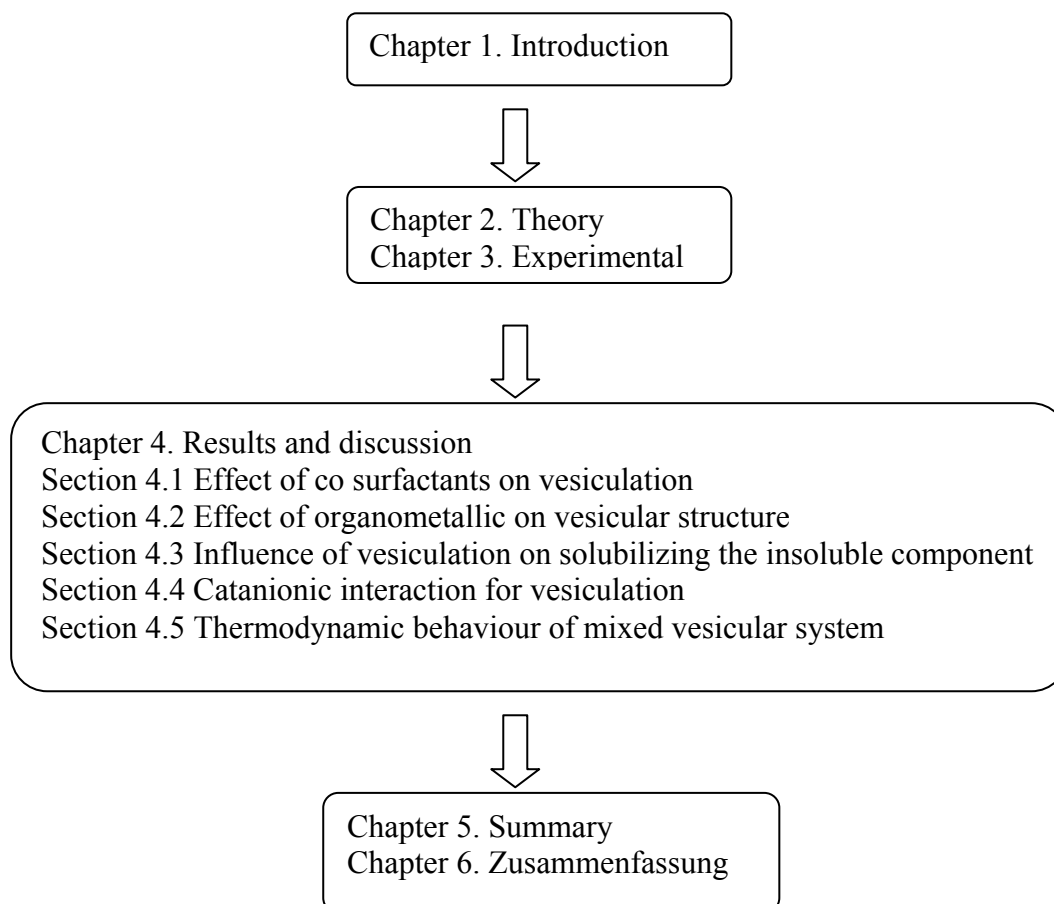
The central aim of this thesis is to experimentally investigate the effects of mixing anisometric colloidal particles with different shapes on their lyotropic phase behaviour. Many of the studies to be described in this thesis have been triggered off by recent experimental observations in mixtures of colloids with well-controlled shapes and interactions. In particular, it can be mentioned that the experimental work of Gradzielski, M. et al⁴³ and Söderman, O. et al⁴⁴ who investigated a number of mixtures which display many interesting phenomena left open for further investigation and interpretation. One of the primary goals in this work is to account for these experimental observations and further investigate the open areas by constructing simple, yet realistic analysis for the colloidal systems under consideration and by scrutinizing relevant aspects of their phase behaviour.

The present investigation is divided into a few sections in terms of the kind of surfactant system used. Firstly the phase behaviour and self aggregation nature of Na-oleate with two different co surfactants with similar alkyl-chain-length [1-octanol and 3,7-dimethyl-trans-2,6-octadien-1-ol (geraniol)] will be discussed. Although both the co surfactants octanol and geraniol are alcohol with a single alkyl chain, but their interactions with the surfactant, Na-oleate are very different. Their aggregation property and derivative structures will be analyzed by means of many different instrumental methods like rheometry, microscopy, spectrophotometry, conductometry and scattering techniques. Moreover, the addition of electrolyte and the effects of counter ions on the aggregation behaviour of surfactant with co surfactants will also be interpreted.

In order to observe the effect of an organometallic component on the self aggregation of previously studied vesicular composition the interaction of $\text{Ti}(\text{OBu})_4$ will be discussed in the subsequent section 4.2. Spectrophotometric measurements will be performed to know the kinetics of vesicle formation and the effect of $\text{Ti}(\text{OBu})_4$ on it. In the next section 4.3 the acid-base-like interaction of parent compound, oleic acid with decyltrimethyl ammonium hydroxide will be analyzed. The phase behaviour will be monitored and the microstructures in different single-phases will be investigated using different methods.

In the next part of this work, catanionic interaction, an alternative way of forming unilamellar vesicles will be explored. The thermodynamic behaviour of two oppositely charged surfactants will be analyzed monitoring their phase behaviour with different mixing compositions. Microstructure in single phase will be analyzed by different methods to prove that they can form vesicles. It will be shown that Na-oleate can form two different types of vesicles with C_{14}TAB . Finally the thermodynamic behaviour of mixed vesicular i.e. interaction between anionic aggregation with catanionic aggregation will be analyzed in the last section.

The structure of this dissertation is shown in the following flowchart:



Chapter 2: Theory

2.1 General

The solubility pattern with respect to solvent properties of a non-polar compound like an alkane is in sharp contrast to that of a charged or otherwise strongly polar chemical species. If these two features occur simultaneously in the same chemical entity, interesting compromises are observed. For aqueous solutions, one well-known situation is the polar group is located in the solution while the non-polar part seeks to avoid the aqueous environment by stretching into the gas phase or into an adjacent non-polar phase. An alternative possibility to avoid the unfavourable contact between non-polar groups and water is by self-association into various types of aggregates where hydrophobic chains shielded from the contact with water by hydrophilic head groups. The hydrophilic-hydrophobic nature of amphiphilic molecules leads to their self-assembly into a variety of structures in aqueous media. Micelles are one of the main types of structures formed by the self-association of amphiphiles. They consist of core of a hydrophobic chains shielded from the contact with water by hydrophilic head groups, which maybe ionic or polar. Micelles can either be spherical or extended into ellipsoidal or rod-like shape. This difference in shape depends on numerous features of the surfactants and their surrounding environment. In this chapter theoretical background for mechanism of aggregation will be manifested whereby short- and long-range interaction can be possible. In addition, driving forces in the course of phase transition will also be explained theoretically.

2.2 Micellization

There are two common approaches to the theoretical treatment of amphiphile aggregation². In one, the so called phase separation model, micelle formation is considered as analogous to a phase separation. The *cmc* is then the saturated concentration of the amphiphile in the monomeric state and the micelles constitute the separated pseudo-phase. According to other approach, the equilibrium model, micelle formation is treated analogous to a chemical equilibrium. Analyses of the equilibria show that for the operative formation of large

aggregates, the onset of micelle formation effectively takes place in a quite narrow concentration range. This observation makes the term critical micelle concentration most useful from a practical point of view, since it gives an approximate figure well characterizing the self association pattern of a certain amphiphiles. The equilibrium in formation of micellar aggregate can be formally written in two equivalent ways. Either one has a stepwise growth of the micelles according to the scheme



Or one can regard each aggregate to be formed directly from the monomers



To consider the self-aggregation, one should treat thermodynamics subjective to monomer (unassociated molecule) and aggregate^{45, 46}. According to the equilibrium thermodynamics for a molecular system forming an assembly structure in a solution, chemical potential of identical chemical species involve in various assemblies should be equal to one another. The chemical potential of unimers in aqueous phase may be expressed as

$$\mu_{aq} = \mu_{aq}^0 + k_B T \ln f_1 X_1 \quad (2.3)$$

where μ_{aq}^0 is the standard chemical potential, k_B is the Boltzmann constant f_1 is the activity coefficient and X_1 is the monomer concentration in aqueous phase. For reaction (2.1) equilibrium constant is

$$K_n = \left(\frac{f_n X_n}{n} \right) / \left(\frac{f_1 X_1 \cdot f_{n-1} X_{n-1}}{n-1} \right) \quad (2.4)$$

and the aggregation process is determined through the values of the constant K_n . Here X_n is the fraction of monomers in aggregation. An alternative formulation is obtained by writing the chemical potential μ_n of the aggregate M_n as

$$\mu_n = n\mu_n^0 + kT \ln \frac{f_n X_n}{n} \quad (2.5)$$

where μ_n^0 is the standard chemical potential per monomer in the micelle. The chemical potentials of monomer in micelle and in the aqueous solution are equal at equilibrium and from equation (2.3) and (2.5) one can write

$$n\mu_n^0 + kT \ln \frac{f_n X_n}{n} = \mu_{aq}^0 + kT \ln f_1 X_1 \quad (2.6)$$

for all n. The mole fraction of aggregate n is

$$\frac{X_n}{n} = (f_1 X_1 \exp \frac{\mu_{aq}^0 - \mu_n^0}{kT})^n / f_n \quad (2.7)$$

Together with the expression for the total concentration S of surfactant molecules

$$S = \sum_i X_i \quad (2.8)$$

Equation (2.7) determines the size distribution of the micellar solution. The essential condition for the aggregation of surfactant molecules is $\mu_{aq}^0 > \mu_n^0$ at arbitrary n . The equation (2.4) and (2.6) are related through

$$-kT \sum_{i=2}^n \ln K_i = n(\mu_n^0 - \mu_{aq}^0) \quad (2.9)$$

Depending on the actual application either equation (2.4) or (2.6) is the most convenient one to use in a description of surfactant aggregation to micelles. At a certain critical concentration, X_1^{crit} , the chemical potential in the aqueous phase equals that of the micellar pseudo-phase

$$\mu_{aq}(X_1^{crit}) = \mu_{mic}^0 \quad (2.10)$$

The critical concentration is then identified as the critical micelle concentration, $X_1^{crit} = cmc$. Below the cmc only the monomers and possibly non-micellar aggregates exist, while above the cmc the concentration of non-micellar molecules stays independent of the total amphiphile concentration (see figure 2.1). This result has important consequences. The concomitant changes in a few illustrative physico-chemical properties are schematically presented in figure 2.1. The quite pronounced changes in the concentration dependence of a large number of properties in the region where micelle formation starts, makes it useful to introduce the concept of critical micelle concentration^{47, 48}.

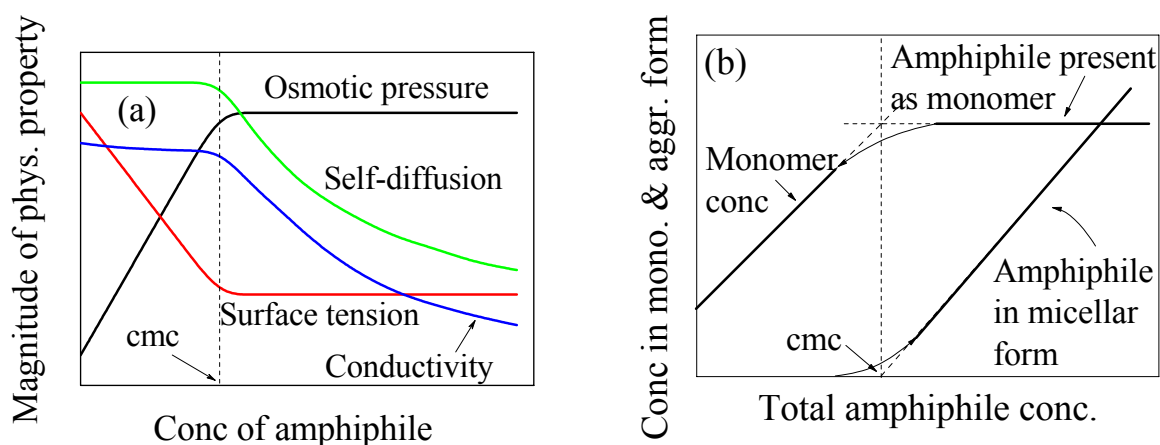


Figure 2.1: Schematic representations of some physical properties which exhibit a sudden change or discontinuity at cmc (a) [from ref. 49]. Figure (b) represents the concentration profile of monomeric and micellized amphiphile against the total concentration of surfactant [from ref. 2].

2.3 Krafft Temperature

In order to utilize the surfactant efficiently, it is necessary to know the concept of Krafft temperature corresponding to the solubility of hydrated surfactants. The schematic diagram to present Krafft point is shown in figure 2.2. The Krafft point is defined as the temperature below which micelles are insoluble in water⁵⁰ i.e. where the monomer solubility is too small for micelle formation. At Krafft point, micelles begin to form⁵¹. Above the Krafft point, most surfactants have a narrow temperature region where they form micelles but not liquid crystals³. Graphically Krafft point can be represented as the temperature at which the solubility versus temperature curve intersects the CMC versus temperature curve⁵² (see figure 2.2). The progress of the conceptual understanding of the Krafft point begins with the initial work published in 1895 until 1988 is summarized in the paper by Moroi and Matuura⁵¹. It may be assumed that complete mixing of molecules occurs below the saturated concentration of molecular dispersion and that the micellar molecules can be treated as if they were perfectly arranged. Thus the solubility below the Krafft point and the CMC can be explained by the concept of the regular solution. The solubility of the surfactant dramatically increases above the CMC. The reason is that the bulk becomes unsaturated by forming micellar aggregation and solubility curve rises steeper.

The Krafft temperature usually increases as the alkyl chain length increases⁵³. However the increase is not regular but displays an odd-even effect⁵⁴. Similarly, the head group and the surrounding counter-ions influence the Krafft point⁵⁵, whereas there are no general trends for the counter-ion dependency. Addition of inorganic salts typically raises the Krafft point for ionic surfactants because of the counter-ion condensation⁵⁶, while it is not the case for zwitterionic surfactants⁵⁷. A longer alkyl-chain surfactant is generally more efficient but its solubility is limited because of its hydrophobic nature. There is commonly a delicate compromise in the design of surfactants. Attempts to lower the Krafft point had mainly been directed towards the conditions in the solid state. The surfactants with lower Krafft point can be developed by structural co-ordination: chain branching in the alkyl chain⁵⁸, introduction of an unsaturated bond in the alkyl chain⁵⁹, alternating the alkyl chain with siloxane chain⁶⁰ and so on. Thus one can develop a surfactant condition on the basis of necessary criteria by introducing optimum changes in the hydrophobic part of the surfactant.

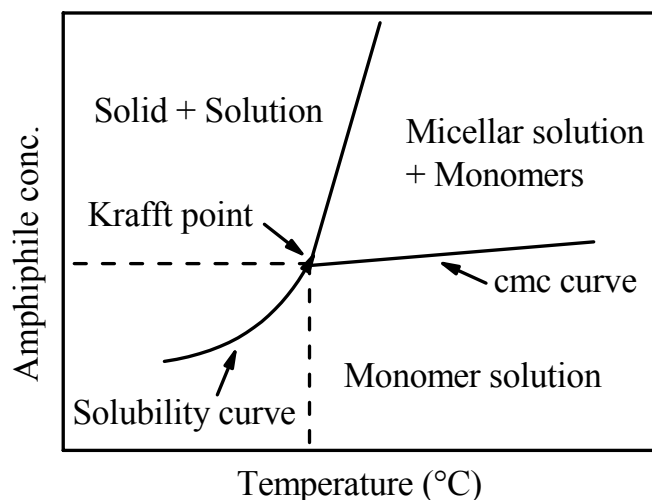


Figure 2.2: Schematic representation of Krafft temperature

2.4 Colloidal Forces

Here under this title it is aimed to understand the various forces that can act between colloidal particles in solution and how these forces (such as electrostatic interaction between two electrically charged surfaces and the ubiquitous van der Waals interaction) can alter the stability of a colloidal dispersion. The mechanisms by which small particles interact in a liquid phase are important in numerous technical applications.

2.4.1 Van der Waals Force

One of the famous theories for stability of colloidal particle is DLVO theory which deals with two different components: a repulsive double-layer force calculated via Poisson-Boltzmann equation and an attractive van der Waals force.

Van der Waals in 1873 noted the non-ideality of gases and attributed it to the existence of molecular or atomic interaction. These interactions were correctly thought to be due to interacting dipoles but incorrectly treated statically. London⁶¹ treated the interacting two-atom system as dynamic and attributed van der Waals force to the dispersion effect. Van der Waals force exists not only between individual atoms and molecules but also between particles. Hamaker⁶² used the additivity concept proposed by London to determine the equations for the van der Waals force between the particles. The additivity concept allows the

force to be calculated based on the interaction between individual atoms making up the particles. The non-retarded energy of interaction between two particles 1 and 2 of volume V_1 and V_2 containing q_1 and q_2 atoms per unit volume is:

$$E = -\int_{v_1} dv_1 \int_{v_2} dv_2 \frac{q_1 q_2 \lambda_{1,2}}{D^6} \quad (2.13)$$

where $\lambda_{1,2}$ is the co-efficient concerning the inter-atomic pair potential. The van der Waals force will be given by

$$F_{VDW} = \frac{\partial E}{\partial D} \quad (2.14)$$

Equation (2.13) combined with equation (2.14) has been solved for the van der Waals force between the bodies of regular geometric form⁶² with two spherical vesicles of radii R_1 and R_2

$$F_{VDW} = \frac{H_a R}{12D^2} \quad (2.15)$$

where R is the reduced radius or $R = \frac{2R_1 R_2}{R_1 + R_2}$ (2.16)

and H_a is called Hamaker's constant and is equal to:

$$H_a = \pi^2 q_1 q_2 \lambda_{1,2} \quad (2.17)$$

The Hamaker constant of most condensed phase is found in the range of $0.4 - 4.0 \times 10^{-19}$ J. But the force between a sphere of radius R and a plane surface may be expressed as

$$F_{VDW} = \frac{H_a R}{6D^2} \quad (2.18)$$

For two plane surfaces, the solution of equation (2.13) is expressed as a pressure, P , or van der Waals force per unit area of contact:

$$P_{VDW} = \frac{\partial F_{VDW}}{\partial H_a} = \frac{H_a}{6\pi D^3} \quad (2.19)$$

Equation (2.15), (2.18) and (2.19) describe non-retarded van der Waals forces for perfectly smooth surfaces. The approach of Hamaker assumes complete additivity of forces between individual atoms and is called the microscopic approach to van der Waals forces.

Lifshitz⁶³ developed the macroscopic theory (also called the modern and continuum theory) of van der Waals forces between and within continuous materials while he assumes that interacting particles and dispersion medium are continuous. He argued that the concept of additivity was unsatisfactory when applied to closely packed atoms in a condensed body. He attributed the non-additivity to the thermodynamic fluctuations always present in the interior of a material medium. The presence of spontaneous electromagnetic fluctuations in any

region will, by Maxwell's equations, change the fluctuation field in any surrounding region. This phenomenon is called screening.

Lifshitz derived the free energy per unit area for two half spaces with plane-parallel boundaries from Maxwell's equations. [Ed. Note: Imagine two large blocks of material separated.] If the half spaces are made of different materials 1 and 2 and are separated by a distance D filled with a vacuum or gas, the non-retarded approximation is given as Hough et al⁶⁴ and Prieve et al⁶⁵ in terms of surface modes of reciprocal length κ :

$$E_{1,2} = \frac{kT}{2\pi} \sum_{n=0}^{\infty} \int_0^{\infty} \left[\ln(1 - \Delta_{1,n} \Delta_{2,n} e^{-2\kappa D}) \right] \kappa d\kappa \quad (2.20)$$

$$\text{where } \Delta_{j,n} = \frac{\varepsilon_j \{i\xi_n\} - 1.0}{\varepsilon_j \{i\xi_n\} + 1.0} \quad (2.21)$$

$$\text{and } \xi_n = n \left[\frac{2\pi k_B T}{h/2\pi} \right] \text{ with } n = 0, 1, 2, \dots \quad (2.22)$$

where T is the temperature in Kelvin scale, k_B is Boltzmann constant and h is Planck's constant. ξ_n is the frequency of n -th thermal fluctuation mode. The prime on the summation in equation (2.20) and many following equations indicate that the $n = 0$ term is given only half weight. The quantity $\varepsilon_j \{i\xi_n\}$ is related to the complex dielectric permeability $\varepsilon\{\omega\}$. The complex dielectric permeability is a macroscopic property that represents the electrical response of a bulk material to an external electric field. It is related to the microscopic polarizability of the constituent atoms of a material.

By replacing $2\kappa D$ with x , the integral in equation (2.20) can be solved as an infinite series in the form⁶⁴:

$$E = -\frac{H_a}{12\pi D^2} \quad (2.23)$$

$$\text{where } H_a = \frac{3kT}{2} \sum_{n=0}^{\infty} \sum_{S=1}^{\infty} \frac{(\Delta_{1,n} \Delta_{2,n})^S}{S^3} \quad (2.24)$$

Taking the derivative of equation (2.23) with respect to the separation distance H , gives the same force per unit area of contact equation as derived by Hamaker (Equation 2.19) using the additivity concept. However, the Hamaker constant, H_a , now depends on the macroscopic material properties of the interacting particles through the functions $\varepsilon_j \{i\xi\}$. This approach is more realistic than Hamaker's which assumes constant, H_a , depends on $\lambda_{i,j}$, a microscopic property of two interacting atoms.

2.4.2 Electric Double-Layer Force

The electric double layer, which describes the diffuse layer of counter-ions in the electrolyte next to a charged surface or about a charged colloid particle, is fundamental to colloid and surface science as it determines the stability of dispersions, the adhesion of particles, and the mobility in applied electric fields. Techniques have been developed to describe accurately the electric double layer taking into account the size of the ions and the correlations between them. Asymptotic analysis has shown how to correct the mean-field Poisson-Boltzmann approximation to include these effects. Van der Waals force between identical species is always attractive; it would have seemed that the dissolved particles embrace one another to form a bigger aggregation and be coagulated, if van der Waals force alone were operative. However, because the particles dispersed in the solution are experiencing many other type of forces including electric double-layer force, resulting in hindrance of coalescence by electrostatic repulsion. The origin of this electric double-layer, surface charge originates from two processes: (1) ionization or dissociation of a functional group on the surface, or (2) ionic adsorption onto the non-charged surface from solution.

The diffused double layer occurs at the interface between the colloidal surface and its adjacent solution. It is made up of the permanent negative charge (for example with oleate surface) of the colloid and the counter-ions in the solution that balance the negative charge. The counter-ions are influenced by two equal but opposing forces – the electrostatic attraction of positive counter ions toward the negative surface, and the diffusive or thermal forces (responsible for Brownian motion) which tend to move the cations away from the surface. The balance of these two forces gives rise to a distribution of cations in the solution adjacent to the colloid surface. This distribution, described as a diffuse electrical double layer or simply diffuse double layer, is made up of the negative colloid surface and the spread-out (diffuse) distribution of the counter-ions. In this diffuse double layer model, the ionic atmosphere is supposed to consist of two regions. Adjacent to the colloidal surface counter-ions tend to predominate due to strong electrostatic forces and here charge density is very high. Ions farther away from the surface of colloids are assumed to be organized more diffusely, according to a balance of electrical force and resulting random Brownian motion. In this outer region the concentration of counter-ions thus decreases gradually away from the surface. For the Stern-Helmholtz model, another single layer is formed over the surface. This outer layer and inner layer are termed as Helmholtz layer and Stern layer respectively (Figure 2.3). Inside

of both the layers potential is decreased proportionally, which is expressed by the following equation:

$$\psi = \frac{4\pi\sigma_e\delta}{\epsilon_\delta\epsilon_0} \quad (2.25)$$

where ψ is the potential, σ_e the charge density, δ is the thickness of the Stern-Helmholtz layer, and ϵ_δ and ϵ_0 are the permittivity in the Stern-Helmholtz layer and of vacuum, respectively.

The ion density on the colloidal surface obeys the Boltzmann distribution:

$$C_s = C_{zp} \exp\left(-\frac{Ze\psi}{k_B T}\right) \quad (2.26)$$

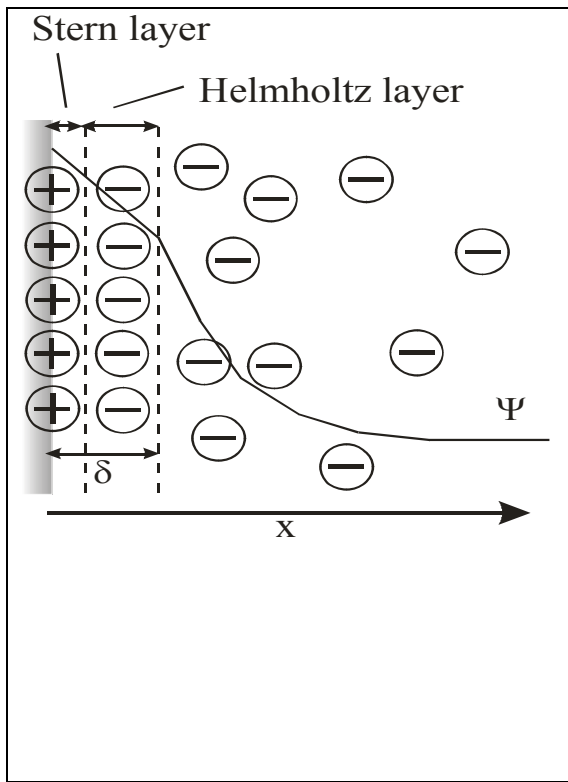


Figure 2.3: Stern-Helmholtz Double layer which indicates the surface charge potential is linearly dissipated from the surface to the bulk of the system. The attracted ions are assumed to approach the colloid surface and form a layer balancing the colloid charge, the distance of approach is assumed to be limited to the radius of the ion and a single sphere of solvation round each ion. The overall result is two layers of charge (the double layer) and a potential drop which is confined to only this region (termed the Outer Helmholtz Plane, OHP) in solution. The result is analogous to an electrical capacitor.

where Z is the number of charge per ions and e is the unit charge, ψ is the electrostatic potential of the colloidal surface, and C_{zp} is the ionic density at zero surface electrostatic potential. The diffuse double layer or the outer diffuse region away from the Stern-Helmholtz layer can be described by the Gouy-Chapman equation, which is a solution of the Poisson-Boltzmann equation for a planar diffuse double layer. The Poisson-Boltzmann equation is:

$$\frac{d^2\psi}{dx^2} = \rho_{net} = -\frac{Ze\rho_0}{\epsilon_r\epsilon_0} \exp\left(-\frac{Ze\psi}{k_B T}\right) \quad (2.27)$$

And the Gouy-Chapman solution is:

$$\psi = -\frac{4k_B T}{e} \tanh\left(\frac{e\psi_0}{4k_B T}\right) \exp(-\lambda_D x) \quad (2.28)$$

where x is the distance between from the middle of two planes, ρ_0 is the normalization constant with the dimension of density, ϵ_r is the relative permittivity of solution. λ_D is given as follows

$$\lambda_D = \left(\frac{e^2 \sum_i C_i Z_i}{\epsilon k_B T} \right) \quad (2.29)$$

The quantity $1/\lambda_D$ has the dimension of length and it is called Debye screening length. In the case of $\frac{Ze\psi_0}{k_B T} \ll 1$, i.e., for a system where the thermal diffusion energy $k_B T$ is much

dominant rather than the surface potential ψ_0 and/ or the electrolyte is weakly charged, then the potential simplifies to

$$\psi = \psi_0 \exp(-\lambda_D x) \quad (2.30)$$

This equation is known as Debye-Hückel equation. When $\frac{Ze\psi_0}{k_B T} \gg 1$, the potential at arbitrary position x can be obtained from the equations (2.25) and (2.28).

2.4.3 DLVO Theory

According to the DLVO theory, the dispersed particles are subjected to two independent forces: the van der Waals force of attraction and the electrostatic force of repulsion arising from the presence of electrical double-layers at the particle surfaces. The net interaction between the colloidal particles is obtained by summing these two terms. This ascribes the total force on a sphere of radius r and surface charge density σ_t a distance D ($D \ll r$) from a plane surface of charge density σ_s to the sum of Coulomb and van der Waals interactions⁶⁷

$$F_{DLVO}(D) = \frac{4\pi\sigma_s\sigma_t r\lambda_D}{\epsilon\epsilon_0} \exp\left(-D/\lambda_D\right) - \frac{H_a}{6D^2} \quad (2.31)$$

Here λ_D is the Debye screening length and H_a is the Hamaker constant, ϵ and ϵ_0 are the relative dielectric constant of the medium and the dielectric constant of vacuum respectively. Van der Waals attraction would be greater than electric double layer repulsion whenever the distance between two particles is enough small, because the attraction increases exponentially

with decreasing distance, while the repulsion increases rather slowly. The comparative relationship of both the forces as a function of distance is shown in figure 2.4.

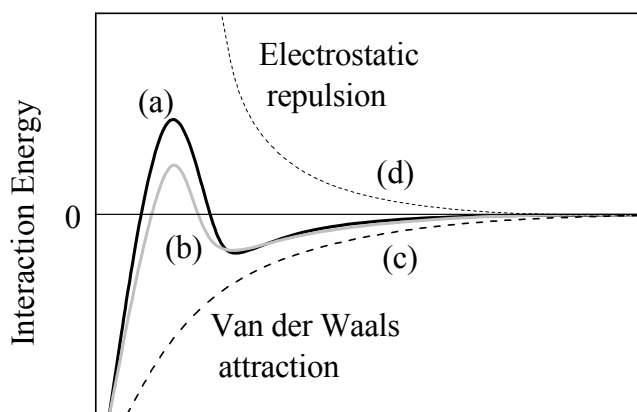


Figure 2.4: Schematic representation of DLVO interaction versus distance profile.

(a) \rightarrow (b): decreasing surface potential with increasing electrolyte concentration (e.g. addition of inorganic salts).

In case of strongly charged particles the repulsion potential exceeds the attraction potential and an energy barrier opposing collision results. The energy barrier allows the particles not to approach towards each other and in such a situation the colloidal particles settle down at the minimum i.e., keep a constant distance away from one another. If the magnitude of this energy barrier exceeds the kinetic energy of the particles, the suspension is stable. On the other hand, reduction of charge density or potential suppresses the energy barrier, resulting in coagulation or flocculation and the colloidal system therefore is unstable. The van der Waals negative potential becomes significant only when the distance between the particles is quite small. At intermediate distances, the repulsive potential is larger than the attractive potential. Attention should be taken on application of the DLVO theory, which was originally developed for inorganic sols, because in certain circumstances experimental results on some model systems seem to depart from the DLVO predictions. In the Coulombic attraction theory (CAT), first proposed by Sogami ⁶⁸ in 1983, the mean field interaction between charged particles has a weak, long-range attraction via their counterions, whereas in DLVO theory the long-range interaction is purely repulsive. This leads to differences in predicted behaviour for dilute systems where the particles apart from each other.

2.4.4 Hydration Force

The hydration force between amphiphilic self-assemblies is proposed originally by Langmuir⁶⁹. A mono-charged or zwitterionic aggregation when immersed in aqueous solution results in one or several well-defined layers of water molecules hydrating the surface in the same way as a dissolved ion has a hydration sphere. Hydration force is a general phenomenon; it represents a measure of the resistance to remove the hydrated water from a hydrophilic surface. Structural or H-bonding polarization at the surface has been suggested as the cause for this force. A number of possible origins of this phenomenon have been discussed in various theoretical and experimental descriptions⁷⁰⁻⁷³. Here I used the empirical definition: hydration force is the hydration pressure which maintains the chemical equilibrium of hydration water that is attached to a hydrophilic surface with a water phase existing under reference conditions (see also references 74 and 75). Hydration force, F_p , shows an exponential decay on hydration in case of lamellar phases⁷⁴. This dependence is usually described by:

$$F_p = P_{h,0} \exp(-R_w / R_{w,0}) \quad (2.32)$$

where $P_{h,0}$ and $R_{w,0}$ are the hydration force at zero hydration and decay constant at zero hydration respectively. The hydration can also be described by the water layer distance, d_w . In the case of non-lamellar phases the curves of hydration force vs. hydration can be more complex.

Hydration force often exceeds the DLVO force in short range and prevents from coalescence of bilayers, vesicles and bio-membranes. Very strong short-ranged repulsive forces have been found to act between lipid bilayers⁷⁶. The range is somewhere between 10 and 30 Å and the repulsion is found to decay exponentially with separation^{77, 78}. Pfeiffer et al⁷⁹ observed that non-exponential decay is also possible when the surfactants aggregation is non-lamellar. Because non-lamellar phase structures are composed of arrangement of curved layers and the curvature contributes to the non-exponential behaviour and it can be similar for the case of spherical vesicles. In fact, for some phospholipid systems it is known that the hydration dependence for non-lamellar phases is strongly influenced by the curvature energy of the layers⁸². This dependence is determined by the bending modulus, especially at higher hydration. A theoretical explanation for the inverse hexagonal phase of phospholipids which shows a rational decay function of hydration force is reported by Rand et al⁸⁰.

$$F = K_0 \left(\frac{1}{R_{pp}} - \frac{1}{R_0} \right) \left(\frac{-1/R_{pp}^2}{A_{pp}/2} \right) \quad (2.33)$$

In their nomenclature, F is the contribution of the bending energy to the osmotic pressure, K_0 the bending module, R_0 the minimum energy radius, R_{pp} a curvature radius and A_{pp} the cross sectional area.

2.4 Vesicle Formation

The thermodynamic properties of surfactant-water systems exhibit a peculiar polymorphism: micellar aggregations and extended phases of hexagonal, cubic, and almost flat lamellar structures were found as lyotropic phases. In addition to these, vesicles and liposomes can also be developed exclusively within the fluid lamellar state, the L_{ves} -phase, under the conditions that the membranes are soft enough to bend into closed shells and can thus decrease the overall energy of the system by avoiding unfavourable hydrophobic contributions. The formation and the stability of the respective structures are the result of the interactions between the molecular species involved and the solvent (usually water), but also of the bending energy of the surfactant arrangement. Especially, the stable average shapes of lipid vesicles are set by minima of the bending elastic energy. Once such closed objects did form, they were reported to exhibit upon temperature changes, within the L_{ves} -phase, a series of different shapes, at constant topology.

Vesicles aggregated from surfactants are of both scientific and technological interest. A central point concerned with the observation of vesicles is the question of their preparation, as in many situations their formation requires the input of external energy. For instance, often vesicles are formed by dispersion of lamellar bilayers where this dispersion may take place by dilution or by the input of external energy. In the onward, a brief review of various methods by which vesicles can be formed is discussed. It should be noted that the size distribution of the vesicular dispersion is strongly affected by the method of preparation^{24, 81}.

A classical way of forming phospholipid vesicles is by the method of sonication of aqueous dispersion of the lipid⁸²⁻⁸⁴. In some situations, vigorous shaking or vortexing is necessary to get a homogeneous mixture of the sample components and this mechanical energy will be sufficient for the formation of vesicles^{21, 22}. Because in many cases external vigorous energy is needed to make a homogeneous mixture, where simple components do not make them similar composition everywhere.

2.5.1 Shear Induced Formation of Vesicles

Shear has a profound influence on the formation of vesicles because it needs a transformation in structure and orientation of complex fluid^{85, 86}. As mentioned above, in order to observe the formation of vesicles, it is often necessary to have external force acting on the planar lamellar bilayers. Such shear induced transition from simple micelles to vesicles has been subjected to a large number of investigation^{87, 88}. It has been shown that originally present planar lamellae become first properly oriented by the shear field of low shear rate, while the transformation to vesicles takes place at high shear rate. Moreover, it has been observed that the size of the onions can be scaled with the inverse of the square root of the shear rate^{87, 88}. The formation of multi-lamellar vesicles is always accompanied by a pronounced shear thickening where the viscosity rises significantly compared to that of the micellar phase or simple planar bilayer phase⁸⁹⁻⁹². This is due to the fact that micelles and planar bilayers can slide along each other without offering much flow resistance, while the multi-lamellar vesicles produce a relatively densely packed system of aggregation. For further increase of shear rate, the produced onion-like vesicles may strip off successively and a shear-thinning behaviour can be observed⁹³. For such a vesicular system viscosity can be described by the following empirical relation over a large shear rate range⁹⁴

$$\eta = \eta_{\infty} + \frac{C}{\dot{\gamma}} \left[1 - \exp\left(-\frac{\eta_0 - \eta_{\infty}}{C} \dot{\gamma}\right) \right] \quad (2.34)$$

where η_0 and η_{∞} are the limiting value of viscosity at low and high shear rates respectively, and C is a constant that can be described in terms of a critical shear rate, $\dot{\gamma}_c$ at which the viscosity reaches a value of $\eta = 0.5 (\eta_0 + \eta_{\infty})$. Accordingly C can be written as¹⁵

$$C = \frac{\eta_0 - \eta_{\infty}}{1.594} \dot{\gamma}_c \quad (2.35)$$

The transformation of planar lamellae to vesicles does not necessarily depend on the shear rate, but in many situations it is controlled by the strain $\gamma = \dot{\gamma} t$ as has been shown for the system alkyl-dimethyl-amine-oxide with alcoholic co-surfactants⁹⁵ where a critical strain for the onset of vesicle formation could be defined from the shear thickening behaviour. It might be mentioned here that in some special situations it has also been observed that application of shear can induce a transition from vesicles to micellar phase^{96, 97}.

2.5.2 Spontaneous Formation of Vesicles

After having above discussion a question normally arises whether spontaneous formation of vesicles is possible. In many circumstances vesicles are formed after inputting external stimulation. However, it is very ambiguous how one defines the process of spontaneous vesicle formation, since in almost all circumstances it is necessary to apply some sort of shear to the system for the preparation of samples in order to homogenize them. Therefore, it is always a question whether this shear applied during homogenization has a potential role for the formation of vesicles. In some cases, samples do not transform into vesicles after immediate homogenization. This is one of the indications that system is transformed into vesicles when there was no shearing and the samples were in quiet rest.

It can be a useful thought that some other types of energies like electrostatic energy or chemical energy is potentially acting to transform this morphological change. There are some observations of spontaneous vesicle formation where counter ions play a potential role for such morphological transformation. For example, dialkyl dimethyl ammonium surfactant does not form vesicles when halide counter ions are present in the system, but replacement of this counter ion by hydroxide ion can stimulate the system to transform into vesicles^{98, 99}. The reason for this difference in behaviour is that hydroxide ion has much higher affinity for water and therefore resides on average further away from the charged bilayer surface. Therefore the repulsive interaction between the head groups and hence the head-group area at the amphiphilic interface becomes larger. Accordingly, they do not form planar bilayers, but have a tendency to form curved bilayers, i.e., vesicles. A similar strong dependence of the formation of vesicles on the counter ions has been observed for anionic surfactants¹⁰⁰.

A classical situation for spontaneous formation of vesicles is that of catanionic systems, where vesicles are obtained by simply mixing a cationic and anionic surfactants. For such “catanionic” systems, vesicle formation has been observed for a large variety of different situations¹⁰¹⁻¹⁰³. Equimolar composition of cationic and anionic surfactants usually forms precipitation, while an excess of either cationic or anionic surfactant composition forms stable unilamellar vesicles¹⁵. The length of the alkyl chain and the nature of the head-group have a strong influence on the formation of precipitate. It is often observed that vesicular bilayers become stable when ionic salt is added to the system. It should be noted here that mixing of cationic and anionic surfactants leads not only to the formation of catanionic vesicular bilayers but also an equal amount of salt being formed by the corresponding counter-ions.

This means that such systems possess a substantial ionic strength which typically stabilizes the vesicles by effective shielding of bilayer charges.

2.6 Phase Transition

A phase transition is the transformation of a thermodynamic system from one phase to another. The distinguishing characteristic of a phase transition is an abrupt change in one or more physical properties, in particular the heat capacity, with a small change in a thermodynamic variable such as the temperature. The first attempt at classifying phase transitions was the Ehrenfest classification scheme, but that is an inaccurate method of classifying phase transitions, for it is based on the mean field theory of phases. Mean field theory is inaccurate in the vicinity of phase transitions, as it neglects the role of thermodynamic fluctuations. In the modern classification scheme, phase transitions are divided into two broad categories. The first-order phase transitions are those that involve a latent heat. During such a transition, a system either absorbs or releases a fixed amount of energy. Because energy cannot be instantaneously transferred between the system and its environment, first-order transitions are associated with "mixed-phase regimes" in which some parts of the system have completed the transition and others have not. This phenomenon is familiar to anyone who has boiled a pot of water: the water does not instantly turn into vapour, but forms a turbulent mixture of water and water vapor bubbles. The second class of phase transitions are the continuous phase transitions, also called second-order phase transitions. These have no associated latent heat. Examples of second-order phase transitions are the ferromagnetic transition, the superfluid transition, and Bose-Einstein condensation.

2.6.1 Concentration-induced Phase Transition

Phase transition dynamics of a surfactant system from a stable to unstable regime and then stable regime again in the phase diagram depends on several parameters. Among them concentration is an important parameter which plays a potential role in transforming the phase from one to another. There are many different approaches which have been used in the thermodynamical description of phase transitions, of them pseudo-phase transition and mass action models are well-known. A very low concentrated surfactant solution is monomeric

where isolated surfactant molecule exists. But with higher concentration surfactant molecules aggregate together and form micelles. This suggests that one might treat the micellar solution as a two phase system where the cmc is the concentration where the system enters the two phase region with a thinking that above cmc the concentration of non-micellar molecules is constant. This indicates that the mean value of any molecular property should vary linearly with concentration above cmc. Although broad thinking says that micellar system is one phase system, but the measurement of some physical parameters indicates that the prediction is approximately correct ².

Depending on thermodynamic variables surfactants show a rich variety of structures ranging from micellar, lamellar, hexagonal and cubic phases. These are composed of small isotropically distributed aggregates, stacked layers, infinite cylinders packed on a two dimensional hexagonal array and a three dimensional net works of interwoven but otherwise unconnected system of cylinders respectively ^{104, 105}. Most of the cases system does not undergo from one phase to another continuously, but with a distinct phase separation. In dilute micellar solution micelles undergo uni-axial or biaxial growth with increasing the concentration of surfactants, depending on the energetic preference. Oetter et al ¹⁰⁶ showed that there is a relation between the interfacial tension and liquid crystalline structure and they observed that a different liquid crystalline structure at higher concentration. The structures are described by theoretical concepts based either on packing considerations of the surfactants in the aggregates or on the spontaneous curvature, which the surfactant film tries to realize. In this case optimal head group area is one of the important parameters in phase transition. Increment in concentration causes hydration of hydrophilic moiety of surfactant to reduce, resulting in the suppression of repulsive force between not only aggregates but also within head groups. As a consequences, the higher the concentration, the higher the packing constrain is. Thus the concentration-dependent phase transition arises from the suppressed head group area.

2.6.2 Effect of Additives

Surfactants in solution exhibit complex aggregation behaviour as a result of a delicate balance of different forces especially with addition of some additives. An important aspect of surfactant systems is the relation between the chemical composition and the shape of the aggregates. In the case of the presence of additive in surfactant solution, the aggregate

structure depends strongly on the character of additives. If the additive has polarity, the interfacial curvature is reduced upon addition of the additives because of its interaction with water or hydrophilic head groups. Often the polar additives are termed as co-surfactants, which potentially form no aggregate by themselves, while cooperate with amphiphiles they produce different morphological structures than pure surfactant itself. Because of this interaction from co-surfactant, surfactant introduces the negative curvature change due to the moderate head group repulsion, and form a different morphology. It also introduces some more elasticity to the surfactant film which gives more softness. This softness of surfactant film plays a significant role in microemulsion¹⁰⁷ and lamellar morphology¹⁰⁸. A non-polar alkane, on the other hand, can solubilize easily into the inner core of micelle, the curvature effect then comes to be more positive. Addition of more oil (non-polar additives) introduces different solubilizing character for non-polar chain of surfactant and sometimes causes breakdown the structure.

When inorganic salts are dissolved into surfactant solution, they become dissociated into their corresponding ions and create an electric double-layer structure on the micellar or otherwise aggregated morphological surfaces according to their nature of the charge. For ionic surfactants, the interaction is dominantly electrostatic and the added salts can effectively reduce the inter-surface repulsion by screening effect and the two adjacent surfaces can come close to each other without facing a strong repulsion from neighbouring one, while for the non-ionic surfactants the effect of added salt is much more complicated. In this case ions are coming from the dissociation of inorganic salts interact with the hydration-water of surfactant head groups and affect the water structure which is well-known as *salting-in* and *salting-out*. For both the phenomena, the anionic species rather than the cationic one influences the water structure more because anions hydrate more strongly than cations; for the same ionic radius as water hydrogen atoms can approach (about 0.8 Å) more closely than the water oxygen atoms, i.e. the *salting-out* anions such as SO_4^{2-} prevent the head group from hydration, while the *salting-in* one, like SCN^- promote to hydrate the head group. According to their effective interaction Hofmeister¹⁰⁹ expressed some anions in a series:

For anions: Citrate³⁻ > SO_4^{2-} > HPO_4^{2-} > F^- > Cl^- > Br^- > NO_3^- > I^- > ClO_4^- > SCN^-

For cations: Al^{3+} > Mg^{2+} > Li^+ > Ca^{2+} > H^+ > Na^+ > K^+ > Rb^+ > Cs^+ > NH_4^+ > $[\text{N}(\text{CH}_3)_4]^+$

The anions and cations reside in the left side of the series correspond to the strongly hydrated ions and are known as *salting-out* while the right hand side ions are more effective to *salting-in* process. These salting-out and salting-in effects have a significant influence on cloud-point¹¹⁰, cmc¹¹¹ and stability of liquid crystal¹¹². The Hofmeister series has a distinct meaning

which indicates that the salting in ions have less charge density and because of their high polarizability they cannot be strongly hydrated, so they influence the head groups to be hydrated; on the other hand, the salting out ions prefer to be hydrated by water because of their high charge density. So water molecules surrounding the surfactants head-groups form a strong hydrogen bond with these ions rather than the surface of aggregation and form a network structure. It can be noted here that anions are far more polarizable than cations (*cf.* Na^+ 0.12; K^+ 0.78; Cl^- 4.00)¹¹³ due to their more diffused extra electron(s) and breaking hydrogen bonds around anions is relatively slow due to the difficulty in finding a new hydrogen-bonding partner¹¹⁴. From this discussion it is clear that *salting-in* ions bound strongly with surfactants head-group and the others bound loosely. Sometimes, the ions with high and low binding degrees with head group are called hydrophobic and hydrophilic counter-ions respectively.

2.6.3 Temperature-induced Phase Transition

Temperature has a considerable influence on phase transition, because thermal energy, kT directly depends on temperature. If the surfactant solution forms a liquid crystalline phase or any other specific ordered phase, then change of temperature can disorder the system. Such phase transition is denoted by symmetry change, i.e. by transformation of orientational and translational ordering in the system. For example, a phase transition from lamellar phase to micellar phase is defined by the break of translational order in one dimension. The layered structure, which is characterized by a periodic alternation and repetition, can be disordered or reformed by incorporating some thermal energy which is a direct influence of temperature.

Most of the non-ionic surfactants exhibit inverse solubility with temperature. The solubility of these surfactants in water decreases as temperature increases, with materials that are fully soluble at room temperature becoming partially insoluble forming separate phases at higher temperatures. The temperature at which a solution of surfactant starts to form molecular aggregation or start to change from one structure (isotropic) to another is known as the "cloud point temperature" or simply "*cloud point*" because, at this temperature the previously clear solution becomes cloudy (figure 2.5(a)). This cloud point temperature can be explained as the solubility limit of that specific phase in that particular solution, beyond that temperature system enters into different phase. This behavior is characteristic of nonionic surfactants, which are often soluble at low temperatures but "cloud out" at some point as the temperature is raised. Clouding phenomenon relates to the micellar growth, resulting in the macroscopic

scattering of light. Therefore, smaller micelles may exist below the cloud point, but after this temperature micellar growth is big enough to scatter sufficient photons that make the system cloudy. The topological variation is the responsible parameter in the course of clouding has been argued using different models^{115, 116}.

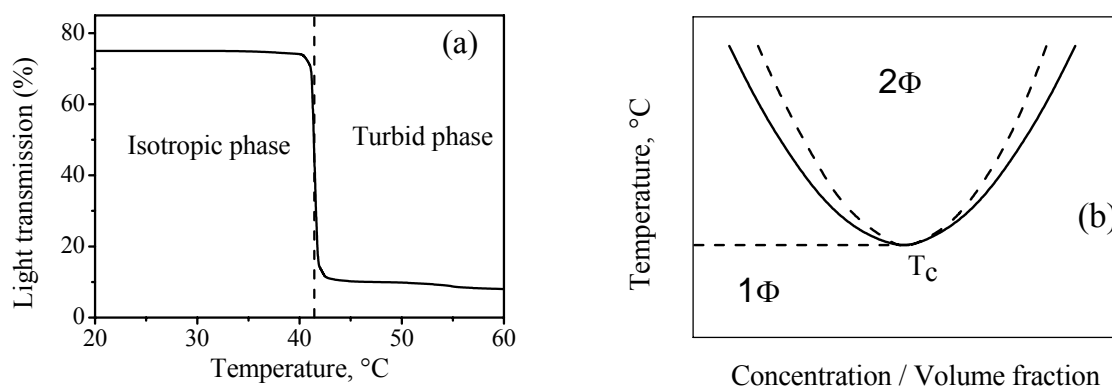


Figure 2.5: Schematic representation of influence of temperature on phase transition. Figure (a) indicates that an isotropic surfactant solution becomes turbid when it crosses the cloud point temperature. Figure (b), on the other hand represents the temperature-composition phase diagram. T_c is the lower critical solution temperature (LCST) at which the distinction between co-existent phases vanishes. Here 1Φ and 2Φ refer to the isotropic phase and two-phase regions respectively.

Certain water-soluble polymers are known to be thermo-sensitive and phase separate or precipitate when the temperature rises to a critical solution temperature. This temperature is called as the lower critical solution temperature, T_c above which there is a phase separation into one with surfactant-rich and one with surfactant-poor solution (Figure 2.5(b)). The onset of phase separation is manifested by a cloudiness of the solution, and further increasing temperature induces the system to separate into two phases. This phenomenon can be explained on the basis of Gibbs free energy. If the change in free energy of homogeneous mixture, ΔG_m is less than that of the pure components, the system is completely miscible. If there is a temperature, however, at which ΔG_m is greater than that of two co-existing phases, then the phase separation will occur. Below T_c , ΔG_m for a mixture is always less than that of the pure components, so a homogeneous phase is stable.

As mentioned above, thermo-sensitivity and phase separation is typically observed for the aqueous solution of non-ionic surfactants¹¹⁷ and dehydration of surfactant molecules is a potential cause of this phenomenon. A few cationic surfactant solutions especially in presence

of high electrolyte concentration also show such behaviour^{118, 119}. This phenomenon originally termed as coacervation, and has been first observed for the mixture of cationic surfactant with inorganic salts like KSCN and potassium chloride¹²⁰.

2.6.4 Shear-induced Phase Transition

Concentrated suspensions of colloidal particles undergo dynamical microstructural transitions under shear. Membrane phases are one example of the variety of complex fluid structures formed by surfactant molecules in solution. The diagram in figure 2.6 shows the regularly stacked lamellae of the L_α phase and the convoluted meandering channels of the “sponge” or L_3 phase. The topological distinctions between these two phases result in very different macroscopic properties. The anisotropic lamellar phases are usually birefringent and viscous, with complicated flow responses, while the isotropic sponge phases are clear and generally flow freely with constant viscosity. However, these very distinct phases are adjacent in the phase diagrams of many systems, and very dilute sponge phases exhibit a transient birefringence when shaken, which suggests a shear-induced transition to a lamellar state. Due to the experimental challenges of studying both the structure and rheology of such dilute phases, the exact nature of the transient birefringence has remained somewhat controversial. After such observation Cates and Milner¹²¹ predict that the lamellar phase is topologically similar to sponge phase, and therefore expect the relationship to extend to such systems as well. Their analysis indicates that the shear-induced transformation from sponge phase to lamellar phase is a result of quasi-first order phase transition. For such phase transition, one

can write the critical shear rate; $\dot{\gamma}_c = \frac{k_B T \left(\frac{\phi}{\delta}\right)^3}{\eta_s}$ (2.36)

Where k_B is Boltzmann constant, T is temperature in Kelvin scale and η_s is solvent viscosity.

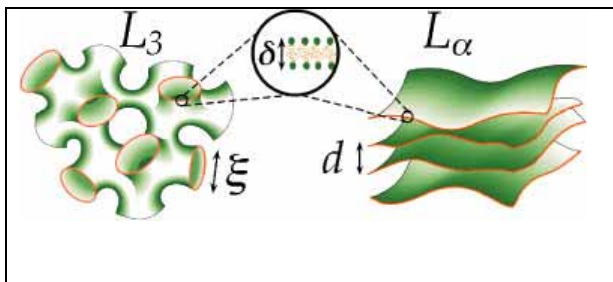


Figure 2.6: Representations of two types of membrane morphologies: the sponge, L_3 and lamellar, L_α phases with their corresponding characteristic lengths.

From this equation, it is clear that transient birefringence, occurring at low shear rates, requires very dilute samples, i.e., having small ϕ . Furthermore, the ϕ^3/η_s dependence suggests that increasing solvent viscosity to slow membrane fluctuations would relax this requirement.

The bilayer structures are stabilized dominantly by the electrostatic interaction between charged membranes and the undulation introduced by Helfrich¹²². This undulation force seems to be destabilized by shear flow. Diet et al¹²³ have observed a relation between the size R , of lamellar droplets in an onion phase and the applied shear rate: $R \approx 1/\sqrt{\dot{\gamma}}$. They

calculated the characteristic size of the onions by balancing two forces: the elastic force, f_{el} and the viscous force, f_{vis} according to following equations¹²⁴

$$f_{el} = \frac{4\pi(2\kappa + \kappa')}{d} \quad (2.37)$$

$$f_{vis} = \eta R^2 \dot{\gamma} \quad (2.38)$$

where d is the distance between two repeating bilayers, η is the viscosity and $\dot{\gamma}$ is the applied shear rate. When the elastic force balances the viscous force, according to the equations (2.37) and (2.38), the equilibrium size for the steady state can be calculated

$$R = \sqrt{\frac{4\pi(2\kappa + \bar{\kappa})}{\eta d \dot{\gamma}}} \quad (2.39)$$

They described that the results from this theoretical calculation agree fairly with the empirical results. Van der Linden et al¹²⁵ furthermore addressed the volume function dependence on the onion size. They used different method of balancing between Laplace pressure and the local shear stress during shear. During shearing, the difference in curvature of the droplet surface with respect to its surroundings would imply a surface stress and that is equal to the Laplace pressure, $4\sigma_{eff}/R$, where σ_{eff} refers to the effective surface tension of the droplet. The surface stress due to the curvature of the surface, created at a certain shear rate $\dot{\gamma}$, balances the shear stress, $\eta\dot{\gamma}$. Using this formulation one can find the diameter of onion

$$R = \frac{4\sigma_{eff}}{\eta\dot{\gamma}} \quad (2.40)$$

Evans¹²⁶ pointed out that the imposition of steady, isothermal and isochoric shear can melt a soft-crystalline aggregate to a normal-shearing fluid. He concluded that different fluid phases can be produced by shearing of crystalline aggregation of colloidal dispersion. Clark and Ackerson¹²⁷ made the similar conclusion after performing their experimental observations.

Cates and Milner¹²⁸ theoretically studied the phase transition $L_3 \rightarrow L_\alpha$ in the presence of shearing and they concluded that it is a fluctuation-induced first-order phase transition. Hoffmann and Rehage^{129, 130}, on the other hand, experimentally found out an analogous phase transition, $L_3 \rightarrow L_\alpha$ under shear rate. It is well-known that the sponge phase becomes birefringent once the shear field is exposed¹³¹, and recently Yamamoto et al¹³² also showed the sponge-lamellar phase transition under shearing experimentally. Using many different experimental techniques like Rheology, SANS, birefringence and SALS experiments from a defective lyotropic lamellar phase Berghausen et al¹³³ showed that shear flow can lead to different states of lamellae orientation. They explored that both surfactant solution and block copolymer melts revealed a reorientation from perpendicular to parallel alignment or vice versa where oscillatory shear is applied. This indicates that the morphological transition might be a general feature of complex fluid when it is subjected to under shear flow.

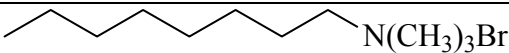
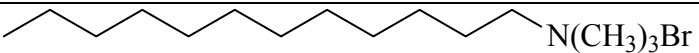
Chapter 3: Experimental

3.1 Chemicals

3.1.1 Surfactants

Several surfactants were used in the present study and they can be categorized into two different groups – (1) anionic surfactant and (2) cationic surfactant, since they can be ionised into anionic and cationic group when they are in aqueous solution. Of them the former one was most commonly used and the later one was used when cationic and mixed vesicular systems were studied. The chemical structures of all the surfactants are shown in table 3.1.

Table 3.1: Chemical structures of different surfactants used in the present study

Surfactant and its cmc ¹³⁴	Chemical structure
Oleic acid (cis-9-octadecenoic acid) (cmc of Na-oleate = 0.9 mM)	$\text{CH}_3(\text{CH}_2)_7 \begin{array}{c} \diagdown \\ \text{C} \\ \diagup \end{array} = \begin{array}{c} \diagup \\ \text{C} \\ \diagdown \end{array} (\text{CH}_2)_7\text{COOH}$ $\begin{array}{c} \text{H} \\ \diagup \\ \text{C} \\ \diagdown \\ \text{H} \end{array}$
Octyltrimethyl ammonium bromide (cmc = 257.4 mM)	
Decyltrimethyl ammonium bromide (cmc = 64.6 mM)	
Dodecyltrimethyl ammonium bromide (cmc = 16.0 mM)	
Tetradecyltrimethyl ammonium bromide (cmc = 3.6 mM)	

Sodium oleate (Na-oleate) was prepared by pH-metric titration of oleic acid which was purchased from Fluka in technical quality, according to the method of Flockhart and Graham ¹³⁵ in aqueous solution. Titration was performed in a closed environment, so that atmospheric

CO₂ cannot be absorbed in the solution, since equivalent point of the titration is in basic region (see figure 3.1). The titration curve is shown in figure 3.1. From the figure one can easily see that the point of inflection appeared at the volume of 102.5 ml of NaOH solution (titrisol, Merck) which is 2.5 ml more than expected volume. This indicates that oleic acid may contain some organic acid with shorter alkyl chain. It took continuously about two days time to complete the titration. Such long duration is necessary to complete the titration, because oleic acid is fairly insoluble in aqueous medium and when titration was performed the acid was encapsulated inside of the emulsion and that is why solution was initially very turbid. This indicates that the reaction between acid and base was slow because of the absence of free acid in the solution.

Other cationic surfactants were directly used without further purification or treatment as they were purchased from Fluka with purity $\geq 98\%$ except Tetradecyltrimethyl ammonium bromide. This surfactant was purchased from Aldrich with purity $\geq 99\%$.

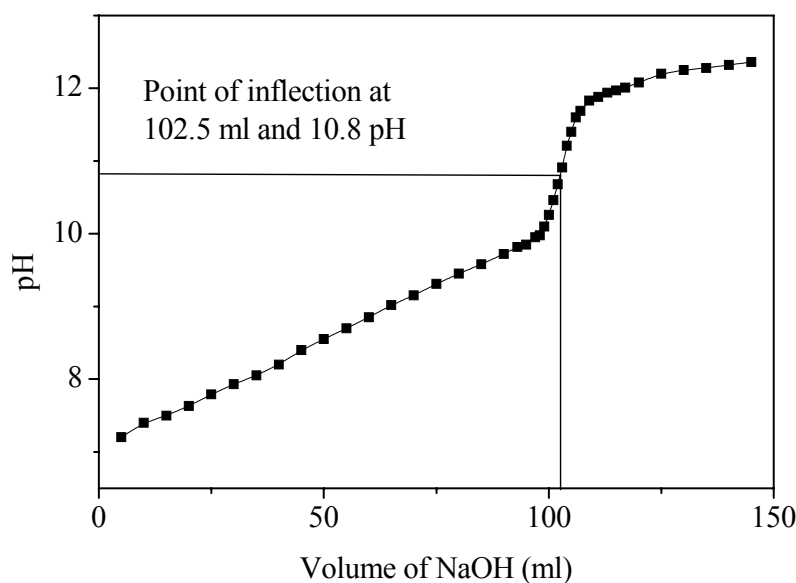
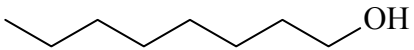
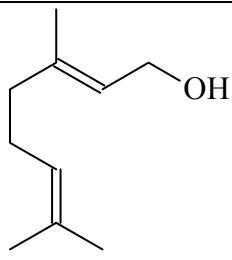


Figure 3.1: Titration curve of oleic acid against standard Na-hydroxide solution at room temperature (22°C); pH is plotted as a function of volume of standard NaOH solution. The quantity of oleic acid taken in this titration was equivalent to 100 ml Na-hydroxide solution.

3.1.2 Co-surfactants

In the present study, two alcoholic co-surfactants were used and their chemical structures are shown in the table 3.2. Of them 1-octanol has a normal alkyl chain while, geraniol has the same number of carbons in its main alkyl chain, but in addition it has two branched-methyl groups and two double bonds. Because of that, its interaction with surfactant aggregation is different from 1-octanol which was observed in comparative study with Na-oleate. Geraniol is well familiar by its trivial name, but in SI system its name is 3,7-dimethyl-trans-2,6-octadien-1-ol.

Table 3.2: Chemical structures of different co-surfactants used in this study

Co-surfactant	Chemical structure
1-octanol [octan-1-ol]	
Geraniol [3,7-dimethyl-2,6-octadien-1-ol]	

3.1.3 Other Chemicals

Many other chemicals were used in the present investigation. Of them some were used to prepare the surfactants in useful form, for instant NaOH solution (titrisol, Merck) was used to prepare Na-oleate from oleic acid, ion exchange resin (strongly basic and acidic resin for anion and cation exchanger respectively) was used to convert DTAB to DTAOH and so on. Ion exchange capacity of anion exchanger was ≥ 0.9 mM/ml, but that of cation exchanger was ≥ 1.7 mM/ml. All chemicals used in the present work are listed in table 3.3.

Table 3.3: Specification of all additive chemicals with purity and suppliers

Chemicals	Formula	Purity	Supplier
Na-hydroxide titrisol	NaOH	$\geq 99.9\%$	Merck
Na-hydroxide granular	NaOH	$> 99\%$	Merck
Na-chloride	NaCl	$> 99.5\%$	Merck
Cs-hydroxide	CsOH	$> 99\%$	Merck
Cs-chloride	CsCl	$> 99\%$	Merck
Tetra-methyl ammonium hydroxide	Me ₄ NOH	$> 95\%$	Fluka
Tetra-methyl ammonium chloride	Me ₄ NCl	$> 95\%$	Fluka
Tetraethyl ammonium hydroxide	Me ₄ NOH	$> 95\%$	Fluka
Tetraethyl ammonium chloride	Et ₄ NCl	$> 95\%$	Fluka
Hydrochloric acid, titrisol	HCl	$\geq 99.9\%$	Merck
Ti-tetrabutoxide	Ti(OBu) ₄	$> 97\%$	Fluka
Hexamethyl disilane	Me ₃ Si-SiMe ₃	$> 98\%$	Fluka
Lithium hydroxide	LiOH	$> 99\%$	Merck
Lithium chloride	LiCl	$> 99\%$	Merck

3.2 Phase Study

To understand a surfactant and its interaction with other components of the system, the phase study is important. For instance the phase behaviour reveals characteristic points that could tell us whether these additives involve in the interaction with aggregates, or not. Each associating structure can be identified by several experimental methods.

3.2.1 Single Phases

Surfactants form a variety of microstructures in aqueous media, ranging from simple micelles at low surfactant concentration to complex mesophases, such as lamellar, hexagonal and cubic phases at high concentration. These are composed of small isotropically distributed aggregates, stacked layers, infinite cylinders packed on a two dimensional hexagonal array

and three dimensional networks of interwoven but otherwise system of cylinders, respectively¹³⁶⁻¹³⁸. This transformation from one type of aggregation to another is possible mostly through a biphasic region³. Every single phase with individual aggregate can be identified by several experimental methods. For instance, a liquid crystalline aggregate such as lamellar or hexagonal liquid crystalline sample can be identified by optical anisotropy, since this type of solution shows birefringence when placed between a polarizer and an analyzer which are crossed perpendicularly. Liquid crystalline structures are capable of rotating the light about the direction of light propagation. The other structures, on the other hand, cannot rotate the plane polarized light about its propagating direction and hence no light is transmitted when the polarizer and analyzer are combined together.

3.2.2 Phase Rule and Tie Line

A phase transition is the transformation of a thermodynamic system from one phase to another. The distinguishing characteristic of a phase transition is a sudden change in one or more physical properties, in particular the heat capacity, with a small change in a thermodynamic variables. In work on heterogeneous equilibrium published in 1875-1876, J. Willard Gibbs derived a simple rule which determines the number of degrees of freedom for a heterogeneous system in equilibrium. The number of degrees of freedom for a system is the number of intensive variables (often taken as the pressure P , temperature T , and composition fraction) that may be arbitrarily specified without changing the number of phases. If a system in equilibrium contains P phases and C components then the phase rule states that the number of degrees of freedom is given by

$$F = C - P + 2 \quad (3.1)$$

Note that great care must be taken in correctly determining C , which is the number of *chemically independent* species. Specifically, attention must be paid to the equilibrium among chemical species. If there is a first order character of phase transition, a two-phase or three-phase region must exist between two adjacent single phases. During such a transition, a system either absorbs or releases a fixed amount of energy. Because energy cannot be instantaneously transferred between the system and its environment, first-order transitions are associated with "mixed-phase regimes" in which some parts of the system have completed the transition and others have not. The separated two- or multi-phases should be consisted of the neighbouring phases, governed by the tie lines. For a binary system, here referring to a water/

surfactant system, the tie line must be connected horizontally from one to another single phase at constant temperature. The end point of the tie line will give the composition of two phases in equilibrium. For a ternary system such as two surfactants/ water or, surfactant/ water/ oil, the phase behaviour becomes complicated due to the value of degree of freedom $F = 2$ at constant temperature. Namely, the phase rule permits to three co-existing phases. The tie line can no longer be drawn by the same way as the binary system. One would be able to determine the tie line by quantitative methods¹³⁹, since the relative amount of two or three phases are related to the lever rule along the tie line. Transition between phases in surfactant systems are generally of the first order, implying that there is a narrow or wide two-phase region between two single-phase regions. The two-phase region may sometimes be difficult to be found out visually when they are miscible, for instance a two-phase region consists of two liquid crystals.

3.3 Rheology

The term “rheology” may be defined as the study of flow of fluids and deformation of matters under stress and strain. One of the tasks of rheology is to empirically establish the relationships between deformations and stresses, respectively and their derivatives by adequate measurements. Such relationships are then amenable to mathematical treatment by the established methods of continuum mechanics. Specifically it is concerned with the description of mechanical properties under various deformation conditions. Dilute solution of surfactant systems usually behave as Newtonian liquids. The viscosity of these solutions is related to the size and shape of aggregates. At higher concentration, the surfactant solutions show a complicated rheological behaviour. They come to be elastic and their viscosities depend on the shear time or the shear rate. Generally, viscosity increases with the surfactant concentration; however, there are some systems which have very low viscosities even at very high surfactant concentration, while there are some other systems which show opposite behaviour. Experimentally well defined zero shear viscosities can be interpreted in terms of two independent parameters: a structural parameter, shear modulus, and a dynamic parameter, structural relaxation time. Both quantities should be determined separately, which had become possible through the dynamic measurement in a linear range of deformation.

3.3.1 Newtonian Fluid

A fluid is classified as being Newtonian if it confirms to Newton's friction law, i.e. if viscosity remains constant with agitation or varying the shear rate (see figure 3.2a) and its shear rate being proportional to the velocity gradient vertical to the direction of flow. Here one can consider a coordinate system with the x-direction perpendicular to the shearing plane and a fluid has two layers separated by dy . When a shear stress, σ is applied to upper layer, forcing it to move towards x-direction with a velocity, $dv = dx/dt$, at that time, dv/dy defines the velocity gradient. Newton's law of viscosity states that F/A (force per unit area) is proportional to dv/dy or shear rate, $\dot{\gamma}$. So, one can write

$$F/A = \sigma \approx dv/dy \quad (3.2)$$

$$\sigma = \eta \dot{\gamma}$$

From this relation one can say, Newtonian fluid may be defined as the relation that the applied stress is proportional to the resulting rate of deformation or simply the rate of shearing¹⁴⁰. And the proportionality constant of this relation is Newtonian viscosity.

3.3.2 Non-Newtonian Fluid

The apparent viscosity (η_{app}) for a non-Newtonian fluid strongly depends on shear stress or shear rate. Although the concept of viscosity is commonly used to characterize a material, it can be inadequate to describe the mechanical behaviour of a substance, particularly non-Newtonian fluids. They are best studied through several other rheological properties which relate the relations between the stress and strain tensors under many different flow conditions, such as oscillatory shear, or extensional flow which are measured using different devices or rheometers. The rheological properties are better studied using tensor-valued constitutive equations, which are common in the field of continuum mechanics. One can see and compare the flow property of Newtonian and non-Newtonian fluid in figure 3.2.

Shear thinning is one of the very common properties for many non-Newtonian fluids. For a dilute system, shear thinning can be due to the flow orientation of the aggregated particles or the change in conformation of the polymer molecules or elongated micelles. Thus, when the shear rate is larger than the rate of thermal reorientation of the particles will be aligned in the

direction of flow. For the concentrated system, shear thinning appears when shear rate is larger than the rate of build-up of the equilibrium supra-particle structures. For a shear-thinning or a pseudo-plastic system, η_{app} decreases with increasing shear rate. Bingham plastics are characterised by a finite yield stress value, i.e. a certain stress is needed to start flowing a system and before exceeding this stress, the system does not flow.

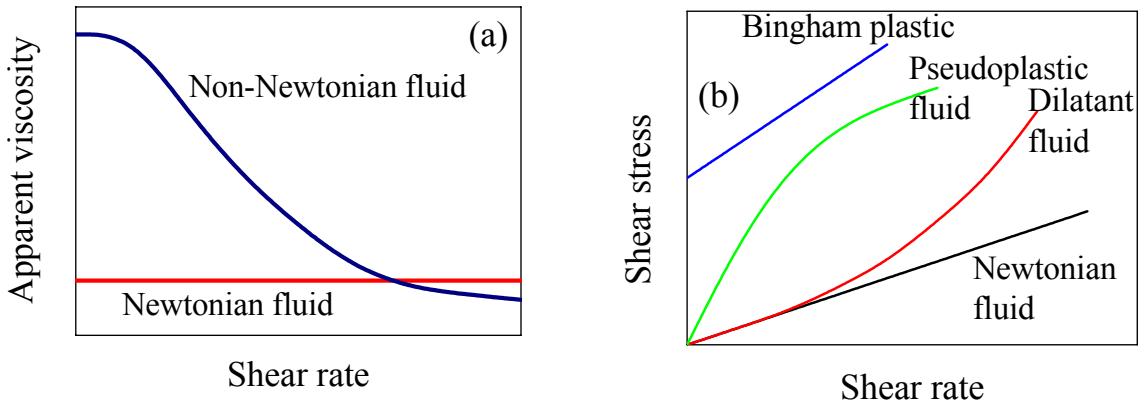


Figure 3.2: Comparative representation of viscosity of Newtonian and non-Newtonian fluids (a). Graphical illustration expresses the relationship between shear stress and shear rate for different colloidal structures (b).

One can measure the characteristic viscosities for a shear thinning system. At very low shear rate there exists a region where viscosity remains constant for non-Newtonian system too. This viscosity normally termed as zero-shear viscosity, η_0 . At intermediate shear rate there is a non-linear region where the viscous resistance falls with increasing the shear rate and the system shows shear thinning behaviour. But at very high shear rate, viscosity becomes constant again and it is termed as limiting viscosity at infinite shear, η_∞ . Under this condition, anisometric particles are aligned in the streaming solutions or a super-molecular network structure has been destroyed by the shearing force. In such case one can use the Cross model¹⁴¹

$$\frac{\eta_0 - \eta}{\eta - \eta_\infty} = (K\dot{\gamma})^m \quad (3.3)$$

where K and m are the constant parameters with dimension of time and dimensionless respectively. It is informative to make certain approximations to the Cross model and by this way one can introduce some other models. When $\eta \ll \eta_0$ and $\eta \gg \eta_\infty$, the Cross model reduces to

$$\eta = \frac{\eta_0}{(K\dot{\gamma})^m} \quad \text{or} \quad \eta = K_2\dot{\gamma}^{n-1} \quad (3.4)$$

This is the well known “*power-law*” model and n is called the power-law index. K_2 is called the consistency. The inverse of K in Cross model is often called the critical shear rate where one can find the system starts to show shear thinning behaviour.

It has been shown for many viscoelastic solutions that there exists a simple correlation between dynamic and steady state shear flow which is known as Cox-Merz rule ¹⁴². According to this rule it has been observed that the complex viscosity $|\eta^*|$ at a certain frequency ω gives the same information as the steady state value of the shear viscosity η at the corresponding shear rate $\dot{\gamma}$. A good agreement between the viscosities has been reported in polymer solutions ¹⁴³ and rod-like micellar solution ¹⁴⁴. The rule does not satisfy very well with more complex structured fluids like vesicles ¹⁴⁵, liquid crystalline polymers and concentrated colloidal dispersions. Experimental data of complex structured fluids reveals a very less agreement or no agreement between the complex viscosity curve in oscillatory measurement and the simple shear viscosity curve ^{146, 147}. Monero et al ¹⁴⁸ explained the deviation from the Cox-Merz rule that the steady shear curve is governed by a larger relaxation time than that of complex viscosity. To comply with the Cox-Merz rule, it is necessary that $\tau_S = \tau_\infty$, where τ_S and τ_∞ indicate the characteristic time at high deformation rate and structural relaxation time respectively. When $\tau_S > \tau_\infty$, the shear viscosity is shifted downwards with respect to the complex viscosity. At high frequency complex viscosity approaches to a specific asymptote.

$$|\eta^*(\omega)| \rightarrow G_0\tau_R \quad (3.5)$$

This implies that $\tau_R = \tau_\infty$ permits to the Cox-Merz rule at high frequency or shear rate. The Maxwell model with the single relaxation time would follow the Cox-Merz rule, however, the relaxation mode of a real system is governed by some independent time constants arising from different motions at each time scale ¹⁴⁹⁻¹⁵¹.

3.3.3 Viscoelastic Fluid

The Word “viscoelastic” means the simultaneous existence of viscous and elastic properties in a material. It is not unreasonable to assume that all real materials are viscoelastic, i.e. in all materials; both viscous and elastic properties coexist. Most surfactant solutions show such

viscoelastic flow behaviour. The rheological properties of these solutions can often be represented by a mechanical model which, at least qualitatively, behaves in an analogous manner. The basic elements of the mechanical models are an elastic spring to represent Hookian law and a dashpot which obeys Newtonian law. Each spring element is assigned for stiffness analogous to the shear modulus G_0 and each dashpot represents a viscosity η . To simplify the model one can consider that a viscoelastic surfactant solution is consisted of one spring combined with one dashpot in series (Maxwell model). If the applied force is assumed to be analogous to the shear stress and displacement analogous to shear strain, the spring constant can be interpreted as the elastic shear modulus and the dashpot as the shear viscosity. Since real solutions generally exhibit non-linear behaviour under large deformation, such model is appropriate only for small displacements. The region where the response of a viscoelastic material is only a function of time for all magnitude of stress or strain is called the linear viscoelastic regime. Figure 3.3 shows an example of the linear and non-linear regimes for a viscoelastic solution which can be determined by the variation of rheological parameters as a function of stress or strain.

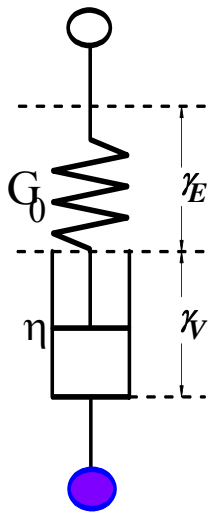


Figure 3.3: Schematic representation of Maxwell model.

On the basis of the model depicted in figure 3.2, a viscoelastic solution can be represented by a linear differential equation. When a certain stress is applied to the solution, the spring stretches instantaneously, while the dashpot elongates steadily at a rate of σ/η . The total strain is the sum of the elastic strain γ_E and viscous strain γ_V .

$$\gamma_T = \gamma_E + \gamma_V \quad (3.6)$$

Differentiating this equation with respect to time yields

$$\dot{\gamma}_T = \dot{\gamma}_E + \dot{\gamma}_V = \frac{1}{G_0} \cdot \frac{d\sigma}{dt} + \frac{\sigma}{\eta} \quad (3.7)$$

When the deformation process is suddenly stopped, the Maxwell model relaxes with a time constant τ which is given by the ratio of the viscosity and the elastic modulus. By setting $\dot{\gamma} = 0$ in equation [3.7], the stress relaxation can be expressed by

$$\sigma = \sigma_0 \exp(-t/\tau) \quad (3.8)$$

Thus the stress relaxes exponentially to zero.

Dynamic experiments can be performed to get further information about viscoelastic behaviour of the solution. The dynamic measurement allows one to have information on the equilibrium state of the surfactant solution without destructing the super-molecular structures. In such case, generally a sinusoidal deformation or strain is applied to the solution. If the solution obeys Newtonian law, the stress will lead the strain by 90° and for an elastic soft solid the shear stress will be in phase with the shear strain (see figure 3.4). For viscoelastic materials, therefore, it is expected that the phase difference between stress and strain would be between 0° and 90° .

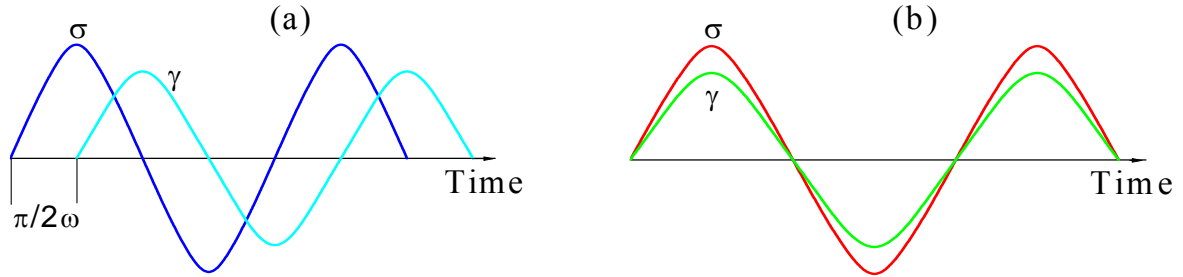


Figure 3.4: Phase difference between stress (σ) and strain (γ) for a Newtonian solution (a) and for an elastic body (b).

The response of Maxwell model to the periodic change of frequency ω consists of a sinusoidal shear stress is made up of two components; the first component is in phase with the deformation and the second one is out of phase with the strain. From these quantities, the storage modulus G' and loss modulus G'' can be calculated according to the equation

$$G' = \frac{\hat{\sigma}}{\hat{\gamma}} \cos \delta \quad G'' = \frac{\hat{\sigma}}{\hat{\gamma}} \sin \delta \quad (3.9)$$

where $\hat{\sigma}$ and $\hat{\gamma}$ indicate the amplitude of the shear stress and of the deformation. It is convenient to express the periodically varying function in terms of the complex viscosity η^* , the magnitude of which can be defined as

$$|\eta^*| = \frac{(G'^2 + G''^2)^{1/2}}{\omega} \quad (3.10)$$

The behaviour of the Maxwell materials under harmonic oscillations can be obtained from the equations

$$G'(\omega) = G_0 \frac{\omega^2 \tau^2}{1 + \omega^2 \tau^2} \quad (3.11)$$

$$G''(\omega) = G_0 \frac{\omega \tau}{1 + \omega^2 \tau^2} \quad (3.12)$$

It has been seen that for $\omega\tau \gg 1$, G' approaches a limiting value which is identical to the shear modulus G_0 . Under such experimental conditions, the model behaves like an elastic body. At low frequencies, when $\omega\tau \ll 1$, G' becomes proportional to ω^2 . This region is called the terminal zone and the Maxwell model behaves as a liquid.

3.3.4 Equipments

The rheological measurements were performed by a Haake RS600 with a cone-plate sensor and a Haake RS300 with a double gap cylindrical sensor. These two different sensor systems were used according to the viscosity of the solutions: RS600 was used for highly viscous fluid or gel and RS300 was used for low viscous liquids. During the measurement the temperature was controlled to an accuracy of $\pm 0.1^\circ\text{C}$ by a thermo-controller (Haake TC81) for RS600 and by an ethylene glycol circulator with an accuracy of $\pm 0.5^\circ\text{C}$ for RS300. The measurements were operated by the software, Haake RheoWin Job Manager and the measured data were analysed by Haake RheoWin Data manager. Geometrical information about these two Rheometers is listed in table 3.4.

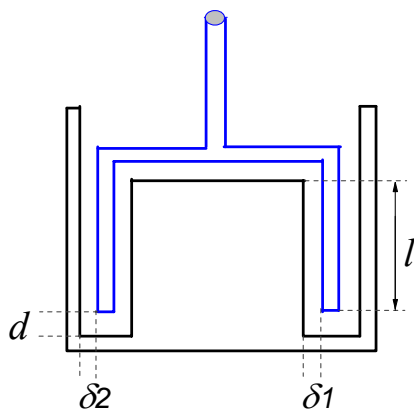


Figure 3.5: Schematic representation of double gap cylindrical geometry of RS300. One can find the measure of different parameters described in table 3.4.

Table 3.4: Geometric information about cone-plate and double gap cylindrical sensors

Sensor	Radius of cone [mm]	Cone angle	Distance between cone-plate [mm]	
Cone-plate	30 ± 0.01	1°	0.052	

Sensor	Gap δ_1 [mm]	Gap δ_2 [mm]	Length l [mm]	Distance d [mm]
Double gap cylinder	0.25	0.3	55 ± 0.006	5.1

3.4 Dynamic Light Scattering (DLS)

Colloidal particles in solution always undergo Brownian motion, which results in the fluctuation of scattering intensity. DLS is a technique to investigate the scattering intensity fluctuation and obtain the size information of the particles. When a laser beam passes through a colloidal dispersion, the particles scatter some of the light in all directions. When the particles are very small compared with the wavelength of the light, the intensity of the scattered light is uniform in all directions (Rayleigh scattering); for larger particles (above approximately 250 nm diameter), the intensity is angle dependent (Mie scattering).

3.4.1 Principle of Dynamic Light Scattering

Dynamic light scattering (DLS) is also known as "photon correlation spectroscopy" and uses the scattered light to measure the rate of diffusion of the aggregated particles. This diffusion data is conventionally processed to derive a size distribution for the particles, where the size is given by the hydrodynamic radius, R_h . Classical light scattering involves measuring the amount of light scattered by the particles in a solution at some angle relative to the incident laser beam. For spherical aggregation, the intensity of the scattered light is uniform in all directions, so it is only necessary to measure scattering at a single angle (usually 90 degrees). In dynamic light scattering one measures the time dependence of the light scattered from a very small region of solution, over a time range from centies of a microsecond to the second range. The fluctuation in the intensity of the scattered light is related to the rate of concentration fluctuations in the region studied, and the data can be analyzed to give the

collective diffusion coefficients of the system. In a first approximation the collective diffusion is equated with the individual motion of particles (Brownian motion). When multiple species are present, a distribution of diffusion coefficients will be interpreted.

Traditionally, rather than presenting the data in terms of diffusion coefficients, the data are processed to give the "size" of the particles (radius or diameter). The relation between diffusion and particle size is based on theoretical relationships for the Brownian motion of spherical particles, originally derived by Einstein. The "hydrodynamic radius" or "Stokes radius", R_h , derived from this method is the size of a spherical particle that would have a diffusion coefficient equal to that of the aggregates, and the data is commonly presented as the fraction of particles as a function of their radius or diameter.

3.4.2 Correlation Function

Light will be scattered by a molecule in solution if the molecule has polarizability different from its surroundings. In this case, oscillating dipole moment induced by the electric field of the incident light beam will radiate light in all directions. The intensity of the scattered light will be related to the direction of polarization of the incident light, scattering angle and solution parameters.

DLS measurements involve the analysis of the time dependent autocorrelation function of scattered light as performed by a digital correlator. The normalized time dependent autocorrelation function of the intensity of the scattered light $g^{(2)}(\tau)$ for a given delay time τ is given by ¹⁵²

$$g^{(2)}(\tau) = \frac{\langle I(t)I(t+\tau) \rangle}{\langle I(t) \rangle^2} \quad (3.13)$$

where $I(t)$ and $I(t + \tau)$ are the intensities of the scattered light at time t and $(t + \tau)$ respectively, and the braces indicate averaging over t . In most cases of practical interest the intensity time autocorrelation function may also be expressed in terms of the field – field time autocorrelation function $g^{(1)}(\tau)$ as

$$g^{(2)}(\tau) = B + \beta [g^{(1)}(\tau)]^2 \quad (3.14)$$

with $g^{(1)}(\tau)$ is given by

$$g^{(1)}(\tau) = \frac{\langle E(t)E^*(t+\tau) \rangle}{\langle E(t)E^*(t) \rangle} \quad (3.15)$$

where $E(t)$ and $E(t + \tau)$ are the scattered electric fields at time t and $(t + \tau)$ respectively, and β is a factor that depends on the experimental geometry. Equation (3.14) is known as the Siegert relation¹⁵³. The factor B , commonly referred to as the baseline, is the long-time value of $g^{(2)}(\tau)$. Although the factor B should be equal to 1, in practice, a small amount of noise in the measurement can result in values that differ from unity by small ($\sim 10^{-4}$) amounts¹⁵⁴. In this case assuming that the baseline is one changes the parameter estimates and increases the deviation of the fit from the data. Larger deviations of the baseline from one can indicate that there is a problem with the data¹⁵⁴ or that it is a non-ergodic system.

For monodisperse particles in solution the field correlation function decays exponentially, $g^{(1)}(\tau) = 1 + \exp(-\Gamma \tau)$ with a decay rate of $\Gamma = 2Dq^2$, where D is the diffusion coefficient of the particles and q is the magnitude of the scattering wave vector¹⁵⁵. The scattering wave vector q is defined as the difference between the incident and the scattered wave vectors, and its magnitude q is given by

$$q = \frac{4\pi n}{\lambda_0} \sin(\theta/2) \quad (3.16)$$

where n is the refractive index of the solvent, λ_0 is the wavelength of the laser in vacuum and θ is the scattering angle. The relation between diffusion coefficient, D and hydrodynamic radius, R_h of the particles is given by Stokes-Einstein equation¹⁵⁵

$$R_h = \frac{k_B T}{6\pi\eta D} \quad (3.17)$$

Where k_B is the Boltzmann's constant, T is the temperature in Kelvin scale and η is the dynamic viscosity of the medium. For a polydisperse sample, $g^{(1)}(\tau)$ can no longer be represented as a single exponential and must be represented as a sum or an integral over a distribution of decay rates $G(\Gamma)$ by¹⁵⁶

$$g^{(1)}(\tau) = \int_0^\infty G(\Gamma) \exp(-\Gamma \tau) d\Gamma \quad (3.18)$$

where $G(\Gamma)$ is normalized so that

$$\int_0^\infty G(\Gamma) d\Gamma = 1 \quad (3.19)$$

3.4.3 Method of Cumulants

Finding the precise functional form for the distribution of decay rates $G(\Gamma)$ is problematic because the correlation function is measured discretely over an incompletely range of τ and

there is always noise associate with the data ¹⁵⁷. There are several ways of using DLS data to characterise $G(\Gamma)$, ¹⁵⁷ but one of the simplest is the method of cumulants first proposed by Koppel ¹⁵⁶. This method is based on two relations: one between $g^{(1)}(\tau)$ and the moment-generating function of the distribution, and one between the logarithm of $g^{(1)}(\tau)$ and the cumulant-generating function of the distribution. It is appropriate only for the use in case in which $G(\Gamma)$ is monomodal ¹⁵⁴.

In fact, as was discussed by Koppel ¹⁵⁶, the form of $g^{(1)}(\tau)$ as given in equation (3.18) is equivalent to the definition of the moment generating function $M(-\tau, \Gamma)$ of the distribution ¹⁵⁸ $G(\Gamma)$

$$M(-\tau, \Gamma) = \int_0^{\infty} G(\Gamma) \exp(-\Gamma \tau) d\Gamma \equiv g^{(1)}(\tau) \quad (3.20)$$

The m th moment of the distribution $m_m(\Gamma)$ is given by the m th derivative of $M(-\tau, \Gamma)$ with respect to τ :

$$m_m(\Gamma) = \left. \frac{d^m M(-\tau, \Gamma)}{d(-\tau)^m} \right|_{-\tau=0} = \int_0^{\infty} G(\Gamma) \Gamma^m \exp(-\Gamma \tau) d\Gamma \Big|_{-\tau=0} \quad (3.21)$$

Similarly the logarithm of field correlation function is equivalent to the definition of the cumulant-generating function ¹⁵⁸ $K(-\tau, \Gamma)$

$$K(-\tau, \Gamma) = \ln[M(-\tau, \Gamma)] \equiv \ln[g^{(1)}(\tau)] \quad (3.22)$$

where the m th cumulant of the distribution $\kappa_m(\Gamma)$ is given by the m th derivative of $K(-\tau, \Gamma)$:

$$\kappa_m(\Gamma) = \left. \frac{d^m K(-\tau, \Gamma)}{d(-\tau)^m} \right|_{-\tau=0} \quad (3.23)$$

By making use of the fact that the cumulants, except for the first, are invariant under a change of origin, one can write the cumulants in terms of the moments about the mean as

$$\kappa_1(\Gamma) = \int G(\Gamma) \Gamma d\Gamma \equiv \bar{\Gamma} \quad (3.24)$$

$$\kappa_2(\Gamma) = \mu_2 \quad (3.25)$$

$$\kappa_3(\Gamma) = \mu_3 \quad (3.26)$$

$$\kappa_4(\Gamma) = \mu_4 - 3(\mu_2)^2 \dots \quad (3.27)$$

where μ_m are the moments about the mean, as defined by

$$\mu_m = \int G(\Gamma) (\Gamma - \bar{\Gamma})^m d\Gamma \quad (3.28)$$

The first cumulant describes the average decay rate of the distribution. The second and third cumulants correspond directly to the appropriate moments about the mean. The second moment corresponds to the variance and the third moment provides a measure of the

skewness or asymmetry of the distribution. The first two cumulants must be positive, but the third cumulant can be positive or negative.

The basis of the cumulant expansion that is usually used in the analysis of DLS data lies in expanding the logarithm of $g^{(1)}$ in terms of the cumulants of the distribution. This relation follows from the fact that m th cumulant is the coefficient of $(-\tau)^m / m!$ in the Taylor expansion of $K(-\tau, \Gamma)$ about $\tau = 0$, as given by

$$\ln[g^{(1)}(\tau)] \equiv K(-\tau, \Gamma) = -\bar{\Gamma} \tau + \frac{\kappa_2}{2!} \tau^2 - \frac{\kappa_3}{3!} \tau^3 + \frac{\kappa_4}{4!} \tau^4 \dots \dots \dots \quad (3.29)$$

To take advantage of this form and use linear least square methods to fit this function to the data requires that a key assumption be made about the data. The base line must be assumed to be exactly one. Then a fit can be made to

$$\ln[g^{(2)}(\tau) - 1] = \ln \frac{\beta}{2} - \bar{\Gamma} \tau + \frac{\kappa_2}{2!} \tau^2 - \frac{\kappa_3}{3!} \tau^3 + \frac{\kappa_4}{4!} \tau^4 - \dots \dots \dots \quad (3.30)$$

This final equation is the traditional fitting function that is described in many DLS analysis 155, 157, 158

3.4.4 Equipments

ALV DLS/SLS SP 5022F compact goniometer system with an ALV 5000/E correlator was employed for the dynamic light scattering measurements. He-Ne laser of wavelength 632.8 nm served as light source, and most of the samples were measured at 90° scattering angle. Prior to the light scattering measurements the sample solutions were filtered using Millipore Nylon filters with a pore size of 450 nm. Temperature was kept constant during the measurement at 25°C with an equipped water circulator.

3.5 Small Angle X-ray Scattering (SAXS)

SAXS is a technique for studying the structural feature of colloidal particles and their spatial correlation. It is performed by focusing a low divergence x-ray beam onto a sample and observing a coherent scattering pattern that arises from electron density inhomogeneities within the sample. Since the dimensions of samples typically analyzed are much larger than the wavelength of the X-ray used ($\text{Cu-K}_\alpha = 1.54 \text{ \AA}$), the dimensions from tens to thousands of

angstroms can be analyzed within a narrow angular scattering range. This angular range or pattern is analyzed using the inverse relationship between particle size and scattering angle to distinguish characteristic shape and size features within a given sample.

3.5.1 Data Treatment

In order to obtain the absolute scattering intensity $I(q)$ as a function of scattering vector q , the experimental data have to be treated according to the following steps:

- (a) Measurements (capillary, solvent, solutions separately)
- (b) Scattering intensity normalized to the exposure time and the primary beam intensity
- (c) Subtraction of scattering intensity of sample from background (capillary and solvent)
- (d) Desmearing the scattering intensity for the finite dimension of the primary beam

Measurements and Normalization:

The experimental raw data (including scattering intensities of empty capillary, solvent filled capillary and solution filled capillary) should be at first normalized to the exposure time t_0 and primary beam intensity I_0 . To control the scattering intensity, a moving device (in front of the block collimation system with a slit of 34 μm width) and a fest block (before detector with a slit of 100 μm width) are performed to measure the primary beam intensity before and after each measurement. The exposure time of each measurement is set to a few hours to one day, depending on the scattering power and concentration of the sample. $I_0 = 1\text{E}4$ and $t_0 = 600$ s are taken reference values for the primary beam intensity and exposure time respectively, so that the measurements are comparable.

Background Subtraction:

The scattering intensity of particles $I_p(h)$ is then obtained by

$$I_p(h) = I_s(h) - (1 - \phi)I_B(h) - \phi I_C(h) \quad (3.31)$$

where ϕ denotes the volume fraction of the particles; $I_s(h)$, $I_B(h)$ and $I_C(h)$ represent the scattering intensities of solution, background and empty capillary respectively. Obviously, the scattering intensity after the subtraction decreases more rapidly than original data when the distance to centre of primary beam, h is larger.

Smoothing and Desmearing:

For Kratky camera, the key step of data treatment lies in the desmearing of finite dimensions of primary beam. Because of the relatively large statistical error at high q range, smoothing of data before desmearing or thereafter is in most cases necessary. However, this smoothing should not add any artificial structures to the scattering function. To be sure about that, a comparison between the desmeared data with smoothing and that without smoothing should always be done.

3.5.2 Power Law

Since the data on scattering measurements is dealt within the reciprocal space, the structural information is reflected in the inverse q range. The scattering in the large q value gives information in terms of the relatively microscopic structure and small q refers to the large structure. For small-angle scattering one can classify the q values into three different zones as shown in figure 3.6. In the low q range, the dimension of aggregate or particle can be evaluated by the Guinier law¹⁵⁹. The size of a particle, irrespective of whether it is geometrically well defined or irregular in shape, can be conveniently characterized by its radius of gyration according to the Guinier law.

From the figure it is seen that the different shapes of particles can be identified simply by the power law of intensity decay in the intermediate q range

$$I(q) \approx q^{-\alpha} \quad (3.32)$$

The exponent term α is equal to 4 for the spherical particles (three dimensional), 2 for thin discs (two dimensional) and 1 for thin rod (one dimensional), and is thus seen to reflect the dimensionality of the object.

At further large q , the scattering intensity is reflected by the surface fractal of aggregates. Porod¹⁶⁰ proposed for the ideal two-phase model that the scattering intensity should decrease as $\sim q^{-4}$ in the large q range (for sharp interface) and the proportionality constant should be related to the total area S of the boundaries between two phases in the scattering volume. In other words, as $q \rightarrow \infty$

$$I(q) \rightarrow \frac{2\pi(\Delta\rho_e)^2 S}{q^4} \quad (3.33)$$

where $\Delta\rho_e$ is the electron density difference. This power law indicates that the surface of aggregate is smooth, and if the decay is more than -4 , it is likely that the boundaries between the two phases would be indistinct¹⁶¹.

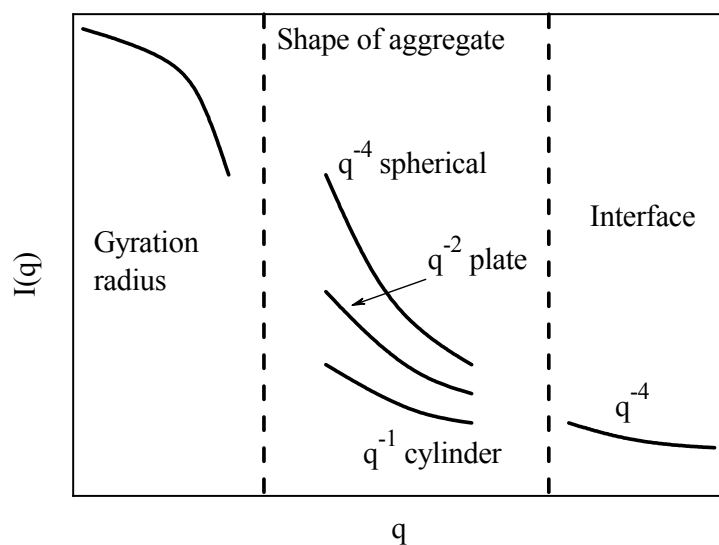


Figure 3.6: Schematic representation of different scattering range and their corresponding structural information.

3.5.3 Equipments

SAXS measurements were performed by a modified Kratky-Compact-Camera which has the X-ray generator Kristalloflex 710H, manufactured by Siemens containing a sealed X-ray tube (AEG FK60-04/12) with copper anode. The operating voltage was 35 kV with an anode current of 30 mA. A nickel filter was used to mask the Cu-K_β line so that only monochromatic X-ray source with the wavelength of 1.54 Å (Cu-K_α line) was used throughout the experiments. The X-ray tube is cooled by circulating water with temperature of $20 \pm 0.2^\circ\text{C}$ to ensure a stable primary intensity. Samples were filled in a quartz glass capillary with a diameter of 1 mm and the wall thickness was 0.01 mm. The inner part of the camera was evacuated using an oil vacuum pump. The primary beam intensity profile was determined by a moving device. The scattering intensity and position were recorded by a linear position-sensitive detector which works under mixed gas of argon and methane (90:10).

3.6 Surface Tension

The cohesive force between molecules located in the bulk of a liquid is shared with all neighbouring molecules. But the molecules at the surface do not have other like-molecules above them and consequently they cohere more strongly to those directly associated with them on the surface. This enhancement of molecular attractive forces at the surface is called surface tension. Surface tension is expressed in units of dyne/cm or mN/m.

In aqueous system, an additive can affect the surface tension in three different ways. Water soluble organic materials, such as ethanol, normally decrease the surface tension monotonically with increasing concentration. Surfactants, on the other hand, show a very large reduction in surface tension at very low concentrations up to the critical micelle concentration, above which surface tension remains practically constant. This large reduction in surface tension is due to the strong adsorption of surfactants at the liquid-air interface. At concentration higher than cmc, all additional surfactants will form new micelles, thus keeping the surfactant monomer activity (concentration) more or less constant. Thirdly, electrolytes normally increase the surface tension. The reason is that the electrolytes are depleted from the surface, i.e. there is a negative adsorption of the ions at the surface.

3.6.1 Gibbs Adsorption Isotherm

Gibbs adsorption equation gives relation between surface tension (σ_s) to the number of moles and the chemical potentials (μ_i) of the components in the interface by the equation¹⁶²

$$d\sigma_s = -\sum_i \Gamma_i d\mu_i \quad (3.34)$$

where Γ_i stands for surface excess concentration of component i . The chemical potentials depend on the activity of the components according to $d\mu_i = RT d \ln a_i$. So at equilibrium in terms of concentration between the surface and bulk phase equation (3.34) becomes

$$d\sigma_s = -RT \sum_i \Gamma_i d \ln a_i \quad (3.35)$$

For sufficient dilute solution activity co-efficient of the solution becomes unity and a_i can be replaced by its molar concentration C_i . For non-ionic surfactant and for one component equation (3.35) takes the form

$$d\sigma_s = -RT \Gamma_1 d \ln C_1 \quad (3.36)$$

But for ionic surfactant, one has to take into account the fact that there is a counter ion associated with surfactant and the surface as a whole electrically neutral. Thus the above equation for ionic surfactant

$$d\sigma_s = -RT(\Gamma_1^+ d \ln C_1^+ + \Gamma_1^- d \ln C_1^-) = -2RT\Gamma_1 d \ln C_1 \quad (3.37)$$

To calculate the surface excess concentration one can use the following equation which comes from equation (3.34)

$$\Gamma_1 = -\frac{C}{RT} \left(\frac{d\sigma_s}{dC} \right)_T = -\frac{1}{RT} \left(\frac{d\sigma_s}{d \ln C} \right)_T \quad (3.38)$$

Assuming monolayer adsorption, one can calculate the cross sectional area per adsorbed molecule, a_s according to following equation

$$a_s = \frac{10^{18}}{N_A \Gamma_1} \quad (3.39)$$

where a_s is expressed in nm²/molecule and Γ_1 is in mol/cm².

3.6.2 Equipments

The surface tension measurements were performed by a Lauda tensiometer TE 1C (Du Noüy ring method) equipped with a thermo-controller. In this method, a ring is pulled through the liquid-air surface and the maximum downward force directed to the ring is measured. The calibration was always performed using the standard ring before each measurement and the samples were measured repeatedly more than three cycles. The deviation from the accepted result was set below 0.2 mN/m in every cycle of measurement.

3.7 UV-visible Spectrophotometry

3.7.1 Turbidity Measurement

Turbidity is defined as an “expression of the optical property that causes light to be scattered and absorbed rather than transmitted in straight lines through the sample”, or in other words, turbidity is the measure of relative transparency of the sample. It is an optical measure from

the interaction of incident light with particulate materials or emulsion droplets in a liquid samples. Turbidity caused by the emulsification of oil in water will cause the incident light beam to be scattered in the directions other than the straight line through the sample. A higher level of turbidity in the sample results in a lower extent of transmitted light reaching to the detector.

3.7.2 Equipments

Turbidity measurements were carried out on the double-beam double-monochromator uv-visible spectrophotometer Lambda 19, Perkin Elmer. Pre-aligned tungsten-halogen lamp served for the visible light source, since all the measurements were performed in the visible range. Sidewindow photomultiplier detector is used to detect the level of turbidity in the sample. The photometer is connected to a computer and the data was stored by a software uv WinLab – version 2.80.03. Temperature was kept constant during the measurement at 25°C with an equipped water circulator.

3.8 Transmission Electron Microscopy

A transmission electron microscope (TEM) works almost in the similar way like a slide projector. In the projector a beam is focusing on the slide and as the light passes through it, the transmitted beam forming an enlarged image of the slide on the viewing screen. In TEM, on the other hand, a beam of electron is focusing on the vitrified specimen (like the slide) and whatever is transmitted, is projected on a phosphor screen for the user to see. A brief description of working procedure of TEM is given below:

A TEM consists of two main parts – illumination part and imaging part. The former part consists of a stream of monochromatic electron emitting device known as electron gun which is a heated tungsten filament. The emitted electron density can be controlled by the voltage applied at the filament. A high voltage field is applied to accelerate the emitted electrons which mainly focused on the condenser lens. The stream of electron is focused to a spot-shaped electron beam by the use of first condenser lens while the second lens is focusing the

electron beam on the sample by an intense and parallel beam of monochromatic electron. The beam can be controlled by a condenser aperture, knocking out the high angle electrons.

The imaging part is build up by the objective lens, intermediate lens and their corresponding apertures, the projector lens, a phosphor viewing screen and the photographic film. The transmitted electron beam is focused on the objective lens. The most imaging part of the imaging system is the objective lens and objective aperture which can either generate a bright-field or a dark-field image of the specimen. The image is passed down the column through the intermediate and projector lens, being enlarged all the way. Finally the image strikes the phosphor image-screen and generated light is allowing the user to see the image. The darker area of the image represents that area of the specimen through where fewer electrons were transmitted. The lighter area of the image represents that area of the sample through where more electrons were transmitted, in other words; it is thinner or less dense area.

3.8.1 Cryogenic Preparation

At first a bare 400- to 600-mesh EM grid is properly placed on a pair of tweezers. A very small droplet of sample is applied on the bare EM grid and the excess fluid is removed by blotting onto a fine filter paper for 1–3 s. This leaves a very thin layer of the fluid spanning the grid holes. The grid should then be instantly shock frozen (within very short time) by rapid immersion into liquid ethane, before significant evaporation occurs from the thinly spread sample and cooled to approximately 90K by liquid nitrogen in a temperature controlled freezing unit (Zeiss Cryobox). After freezing the specimen the remaining ethane was removed using blotting paper. The specimen was inserted into a cryotransfer holder and transferred to a Zeiss EM922.

3.8.2 Equipments

In this work, TEM images were taken by a Zeiss EM 922 electron microscope operated at acceleration voltage of 200 kV and at the temperature of around 90K. Zero-loss filtered images ($\Delta E = 0$ eV) were taken under reduced dose conditions (100 – 1000 e / nm²). All images were registered digitally by a bottom mounted CCD camera system (Ultrascan 1000) combined and processed with a digital imaging processing system (Digital Micrograph 3.10 for GMS 1.5). The machine is equipped with an in-column energy filter which is important

for analytical purposes such as electron spectroscopic imaging and electron energy loss spectroscopy. So these machines are also called energy filtering transmission electron microscopes.

3.9 Conductometry

The term that is the opposite of resistance is conductance. It is a measure of how much easily electricity passes through a certain solution. The factors that affect the magnitude of resistance are exactly the same for conductance, but they affect conductance in the opposite manner. Therefore, conductance (C) is directly proportional to area (A), and inversely proportional to the length (l) of the material.

$$C = \kappa \cdot \frac{A}{l} \quad (3.40)$$

where κ is the conductivity of the system. So, conductivity is the conductance of a system with unit cross sectional area and length. For electrolytic solution conductivity can be calculated using an expression as a weighted sum of the equivalent conductivity λ_i of each ionic species present in the solution ¹⁶³

$$\kappa = \sum_i z_i c_i \lambda_i \quad (3.41)$$

The quantities z_i and c_i are the valence and molar concentration of the species, respectively. At low concentrations, the equivalent conductivity is practically constant and at that time the solution conductivity is proportional to concentration of electrolyte. At higher concentrations, the equivalent conductivity decreases noticeably with increasing concentration. Therefore, accurately estimating pure solution conductivity requires accurately estimating the equivalent conductivity. On the other hand, Kohlrausch's law illustrates that the molar conductivity of an electrolytic solution is equal to sum of the molar conductivities of its constituting ions

$$\Lambda = \nu^+ \Lambda^+ + \nu^- \Lambda^- \quad (3.42)$$

Here ν^+ and ν^- are the number of cations and anions, respectively in the solution. Using this equation one can theoretically calculate the conductivity of an electrolyte solution when concentration is not so high.

3.9.1 Equipments

Conductivity measurements were performed with a microprocessor conductivity meter LF 197i. It has a thermal sensor connected to the cell, so the device is capable to measure conductivity and temperature (accuracy $\pm 0.1^\circ\text{C}$) of the solution simultaneously. A standard-conductivity cell TetraCon 325 with cell constant $0.475\text{ cm}^{-1} \pm 1.5\%$ was used with conductivity meter. The instrument has been calibrated from time to time by measuring the standard aqueous KCl solution.

3.10 pH-measurements

A pH meter measures the H^+ ion concentration (pH) of solutions using an ion selective electrode. An ion selective electrode ideally responds to only one specific type of ions, though in reality several types of ions are present in the solution. There are always some degrees of interference from the other ions in the solution.

pH measurements were performed with a pH meter of model pH 197i from Wissenschaftlich-Technische Werkstätten which can provide the accuracy in pH measurement up to ± 0.01 and in temperature $\pm 0.1^\circ\text{C}$. The pH meter was connected to a pH combined electrode SenTix 41. To avoid dryness of the electrode, it was always kept in such a manner that its tip was submerged in a dilute aqueous KCl solution. Before going to use the pH meter, it was always calibrated with three different buffer solutions of pH 2.0, 7.0 and 9.0.

Chapter 4: Results and discussion

4.1 Surfactant with Co-surfactants

4.1.1 Phase Behaviour

It is generally known that the mean spontaneous curvature on micellar interfaces is continuously lowered when co-surfactants are mixed with single chain surfactants¹⁶⁴. The reason for this change in curvature is due to the small area which a co-surfactant occupies at a micellar interface. As a consequence of this continuous change in the curvature, the systems undergo several phase transitions with increasing the concentration of co-surfactants¹⁶⁵. The systems try to come as close as possible to the spontaneous mean curvature without causing much bending energy by adjusting the two principal curvatures on the micellar aggregates. By doing this the systems have to switch the micellar structures from spheres to rods, to bilayers and to vesicles with increasing the co-surfactant concentration. These changes in structures, phases and their properties have recently been systematically studied in details for the system Na-oleate with octanol as co-surfactant^{43, 166}. A phase diagram for the system of Na-oleate (see the description in experimental section 3.1) with increasing concentration of octanol and geraniol is given in figure 4.1.1.

The binary system, Na-oleate and water, forms a visually transparent single phase solution with no birefringence. On gradual addition of increasing amount of co-surfactants into 200 mM Na-oleate, the system undergoes a phase transition. The solutions of Na-oleate with low concentration of co-surfactants form micellar solution with somewhat spherical or elongated micelles^{167, 168}. The increasing co-surfactant concentration induces the phase transitions: isotropic (no birefringence) \rightarrow 2Φ (Upper layer is very thin and more turbid/ oily, hard to realise from photography, shaking the samples makes whole sample turbid.) \rightarrow Vesicle phase (partially turbid and highly viscous) \rightarrow Vesicular gel. Gradzielski et al⁴³ have also been experienced the similar observation for the system of aqueous Na-oleate with octanol. It has been reported⁴³ that there is a biphasic region (octanol concentration from about 80 mM to 120 mM with 200 mM Na-oleate) between L_1 phase and vesicular phase for the same system;

but in their work the 2Φ region is very narrow compared to the present investigation. In this study it was observed that the biphasic region is spread from 75 mM to 225 mM octanol concentration which is much broader. This difference in phase behaviour may arise because of the difference in the quality of surfactant, since technical Na-oleate (see section 3.1) is used in this investigation.

The appearance of 2Φ region which is started at 75 mM for octanol and 90 mM for geraniol with 200 mM aqueous Na-oleate, is like an oily layer is swimming on aqueous layer. In this 2Φ region the lower partially turbid layer has vesicle structure, as will be shown later on by dynamic light scattering and cryo-TEM measurements. Further addition of co-surfactants the system transformed into a large single phase region where the micellar aggregation produced to vesicular structure. At 300 mM octanol concentration, the sample was partially turbid and very viscous, and flowing slowly by its own weight; but with increasing octanol concentration at 400 mM turbidity of equilibrium solution disappears. At this composition sample becomes stiff gel which does not flow under its own weight in the test tube. This means that just by allowing the octanol to diffuse from its emulsion droplets to the micellar solution one has a transformation of simple micellar aggregates to a highly ordered gel phase of vesicles. Sample with 350 mM geraniol, on the other hand, is a flowing liquid and partially turbid. Similar to octanol, increasing the geraniol concentration sample losses its flow property under its own weight, but the turbidity increases with increasing geraniol concentration.

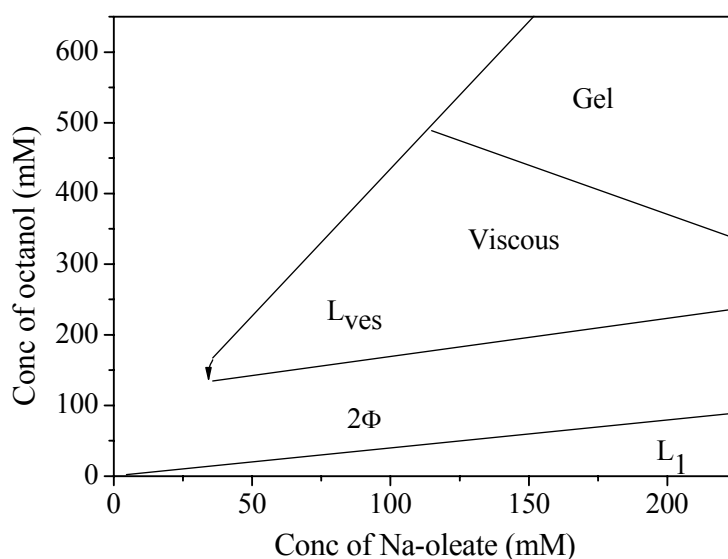


Figure 4.1.1(a): Phase diagram for the ternary system Na-oleate/ water/ octanol at 25°C.

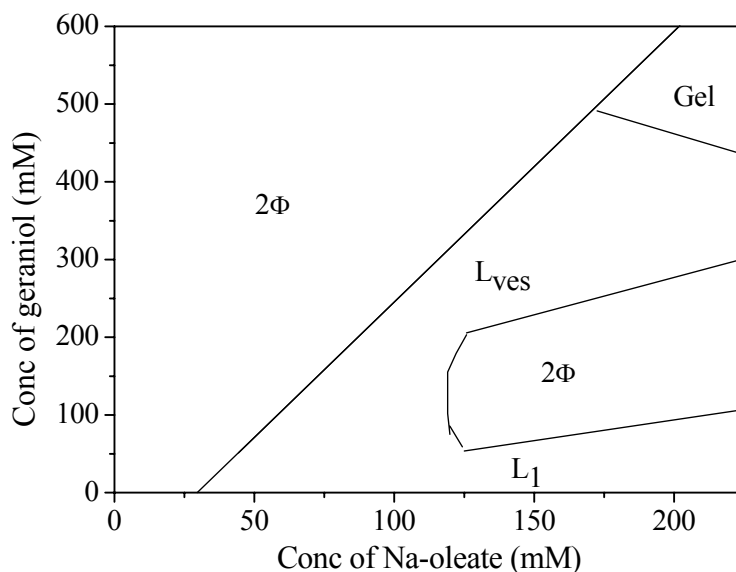


Figure 4.1.1(b): Phase diagram for the ternary system Na-oleate/ water/ geraniol at 25°C.

The phase behaviour for the ternary systems Na-oleate/ water/ octanol and Na-oleate/ water/ geraniol at 25°C were investigated up to the concentration of 200 mM Na-oleate and 600 mM co-surfactants. The obtained phase diagrams are displayed in figure 4.1.1 as a function of surfactant and co-surfactants concentration. Both the phase diagrams have been drawn on the basis of visual observation of physical state after one week equilibration of the samples in a thermostat at 25°C. The diagrams show that the systems form either micellar or biphasic region at lower concentration of surfactant with both the co-surfactants. No sign of vesicular structure was observed in this lower concentration (<50 mM) region.

In case of Na-oleate/ water/ octanol system isotropic L_1 phase transformed into vesicular phase with increasing co-surfactant concentration via a two-phase region where relatively narrow turbid/ oily layer was floating on the partially bluish and isotropic vesicular layer which indicates that the phase transformation occurred following the first order phase transition rule. This partially bluish colour was observed because of the scattering of light by the bigger aggregates and this characteristic bluish colour is a sign of vesicular aggregation¹⁶⁹ and this observation is in good agreement with the results obtained from DLS and cryo-TEM measurements (see figures 4.1.3 and 4.1.5). Further increasing the concentration of both surfactant and co-surfactant they produce a stiff gel structure which possesses a high yield stress.

On the other hand, in case of Na-oleate/ water/ geraniol system, the phase diagram has different nature from the system with octanol. At higher surfactant concentration from 150 mM to 200 mM, the isotropic L_1 phase is transformed into vesicular phase with increasing the geraniol concentration via a two-phase region which is similar to the system with octanol. But at lower surfactant concentration for instance at 100 mM Na-oleate, the isotropic L_1 phase slowly transformed into vesicular phase without producing a biphasic region. Cryo-TEM for this sample clearly reveals that this system has a mixture of micellar and vesicular structure which indicates that the transformation of micellar structure to vesicular one is in equilibrium at this composition (see figure 4.1.2a). To check the results, dynamic light scattering measurements have also been performed for 100 mM Na-oleate with increasing concentration of geraniol. The autocorrelograms (see figure 4.1.2b) of these measurements clearly indicate that the system is transformed into vesicular structure when the geraniol concentration was raised from 40 mM to 60 mM. Further calculation revealed that the aggregate radii in pure Na-oleate solution, with 40 mM and 60 mM geraniol are respectively 1.2 nm, 2.6 nm and 21.0 nm. This is in good agreement with the observation by cryo-TEM (figure 4.1.2a). These results illustrate that the system has been transformed to vesicular aggregate when the concentration of geraniol has been raised to 60 mM. Such sudden transformation from micellar phase to vesicles without phase separation has not been observed in case of system with octanol.

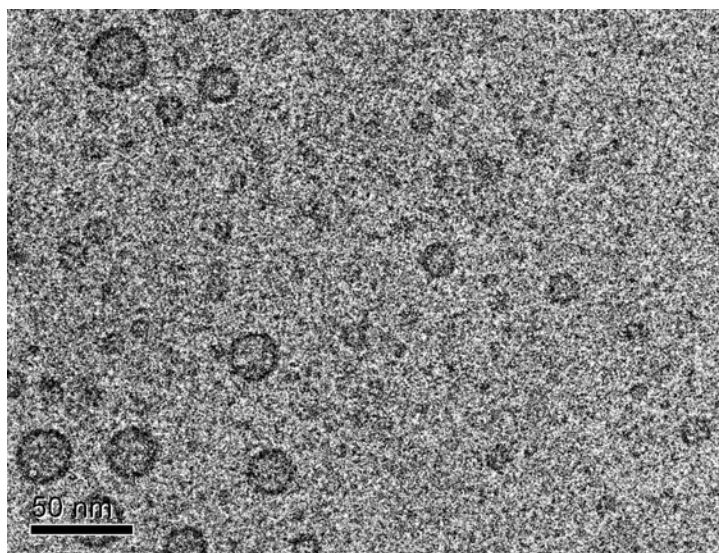


Figure 4.1.2 (a): The cryo-TEM image of 100 mM Na-oleate with 60 mM geraniol shows that there are some unilamellar vesicles present in system, but the quantity of surfactant involved in vesicle formation does not match with the total surfactant concentration. So, rest of the surfactants are remaining in micellar condition which is not visible. The bar length in cryo-TEM corresponds to 50 nm.

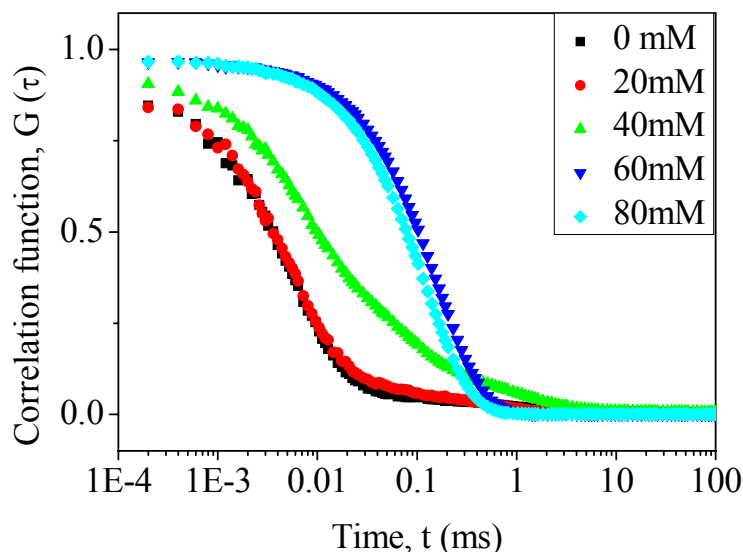


Figure 4.1.2(b): Gradual transformation of micellar phase to vesicular phase without forming a biphasic region. The figure displays the autocorrelograms of 100 mM Na-oleate with increasing concentration of geraniol. The autocorrelograms of these measurements clearly indicate, how the system is transforming into vesicular structure with increasing the geraniol concentration

This difference of geraniol in interaction with Na-oleate and hence in phase behaviour may be explained on the basis of π -electrons present in the molecules. From the molecular structure it is known that both geraniol and Na-oleate have π -electrons. The self assembly of amphiphile is mainly driven by the hydrophobic effect, but the π - π stacking interaction becomes another dominating factor that enhances the geraniol system to transform into vesicular structure without forming a biphasic region, which is completely absent in octanol, since it has no π -electron. Recently Song et al.¹⁷⁰ have also been observed such phenomenon with other systems where π -electron plays a potential role in forming a stable micellar structure.

4.1.2 Hydrodynamic Radii and Polydispersity

Figure 4.1.3 shows the normalized intensity correlation function at different concentration of surfactant and co-surfactants i.e., Na-oleate/water/octanol and Na-oleate/water/geraniol system at the scattering angle of 90° . The long decay time indicates that the samples have some bigger aggregates (vesicles) which are diffusing slowly.

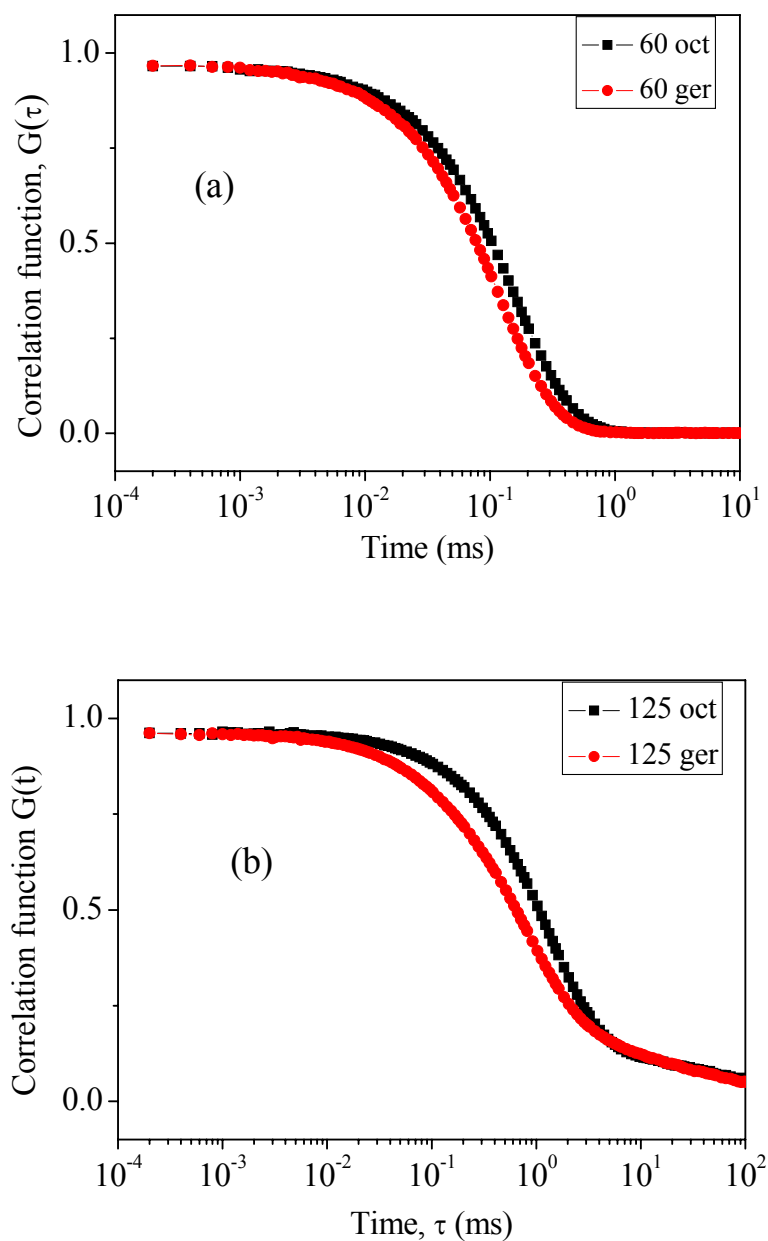


Figure 4.1.3: Normalized intensity correlation function is plotted against time for different concentration of surfactant and co-surfactants at 25°C and at an angle of 90°. Figures (a) and (b) are 100 and 200 mM Na-oleate respectively with indicated concentration of octanol and geraniol.

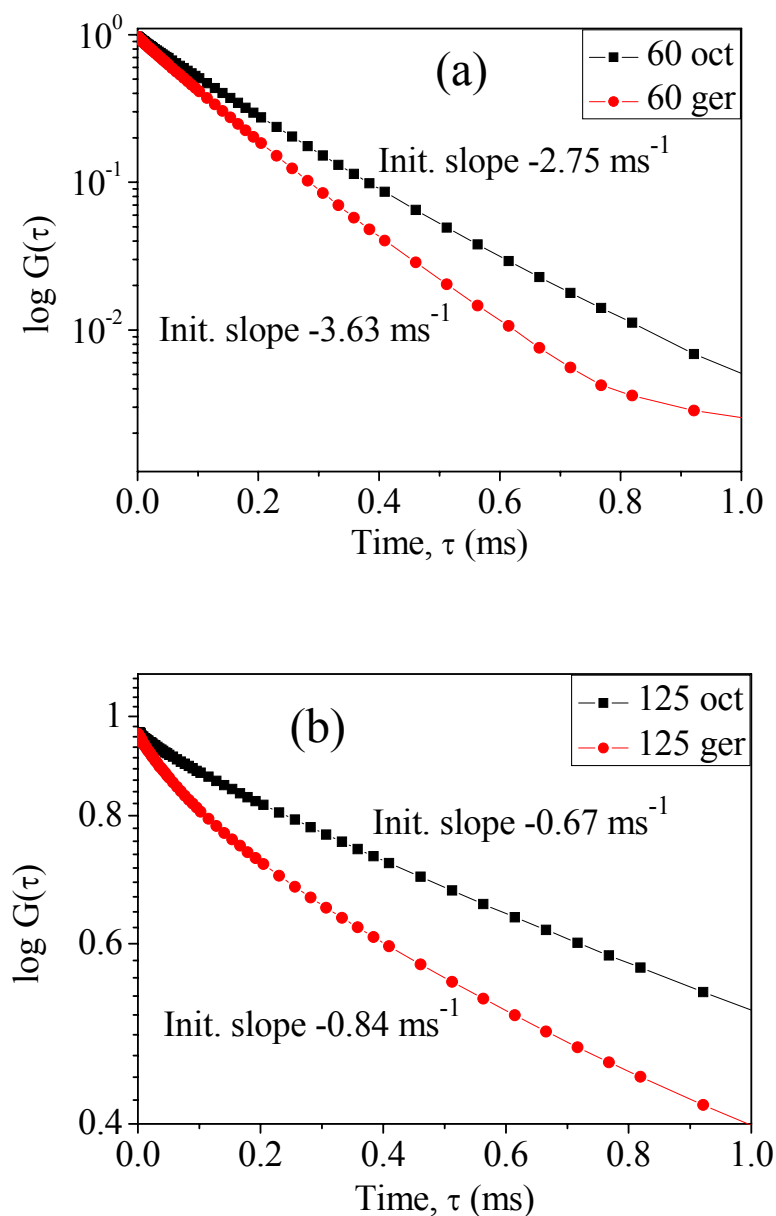


Figure 4.1.4: Correlation function $G(\tau)$ for the vesicle system as a function of time for different concentration of surfactant at 25°C and at a fixed angle of 90° . For the case of geraniol non-linear decay is more pronounced. Figure (a) and (b) are 100 and 200 mM Na-oleate respectively with indicated concentration of octanol and geraniol.

The autocorrelograms do not decay linearly especially at higher co-surfactant concentrations which become clearer in figure 4.1.4. This implies that the systems may have polydispersity and indeed a high polydispersity index is calculated (see table 4.1.1). The initial and numerically bigger negative slopes in figure 4.1.4 indicate that the samples have some smaller

vesicles which diffuse faster whereas the successive smaller slope indicates that there may have some vesicles with bigger sizes that diffuse slowly. Cryo-TEM images of the samples clearly reveal the information of co-existence of smaller and bigger vesicles together (see figures 4.1.5 and 4.1.6). The polydispersity index of size distribution along with diffusion coefficients and hydrodynamic radii are given in table 4.1.1. Tabulated results are showing that there is no systematic trend in vesicle size following with concentration of surfactant. It is clearly revealed from this result that 100 mM Na-oleate forms vesicles with lower concentration (60 mM) of co-surfactants, while from the phase sequence it has been observed that 60 mM co-surfactant forms a clear isotropic L_1 phase with 200 mM surfactant. This observation implies that the vesicle formation with lower surfactant concentration can be possible with lower co-surfactant concentration.

Table 4.1.1: Diffusion coefficients, hydrodynamic radii and polydispersity index of Na-oleate with octanol and geraniol in the vesicular phase.

Conc. of Na-oleate (mM)	Conc. of co-surfactant (mM)		Diffusion coefficient (m^2s^{-1})	Hydrodynamic radius (nm)	Polydispersity index
100	60	Octanol	9.08E-12	27	0.19
		Geraniol	1.20E-11	21	0.31
	100	Octanol	5.97E-12	41	0.25
		Geraniol	7.42E-12	33	0.40
200	125	Octanol	2.21E-12	110	0.32
		Geraniol	2.77E-12	88	0.39
	200	Octanol	2.81E-12	87	0.36
		Geraniol	2.80E-12	87	0.42

4.1.3 Microscopic Observation

Cryogenic transmission electron microscopy (cryo-TEM) was used to investigate the structure in the systems of both Na-oleate/ water/ octanol and Na-oleate/ water/ geraniol. The aim was to relate the macroscopic appearance in phase diagram to microstructures in terms of vesicular or other types of self-assembled structures. The macroscopic behaviour may, of course, be due to the variety of coexisting aggregates structure.

Figure 4.1.5 shows the cryo-TEM micrographs of vesicular dispersion containing 100 mM aqueous Na-oleate with 100 mM co-surfactants. The micrographs clearly reveal the presence of unilamellar vesicles only. This is a good indication that the micrographs were taken from a sample of single phase region. The most notable observation is the presence of a large number of vesicles with a little polydispersity. The slides of micrograph illustrate that the vesicles are completely spherical in shape and the diameter is ranging from 20 nm to 60 nm; but most of them are with a diameter of about 40 nm. In cryo-TEM images, unilamellar vesicles appear as uniformly dark circular rings; contrast in the image is generated by the variation of the projection of the electron beam, which is normal to the image in these figures, through the vesicle membrane. Figure 4.1.5(a) illustrates the cryo-TEM micrograph of 100 mM Na-oleate with 100 mM octanol. In this micrograph a noticeable observation is the presence of a large number of well-shaped vesicles. Different zones of the vitrified film were investigated under TEM but no significant change in morphology was observed.

On the other hand figure 4.1.5 (b) exhibits the micrograph of 100 mM Na-oleate with 100 mM geraniol. Here number density of vesicles is not as high as with octanol. This finding indicates that total concentration of surfactant, probably, did not form vesicles with geraniol as observed with octanol. This micrograph also reveals that there are a number of very small objects (may be micelles) and they do not have well-defined vesicular-spherical rim. Such phenomenon has not been observed in the cryo-TEM images for the system with octanol. In addition to this average and spherical unilamellar vesicles a very few large and bilamellar vesicles were observed in the same sample with geraniol at different zone of the vitrified film (see figure 4.1.6). In this micrograph large- and bilamellar-vesicle (joined together) with elliptical and elongated shape along with large fraction of small unilamellar vesicles were observed. This micrograph is clearly exposing the co-existence of smaller and bigger vesicles in the sample. The diversity of the shape of the particles illustrates that the membrane of the vesicles is flexible. The lamellar spacing between two bilayers is about 24 to 27 nm. At the joining point of two bilamellar vesicles the inter-lamellar space is even bigger and is about 50 nm.

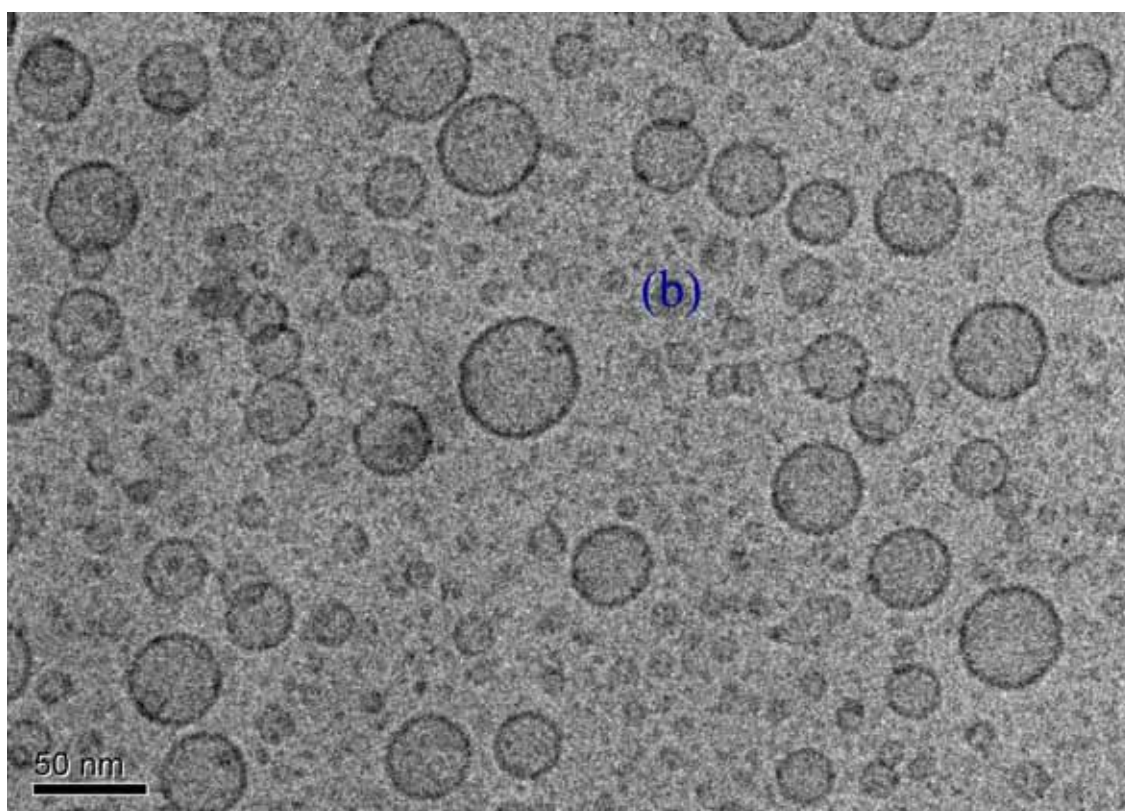
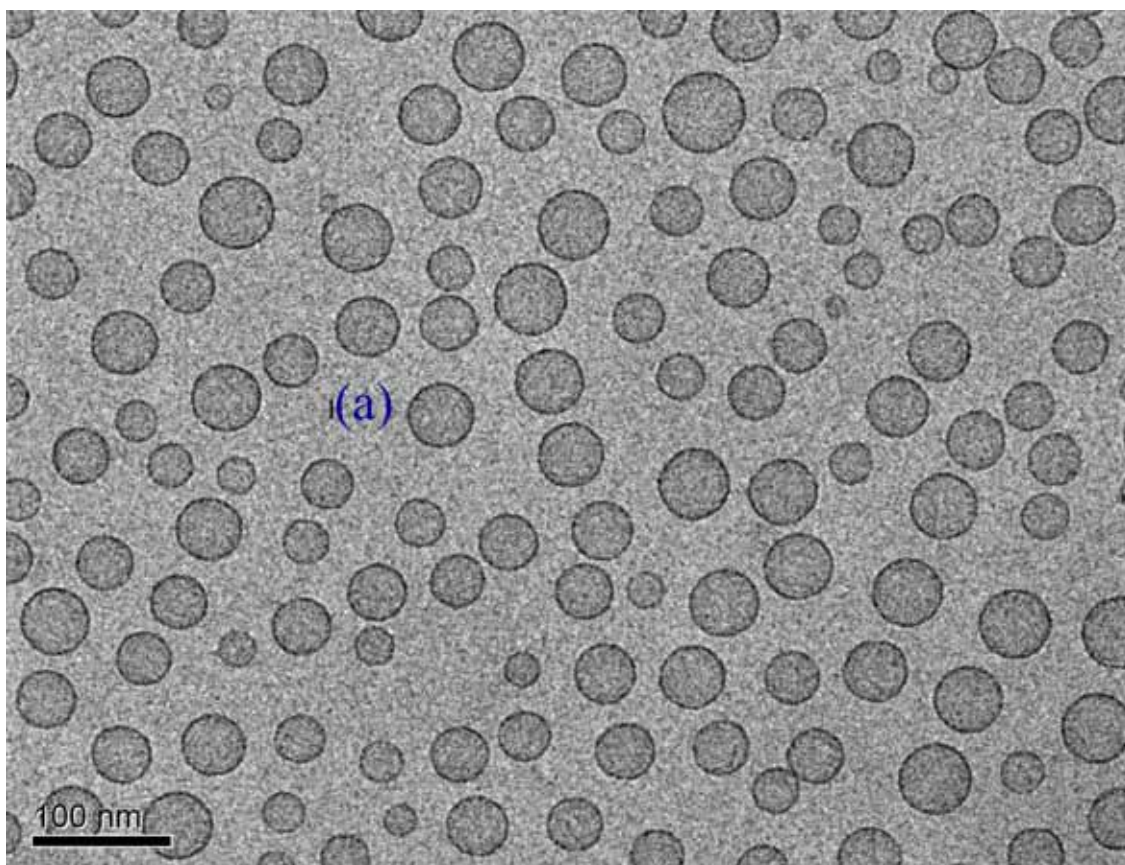


Figure 4.1.5: Cryo-TEM micrographs for the sample of 100 mM Na-oleate with 100 mM octanol (a) and with 100 mM geraniol (b). The micrographs clearly reveal that the samples contain spherical and unilamellar vesicles. The bar length is corresponding to 100 nm and 50 nm for (a) and (b) respectively.

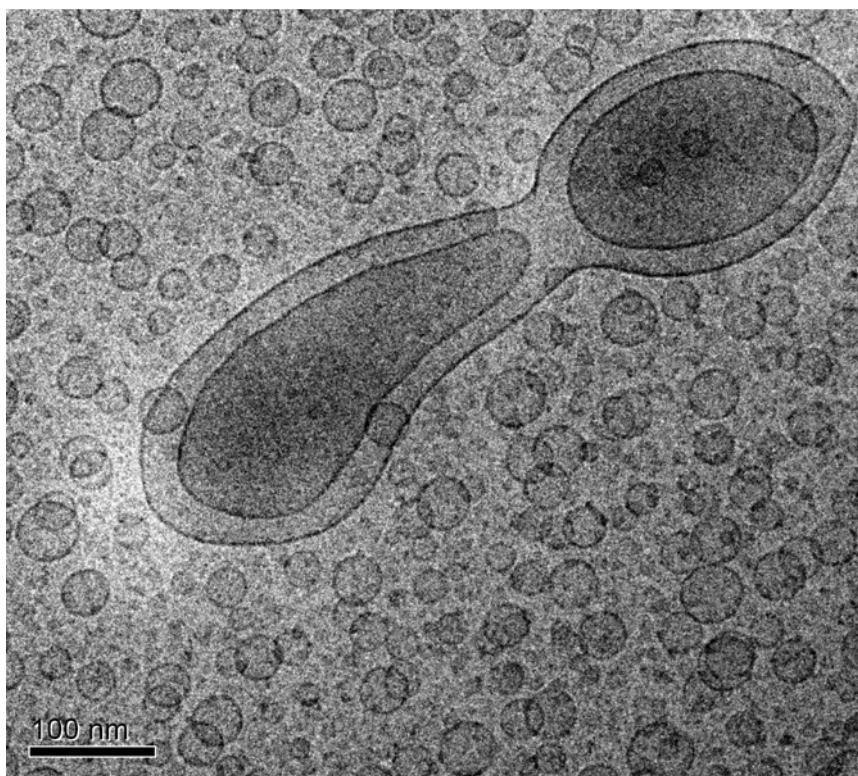


Fig 4.1.6: Cryo-TEM micrograph for the sample of 100 mM Na-oleate with 100 mM geraniol. The unilamellar spherical vesicles (appear as open rings) coexist with very big bilamellar vesicle. The bar length corresponds to 100 nm.

Understanding the magnitude and origin of the forces between bilayer membranes is essential to understand the stability of unilamellar vesicles against adhesion and fusion¹⁶. This is important especially for differentiating between metastable mechanically or chemically formed unilamellar vesicles and equilibrium unilamellar vesicles^{171 - 178}. Unilamellar vesicles can be stabilized against the formation of multilamellar liposomes by either (i) thermal fluctuations that lead to a net repulsive interaction between bilayers¹⁷⁹ or (ii) a spontaneous curvature that picks out a particular vesicle radius with either bilayer curvature being prohibited energetically^{102, 180, 181}. Theory and experiments have shown that surfactant mixing with co-surfactant can lead to sufficiently low values of κ , the bending modulus^{182 - 184}. For the mechanism (ii), non-ideal surfactant mixing can cause the interior and exterior monolayers of the vesicle bilayer to have different compositions, leading to a spontaneous bilayer curvature^{180, 181}. If the bilayers are sufficiently rigid ($\kappa \gg k_B T$), the curvature energy of adding a second bilayer to the vesicle can overcome the attractive interaction between bilayers, leading to unilamellar vesicles. However, although the concept of spontaneous

curvature is well accepted theoretically,^{34, 180, 181} there has been no definitive experimental proof of a spontaneous curvature in bilayers at equilibrium¹⁸⁵.

The equilibrium size distribution of a population of unilamellar vesicles is determined by a subtle competition between the entropy of mixing and the curvature elasticity of the bilayers^{186, 187}.

$$C_N = \left\{ C_M \exp \left[\frac{-8\pi K}{k_B T} \left(1 - \frac{R_0}{R} \right)^2 \right] \right\}^{\frac{R^2}{R_0^2}} \quad (4.1)$$

where C_M and C_N are the molar number fractions of vesicles of size M and N respectively, R_0 is the radius of the minimum energy vesicle and K is an effective bending constant. A consequence of equation (4.1) is that the vesicles stabilized by thermal fluctuation ($K \sim k_B T$) have a much broader size distribution than vesicles stabilized by the spontaneous curvature ($K \gg k_B T$)¹⁸⁷. This result is the opposite of vesicle size distribution models that do not include a spontaneous curvature^{46, 182}.

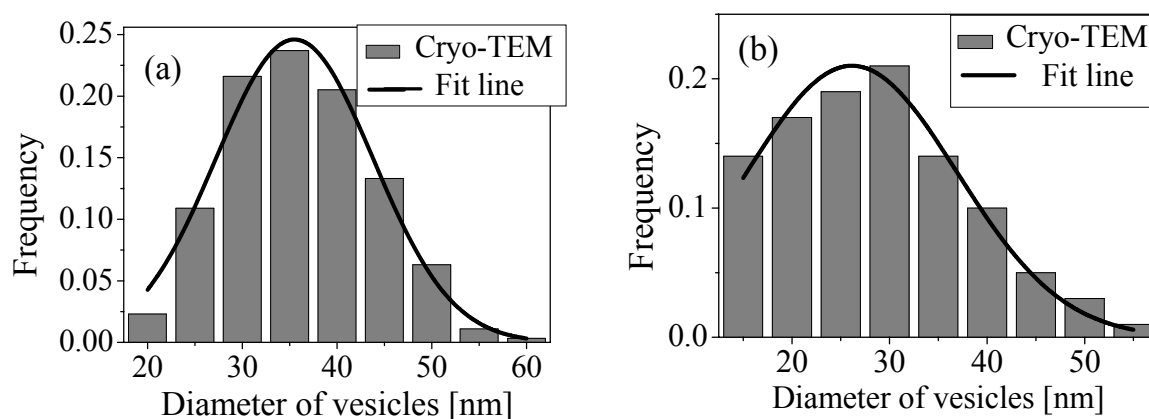


Figure 4.1.7: Number averaged vesicle size distribution histogram determined from the measurements of more than 1500 vesicles from many cryo-TEM images of 100 mM Na-oleate with 100 mM octanol (a); and (b) is that with geraniol, but the number of vesicles considered here were a little more than 1200. The solid line in each plot is the best fit of the equation (4.1) derived by Jung et al¹⁸⁶.

To extract R_0 and K , it is necessary to determine the vesicle size distribution calculated from the image taken by cryo-TEM. A histogram of the size distribution is built up by measuring the size of more than 1500 and 1200 spherical vesicles taken from different slides of micrograph of cryo-TEM images of 100 mM Na-oleate with 100 mM octanol and geraniol

respectively (figure 4.1.7). The experimentally measured distribution of vesicular diameter from cryo-TEM is fitted to equation (4.1) to determine R_0 and K values. It can be mentioned here that, in addition to the unilamellar spherical vesicles, there were also a very few elongated and bi-lamellar vesicles (see in figure 4.1.6) observed with geraniol system. These very few elongated vesicles were not included in fitting the distribution of unilamellar and spherical vesicles.

A best fit of equation (4.1) to the histogram built for the size distribution of classified vesicles resulted $K = \kappa + \bar{\kappa}/2 = 0.42 \pm 0.03 k_B T$, the sum of the Helfrich mean (κ) and Gaussian ($\bar{\kappa}$) curvature moduli and $R_0 = 36 \pm 0.6$ nm for the system with octanol, while $K = 0.18 \pm 0.01 k_B T$ and $R_0 = 29 \pm 0.9$ nm for the system with geraniol. The fit of equation (4.1) to the histogram for both the systems with octanol and geraniol revealed that the effective bending constant K is in the order of $k_B T$ ($K \sim k_B T$) which implies that there is a much broad vesicles size distribution¹⁸⁷. This observation is very good in agreement with high polydispersity index found in DLS measurements.

On the basis of different vesicular size distribution total surface area of classified vesicles has been calculated. From the summation of calculated total surface area of all the classified vesicles present in the same area of cryo-TEM micrograph for both the systems, it has been observed that same concentration of surfactant with geraniol produce about 18% less surface area compared to the system with octanol. This observation indicates that some surfactant does not produce vesicles with geraniol system and it is probably remained in micellar state.

4.1.4 Conductivity and pH Measurements

The samples were prepared and kept in a thermostat at 25°C for a week for equilibration. Then pH and conductivity were measured at room temperature (23°C) when the samples were completely in rest. No stirring or agitation was performed during the measurement. After dipping the electrode into the solution it has been observed that both the conductance and pH were changing with time. To get a constant and equilibrium value, enough time (about 30 minutes) was given for every measurement. The results of pH and conductivity measurements are displayed in figure 4.1.8.

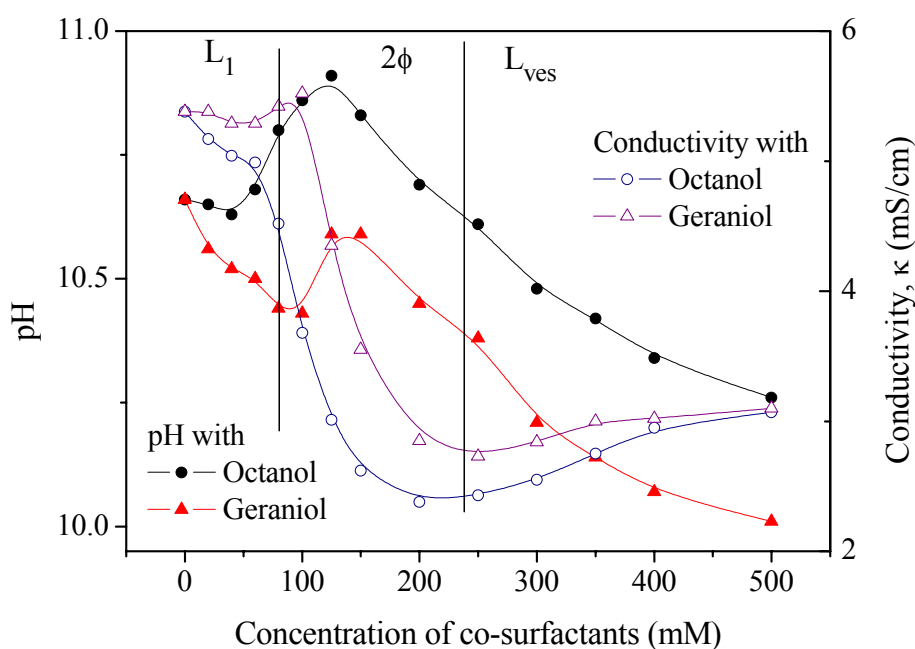


Figure 4.1.8: pH and electrical conductivity as a function of co-surfactant concentration in 200 mM aqueous Na-oleate solution. All the measurements were performed when the samples were under rest and at the temperature of 23°C.

In the lower concentration range of co-surfactants where the system was transparent and isotropic and when the self-association was mainly micellar, the concentration of co-surfactants has very minor effect on pH. After reaching the concentration of the co-surfactants at 75 mM for octanol and 90 mM for geraniol when the systems start to enter into a biphasic region, pH increases with increasing co-surfactant concentration and attains the maximum value of pH at the concentration of 125 mM for both the co-surfactants. Afterward it decreases again with increasing co-surfactant concentration. This decrease in pH indicates that the formation process of vesicular structure facilitates the system to release protons. The increasing concentration of alcohols in the vesicular bilayer can make an effective hydrogen bond with surfactant head-groups and partially neutralize the carboxylate ($-\text{COO}^-$) ions of bilayer surface. This partial neutralization of bilayer surface facilitates to weaken the interaction between negatively charged carboxylate groups and positively charged protons attached on the vesicle surface. As a consequence, pH of the system is decreasing with increasing the concentration of co-surfactants in the range of vesicular composition.

The conductivity, on the other hand, shows opposite character with co-surfactant concentration. The initial (almost) steady value of conductivity at low co-surfactant concentration range is in a good agreement with pH measurement, suggesting that the co-surfactant concentration has almost no effect in changing the structure in this single phase region. After reaching the concentration of phase separation, conductivity drops very fast with increasing co-surfactant concentration. The change in conductivity should be considered in the view of formed aggregate structures. In phase behaviour section (see 4.1.1) it is described that the lower and main aliquot of the system has vesicular structure in this biphasic region. So the sudden decrease in conductivity can be explained by the fact that vesicular structures are formed in this region, which entraps a sufficient amount of the counter ions^{43, 182, 188} interior of the structure which has no contribution in the measured conductivity. The conductivity remains almost constant until the end of the composition studied here which indicates that the structure present in the system remains the same with increasing co-surfactant concentration.

Within the L_{ves} phase, a slight increase in conductivity with increasing co-surfactant concentration was observed. This may be explained by the fact that the functional group of co-surfactants in the amphiphilic bilayer interacts with the ionic carboxyl group and will form an effective H-bonding⁴³. This gives rise to a decrease of the surface charge density and thereby leads to an increased degree of dissociation of the counter ions and they are contributing in conductivity.

One can easily compare pH and conductivity of the systems with octanol and geraniol illustrated in figure 4.1.8. The figure expresses that the changing pattern in pH and conductivity with concentration of co-surfactants is almost the same. This indicates that the interaction of co-surfactants with amphiphilic aggregation is similar. Figure 4.1.8 also reveals that pH of the system with octanol is always higher than that of with geraniol. A π - π interaction¹⁷⁰ between geraniol and surfactant moiety may lead to a more stable aggregation and that influences the system to form a more effective hydrogen bond. This interpretation might be reasonable for the fact that the conductivity of the system with geraniol is slightly higher than the system with octanol.

pH of the system without co-surfactant was 10.66; but after interaction, equilibration and formation of vesicles it reduces at 10.26 and 10.01 for the system with octanol and geraniol respectively. This decrease in pH indicates quantitatively 0.028 mM and 0.036 mM H^+ is generated because of the interaction of surfactant with octanol and geraniol respectively in presence of water. Hydrolysis of water may be the source of these generated protons which

can be stabilized by the negatively charged surface of vesicles. Conductivity of the system, on the other hand, is 5.38 mS/cm for pure surfactant solution. Because of the addition of co-surfactants and formation of vesicles it reduces to 2.43 mS/cm (at 250 mM) and 2.84 mS/cm (at 300 mM) for the system with octanol and geraniol respectively. If one considers that this reduction in conductivity is only for the encapsulation of counter ions interior of vesicular structure, then one can conclude that 54.83% and 47.21% of counter ions are trapped inside of the vesicular structure with octanol and geraniol respectively. Larger percentage of entrapped counter ions indicates that octanol may form larger number or bigger vesicles compared to geraniol. This result is qualitatively in good agreement with the findings obtained from cryo-TEM measurement for both the systems.

4.1.5 Rheological Properties

Macroscopic properties of the system can be characterized by rheological measurements. The variation of zero shear viscosity for the system of 200 mM NaOA with increasing concentration of co-surfactants is depicted in figure 4.1.9. The samples before phase separation (with low concentration of co-surfactants) have very low viscosity. In this region aggregate-structure of the samples is mainly micelles and their viscosities are slightly higher than the dispersion medium. After phase separation, on the other hand, viscosity increases rapidly with increasing the co-surfactant concentration and samples were showing strongly viscoelastic property indicating the formation of bigger aggregates like vesicles. In this region one can measure shear moduli of the systems which have a considerable yield stress.

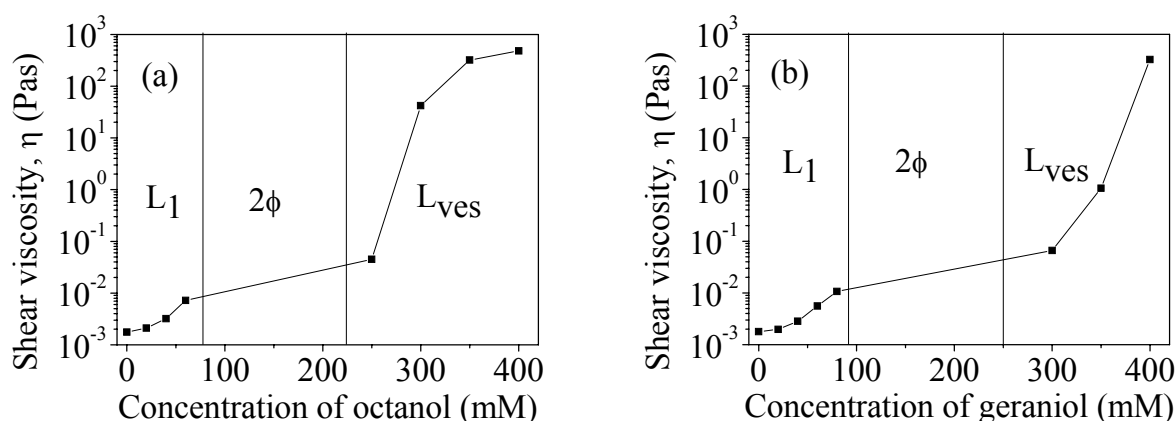


Figure 4.1.9: Zero-shear viscosity as a function of co-surfactant concentration in 200 mM Na-oleate solution at 25°C. Low viscous samples were measured by double gap method and high viscous samples were measured by cone-plate method.

Rheological Behaviour of L_1 Phase

200 mM Na-oleate solution with low concentration (0 – 80 mM) of co-surfactant the systems behave like a Newtonian fluid and exhibit low viscosity. Surfactant solutions that contain micellar structures generally show a low viscosity, which increases with increasing the co-surfactant concentration since micelles grow with increasing the concentration^{189, 190}. Gradual addition of co-surfactant viscosity was gradually increasing, but still behaving like a Newtonian fluid. This reveals that the micelles become bigger with increasing co-surfactant concentration and hence viscosity increases. Figure 4.1.10 shows that the viscosity increases in an exponential manner with increasing the concentration of co-surfactants.

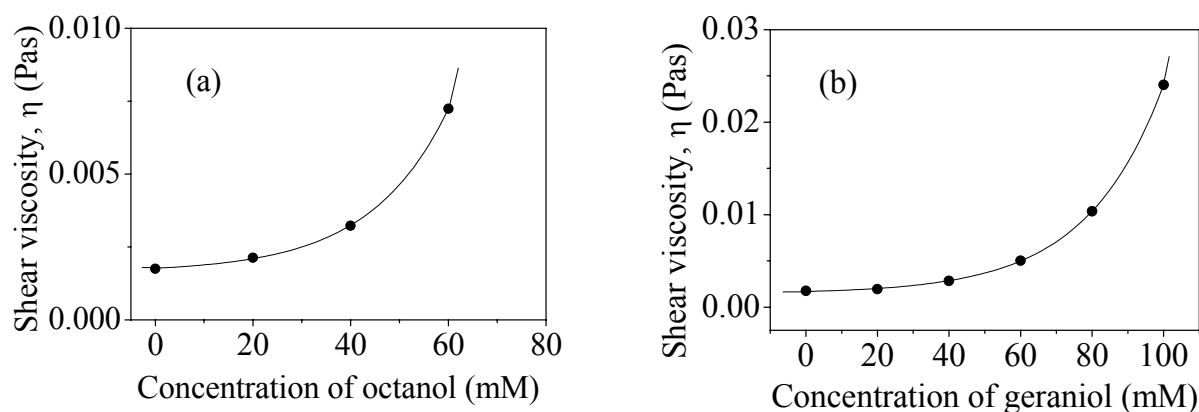


Figure 4.1.10: Steady shear viscosity as a function of concentration of co-surfactants for octanol (a) and for geraniol (b).

Rheological Properties of L_{ves} Phase

De Haas et al¹⁹¹ reported that dilute dispersion of vesicles where vesicles are not interacting with each other shows Newtonian behaviour. It is expected that immediate after two-phase region vesicular dispersion is dilute, and hence it shows Newtonian behaviour without variation in viscosity as a function of shear rate. A large and sharp increase in zero shear viscosity was observed when the co-surfactant concentration was increased in this region. Increasing the concentration of co-surfactant, a Newtonian plateau is visible at low shear rate for the system with 300 mM octanol and 350 mM geraniol while at high shear rate a pronounced shear thinning was observed (see figure 4.1.14); one can mention that it is a

critical concentration, below which samples are showing mainly Newtonian behaviour and above this concentration Newtonian plateau is no longer observed at low shear rate. For such critical concentration where samples are showing Newtonian plateau at low shear rate and shear thinning at high shear rate, one can use Cross equation ¹⁴¹ to evaluate different parameters.

$$\frac{\eta - \eta_{\infty}}{\eta_0 - \eta_{\infty}} = \frac{1}{1 + (K\dot{\gamma})^m} \quad (4.2)$$

where η_0 and η_{∞} refer to the asymptotic values of viscosity at very low and very high shear rates respectively, K is a constant with the dimension of time and m is a dimensionless constant. A best fit of equation (4.2) to the experimentally measured shear viscosity revealed the zero shear viscosity η_0 , viscosity at very high shear rate η_{∞} and the values of constant terms K and m. All the values obtained from Cross fitting are summarised in table 4.1.2 for the system with both octanol and geraniol. Similar K and m values are reported for aqueous dispersion of polymer latex system ¹⁹².

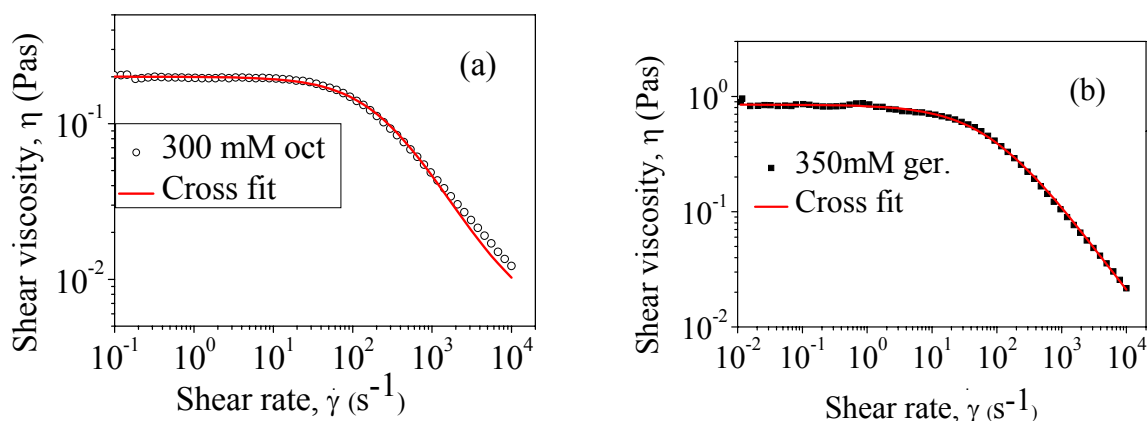


Figure 4.1.11: Fit of Cross equation (4.2) to the experimental shear viscosity data for the system of 200 mM Na-oleate with 300 mM octanol (a) and with 350 mM geraniol (b).

The concentration of co-surfactants at which shear thinning becomes started is determined by rheological measurement, and is 300 mM for octanol and 350 mM for geraniol at the shear rate of 250 s^{-1} and 100 s^{-1} respectively, as shown in figure 4.1.11. This starting of shear thinning can be described in the way that the deformation of the vesicles with high shear rate becomes faster than their ability to reform or regain their original structure ^{193, 194}.

This critical concentration is different for different co-surfactants, indicates that both the co-surfactants are interacting with the surfactant but their effective interaction is different. The phenomenon can be explained on the basis of effective volume fraction rule, while vesicles with higher volume fraction often show shear thinning behaviour¹⁹¹. Samples with critical co-surfactant concentration show a Newtonian plateau at low shear rate region and at high shear rate region exhibit shear thinning behaviour and this shear thinning region broadens with increasing the concentration of co-surfactant since the additional co-surfactant gives a positive contribution to increase the volume fraction. The transition between Newtonian plateau and shear thinning region is the indication of vanishing contribution of Brownian motion, due to a changing particle position distribution¹⁹¹. For higher volume fractions this transition is dominated by a different micro-structural change, which might be related to the details of the interaction at short surface-to-surface distance and the vesicle deformability.

Table 4.1.2: Limiting shear viscosities of the sample with critical concentration along with constant terms obtained from Cross equation for the system of 200 mM Na-oleate with octanol and geraniol.

Conc (mM)	Const. K (s)	Const. m	η_0 (Pas)	η_∞ (Pas)	Critical shear rate $\dot{\gamma}_c$ (s ⁻¹)
300 mM oct.	0.004	0.97	0.2	0.005	250
350 mM ger	0.01	0.85	0.85	0.001	100

Above the critical concentration there would be an expected distinct shear thinning effect¹⁹³⁻¹⁹⁷ and experimentally it was observed that the samples with higher co-surfactant concentration are showing pronounced shear thinning behaviour (see figure 4.1.12). For such pronounced shear thinning behaviour one can use power law¹⁴⁰

$$\eta \approx \dot{\gamma}^{-k} \quad (4.3)$$

The exponent term k reveals the shear thinning rate of viscosity. The slope of declination for both the systems with octanol and geraniol was calculated and observed that the values are in the range of – 0.9 to – 1.0. This high value of k indicates that the thinning rate of viscosity with increasing the shear rate is very high. There are a few possibilities to explain this high shear thinning rate. Vesicular structure can be deformed during shearing or randomly distributed vesicles can come in alignment during shearing or both can happen simultaneously.

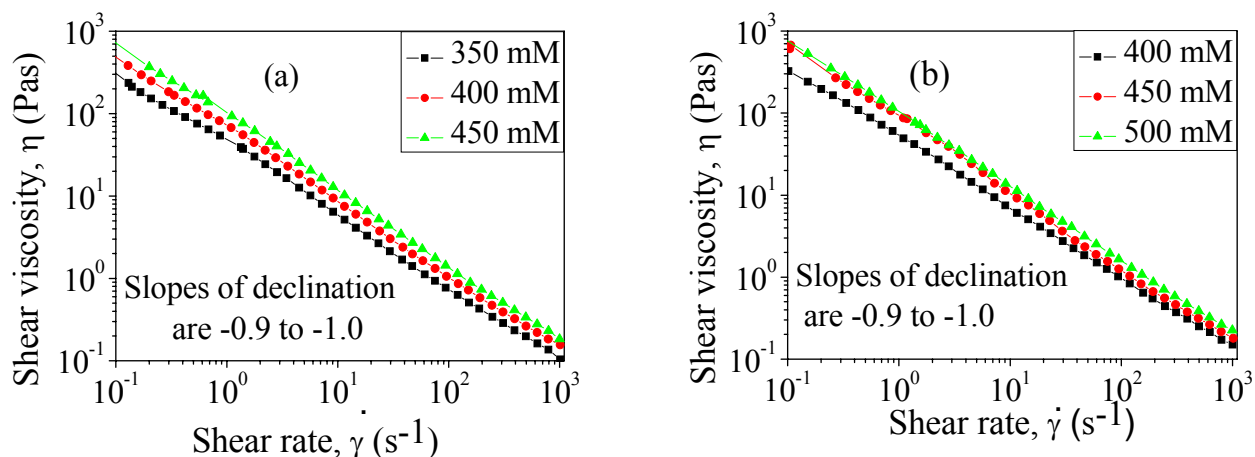


Figure 4.1.12: Double logarithmic plot of shear viscosity against shear rate. Figure (a) and (b) are displaying the shear thinning behaviour of viscosity with increasing shear rate with different concentration of co-surfactant octanol and geraniol respectively.

Such shear thinning is observed in many cases of vesicular systems. The exponent term k for hard spheres has been found experimentally to be about -0.5 over an extended range of shear rates¹⁹⁸. A very similar shear thinning behaviour was observed for uni-lamellar phospholipid vesicles with radii of 250 nm ¹⁹¹. The shear thinning behaviour of multi-lamellar vesicles is also very pronounced i.e. the exponent term k is even smaller than -0.5 , as it has been observed that the multi-lamellar vesicles becomes smaller in size since bilayer shells become successively removed off with increasing shear rate¹⁹⁹. For the systems $200\text{ mM Na-oleate/ water/ }500\text{ mM octanol}$ and $200\text{ mM Na-oleate/ water/ }500\text{ mM geraniol}$, the value of k is calculated as -0.97 which is much more pronounced than in the ideal hard sphere case⁹⁰. These observations of vesicular structure for the stiff gel composition are supporting the findings by DLS and cryo-TEM methods at dilute state that the system has been transformed into vesicular structure with increasing the concentration of co-surfactants.

To assess the effect of co-surfactant on the formation of vesicle and hence rheological properties, frequency sweep measurements have also been performed for vesicular stiff gel samples under the linear deformation range from frequency $f = 0.01$ to 100 Hz . Figure 4.1.13 illustrates the rheograms at different concentrations of co-surfactant and with different co-surfactants. These rheograms are showing characteristic behaviour of viscoelastic fluids.

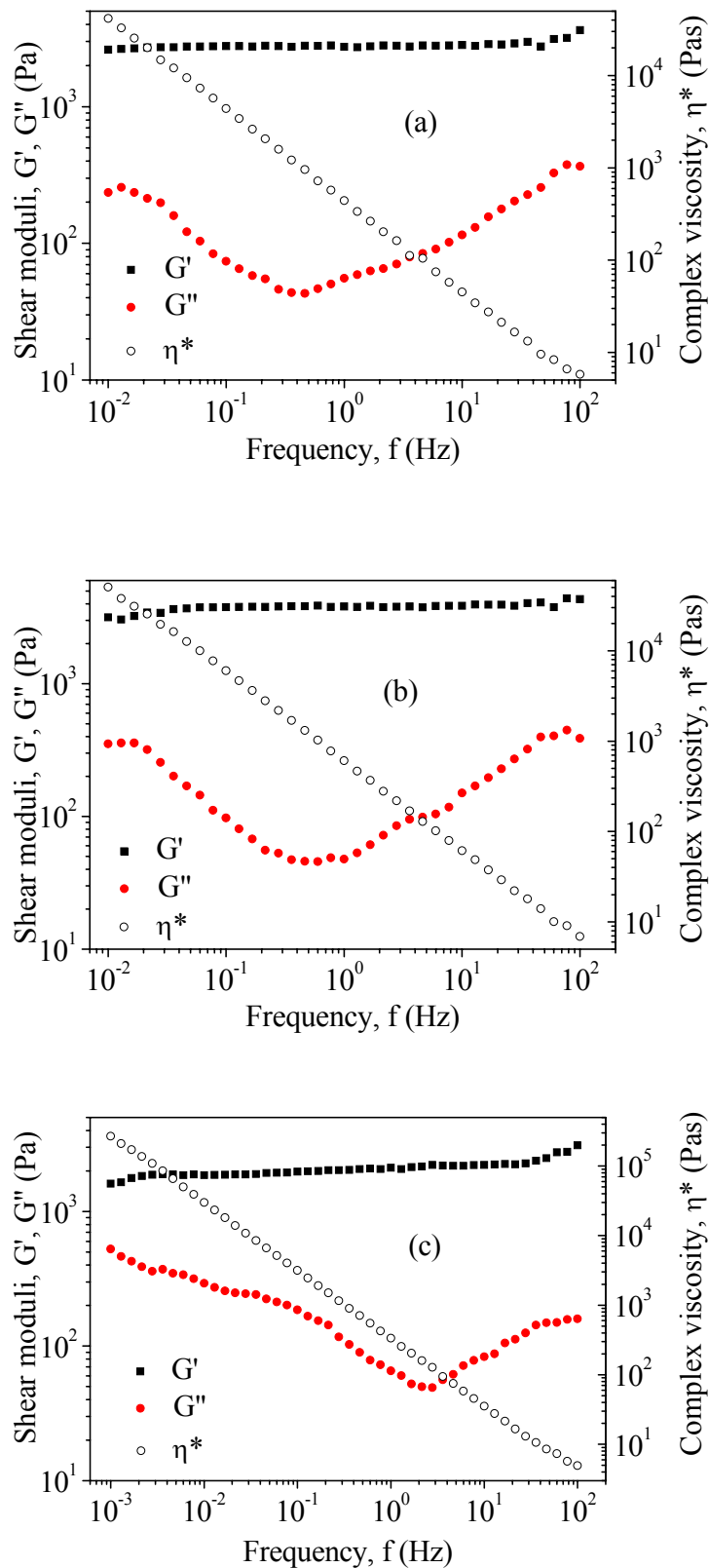


Figure 4.1.13: Frequency sweep oscillatory measurements of vesicular L_{ves} stiff gel at different concentration and with different co-surfactants at 25°C. Na-oleate concentration was 200 mM. Figures (a) and (b) are with 500 mM and 600 mM octanol respectively. Figure (c) is with 600 mM geraniol.

All the rheograms show that the storage modulus G' is almost constant and independent of frequency in the measuring range, and it is higher than loss modulus G'' by about one order of magnitude. The complex viscosity shows no plateau and it decreases double-logarithmically with increasing frequency in whole frequency range which is a typical characteristic feature of viscoelastic gel system^{43, 200, 201}.

Relaxation Time

One can evaluate relaxation time from the oscillatory frequency sweep measurement of the sample. Figure 4.1.14 illustrates the rheograms of 200 mM Na-oleate with 300 mM (figure a) and 350 mM (figure b) geraniol. This figure indicates that both storage and loss moduli are frequency dependent. For the sample with 300 mM geraniol, it was observed that loss modulus is higher than storage modulus at higher frequency range and it (loss modulus) increases with increasing the frequency. The storage modulus, on the other hand, is decreasing initially with the increase of frequency till it meets the loss modulus and afterward it remains almost constant at the higher frequency range. The sample with 350 mM geraniol shows more elastic property than viscous property in most of the frequency window studied here. Both the storage and loss moduli decrease with decreasing the frequency but the rate of decrease for storage modulus is much more pronounced than that of loss modulus and finally they meet each other at 0.01 Hz. This indicates that the elastic property decreases with frequency faster than the viscous property. These rheograms notice that the solutions have finite relaxation time.

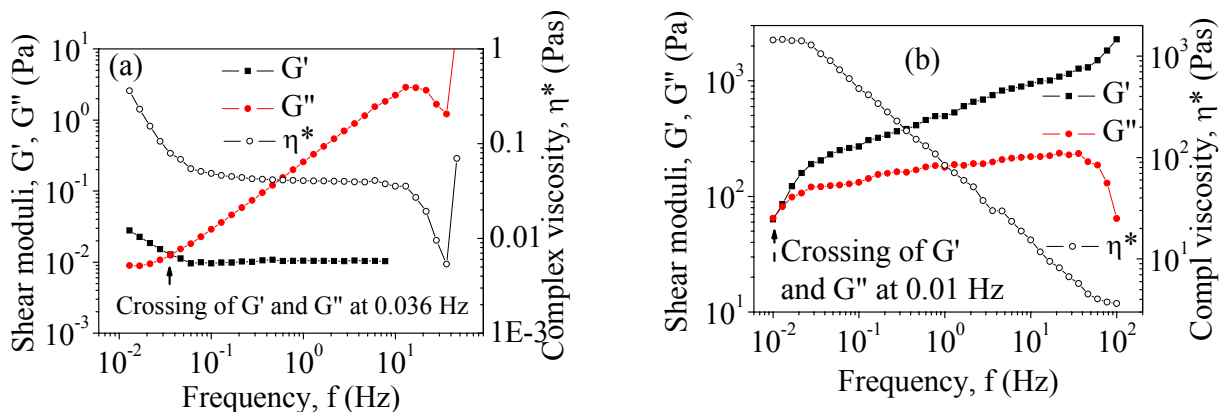


Figure 4.1.14: Frequency sweep oscillatory measurements of vesicular L_{ves} phase of 200 mM Na-oleate with different concentrations of geraniol at 25°C. The concentration of geraniol in the sample was 300 mM (a) and 350 mM (b).

The rheograms in figure 4.1.14 show that the solutions have a single crossing between two moduli. Before and after this crossover point samples attain either more elastic or viscous property. For such system one can easily calculate the characteristic time τ_{cross} called relaxation time, τ_{R} . The relaxation time for 200 mM Na-oleate with 300 mM and 350 mM geraniol is 28 s and 100 s respectively. The crossover shifts towards lower frequency with increasing the co-surfactant concentration, since the system is moving towards more viscous liquid with concentration and for higher concentration no crossover was observed when solution attains stiff gel state.

Yield Stress

The viscoelastic behaviour of associated vesicles becomes evident in the non-linear rheological measurements. During the preparation and homogeneously mixing the samples some air-bubbles were entrapped into some samples with high co-surfactant concentration. The prevention from rising up these entrapped air-bubbles primarily indicated that the samples have a distinct yield stress. Dynamic rheological measurements can be used to determine the yield stress by observing the shear stress as a function of deformation or shear rate for the samples with different co-surfactant concentration. From figure 4.1.15 it is clear that yield stress increases almost linearly with increasing the concentration of co-surfactants (see figure 4.1.15c and d).

True yield stress value is different from finite-long structural relaxation time. One may determine the yield stress value by measuring shear stress against shear rate; the systems with entangled rod-like micelles show this type of apparent yield stress values²⁰². These values are the results of long relaxation time due to the retardation of the movement of the rod-like micelles. To check if the solutions have true values of yield stress the deformation should also be plotted against shear stress as shown in figure 4.1.15a and b. The figure indicates that the gel formation by vesicular structure facilitate by octanol is much faster than geraniol. Linear structure of octanol could be the plausible cause for this faster gelation.

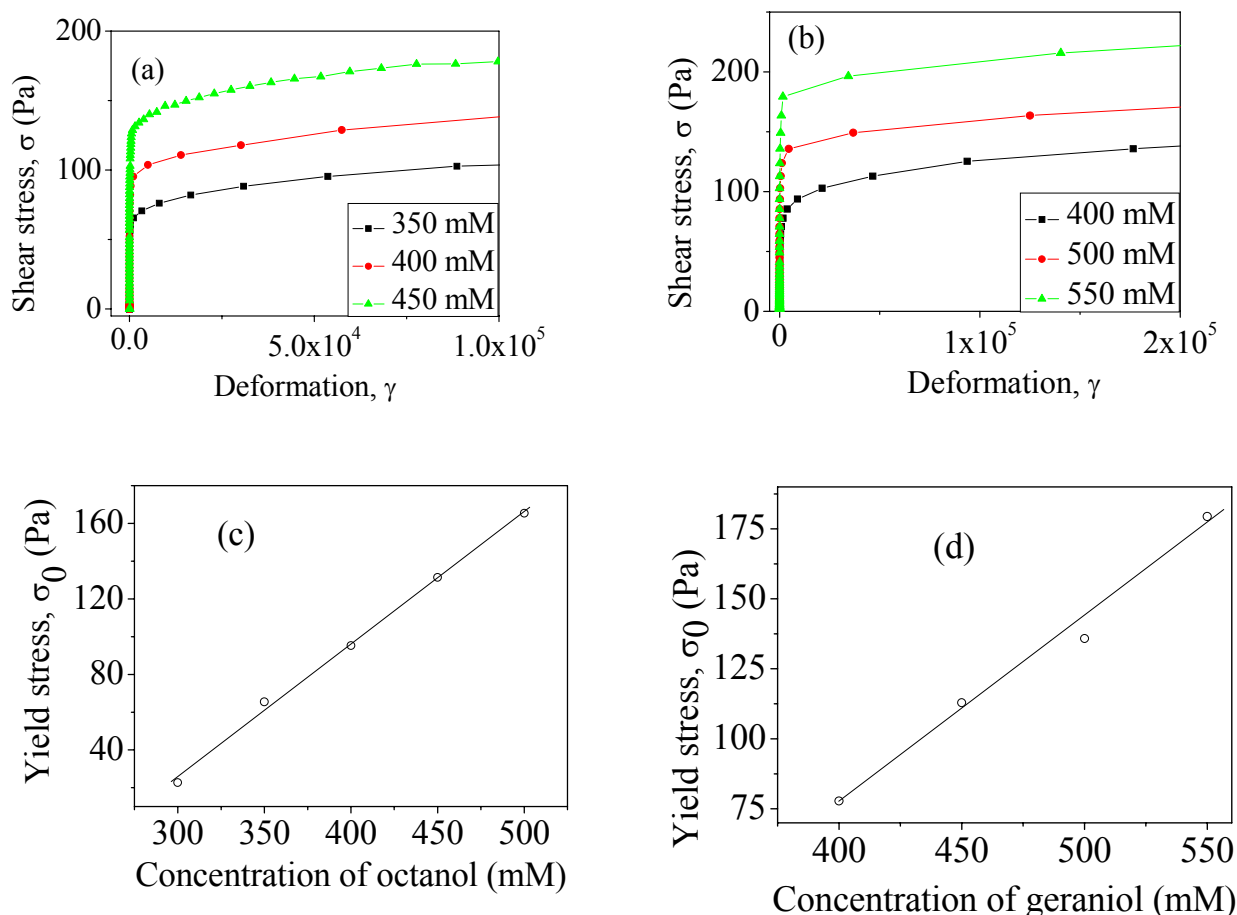


Fig 4.1.15: Shear stress against deformation to determine yield stress of 200 mM Na-oleate with increasing concentration of octanol (a) and geraniol (b). Figures illustrate that yield stress increases linearly with increasing the co-surfactant concentration (c) and (d).

4.1.6 Kinetics of Vesicle Formation

During the preparation of samples it was observed that after addition of co-surfactants and vigorous shaking, the samples became turbid initially because of the emulsification of organic components into aqueous surfactant solution. This turbidity was reducing with time which indicates that organic component was slowly incorporating into micellar structure and transforming from micellar aggregation to bilayers and finally bilayers were forming vesicular structure. In this case the micelle–vesicle transformation was slow enough to be measured by spectrophotometric method. The spectra in figure 4.1.16 are exposing the velocity for

disappearing the emulsified turbidity for the formation of bilayer and afterward vesicular aggregation, by surfactant solution with co-surfactant at 25°C, as a function of time. From this figure one can see that two processes are going on there for both the co-surfactants. The initial and fast declination part of the absorbance spectrum in about 10 minutes can be identified as the dissolution of co-surfactants into the micellar aggregation to form bilayer structure and afterward the formed bilayers are enclosed into spherical vesicular structure. The formed vesicles are ordered into a structural reorganisation through the slow process. Each of the species, on an average, makes a different contribution to the turbidity. Thus by monitoring the turbidity as a function of time and treating the resulting spectrum consisting of two first order relaxation process one can elucidate the two sets of kinetic parameters.

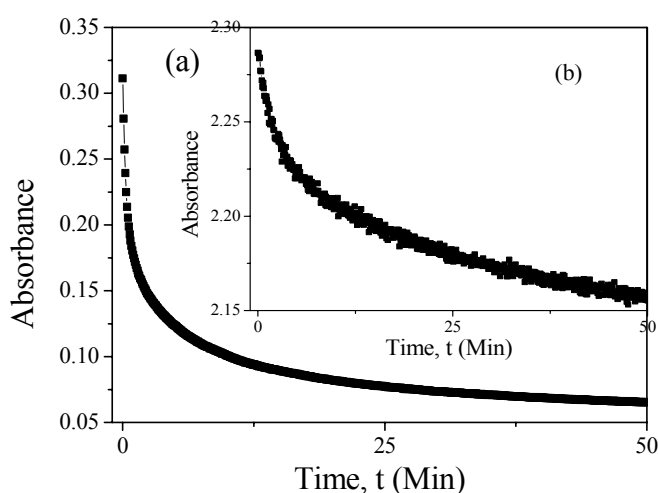


Figure 4.1.16: Spectrophotometric absorbance as a function of time, spectrum obtained directly from uv-visible spectro-photometric measurement at the wavelength of 550 nm. Figure displays the rate of formation of vesicle by 200 mM Na-oleate with (a) 500 mM octanol and (b) 400 mM geraniol.

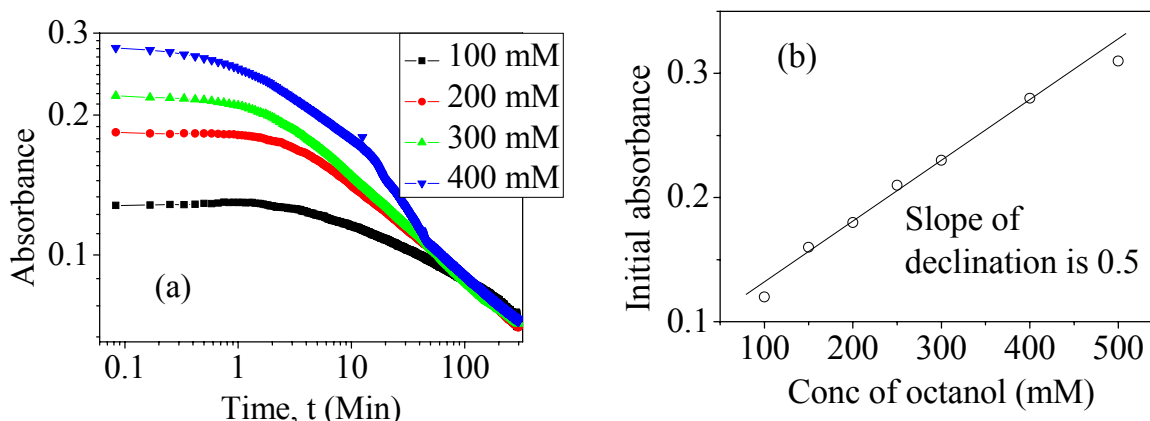


Figure 4.1.17: Double logarithmic plot of absorbance as a function of time (a). Here the surfactant concentration was 200 mM and octanol concentration was varied from 100 mM to 400 mM. In figure (b) initial absorbance is plotted as a function of octanol concentration.

In the first stage it was assumed that 200 mM Na-oleate solution is mainly globular micelles. Finely dispersed (because of strong mechanical vibration) co-surfactants into aqueous phase made the system emulsified initially and because of their very low solubility in aqueous medium (Solubility of octanol is 4.5×10^{-8} M and geraniol is almost insoluble) octanol or geraniol precludes growth by molecular diffusion or Ostwald ripening. The formation of bilayers and hence vesicles is thus likely to proceed by coalescence or aggregation process. When aggregation of two particles occurs immediately at contact, the process is limited by diffusion and in general is fast²⁰³. Figure (4.1.17 a, b) illustrates that the initial absorbance increases with increasing the concentration of octanol, since the system is more emulsified with larger amount of octanol. The initial absorbance is different for different octanol concentration, but after certain time all the absorbance spectra are meeting together (figure 4.1.17a). This phenomenon indicates that the higher concentration of emulsified co-surfactant dissolves significantly faster into the aqueous micellar solution and meeting at a point together and that is the measure of kinetically rapid formation of bilayers and hence vesicles.

Characteristic Time

In this investigation, kinetics for the transformation to vesicles from micelles is studied as a function of concentration of co-surfactants keeping the concentration of surfactant constant at 200 mM. A vesicular structure was observed when the concentration of co-surfactant reached at ≥ 100 mM. It has also been observed that the kinetics of vesicle formation was best described by a double exponential fitting, indicating the presence of two well separated steps for the transformation (figure 4.1.21).

$$y = y_0 + a_1 \exp(-t/\tau_1) + a_2 \exp(-t/\tau_2) \quad (4.4)$$

where τ_1 and τ_2 are the relaxation times for the fast and slow phase respectively while y_0 , a_1 and a_2 are the adjustable parameters. However, in most practical situation, the aggregation time (s) is more important than the aggregation rate (s^{-1}). Figure 4.1.22 displays the characteristic time for the formation of vesicular aggregation for the surfactant with octanol as a co-surfactant. The relaxation time for the fast phase for the formation of vesicles ($\tau_1 \sim 5$ Min) and for the slow phase ($\tau_2 \sim 59$ Min) (Figure 4.1.21a) differed by more than one order of magnitude for octanol system; but for geraniol the difference is even higher ($\tau_1 \sim 13$ Min and

$\tau_2 \sim 1102$ Min) (Figure 4.1.21b). This difference in relaxation time in first and second step is allowing a good discrimination between the two phases.

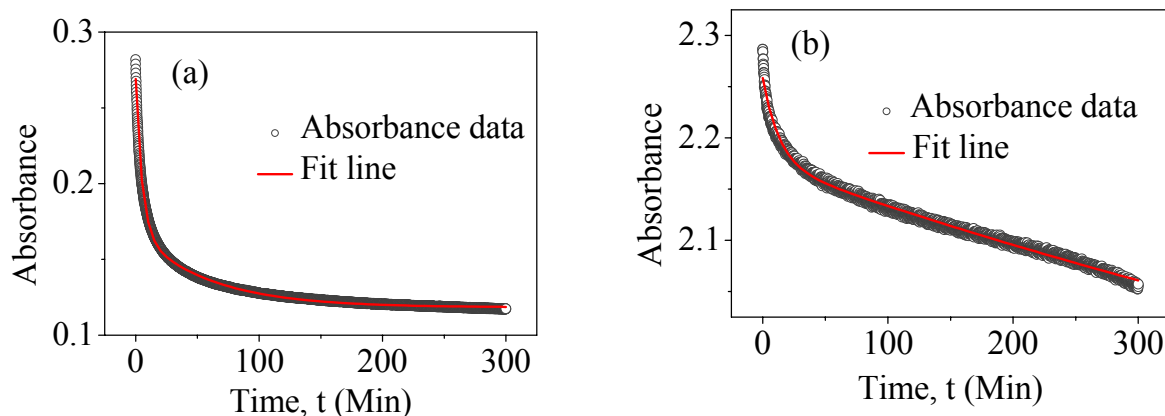


Figure 4.1.18 Biexponential decay fit (red line) with the experimental absorbance measured for the vesiculation of 200 mM Na-oleate with (a) 400 mM octanol and (b) 400 mM geraniol.

Characteristic aggregation-times for micelle-bilayer-vesicles transformation were calculated for Na-oleate/ octanol and Na-oleate/ geraniol systems by fitting the equation (4.4) to the empirical data and the results are illustrated in figure 4.1.19. The figure clearly reveals that the kinetic times for both fast and slow steps are gradually decreasing with increasing the concentration of octanol (figure 4.1.19a and b). This implies that the rate of dissolution of octanol in micellar solution and afterward ordering of vesicles are higher with higher concentration of octanol. On the other hand, kinetic times for the fast process with geraniol system show different pattern. Similar to the system with octanol initially it decreases with increasing the concentration of geraniol up to 300 mM. After exceeding this concentration the time increases very rapidly (see figure 4.1.19c). This indicates that the rate of dissolution of geraniol increases with increasing the concentration up to 300 mM. Beyond this concentration some excess emulsion droplets dissolve very slowly and affect the overall dissolution rate of geraniol. No systematic increase or decrease in characteristic time for slow process with geraniol was observed.

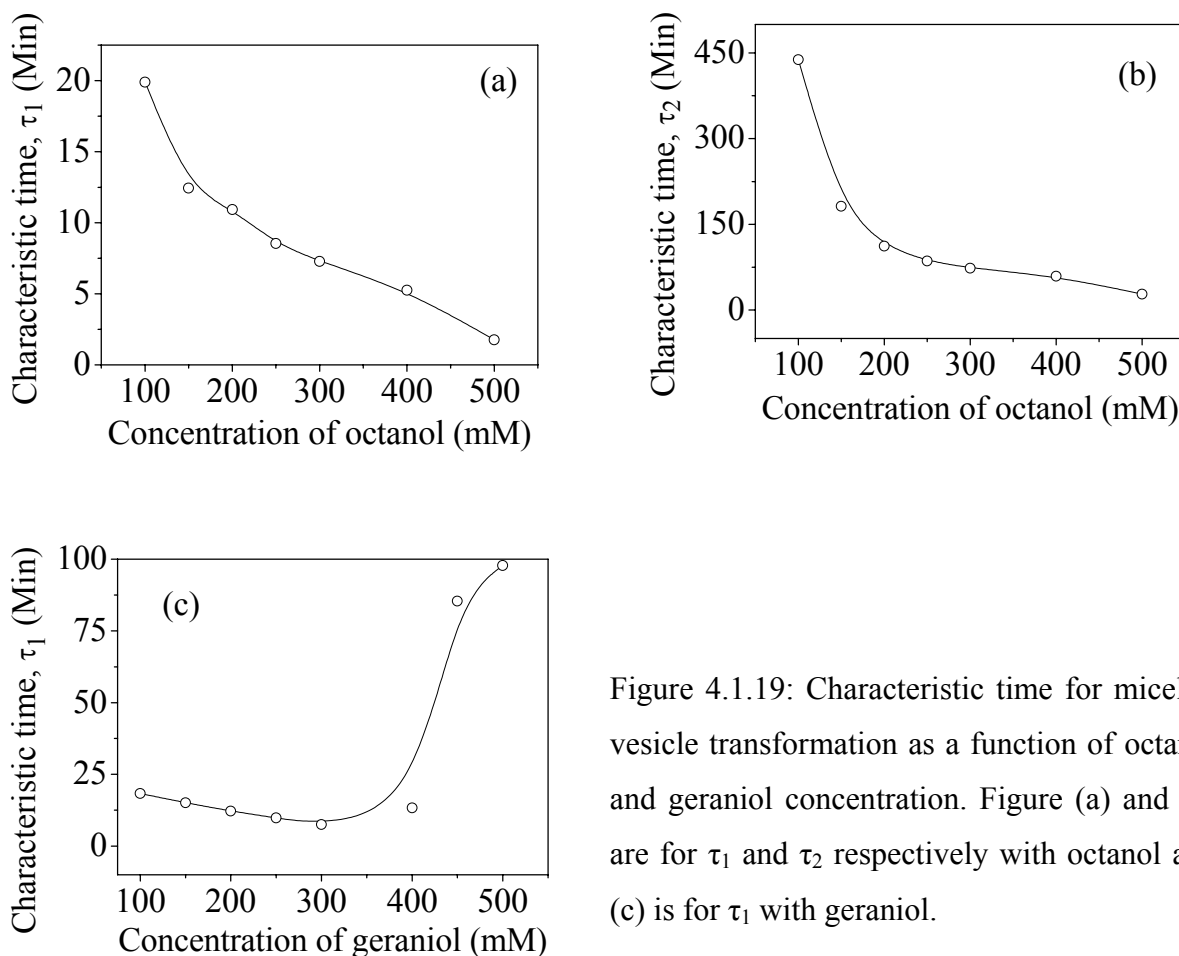


Figure 4.1.19: Characteristic time for micelle-vesicle transformation as a function of octanol and geraniol concentration. Figure (a) and (b) are for τ_1 and τ_2 respectively with octanol and (c) is for τ_1 with geraniol.

Formation Rate of Vesicles

The initial velocities, V_0 for the dissolution of turbidity by the interaction of surfactant solution with emulsified co-surfactants were calculated from the spectrophotometric measurement and the results were displayed in figure 4.1.20. The results indicate that the concentration of co-surfactant has a significant role on initial rate of dissolution of turbidity. Sigmoid nature of the curve with octanol (Figure 4.1.20a) clearly indicates that there are two different phases for the formation of bilayers in the entire concentration range. There is a possibility to explain the sigmoid nature of the curve. The initial sharp increase in rate (from 100 mM to 250 mM) indicates the formation of bilayers for unilamellar vesicles and the rate remains almost constant from 250 mM to 350 mM octanol concentration producing a middle-plateau in the rate figure. This plateau indicates that the system is saturated with unilamellar vesicles. After 400 mM octanol concentration rate of formation of vesicles again increases

with increasing the concentration. In this concentration range sample produces, probably, multi-lamellar vesicles with highly ordered gel structure. On the other hand, the nature of the curve with geraniol is different from that of octanol. Similar to octanol initially rate of dissolution of emulsified turbidity increases with increasing the concentration of geraniol in the range of 100 mM to 300 mM. But at higher concentration (> 300 mM) the rate decreases with increasing the concentration of geraniol (see figure 4.1.20b). This indicates that after exceeding this concentration excess emulsion-droplets solubilise very slowly and consequently overall rate decreases.

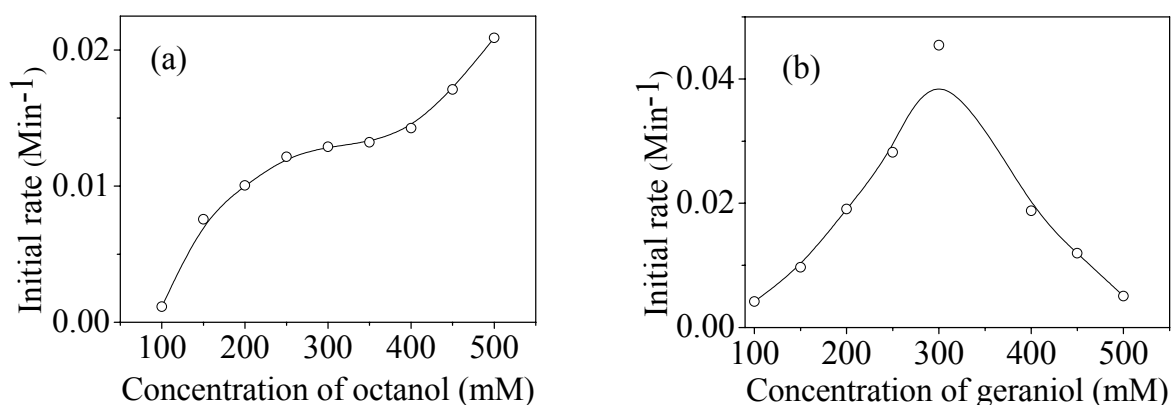


Figure 4.1.20: Initial rate for the dissolution of turbidity as a function concentration of octanol (a) and geraniol (b) at 25°C. The concentration of Na-oleate was 200 mM.

4.1.7 Effect of Electrolytes on Vesicular Gel

It has been observed that 200 mM Na-oleate forms vesicular gel with 500 mM octanol as co-surfactant. The formation of vesicle-gel depends on the size and concentration of the vesicles. To investigate the effect of electrolytes on the formation of vesicular gel five different electrolytes with different cationic groups but the same anionic part were chosen here. It was assumed that mainly cationic group will interact with the vesicular bilayers since Na-oleate forms anionic bilayers with co-surfactant. The nature and extent of interaction of different cationic groups with anionic vesicle surface may be different. Five different electrolytes can be classified into two groups – three electrolytes are mineral salts like alkali (Li^+ , Na^+ and Cs^+) chlorides and the remaining two are quaternary ammonium organic (Me_4N^+ and Et_4N^+) chlorides.

To assess the effect of additional electrolyte on the vesicular gel composition rheological measurements have been performed under different conditions. Frequency sweep measurement of all the samples under the linear deformation frequency, $f = 0.01$ to 100 Hz shows that the samples have characteristic viscoelastic properties. Figure 4.1.21 illustrates some rheograms of vesicular gel with the same composition but different electrolytes. All the rheograms show the storage modulus G' is almost constant and independent of frequency in the range under investigation and it is higher than loss modulus G'' by about one order of magnitude. Loss modulus, on the other hand, has no such regular pattern like storage modulus. At the frequency of about 5 Hz they have been shown the minimum value and then the modulus increases with increasing and decreasing the frequency. No crossing of two moduli within the study range of frequency, 10^{-2} to 10^2 Hz was observed, indicating the absence of finite relaxation time. The complex viscosity shows no plateau and which decreases double logarithmically with increasing the frequency in entire frequency range which is a typical characteristic feature of gel. Two different groups of electrolytes (metallic electrolytes and organic electrolytes with bulky group) were used in this investigation to check whether there is any dependency of interaction with bulky group. But the results indicate that there is no significant change with different electrolytes (see figure 4.1.22).

Rheological measurements of the samples with and without electrolyte show a pronounced shear thinning behaviour; but the thinning rate i.e., the value of constant k in power law (equation 4.3) is not always constant for all the samples. It has been observed from the analysis that the shear thinning rate increases initially with increasing the concentration of metallic electrolyte and after reaching the concentration of about 20 to 30 mM (depending on electrolyte) it is decreasing (see figure 4.1.23a). This almost similar trend in shear thinning rate indicates that the interaction of metallic electrolytes with vesicular surface is similar. The result of shear thinning rate, on the other hand, with organic quaternary ammonium electrolyte gives different trends. Instead of gradual and slow increase (as observed in case of metallic electrolyte) in thinning rate, it increases suddenly at the concentration of 5 mM organic electrolyte and afterward it decreases slowly with increasing the electrolyte concentration (figure 4.1.23b). This difference in the trend of shear thinning rate indicates that the interaction of metallic and organic electrolyte with the vesicular surface is different.

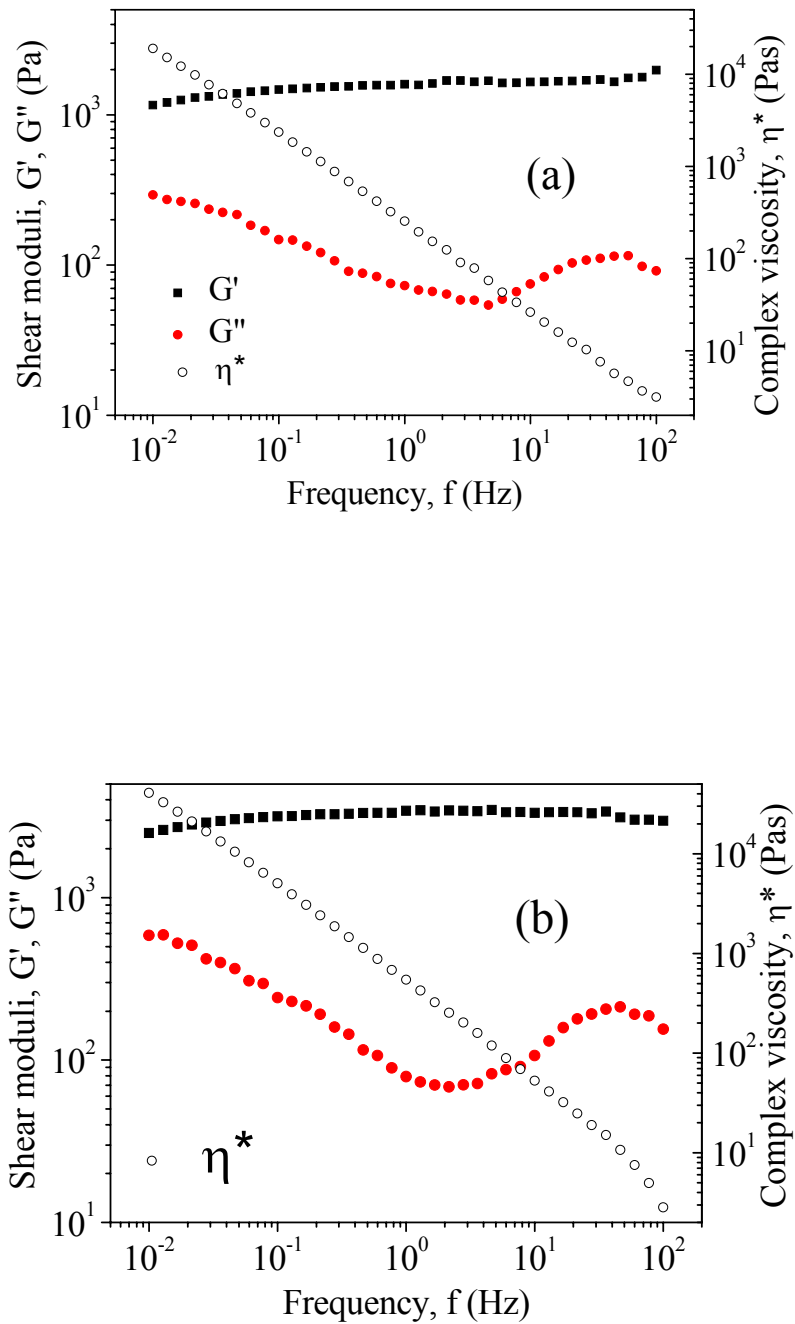


Figure 4.1.21: Frequency sweep oscillatory measurements of vesicular stiff gel at the same composition but with different metallic electrolytes at 25°C. Here the composition of samples was 200 mM Na-oleate + 500 mM octanol + 20 mM electrolyte. Figures (a) and (b) represent the rheogram with 20 mM LiCl and CsCl respectively.

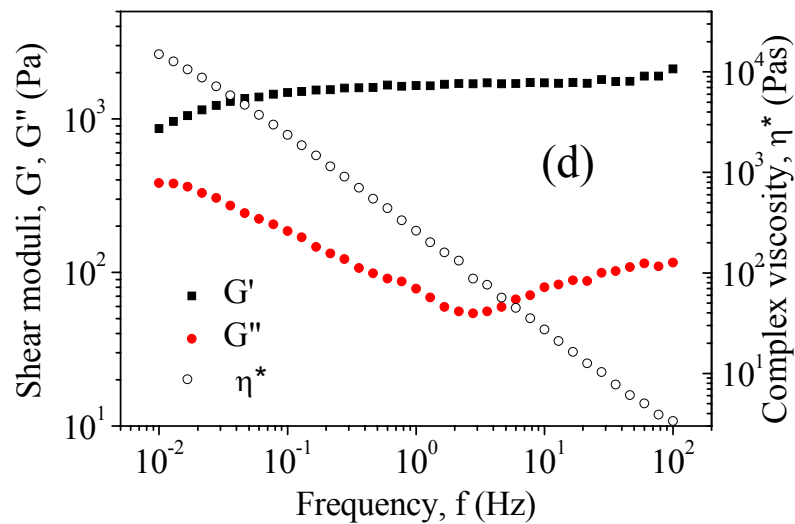
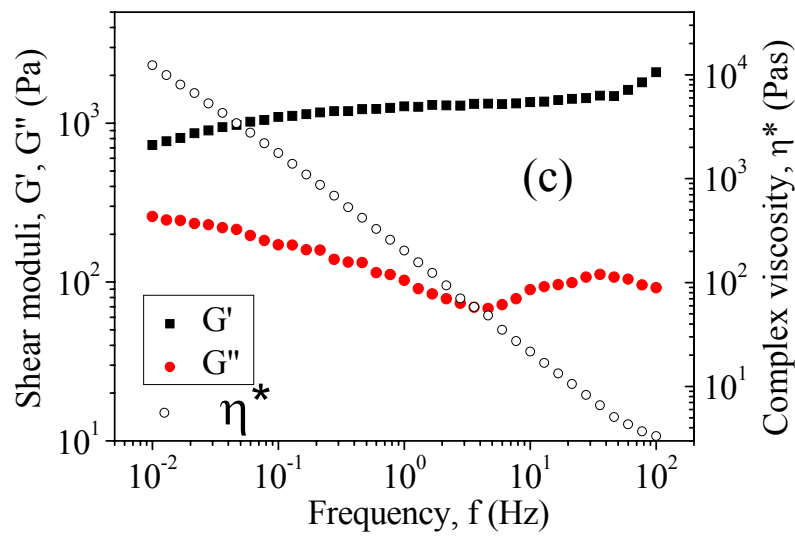


Figure 4.1.21: Frequency sweep oscillatory measurements of vesicular stiff gel at the same composition but with different organic electrolytes at 25°C. Here the composition of samples was 200 mM Na-oleate + 500 mM octanol + 20 mM electrolyte. Figures (c) and (d) represent the rheogram with 20 mM Me₄NCl, and Et₄NCl respectively.

Shear thinning behaviour has been observed for all the samples for steady shear viscosity and complex viscosity. It is observed that the shear thinning given by steady shear measurement does not coincide with that by dynamic measurement with and without added electrolyte. This indicates that the samples do not follow the Cox-Merz rule¹⁴². Hoffmann et al²⁰⁵ reported that vesicular dispersions usually do not follow the Cox-Merz rule.

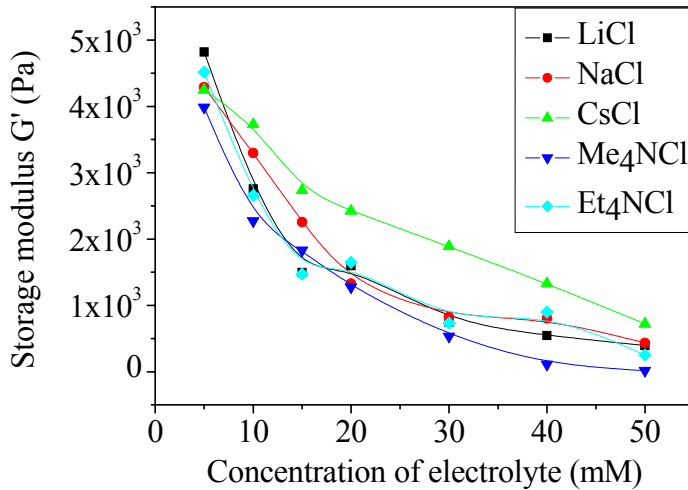


Figure 4.1.22: Storage modulus at frequency $f = 1$ Hz as a function of total electrolyte concentration for the quaternary system of 200 mM Na-oleate/ 500 mM octanol / electrolyte/ water. From this figure it is clear that storage modulus decreases almost single exponentially with increasing the concentration of electrolyte.

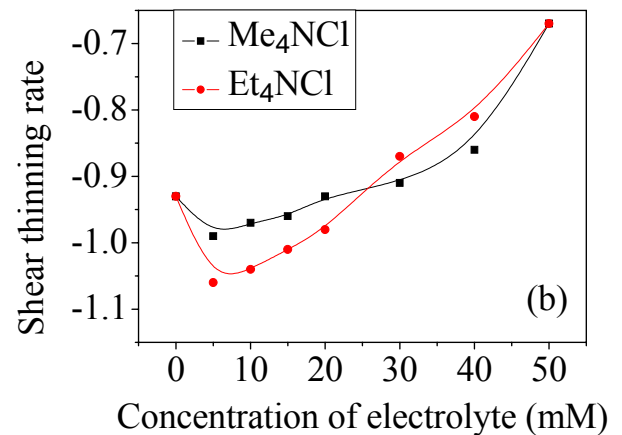
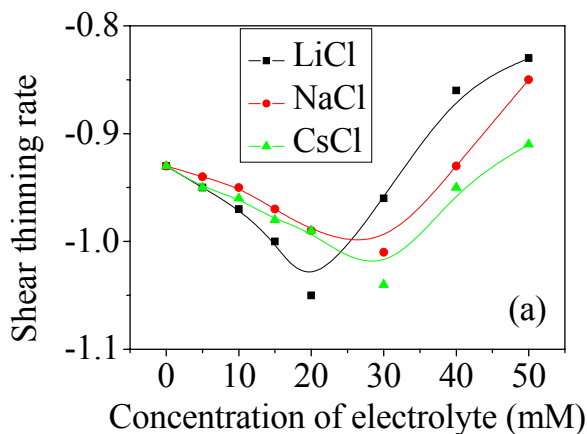


Figure 4.1.23: Slope of shear thinning of the samples of 200 mM Na-oleate and 500 mM octanol with increasing concentration of metallic (a) and quaternary organic (b) electrolytes as a function of electrolyte concentration.

Low frequency oscillations in the linear viscoelastic region provide a sensitive tool to know whether the sample has real yield stress. When the interparticle structure is only marginally affected by the applied oscillations (linear region), the sample with a real yield stress will show solid-like behaviour at all frequencies lower than molecular vibrations, with a constant storage modulus G' that is much larger than the loss modulus G'' ²⁰⁶. Hoffmann et al described that densely packed vesicular dispersion often show yield stress value²⁰⁷ and do not flow as long as the applied shear stress is lower than a characteristic certain value. This characteristic stress value is called yield stress. Dynamic rheological measurement of vesicular gel of 200 mM Na-oleate with 500 mM octanol shows a distinct yield stress value of about 152 Pa. The homogenous mixture of two components produces a greater viscosity and yield stress than those developed by the individual components in the mixture, so it is a synergetic rheological effect. It was observed that addition of electrolyte to this vesicular stiff gel has a significant role on the yield stress and the value is decreasing with increasing the concentration of electrolytes (see figure 4.1.24). This decrease in yield stress may be interpreted by the shielding effect of vesicular charge by the presence of electrolyte. As the concentration of electrolyte increases, the screening effect becomes stronger and the intervesicular interaction becomes reduced. Consequently, the system moves towards more liquid nature.

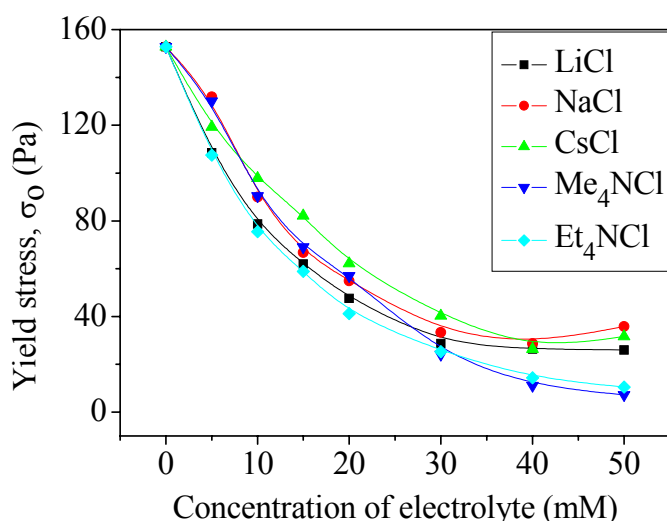


Figure 4.1.24: Yield stresses of the samples with increasing concentration of electrolyte as a function of the concentration of added electrolyte at 25°C.

Physical state of the samples with higher concentration of organic electrolytes loses their solid-like gel structure. They became viscous liquid when the concentration of the electrolyte reached at 40 mM, so the yield stress of the samples at this concentration is very less compared to the samples of similar composition with metallic electrolytes.

4.2 Templating Anionic Vesicles by means of $\text{Ti}(\text{OBU})_4$

4.2.1 Viscoelastic Behaviour

It has been shown in the previous section (section 4.1) that Na-oleate forms vesicles when it mixes with octanol as co-surfactant and the system forms highly ordered vesicular stiff gel when 500 mM octanol was mixed and equilibrated with 200 mM Na-oleate. In order to observe the interaction of $\text{Ti}(\text{OBU})_4$ [Titanium tetra-butyloxide (TTB)], a source of TiO_2 by hydrolysis, with this vesicular stiff gel structure the onset dynamic rheological measurements have been performed. Figure 4.2.1 compares the frequency response of four samples with identical surfactant and co-surfactant concentration, but increasing Ti-precursor concentration. All the rheograms show the typical behaviour of viscoelastic system with a distinct yield stress value. The elastic modulus G' is independent of frequency in the entire measuring range for all the samples and the values of storage modulus G' are higher than that of viscous modulus G'' by a factor of about 10 or more. The complex viscosity shows no plateau; it decreases double logarithmically with increasing frequency in the whole frequency range studied here.

Dynamic rheological data show that the pattern of both shear moduli G' and G'' are similar for all the samples. Increasing the concentration of Ti-precursor up to 3 wt% (figure 4.2.1b) causes no dramatic change in rheology. Further increase in the concentration of $\text{Ti}(\text{OBU})_4$ to 5 wt% (figure 4.2.1c) induces a little difference in rheological response. In this case the difference between two shear moduli was reduced because of the decrease in elastic modulus G' , and the pattern of viscous modulus G'' was also changed. As they do not intercept, this implies that the samples do not have finite relaxation time in the temporal observation window.

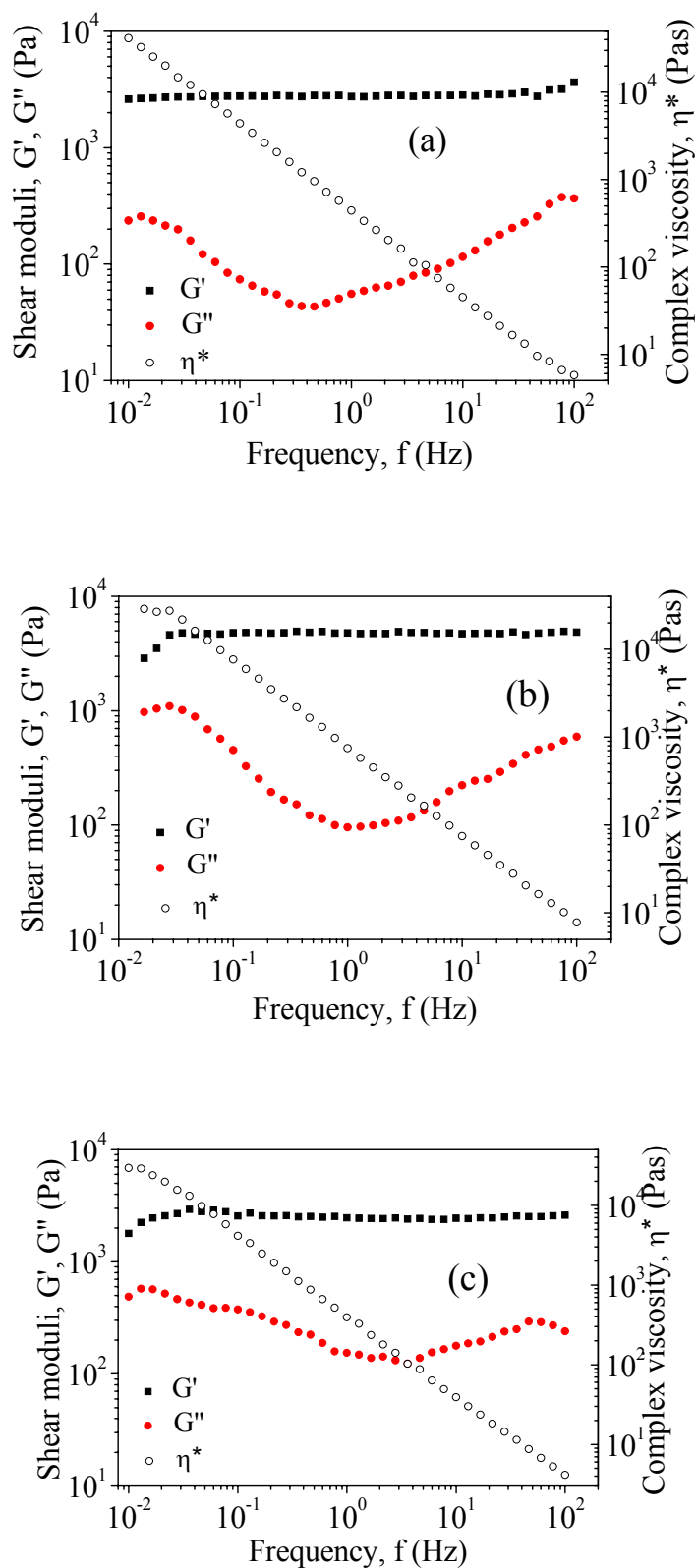


Figure 4.2.1: Frequency sweep oscillatory measurement of stiff gel formed from the colloidal aggregation of Na-oleate/ octanol/ $\text{Ti}(\text{OBU})_4$ system at 25°C . The surfactant and co-surfactant concentrations were 200 mM and 500 mM respectively. Figures (a), (b) and (c) respectively illustrates the increasing concentration of 0 wt%, 0.5 wt%, 3 wt% and 5 wt% of Ti-precursor.

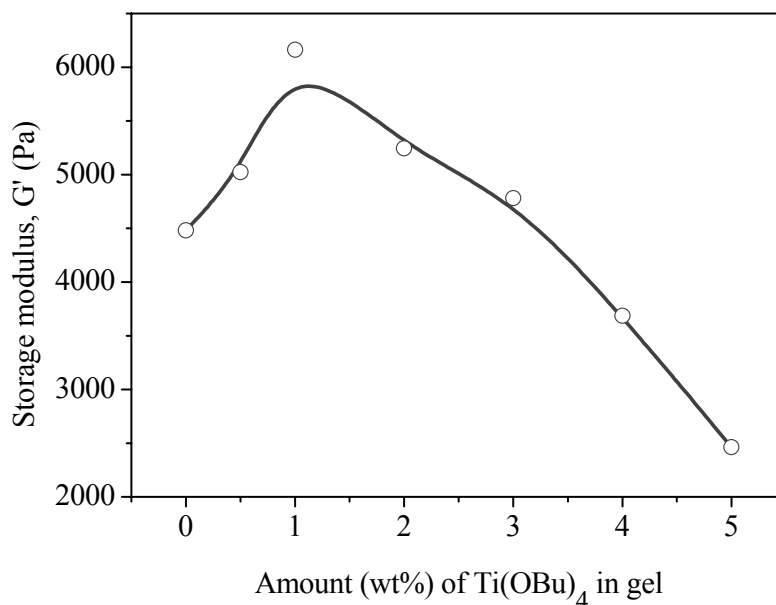


Figure 4.2.2: Elastic modulus G' at $f = 1$ Hz as a function of amount (wt%) of metal precursor in the gel composition of 200 mM Na-oleate with octanol at 25°C .

Figure 4.2.2 shows that the storage modulus varies from ca 2400 Pa to ca 6200 Pa which is a factor of about 2.5. This implies that TTB appears to have only a minor effect on the microstructure of the gel. The elastic modulus, G' , increases initially with increasing the concentration of metal precursor in the gel and it reaches a maximum value when the concentration of TTB was 1 wt% (figure 4.2.2). It can be mentioned here that added TTB has been hydrolysed into TiO_2 and alcohol when it comes into contact with aqueous part of the system. There are two possibilities to explain the initial increase in elastic modulus. The formation of little amount of TiO_2 , the first hydrolysis product of TTB, should strengthen the structure. In addition to this, the vesicle gel can form a more ordered structure due to the presence of butanol, the second hydrolysis product of TTB. Strengthening the vesicular structure or ordering the randomly distributed vesicles or a simultaneous effect of both the processes led to increase the storage modulus at lower TTB concentration. This explanation with strengthening the structure and ordering of vesicles might be right, since the physical observation of samples with such low concentration of TTB did not show much opacity in the gel.

A striking observation is that after this 1 wt% concentration, the storage modulus decreases almost linearly with increasing the concentration of TTB (figure 4.2.2). This decrease in elastic modulus might be explained with the local network structure formed by the hydrolysis product of TiO_2 . At higher TTB concentration, the concentration of TiO_2 is sufficient to form a new network around vesicles and disrupt the original vesicle-gel structure and can form a local phase separation. The formation of local phase separation by the hydrolysis product TTB could be the plausible cause of decreasing the storage modulus. The influence has been become stronger with higher concentration of TTB; consequently the samples have been losing their elastic property simultaneously.

From the above rheological measurements the ratio of two shear moduli, G'/G'' , for the vesicular gel has been calculated and plotted against the frequency of oscillation in figure 4.2.3. The derived plot clearly reveals that each sample produced a pronounced hump with a peak and depending on the concentration of TTB the position of peak shifts from 0.4 Hz at 0 wt% TTB to 4 Hz for 5 wt% TTB. The presence and position of these peaks imply that samples may have an acoustic sonic effect (ringing gel).

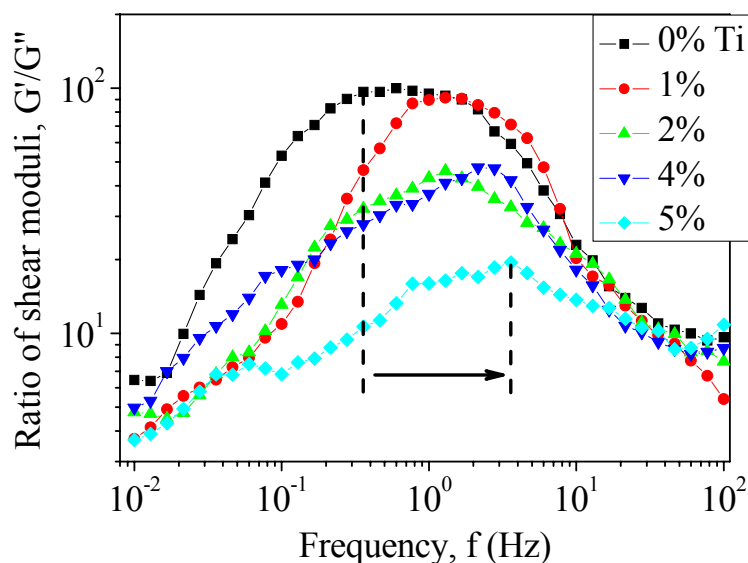


Figure 4.2.3: Ratios of shear moduli, G'/G'' of vesicular gel with increasing concentration of TTB as a function of oscillation frequency at 25°C. The percentage in the side list indicates the amount (wt%) of TTB present in the vesicle gel.

Another noticeable point in figure 4.2.3 is that the ratio of shear moduli G'/G'' remains almost constant until 1 wt% of TTB in the samples. After exceeding this concentration, the amplitude of hump is gradually decreasing with increasing the concentration of TTB. These results indicate that fluidity of the samples increases with increasing the concentration of Ti-precursor. This result is supporting the observation that the sample becomes phase separated and flows by its own weight when the concentration of TTB was 6 wt%.

4.2.2 Non-linear Behaviour

Viscosity measurements as a function of shear rate have been carried out for all the samples and the results are summarised in the figure 4.2.4. The results show that the shear viscosity decreases for all the samples double logarithmically in entire shear range. For such pronounced shear thinning behaviour one can use power law (equation 4.3) to determine the shear thinning rate.

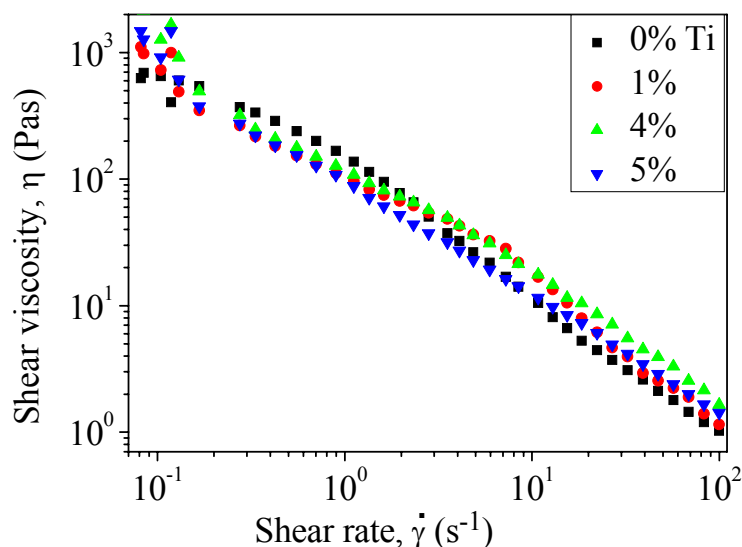


Figure 4.2.4: Double logarithmic plot of shear viscosity against shear rate for the vesicular gel (200 mM Na-oleate with 500 mM octanol) with different concentrations of TTB at 25°C.

The negative slope of shear thinning, k was calculated and observed that the values are lying between 0.9 and 1.0. This value is similar to that of the vesicle gel without Ti precursor, thereby indicating the similar structure build up.

4.2.3 Cox-Merz Rule

A well-known empiricism in the rheology of some viscoelastic systems is the Cox-Merz rule, which relates the linear dynamic measurement of complex viscosity as a function of frequency to the steady shear flow viscosity as a function of shear rate¹⁴². This relationship also allows estimating steady flow viscosity curves from the more readily obtainable dynamic-mechanic rheological measurements. However, this correlation is quite unusual, since the rheological responses of viscoelastic system in dynamic and steady-state are quite independent. Cox–Merz rule works only if flow does not induce substantial variations in morphology. Thus, if the microstructure is affected by flow, it is expected that the dynamic low strain data will not follow the pattern observed for the steady-state flow. The relationship between complex viscosity and steady shear flow viscosity for Na-oleate/octanol/TTB/water has been investigated and the results are depicted in figure 4.2.5.

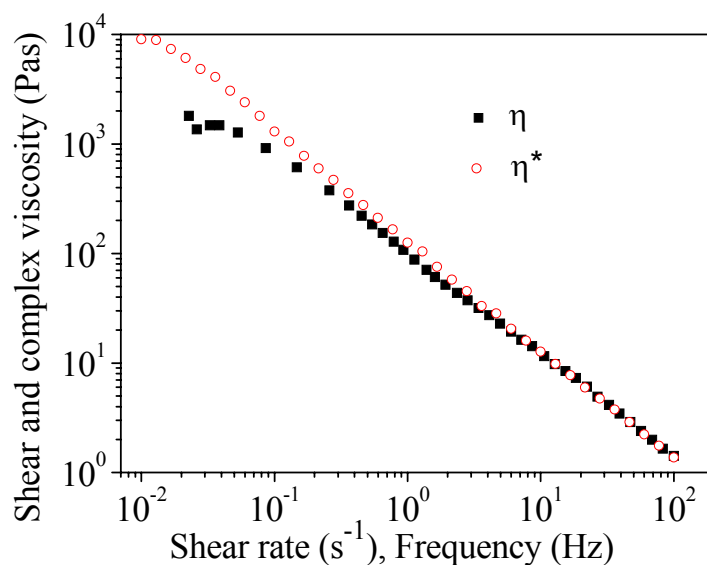


Figure 4.2.5: Comparison of the magnitude of complex viscosity, η^* as a function of frequency and the shear viscosity, η as a function of shear rate for the sample of 200 mM Na-oleate + 500 mM octanol + 5 (wt)% TTB.

Figure 4.2.5 illustrates that the Cox-Merz rule works quite satisfactorily within the limit of frequency and shear rate of 2 and 100 Hz and s^{-1} respectively, owing to the similitude of microstructures during the two types of flow. At lower frequency and shear rate, due to the greater sensitivity of the morphology to the dynamic linear measurement, a significant departure of rheological data have been observed; the steady-state viscosity of vesicular gel

increases slower than complex viscosity, and the difference increases gradually with decreasing the oscillatory frequency. Hoffmann et al.^{208, 209} and recently Yamashita²¹⁰ also reported that Cox-Merz rule does not work quite well with vesicular solutions, since they have also obtained deviated results. However, when there is large-scale structure present in the liquid like vesicles, viscoelastic response is evident on time scales much greater than the molecular diffusion time and for this reason, probably such deviation from Cox-Merz rule appears for vesicular structure.

4.2.4 Yield Stress

Bingham-fluids are characterized by the yield stress. Shear sweeps of vesicular gels for the present investigation are depicted in figure 4.2.6 where yield stress is determined as a function of TTB concentration.

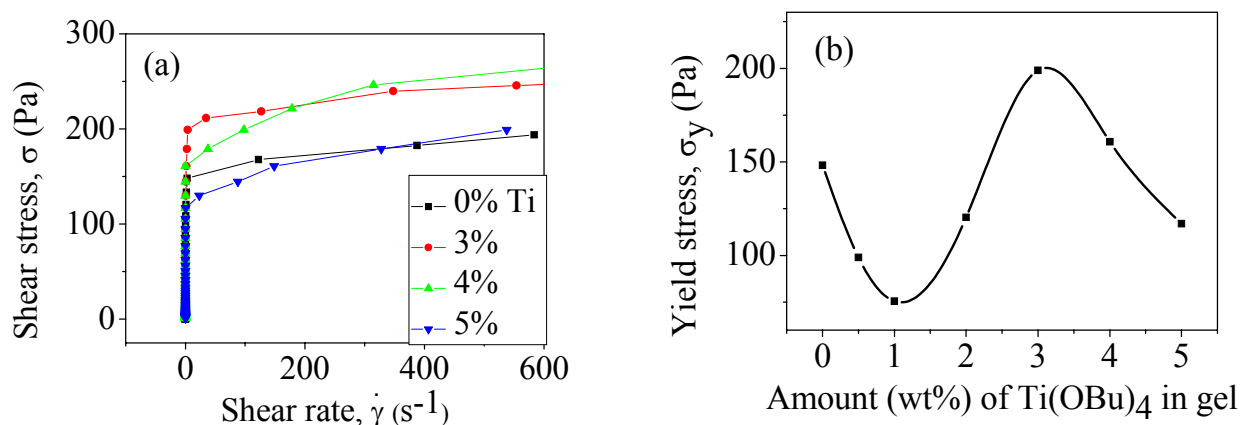


Figure 4.2.6: Shear stress as a function of shear rate for 200 mM Na-oleate/ 500 mM octanol with increasing concentration of TTB at 25°C (a). The number mentioned in the inset is indicating the corresponding percentage of TTB present in the gel. The deduced yield stress values of these systems as a function of weight percent of TTB in the gel (b).

From the figure 4.2.6a it is clear that the systems behave like a Bingham fluid and all the samples have a distinct yield stress value. On the other hand, figure 4.2.6b illustrates that the yield stress values are decreasing initially with increasing the concentration of TTB in the lower concentration region till 1 wt%. Afterward, the values are increasing till 3 wt% and then they are decreasing again. The initial decrease in yield stress indicates that vesicles are no longer densely packed in this concentration range and they can move around each other under

the shear flow. It can be assumed that the alcohol, one of the hydrolysis products of TTB, resides at the amphiphilic interface because of its hydrophilic nature and makes the vesicles in ordered form and consequently the yield stress increases a little. After 3 wt% the values are decreasing again; the phenomenon can be explained on the basis of local network formation by the TiO_2 surrounding the vesicles and hence a local phase separation which is described above. It needs relatively higher concentration of TTB to form a new network surrounding the vesicles. The system is moving towards liquid-nature with further increasing the TTB concentration which can be mentioned here that at 6 wt% the system is phase separated and flowing by its own weight.

4.2.5 SAXS Analysis

First of all, water, micellar solution (200 mM) of Na-oleate and vesicular gel of 200 mM Na-oleate with 500 mM octanol were measured. Likewise, the mixtures of increasing concentration of TTB to the above vesicular gel composition were studied 7 days after preparation and equilibration of the samples, when the solubilization and hydrolysis had been completed. The SAXS scattering intensities of all these samples are displayed in figure 4.2.7.

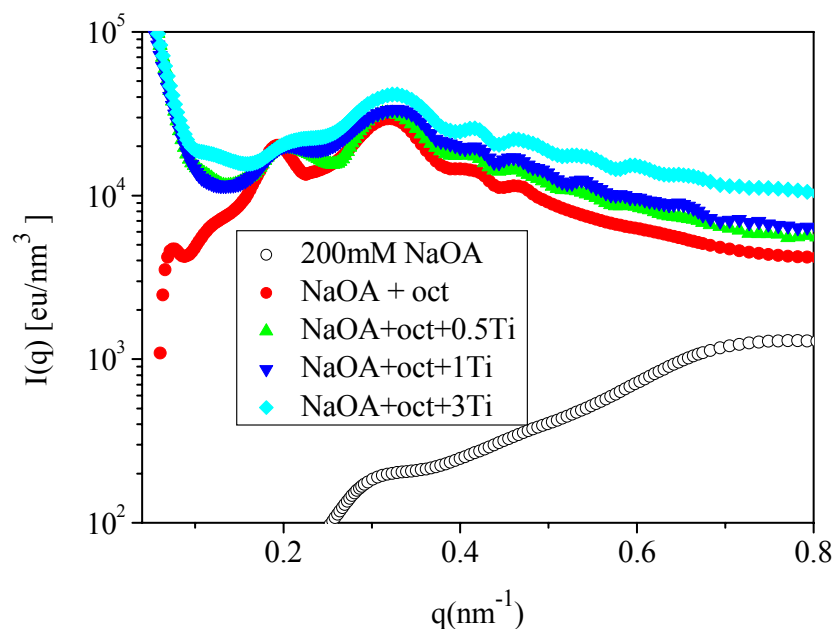


Figure 4.2.7: Desmeared scattering intensities of all samples after subtraction of background as a function of scattering vector q , with preliminary smoothing. Different scattering profiles defined in the inset.

The figure clearly reveals that the scattering intensities of vesicular samples, compared to micellar Na-oleate solution, at low q value are quite high, indicating the presence of bigger aggregates. The scattering intensities are increasing with gradual increase of the TTB concentration in gel composition. Probably the enhanced contrast by the presence of hydrolysis product TiO_2 is the reasonable cause for this. The recorded X-ray scattering pattern for the vesicular samples shows several peaks similar to the former SANS observation⁴³ without metal precursor. It has been observed in previous analysis (see section 4.1) by cryo-TEM measurement in the dilute concentration (100 mM Na-oleate) region of the Na-oleate/octanol system that they form spherical vesicles. Similar X-ray scattering pattern in presence of metal precursor indicates that the incorporation of TTB in bilayers does not change the vesicular shape of the aggregates.

All the vesicular samples (with or without Ti-precursor) are showing the first peak at the q value of 0.18 nm^{-1} . The peaks correspond to the Bragg's repeating distance of 35 nm which can be associated with the diameter of vesicles. This result is very good in agreement with the cryo-TEM results found in previous analysis. The peak positions remain almost the same after adding and increasing the concentration of TTB. This indicates that size of vesicles does not change by adding the metal precursor into vesicular gel.

The scattering intensity for the sample without TTB is going down at very low q values, indicating the presence of repulsive intervesicular interaction. But after adding the metal precursor the scattering intensity is going up proportional to the TiO_2 content due to the formation of TiO_2 .

4.2.6 Kinetic Measurement

When a mixed organic layer (solution of TTB in octanol) was added to an aqueous solution of Na-oleate, two layers were isolated keeping the organic layer floating on the top. Vigorous shaking made the organic layer emulsified into aqueous surfactant solution and made the system very turbid. This turbidity, created immediate after vigorous shaking of two immiscible layers, was gradually reducing with time which indicates that the emulsion droplets were slowly solubilizing into the aqueous phase. This is possible when micellar

surfactant solution can incorporate this emulsified organic layer and transform into a bigger aggregation like vesicle or other morphological structure. So, the speed of reduction of emulsified turbidity is directly measuring the velocity of solubilization of emulsion droplets and thereby transformation from micellar aggregates to a bigger assembly, in this case, a vesicular aggregate. The velocity of disappearing the emulsified turbidity of the samples was measured by UV-visible spectrophotometric method at 25°C and two spectra are shown in figure 4.2.8.

From this figure one can see that two-step process is going on for both the systems [with and without TTB, figure 4.2.9 (b) and (a) respectively] in the formation of vesicular structure – a fast process followed by a steady and slow process. The initial and fast declination part of the absorbance spectrum can be identified as the dissolution of the organic phase into aqueous micellar aggregation to form bilayer structure and afterward, the formed bilayers were enclosed into spherical vesicular structure. The formed vesicles were reorganised into very ordered gel structure through the slow process. Thus by monitoring the turbidity as a function of time and treating the resulting spectrum consisting of two first order relaxation process one can elucidate the two sets of kinetic parameters.

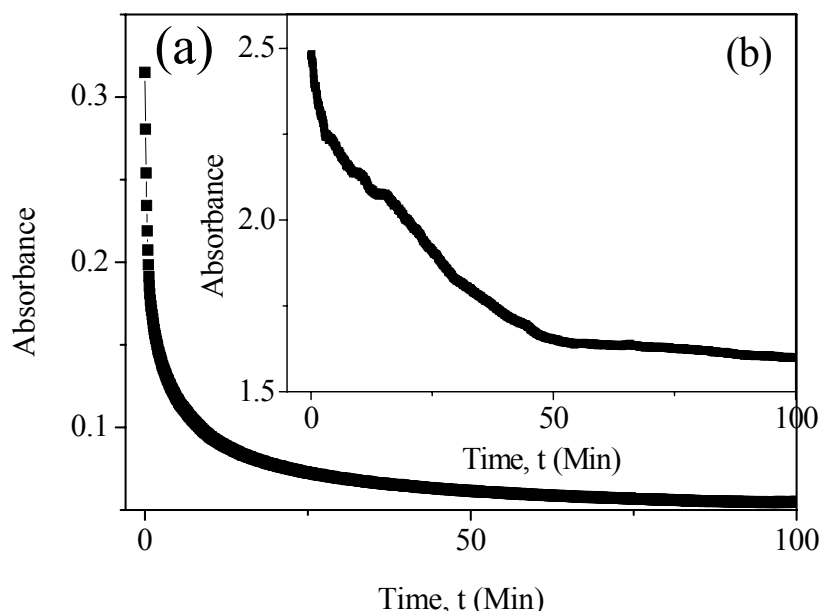


Figure 4.2.8: Spectrophotometric absorbance at the wavelength of 550 nm as a function of time at 25°C . Figure displays the rate of formation of vesicles by 200 mM Na-oleate with 500 mM octanol (a) without TTB (b) with 3(wt)% TTB.

In this investigation, kinetics for the transformation of vesicles from micellar solution is studied as a function of concentration of added TTB keeping the concentration of surfactant and co-surfactant constant at 200 mM and 500 mM respectively. It was observed in the previous study (see section 4.1) that this composition of aqueous surfactant and co-surfactant forms vesicular gel. It has also been observed that the kinetics of vesicle formation was best described by a double exponential fitting (equation 4.4), indicating the presence of two well separated steps for the transformation. Figure 4.2.9 displays the fit of equation (4.4) to experimental data and hence the characteristic time, τ for the formation of vesicular aggregation in presence of metallic precursor was extracted.

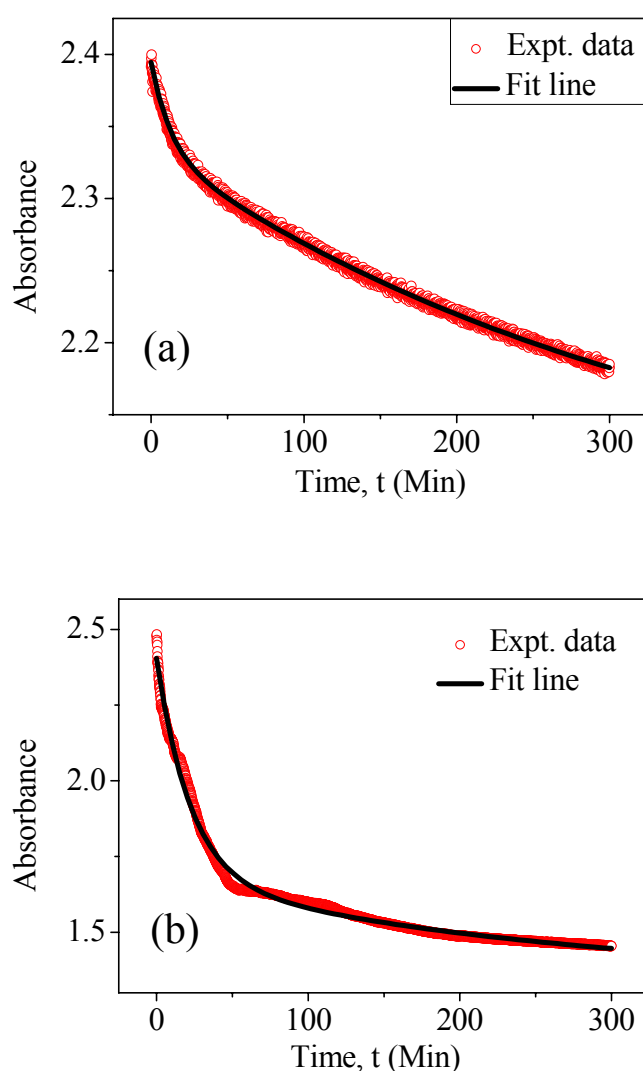


Figure 4.2.9: Double exponential fit of equation 4.4 (black line) for the vesicular gel of 200 mM Na-oleate/ 500 mM octanol with (a) 0.5 wt% TTB (b) 3 wt% TTB.

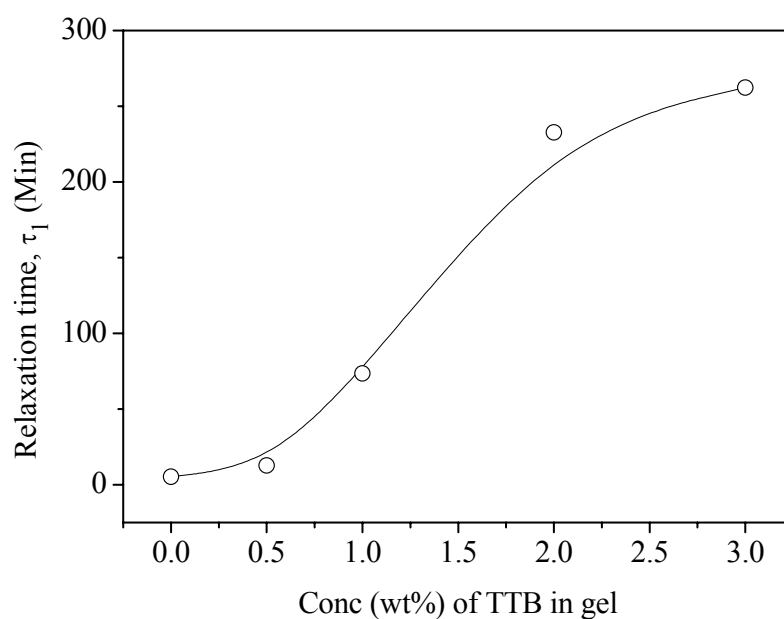


Figure 4.2.10: Relaxation time for the fast mode (τ_1) as a function of concentration (wt%) of TTB in the gel composition.

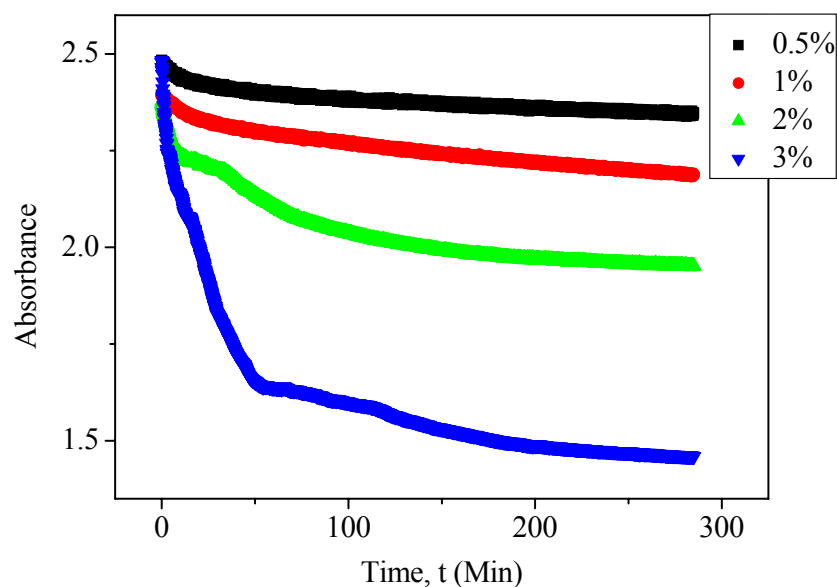


Figure 4.2.11: Absorbance as a function of time to see the effect of metal precursor on the formation of vesicles. The spectra are indicating the rate of solubilization of organic emulsified phase into micellar aqueous solution. The percentage in side menu indicates the percentage of TTB into the gel composition.

In the previous section (4.1) it has been observed that the relaxation time for the fast phase for the formation of vesicular bilayer with octanol was $\tau_1 \sim 5$ Min and that for the slow phase was $\tau_2 \sim 59$ Min. After addition of metal precursor to the vesicular gel composition it has been observed that the relaxation time for the fast phase τ_1 is gradually increasing with increasing the concentration of TTB moiety (see figure 4.2.10); but for the slow phase, the effect is not so systematic. According to assumption, relaxation time for the fast mode is related to the solubilization of organic phase into micellar solution to form vesicular bilayers. The increase in τ_1 values with increasing TTB concentration indicates that metal precursor hinders the solubilisation of organic phase into micellar aggregate to form vesicular bilayer.

It can be mentioned here that initially the organometallic component was solubilized in octanol. When this organic solution has been spread into the aqueous micellar solution as an emulsion, two things happened simultaneously. Dissolution of originally present emulsion droplet into the micellar structure leads to decrease in turbidity. At the same time hydrolysis of TTB proceeds slowly when it comes into contact with aqueous phase of the system which leads to form a network of TiO_2 and that increases the turbidity again, though the contribution of TiO_2 within such a short time is very little compared to the dissolution of turbidity into micellar solution. As the concentration of metal precursor increases the hydrolysis process becomes more significant and hence overall the fast process takes longer time.

4.3 Oleic acid/ C₁₀TAOH System

4.3.1 Phase behaviour

Phase behaviour of the ternary system, oleic acid/ decyltrimethyl ammonium hydroxide [DTAOH (C₁₀TAOH)]/ water has been studied and a phase diagram has been drawn on the basis of visual observation which is depicted in figure 4.3.1. The present work first reports on detailed investigation of dilute oleic acid / C₁₀TAOH in aqueous medium, focusing particularly on the composition dependency of the vesicle formation. It was observed that in lower concentration range, vesicles were formed when half of the molecules in vesicular bilayer were present in anionic form and half of the molecules are in cationic form which has also been observed in many other systems²¹¹⁻²¹³. And most of the experimental work was oriented to identify and characterize this vesicular isotropic region.

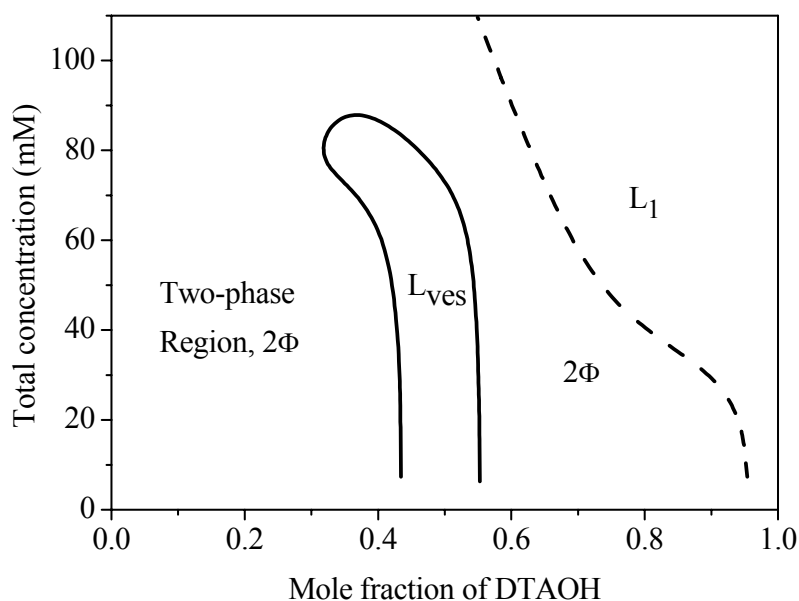


Figure 4.3.1: Phase diagram for the ternary system oleic acid/ decyltrimethyl ammonium hydroxide/ water at 25°C. The total concentration of two surfactant solutions is plotted as a function of mole fraction of DTAOH in the mixture.

The phase diagram presented in figure 4.3.1 reveals the physical state of the mixed surfactant system visually observed after keeping the samples undisturbed for one week in a thermostat

at 25°C. Such a long equilibration time was necessary, since the separation of two phases system often required several days. The phase behaviour for the ternary system has been studied up to the total concentration of 100 mM, since it was observed that system does not form vesicular isotropic phase at this concentration with any composition. The binary system, DTAOH and water, forms a visually transparent and isotropic solution. On gradual addition of increasing amount of oleic acid to this DTAOH solution the system starts to transform from isotropic solution phase to two phases region and this transition is strongly concentration dependent. The system became phase separated with a composition of DTAOH: OA = 9.5:0.5 when the total concentrations were 10 and 25 mM. On the other hand, system can accommodate more amount of oleic acid in L₁ phase without making phase separation (see figure 4.3.1) when the concentration was ≥ 50 mM. At lower concentration aqueous DTAOH was like a solution where all the DTAOH molecules were either ionized or isolated, consequently it could not accommodate oleic acid molecules, a fairly insoluble component in aqueous medium. But at higher (50 mM) concentration the mixed system has a little micellar aggregation, so it can solubilize some oleic acid molecules and probably this is the reason of shifting of tie line to make broader L₁ phase at higher concentration. It can be mentioned here that the cmc of DTAOH is measured as 69.3 mM (see table 4.3.1). The physical appearance of two-phase region was looking like a thin oily layer (mostly oleic acid) was floating on the isotropic layer. As the mixing composition of two surfactant-components approaches closer to 1:1 ratio the lower isotropic layer produces partial turbidity. Formation of bigger aggregation which can scatter light is, maybe, the probable cause for this partial turbidity in lower and bigger layer. When the composition of combined system reaches 1:1 mixing ratio, from the low concentration (10 mM), up to 50 mM, system forms a single phase with white-bluish turbidity which is a characteristic feature of vesicle phase^{173, 214}. Dynamic light scattering and cryo-TEM measurements indicate that the single phase solution with 1:1 mixing ratio of two surfactants is a vesicular solution. Oleic acid is fairly insoluble in water at 25°C. However the addition of more acid component that means, moving towards the acid rich direction made the system phase separated again.

It has been observed in many cases that the vesicles are formed spontaneously when oppositely charged surfactants are mixed together in an aqueous medium. This finding is a direct consequence of strong interaction between oppositely charged head-groups in surfactant aggregates. The effective neutralization of adjacent-lying head-groups reduced the repulsion between head-groups and as a result, the effective surfactant packing parameter

becomes higher. So, the effective neutralization appears when two oppositely charged surfactants mixing composition is 1:1. Interestingly in the present investigation it was observed that the spontaneous vesicles are formed when the composition was exactly 1:1 in the region of lower concentration.

The surprising effect of shifting the L_{ves} phase region from 1:1 composition to the acid rich mixture is observed when the total concentration of surfactants raised more than 50 mM. In this concentration range more acid was accommodated in L_1 phase, i.e. the tie line between L_1 phase and biphasic region was shifted towards more acid rich composition. The composition of isotropic vesicular phase moves towards acid rich direction indicates that more acid molecules can be accommodated into the vesicular bilayers at higher total concentration. This observation is supporting the pH measurement. The extension of vesicular region in phase diagram towards anion rich composition indicates that vesicles become stabilized when it is partially charged.

4.3.2 Surface tension and the Gibbs molecular area

Among the available methods that can be used to estimate the critical micellar concentration (cmc), the surface tension method is versatile not only because cmc can be determined from the plot of surface tension versus logarithmic concentration but also because one can get information on the nature of adsorbed layer at the air/water interface²¹⁵. A typical plot of surface tension versus log concentration for aqueous solutions of DTAB is shown in figure 4.3.2a. The surface tension values decrease almost linearly with log C (concentration) and show a characteristic break and remain constant thereafter. This break point corresponds to cmc value. No minimum around this break point indicates the purity of the surfactant.

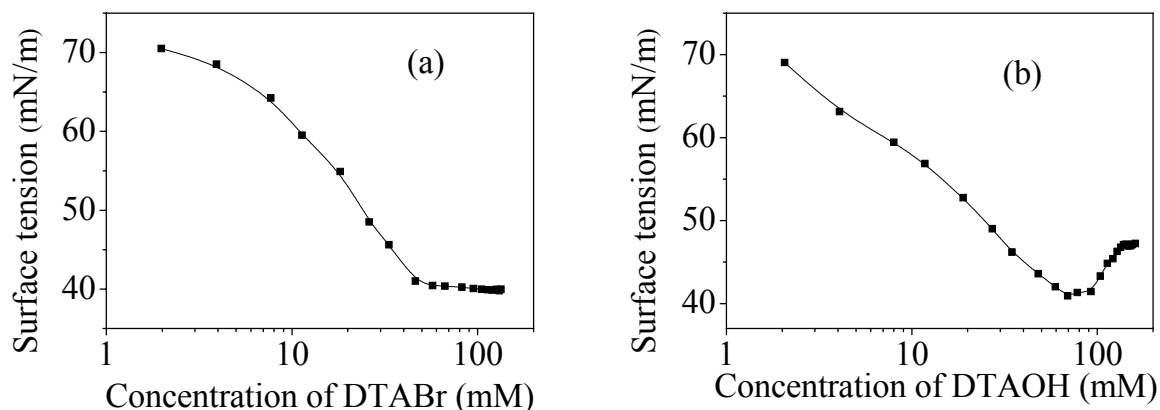


Figure 4.3.2: Surface tension of surfactants as a function of their concentration. Figure (a) illustrates the surface tension profile of DTAB solution in water where one can find no minimum indicating the purity of surfactant. Figure (b) reveals the surface tension of DTAOH solution which was prepared from the above DTAB solution by ion exchanged method.

To estimate the cmc value of freshly prepared DTAOH solution, same procedure was followed like DTAB. But in this case a deep bump was observed at the bottom of surface tension versus log C plot (see figure 4.3.2b). The precaution in careful preparation of DTAOH suggests that there should not be much impurity in the extracted solution. It can be thought that some DTAB may be eluted through the ion exchange column without any exchange reaction with resin matrix, if the efficiency of the column is not enough. To check the presence of DTAB or any impurity, another surface tension measurement was performed for the solution with 70% extracted DTAOH solution mixed with 30% DTAB solution. The result of this experiment compared with pure DTAOH solution is displayed in figure 4.3.3.

In this figure one can easily observe that the presence of 30% added DTAB produced smaller bump compared to the collected pure DTAOH solution. This result indicates that the presence of DTAB or any other impurity may not be the reasonable cause for this deep pronounced bump. Figure 4.3.2(b) shows that the surface tension values decrease almost linearly with log C and after a minimum value it increases with log C and makes a deep bump and after a certain concentration it remains constant. The strong intermolecular hydrogen bond between two adjacent surfactant molecules through OH group is, maybe, the reason for this increase in surface tension after minimum value.

The DTAOH solution is comparatively more dissociative in nature and thus increases the electrostatic repulsion between head-groups, consequently increasing the cmc value as well as the surface area per surfactant head-group. The value of A_m (0.5 nm²) thus obtained is very small and indicates the generation of bilayer structures in dilute aqueous solution ²¹⁶. Similar values of A_m for other surfactants which form bilayer phases, for example, egg phosphatidylcholine ($A_m = 0.72$ nm²)²¹⁷ and *n*-alkylbetains ($A_m = 0.6$ nm²) ²¹⁷ have been reported. However, the A_m value of DTAB (0.4 nm²) is calculated and observed almost identical with DTAOH. This implies that the curvature of the aggregates of both the surfactants would be similar. All the surface properties including Γ_m , and A_m values are summarized in table 4.3.1.

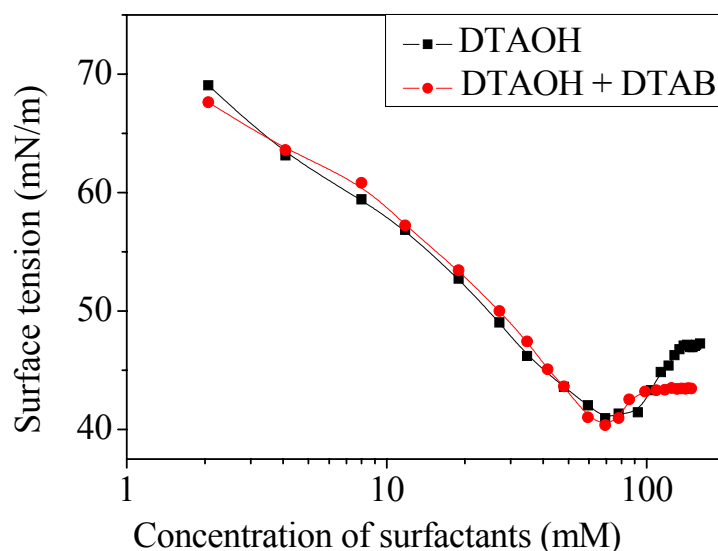


Figure 4.3.3: Surface tension of surfactants as a function of their concentration. The black line implies the surface tension profile of pure DTAOH solution, as collected from the ion exchange column and the red line expresses the surface tension of a mixture of aqueous solution containing 70% DTAOH and 30% DTAB.

Table 4.3.1: Surface and self aggregation properties of DTAB and DTAOH in aqueous solution

Surfactant	cmc (mM)	γ_{cmc} (mN/m)	Γ_m (mol/m ²)	A_m (nm ²)
DTAB	57.2	40.5	4.6e-3	0.4
DTAOH	69.3	40.9	3.3e-3	0.5

4.3.3 Turbidity Measurements

It was observed from the phase diagram that the mixing composition of 1:1 of two surfactants DTAOH and oleic acid produces an isotropic vesicular region and the phase is partially turbid. The turbidity appears because of the scattering of light by the vesicular aggregation of the surfactants. The extent of turbidity depends on the size and population of vesicles. The scattering result indicates that turbidity depends largely on the total concentration of the system. Transmittance was measured in this investigation instead of absorbance, since it was assumed that a part of the incident light is transmitted and rest of the light is not absorbed by the system, because light attenuation was caused by light scattering not by genuine absorbance. The relationship between turbidity and absorbance is ²¹⁸, $\tau = 2.303A/l$ where A stands for absorbance and l is the path length of the sample through which light passes.

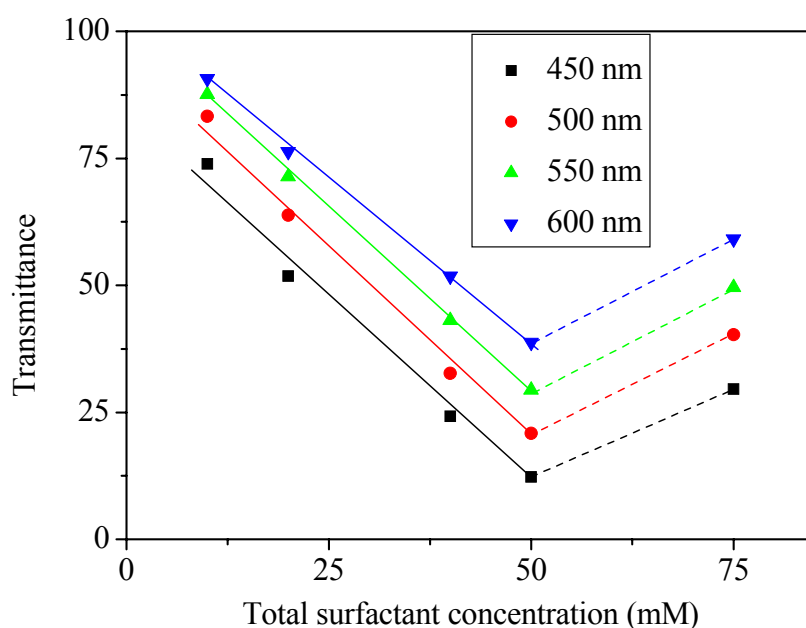


Figure 4.3.4: Transmittance of vesicular isotropic phase of DTAOH/ oleic acid/ water system at different wavelengths as a function of total concentration of surfactant mixture with vesicular composition. The mixing composition of all the samples was 1:1 except 75 mM solution; for this solution (75 mM) the mixing composition was $X_{DTAOH} = 0.4$.

The turbidity of the samples with vesicular composition (DTAOH: oleic acid = 1:1) was measured at different concentrations and wavelengths and the results are illustrated in figure 4.3.4. The results indicate that turbidity increases and hence transmittance decreases initially

with increasing total concentration of surfactants. This can be explained on the basis of the size of the vesicles. The size of vesicles increases as the total concentration of surfactants increases and this result is in good agreement with DLS result which also shows that hydrodynamic radius increases with increasing the concentration up to 50 mM. The calculation explores that transmittance decreases about four times when the total concentration of surfactants was raised from 10 mM to 50 mM and this is caused by the intense scattering of light by bigger aggregation.

One can see from the figure 4.3.4 that the transmittance of vesicular solution at 75 mM total concentration with composition $X_{\text{DTAOH}} = 0.4$ is a little higher than 50 mM solution with equimolar composition. For 75 mM concentration, equimolar composition was phase separated (see phase diagram); as a consequence a different composition, but with vesicular morphology was chosen for the measurement. The increased concentration of oleic acid in vesicular bilayer might be a reason for the reduction of turbidity of the solution. With higher acidic composition the vesicles become charged and their electrostatic repulsion plays a potential role for the solution being clear. It may be explained on the basis of vesicle size too. DLS results showed that hydrodynamic radii of vesicles are smaller when the concentration of solution was 75 mM with $X_{\text{DTAOH}} = 0.4$ composition (see table 4.3.2). Smaller size of vesicles can scatter less light and hence the turbidity decreases.

4.3.4 Conductivity and pH Measurements

In order to monitor the composition of vesicular aggregation of DTAOH and oleic acid from the electrical conducting point of view, pH and conductivity of a series of samples were measured, since it is known that the vesicular aggregation decreases the conductivity drastically. The samples were prepared and kept in a thermostat at 25°C for a week for equilibration. Then pH and conductivity were measured at room temperature at 23°C, when the samples were completely in rest. No stirring or agitation was performed during the measurement. The results of pH and conductivity measurements were displayed in figure 4.3.5. One can see in the figure 4.3.5(a) that the conductivity of pure DTAOH is very high. This high conductivity indicates that the dissociation constant of DTAOH is high and fast diffusive counter ion, OH⁻ is the reason for this high conductivity. Another point of this high conductivity is the concentration of measured solution is below the cmc value. On addition of oleic acid to this DTAOH solution conductivity decreases sharply till the composition reached

1:1. This sharp decrease in conductivity can be explained on the basis of two phenomena: (1) reduction of concentration of counter ions by the neutralisation reaction between two counter ions OH⁻ from DTAOH and H⁺ from oleic acid and (2) trapping of some counter ions into vesicular aggregation. Beyond this 1:1 composition, the conductivity does not increase again, since the solubility of oleic acid in aqueous medium is very less which can be seen from the conductivity of pure oleic acid solution in water. Figure 4.3.5(b), on the other hand, illustrates the conductivity and pH of vesicular phase only. One can easily see here, the conductivity increases with increasing the total concentration of surfactants up to 50 mM, since the number of counter ions are also increasing with concentration. This result suggests that highly dissociating DTAOH is not completely neutralized by acid at this composition and fast diffusive counter ion OH⁻ might be the reason of this high conductivity. On the other hand, the conductivity of vesicular solution at 75 mM total concentration with a composition of $X_{\text{DTAOH}} = 0.4$ resulted a little less conductivity (see figure 4.3.5b). A different composition was chosen for the measurement, since it was observed that 1:1 composition was phase separated at this concentration (75 mM). This indicates that 1:1 composition for vesicular phase has higher conductivity than that of anionic rich composition. This implies that most of the OH⁻ ions are neutralised at the acid rich composition and the system did not produce enough H⁺ ion, because of the low dissociation constant of oleic acid which can be seen from the conductivity of pure oleic acid solution.

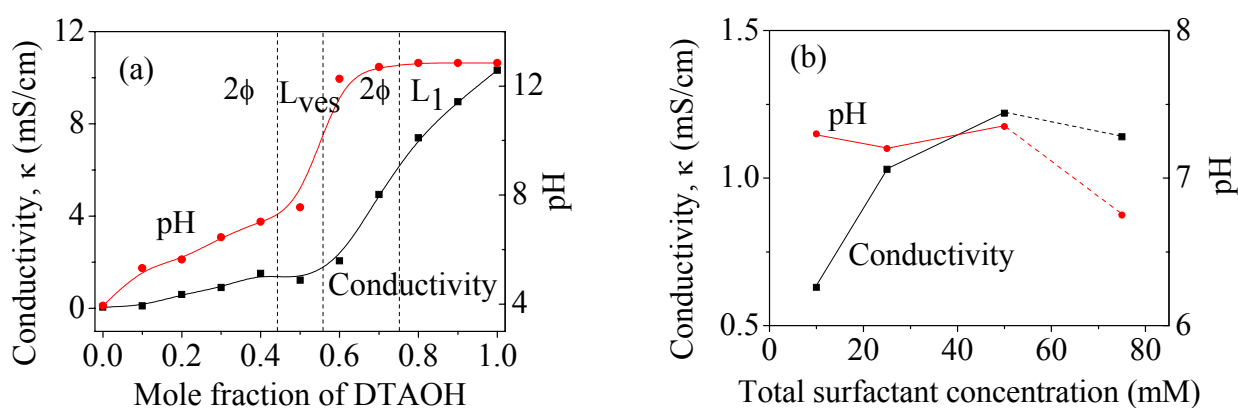
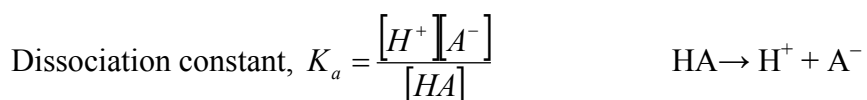


Figure 4.3.5: pH and conductivity of DTAOH/ oleic acid/ water system. Figure (a) illustrates the pH and conductivity of aqueous mixture of DTAOH and oleic acid at different compositions as a function of their mixing ratio at 50 mM total concentration. Figure (b) expresses the pH and conductivity of vesicle phase as a function of surfactant concentration. Solution compositions for vesicular phase were always 1:1 except 75 mM; for this solution composition was $X_{\text{DTAOH}} = 0.4$

There is no direct relationship between conductivity and pH. The conductivity of solutions depends on the concentration of ions in solution, their charges and their speed of diffusion. The pH, on the other hand, specifically tells the concentration of one particular ion, H⁺ in the solution and also indirectly the concentration of OH⁻ ions. This by itself does not uniquely specify the conductivity of the solution, because it does not tell anything about the presence of other ions that may affect the electrical conductivity, or about the speed of diffusion. But in the present investigation, one of the components was weak acid and the other was comparatively strong base; their degree of dissociation can influence the pH of the solution and conductivity as well.

Figure 4.3.5(a) reveals the trend of pH of 50 mM solution with different mixing ratios of DTAOH and oleic acid. Pure aqueous oleic acid shows the pH about 4, indicating the low degree of dissociation in water.



where A⁻ stands for oleate ion. The pH of the solution increases with increasing the mole fraction of DTAOH in the composition. The pH of the solution is more than 7 when the composition of solution is 1:1. This indicates that some oleic acid molecules in vesicle bilayers may remain un-dissociated. Figure 4.3.5(b) expresses the changing pattern in pH and conductivity in vesicular region with total concentration of surfactants. The pH of the vesicle solutions was always a little more than 7 when the composition was 1:1; but pH was a little less than 7 for vesicular composition when the total concentration was 75 mM solution. The composition of this solution was acid rich (X_{DTAOH} = 0.4) indicates that there are some H⁺ ions free in the solution and the source of which are obviously oleic acid.

4.3.5 Microscopic Observation

In cryo-TEM investigations well-defined unilamellar vesicles were observed in the system of total concentration of 25 mM and 50 mM DTAOH and oleic acid with a composition of 1:1 mixing ratio and the micrographs are depicted in figure 4.3.6. The slides of micrograph illustrate that the vesicles are almost spherical in shape and the diameters are ranging from 100 nm to 200 nm. This indicates that small and large vesicles are coexisting in the samples and this is supporting the results observed from dynamic light scattering measurement. One can observe in the cryo-TEM images that only unilamellar vesicles are present in the system.

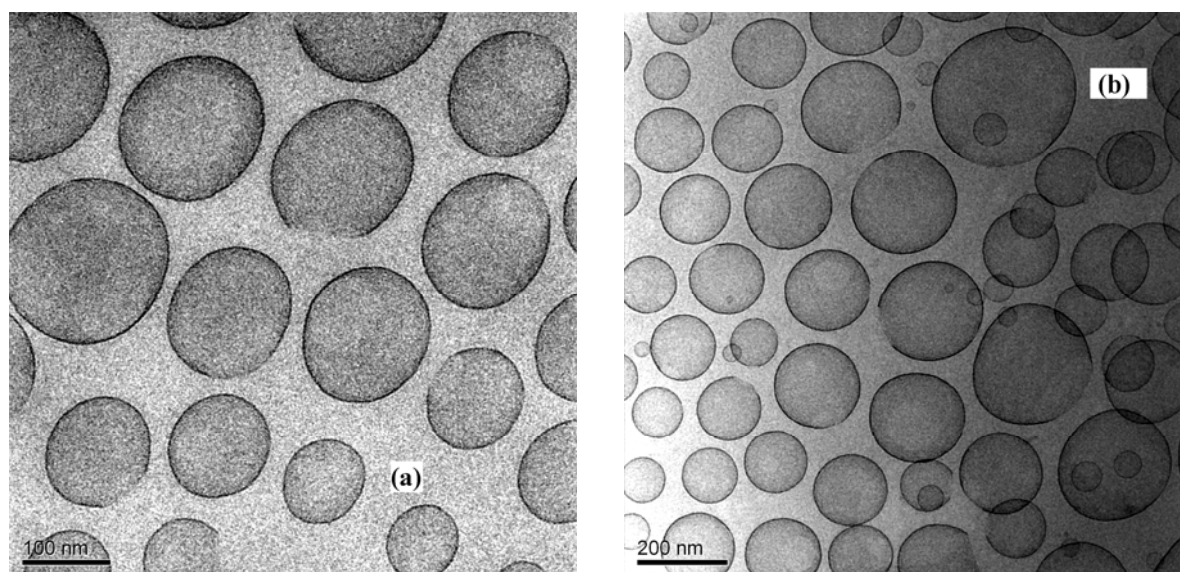


Figure 4.3.6: Cryo-TEM micrographs from the samples of DTAOH and oleic acid with a mixing ratio of 1:1. Figure (a) is a micrograph of 25 mM total concentration and (b) is that of 50 mM total concentration. The bar length underlying at the bottom of the images corresponds to 100 nm and 200 nm for (a) and (b) respectively.

An observation triggered extensive studies of the nature and occurrence of such vesicular structure in different parts of the vitrified specimen under the TEM, but no significant changes in morphology was observed. This indicates that the mixing composition of 1:1 between DTAOH and oleic acid in L_{ves} region produces unilamellar vesicles.

Three main themes will be presented here: (a) Morphology of vesicular particles formed from dispersed micellar aggregates, (b) Perforated bilayers, their structure, nature and formation, and (c) Spontaneous formation of vesicles in a mixture of oppositely charged surfactants i.e. catanionic vesicles.

In addition to the regular shaped vesicles, some perforated vesicles were also observed in different zones where vesicles are open. Typically vesicles were seen as dense-complete rings in the micrographic projection. But in some cases it is observed that the objects are spherical but the rings are not completely closed. A part of the ring is missing and that makes the vesicles open. One can see such vesicles in figure 4.3.7.

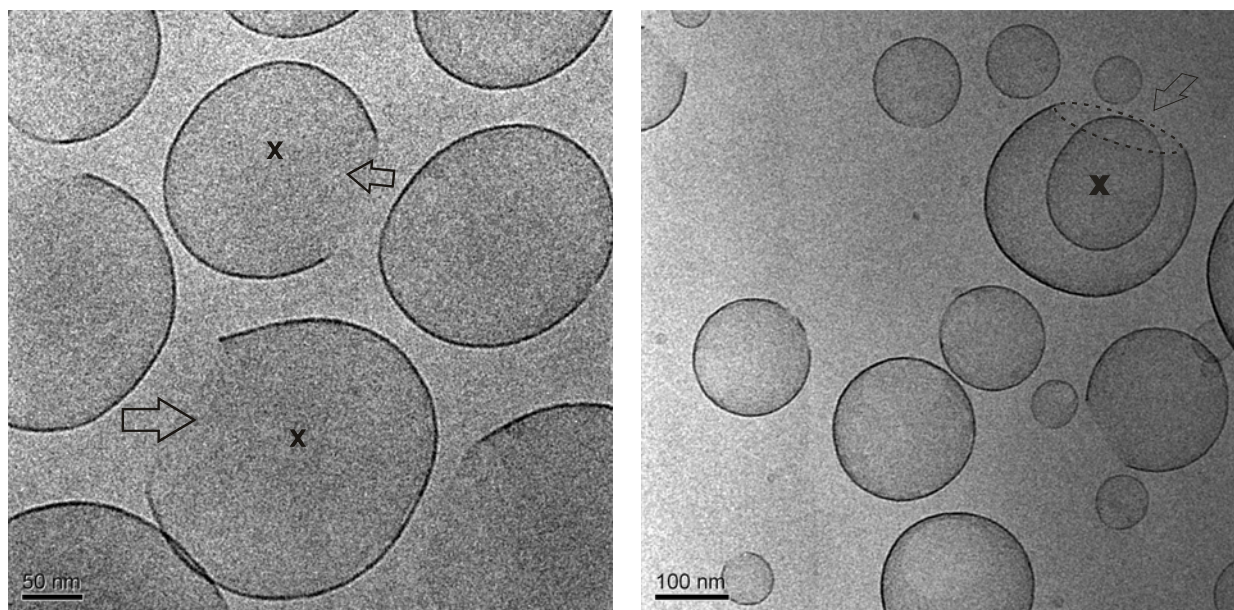


Figure 4.3.7: Cryo-TEM images of vitrified specimen of DTAOH and oleic acid with a mixing ratio of 1:1. In the first image (left) one can see that two well-shaped vesicles (x-denoted) are open (indicated by arrow). In the second image (right) one can easily see that a bigger vesicle (x-denoted) is open (arrow signed) and a smaller vesicle entered into that bigger one through that opening.

If a defect or missing in vesicular ring is positioned in the perimeter of the vesicle with respect to the incident electron beam, it is easily visible in the projection as seen in figure 4.3.7. On the other hand, if the defect is inside the projected area, it will be barely visible due to the low contrast. The structural changes observed in figure 4.3.7 as compared to figure 4.3.7 cannot be ascribed to an instability of the vesicles because the images are taken from different part of the same vitrified film. This indicates that most of the vesicles are well-shaped and very stable, but some of them are open. In fact, such micro-structural changes are typical of membrane solubilization by a surfactant²¹⁹. Walter et al²¹⁹ described that the vesicles seem to have undergone lysis-type reaction producing structures similar to the intermediate structures observed in the vesicle-to-micelle transition in detergent-lipid system. The temporal evolution of the lysis reaction of surfactants depends critically on reaction condition; even a variation of stirring condition can play a significant role²²⁰. From a thermodynamic point of view it is frequently claimed that the catanionic vesicles are stable towards induced conversion because equimolar mixtures of cationic and anionic surfactants may form a lamellar mesophase. But if one component is insoluble (here oleic acid), the system becomes more complex.

In addition to this equilibrium consideration, it is important to recognize that the activity of oleic acid can induce energetic change within a single vesicle leading to a structural instability of the individual vesicle, since the pure acid is fairly insoluble in aqueous medium. The acid is solubilized inside of vesicular bilayers because of the interaction with DTAOH and the presence of polar head group in the molecule. First of all, the activity of acid on the exterior of a vesicle may alter the spontaneous curvature of the vesicular bilayer due to the asymmetric change in molecular composition of the two constituting monolayers of the vesicles. Second, the physical stability of the vesicle may be modified by a coupling between local composition of the bilayer and local curvature of the bilayer. Budding and fission processes may be initiated by such type of couplings, for example, from a local enrichment of oleic acid on the outer monolayer which needs more energy to stay there because of its insolubility in aqueous medium and the segregation of DTAOH from the corresponding region of the vesicle. This indicates that coupling of two different surfactants can play a crucial role in forming bilayers where vesicles remain intact. It is well-known that curvature and thermotropic phase state of vesicles modulate the susceptibility of vesicles to undergo structural changes²²¹. This indicates that the rim of the open-mouth of vesicles may have a composition that is different from the intact part of the vesicular bilayers. Almgren²²² observed such result for other system by NMR analysis with labeling investigation.

Size distribution of vesicles, mean diameter and polydispersity are important experimental parameters describing a colloidal dispersion. For self assembled structures such as equilibrium vesicles, the size distribution is intimately related to characteristic bilayer parameters including the spontaneous curvature^{186, 223} and the Helfrich elastic moduli^{46, 182}. A quantitative size distribution is necessary to apply theoretical methods relating equilibrium vesicle size distributions to fundamental bilayer elastic parameters¹⁸⁶. The size of equilibrium vesicles are determined by a subtle competition between the entropy of vesicles, surfactant mixing and the curvature elasticity of the bilayers^{182, 224, 225}. The vesicle size distribution can be expressed by equation (4.1) where R_0 and K are the radius of the vesicles with minimum curvature energy and the effective bending constant respectively. A consequence of equation (4.1) is that vesicles with $K \sim k_B T$ have much broader size distribution than vesicles with $K \gg k_B T$.

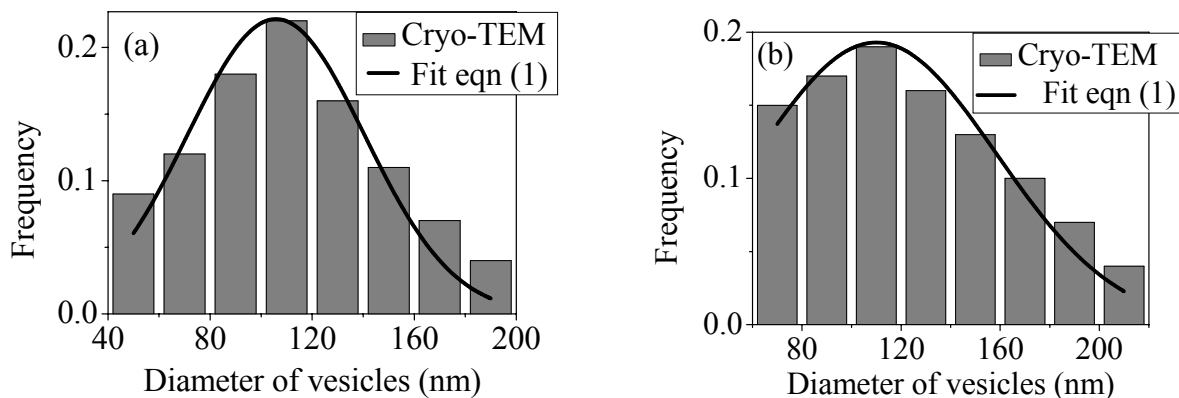


Figure 4.3.8: Vesicle size distribution is plotted in a histogram for the system of DTAOH and oleic acid system with 1:1 mixing composition. Figure (a) is for the total concentration of 25 mM and (b) is for the 50 mM solution.

To extract the value of R_0 and K in equation (4.1), one option is to determine the vesicle size distribution by cryo-TEM. A histogram for the size distribution of vesicles is built up by measuring the size of about 1000 and 1500 vesicles taken from different slides of micrograph of cryo-TEM images at the total concentration of 25 and 50 mM respectively. Figure 4.3.8 shows the distribution of outer vesicle diameter of vesicles prepared from the samples with a composition of DTAOH: OA = 1:1. Consistent with thermodynamic predictions, the distribution is unimodal and roughly Gaussian.

A best fit of equation (4.1) to the histogram built for the size distribution of classified vesicles of total surfactant concentration 25 mM (figure 4.3.8a) results in $K = \kappa + \bar{\kappa}/2 = 0.25 \pm 0.03 k_B T$, the sum of the Helfrich mean (κ) and Gaussian ($\bar{\kappa}$) curvature moduli, and $R_0 = 110 \pm 10$ nm, the spontaneous radius of curvature for vesicles with a reduced chi test = 0.0007; but the fit for 50 mM (figure 4.3.8b) reveals the result in $K = 0.17 \pm 0.02 k_B T$ and $R_0 = 120 \pm 10$ nm with the reduced chi test = 0.0003. The uncertainty in R_0 is quite high when working with such broad distributions, because the model is only weakly sensitive to R_0 ¹⁸⁷. Similar values of K ($0.15 \pm 0.03 k_B T$ ¹⁸⁷ and $0.7 \pm 0.2 k_B T$ ¹⁸⁶) for other surfactant systems which form vesicles have been reported. These results reveal that the effective bending constant K is comparatively higher for the system with lower surfactants concentration and that makes the vesicles smaller in size which is indicated by R_0 value. These results are very good in agreement with the result obtained from DLS measurements which explores that hydrodynamic radius increases with increasing the total concentration of surfactants when the mixing composition was 1:1.

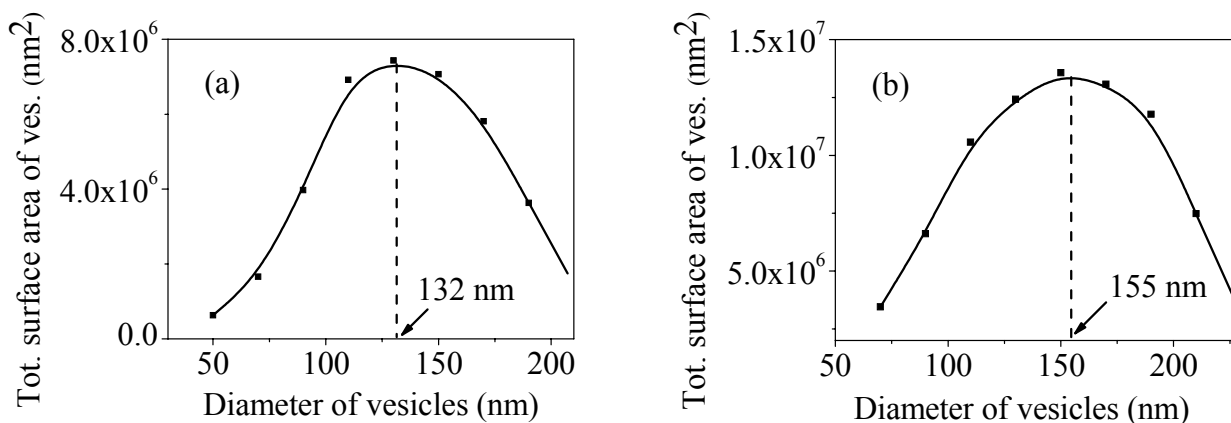


Figure 4.3.9: Total surface areas of classified vesicles formed by the interaction of DTAOH and oleic acid with a mixing composition of 1:1 against the diameter of vesicles. Figure (a) expresses the total surface area distribution of classified vesicles when the concentration was 25 mM, whereas (b) illustrates the total surface area distribution when the concentration was 50 mM.

Total surface area of classified vesicles was calculated on the basis of their vesicle size distribution and plotted against their diameter (see figure 4.3.9). The results reveal that the higher concentration (50 mM) produces much higher (about 24.6% by surface area) outer vesicular bilayer surface area compared to 25 mM solution. Because of this increased vesicular concentration and bigger vesicle size, the solution becomes more turbid with higher surfactant concentration and that is clearly revealed in turbidity measurements. The number averaged vesicular size distribution is plotted against their diameter in figure 4.3.8, and the integral of the surface area of classified vesicles is plotted against their diameter in figure 4.3.9. For both the concentrations one can easily see that the diameter of maximum population, R_0 shifted towards higher values (110 nm to 132 nm for 25 mM and 120 nm to 155 nm for 50 mM) when the integral of vesicular surface area is plotted against their diameter. These results illustrate that the number of vesicles in smaller diameter range is higher than that from bigger diameter range which can easily be seen in Figure 4.3.8.

4.3.6 Dynamic Light Scattering

To check the size of vesicular dispersion in the partially bluish isotropic phase exposed in phase diagram, dynamic light scattering measurement was performed at 25°C. The time-

dependent correlation function of the scattered light intensity was measured at a scattering angle of 90°. The measurements and analysis of the data indicate that the partially turbid phase has the vesicular aggregation. The average vesicle diameter was obtained with the cumulant analysis. The results obtained by this cumulant analysis are presented in table 4.3.2. Although the hydrodynamic radii (R_h) of the vesicles are slightly greater than those obtained from cryo-TEM measurement, these results indicate that the presence of some large vesicles skewed the results towards larger radius.

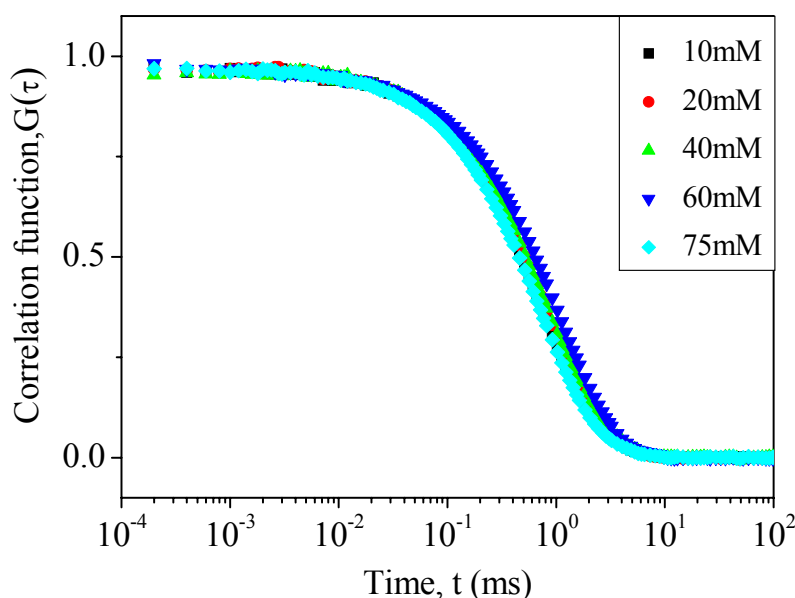


Figure 4.3.10: Normalized intensity correlation function is plotted against time for different concentration of surfactant solutions at 25°C and at a fixed angle of 90°. Figure represents the correlograms at different concentrations indicated in the inset and at a composition of 1:1 except 75 mM. For this (75 mM) solution the composition was $X_{\text{DTAOH}} = 0.4$, since 1:1 was phase separated.

In the DLS experiment, the temporal fluctuations of the scattered intensity, which are due to the particle's Brownian motion, have been analyzed by estimating the normalized temporal autocorrelation function of the scattered light. Figure 4.3.10 shows the normalized intensity correlation function at different concentrations and compositions of surfactants at the temperature of 25°C and scattered angle of 90°. The shape of the correlation function in the figure illustrates that the decay time for the aggregated particles is significantly large. This indicates that the diffusion of particles is slow which implies that comparatively bigger particles are present in the system.

The picture that emerges from this investigation is that the system has polydispersity which becomes clearer from the figure 4.3.11. This figure brought out the result that the system is not decaying linearly which is a sign of polydispersity. So, a cumulant analysis of the intensity autocorrelation function^{156, 226} resulted an apparent diffusion coefficient from the first cumulant and a polydispersity index from the second cumulant. A plot of the correlation function versus time is shown in figure 4.3.11.

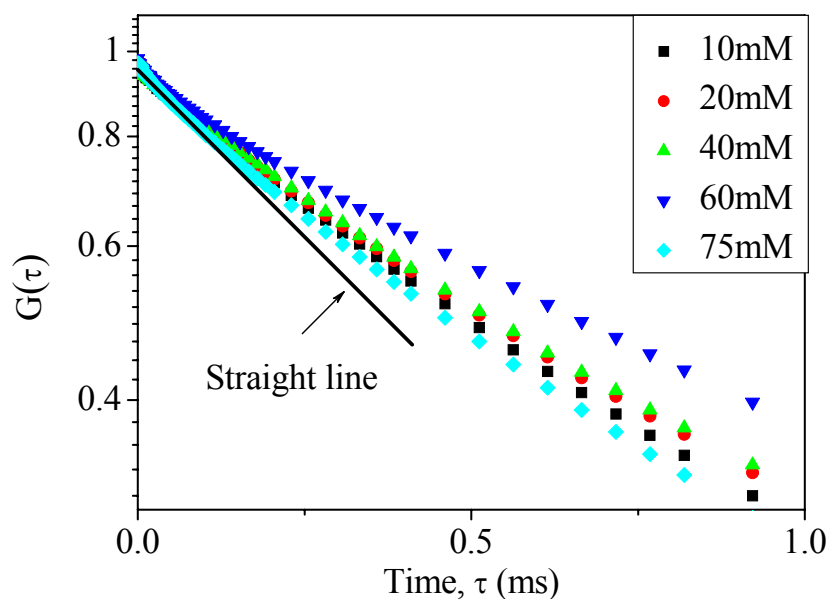


Figure 4.3.11: Correlation function $G(\tau)$ for the vesicle system is plotted against time for different concentration of surfactant at 25°C and at a fixed angle of 90°. Note that, no sample is decaying linearly and this is an indication of presence of polydispersity in the samples.

Figure 4.3.11 shows the normalized correlation function data (at a scattering angle of 90°) at five different concentrations of DTAOH/ oleic acid/ water system. This figure clearly reveals that the correlation functions do not decline linearly with time indicating the presence of polydispersity. Indeed, a relatively high poly-dispersity index (~ 0.43) was recorded in DLS measurement of with 10 mM solution (see table 4.3.2).

Table 4.3.2: Relaxation times, diffusion coefficients and hydrodynamic radii of aqueous mixture of DTAOH and oleic acid for the vesicular region in phase diagram*

DTAOH: OA	Decay time (ms)	Diffusion coeffic. (m ² s ⁻¹)	Hydrodynamic radius (nm)	Polydispersity index
1:1 (10mM)	1.85	2.43e-12	100.8	0.43
1:1 (20mM)	2.22	2.37e-12	103.4	0.42
1:1 (40mM)	2.32	2.25e-12	108.9	0.4
1:1 (60mM)	2.43	2.14e-12	114.5	0.39
4:6 (75mM)	1.74	2.66e-12	92.1	0.4
8:2 (100mM)	0.1	3.09e-11	7.9	

- A total concentration of 100 mM with a composition of 8:2 is also measured to see the micelle size of L₁ isotropic phase.

The diffusion coefficients corresponding to the initial slope of the decay of correlation functions and the hydrodynamic radii are summarised in table 4.3.2. It was observed that the values of slope of decay were increasing with increasing the total concentration of surfactants with composition of 1:1 (see figure 4.3.12a). This indicates that the diffusion of particles becomes slower with higher concentration. The diffusion coefficient, D values are in the range of $\sim 10^{-12}$ m²s⁻¹ which is much smaller than that of normal spherical micelles²²⁷ for which the diffusion coefficient is of the order of $\sim 10^{-11}$ m²s⁻¹. It was also observed in the present investigation for the L₁ phase that the diffusion coefficient is of the order of $\sim 10^{-11}$ m²s⁻¹ (see the table 4.3.2).

One can see from the table that the polydispersity index values are decreasing with increasing the total concentration of surfactants with 1:1 mixing composition; but the values are still very high. This implies that size distribution range is getting smaller with increasing the concentration. For 10 mM solution DLS measurements were performed at different angles, but no significant changes were observed. This indicates that the self-assemblies are smaller compared to wavelength of the radiation and the aggregates have spherical shape. This observation is qualitatively good in agreement with the result obtained from cryo-TEM method which showed that vesicles have spherical shape.

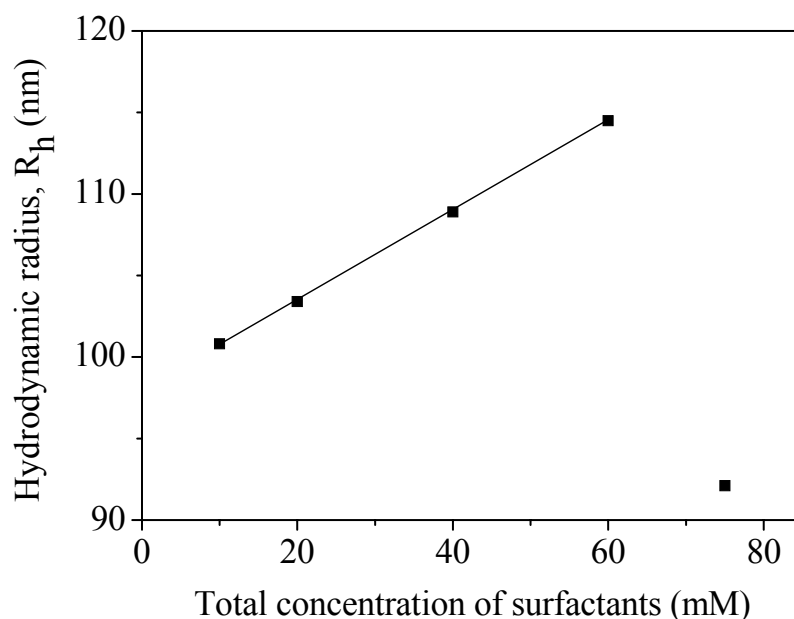


Figure 4.3.12: Plot of hydrodynamic radii, R_h of the self assemblies of DTAOH/oleic acid/ water system as a function of total concentration of surfactants with vesicular composition.

Figure 4.3.12 illustrates that the hydrodynamic radii of the vesicles increase with increasing the total concentration of surfactants when the mixing composition is 1:1. On the other hand, the radius of vesicles is smaller when the total concentration is 75 mM and the composition is $X_{\text{DTAOH}} = 0.4$. Because of the acid-rich composition the vesicles become charged and as a consequence the radius of the vesicles becomes smaller and hence it can diffuse faster than uncharged vesicles with 1:1 composition at lower concentration. The DLS measurements were performed after one week of sample preparation and equilibration at 25°C in a thermostat. These results are consistent with those obtained from other experiments results with respect to polydispersity and vesicular size distribution. The results of DLS studies thus confirm the presence of large vesicular aggregation in partially turbid phase.

4.3.7 SANS Analysis

SANS spectra of C₁₀TAOH/oleic acid system at different concentrations and vesicular compositions are shown in figure 4.3.13. The figure shows the scattering curves for the system at 25°C. The curves are characterised by a q^{-2} decay of the intensity at low and intermediate values of q , which is a signature of scattering from a bilayer structure²²⁸. There

is no minimum in the spectra as would be expected for a monodisperse or a little polydisperse population of vesicles of the size measured by light scattering.

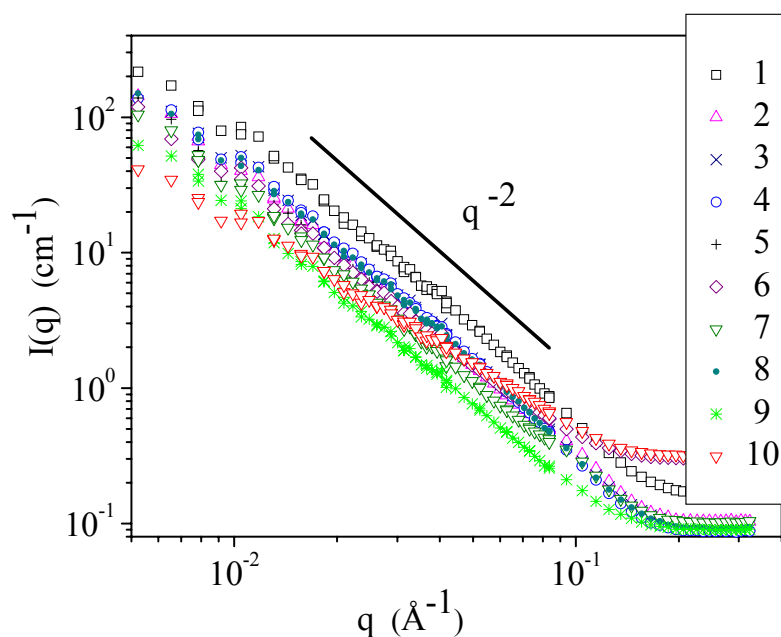


Figure 4.3.13: SANS spectra of C₁₀TAOH and oleic acid system in D₂O at 25°C. Samples were selected from the vesicular region in the phase diagram. The solid line indicates a slope of -2 .

The bilayer thickness was calculated by fitting the empirical data with a model for planar lamellae. It was observed from the extracted results of model fitting that the bilayer thickness is laying around 2.8 nm. The SANS behaviour of scattering from vesicle solutions and the dependence on size and polydispersity is well understood. On the basis of the sizes determined from light scattering, the minimum in the SANS scattering data should be observed in the explored q range if the vesicles were monodisperse. The spectra shown in figure 4.3.13 do not have this feature and therefore contain no information of the vesicle size.

4.4 Catanionic Systems

4.4.1 Phase Behaviour

The phase behaviour and microstructure of several catanionic systems have been explored in this study. The term catanionic surfactants have been coined to refer to a mixture of cationic and anionic surfactants. Mixtures of oppositely charged surfactants exhibit novel solution and interfacial properties. The interplay of electrostatic effects between head-groups and surfactant molecular geometry allows a rich diversity of phase behaviour. Recently, it has been observed that the catanionic mixtures consisting of almost identical cationic and anionic surfactant pair exhibit different phase behaviour between the anionic-rich and the cationic-rich region at high aqueous concentration^{15, 229, 230}. Phase diagrams were composed by studying a large number of different concentrations and compositions of two oppositely charged surfactants and the tie lines were drawn on the basis of visual observation.

Let us begin with the description of phase behaviour of the ternary system Na-oleate/ octyltrimethyl ammonium bromide (C₈TAB)/ water. The oppositely charged aqueous surfactant solutions were mixed together by vortexing (mechanical vibrating mixer) and kept in a thermostat at 25°C. The next day of preparation, the samples were vortexed again and kept them in the thermostat at 25°C for one week. During this time samples were completely in rest to have an equilibrium condition. After one week it has been observed that all the samples have clear, single and transparent phase within the study range of 10 to 200 mM total concentration. Although the pure anionic and cationic samples have almost water-like viscosity, but the viscosity of samples with concentration ≥ 50 mM and with compositions around 1:1 were increasing with increasing the total concentration. The most noticeable point is that no phase separation or transformation from one phase to another was observed.

On the other hand, it was observed for the Na-oleate/ decyltrimethyl ammonium bromide (C₁₀TAB)/ water system that samples have different phases depending on the composition of the mixtures. A phase diagram for the ternary system with C₁₀TAB has been drawn on the basis of visual observation at 25°C and the diagram is depicted in figure 4.4.1. The samples for all the systems have been prepared and treated as described in with C₈TAB system. It was observed from the phase transition that the system with C₁₀TAB showed much more complex

phase behaviour compared to C_8 TAB system. The binary systems, both pure anionic and cationic solutions, form a visually transparent and isotropic L_1 phase. Such solution is known as micellar (after exceeding the cmc) solution with spherical structure³⁴. It can be mentioned that the cmc values of C_8 TAB, C_{10} TAB, C_{12} TAB, C_{14} TAB and Na-oleate are 257.4, 64.6, 16.0, 3.6 and 0.9 mM respectively¹³⁴. On gradual addition of increasing amount of C_{10} TAB to the pure anionic solution (aqueous Na-oleate), when the total concentration was ≥ 25 mM, the system moved from an isotropic L_1 phase to a partially turbid and bluish L_{ves} phase at an equimolar mixing ratio of two component-solutions via a two-phase region. The formation of bigger aggregation which can scatter light is the probable cause for this partial turbidity of the L_{ves} phase. Further increasing the mole fraction of cationic component the system moves from L_{ves} phase to L_1 phase again via another two-phase region. This indicates that the system is transforming from one phase to another phase following the first order phase transition rule.

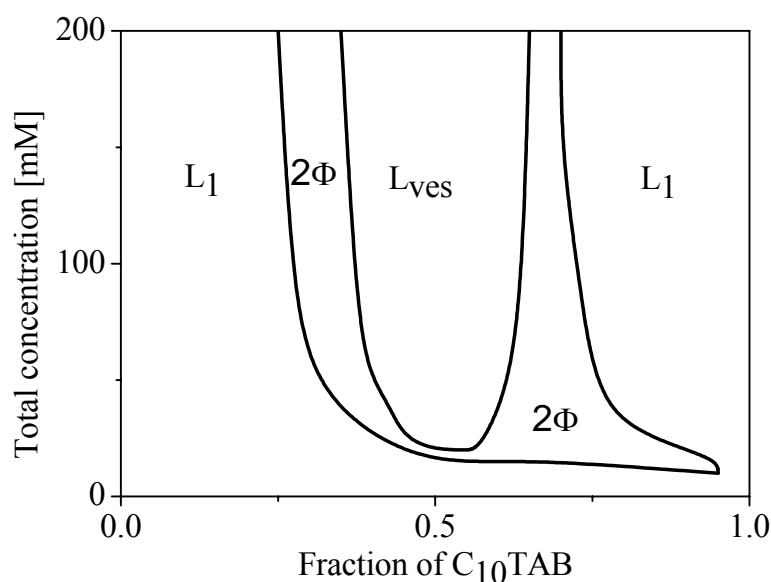


Figure 4.4.1: Phase diagram of ternary system of Na-oleate/ C_{10} TAB/ water at 25°C.

At 10 mM total concentration, samples at all mixing compositions of anionic and cationic components were isotropic and have either L_1 phase or an aqueous solution. The samples were phase separated when the concentration was raised to 15 mM and the compositions were about 1:1 and cationic rich; but no isotropic and partially turbid single phase (L_{ves}) was observed. On the other hand, when the concentration was raised to 25 mM, at the composition of $X_{C_{10}TAB} = 0.43$ the isotropic L_1 phase was transformed into a two-phase region where a narrow and dense turbid phase was floating on the partially turbid but comparatively clear phase. Shaking of the sample made the whole solution turbid. Further increasing the mole

fraction at $X_{C_{10}TAB} = 0.5$ a partially blue coloured single phase, L_{ves} phase, was observed which was very narrow region at this concentration. Such vesicular morphology is commonly observed at equimolar composition of two oppositely charged surfactants^{214, 231} and also in the previous study (see section 4.3). Continuous increasing the fraction of cationic component the system enters again into a two phase region at $X_{C_{10}TAB} = 0.58$. Further increasing the mole fraction of cationic component in the mixture the system entered into an isotropic L_1 phase when the composition was $X_{C_{10}TAB} = 0.9$. On increasing the concentration, the area of vesicular phase became a little wider, but it was following the same sequence of phase transition what was observed at 25 mM total concentration, as one can see in the figure 4.4.1. The phase behaviour of ternary system Na-oleate/ $C_{12}TAB$ / water has been investigated at 25°C and the phase diagram is presented in figure 4.4.2 as a function of concentration and composition of its constituting components. The phase sequence of the present ternary system was similar to the system with $C_{10}TAB$, as one can see in figure 4.4.1 and 4.4.2. In case of $C_{12}TAB$ it was observed that an L_{ves} phase was confined between two two-phase regions, which is similar to the system with $C_{10}TAB$, but the composition of the components for the L_{ves} phase is different for different systems. The position of L_{ves} phase for the system with $C_{10}TAB$ was an equimolar composition and its short surroundings. But the position of L_{ves} phase for the system with $C_{12}TAB$ has been shifted towards anionic rich region. At higher concentration of ≥ 150 mM, the equimolar composition forms a two-phase region which has not been observed for the system with $C_{10}TAB$.

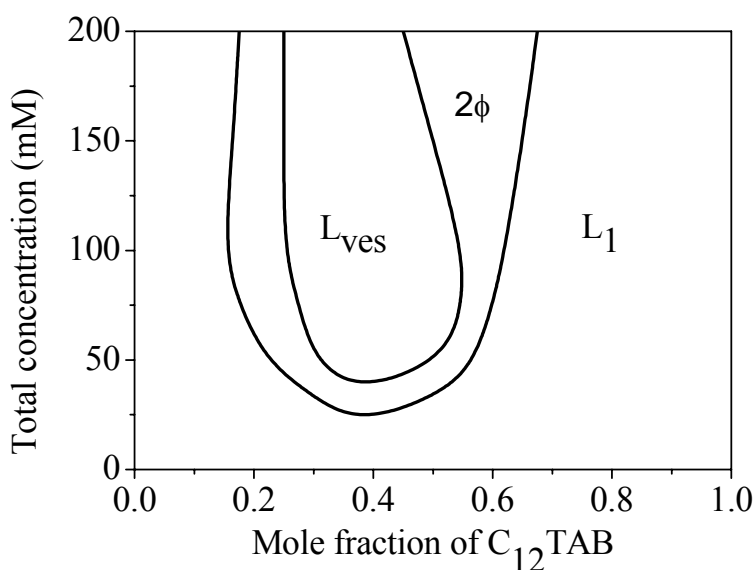


Figure 4.4.2: Phase diagram for the ternary system of Na-oleate/ $C_{12}TAB$ / water at 25°C.

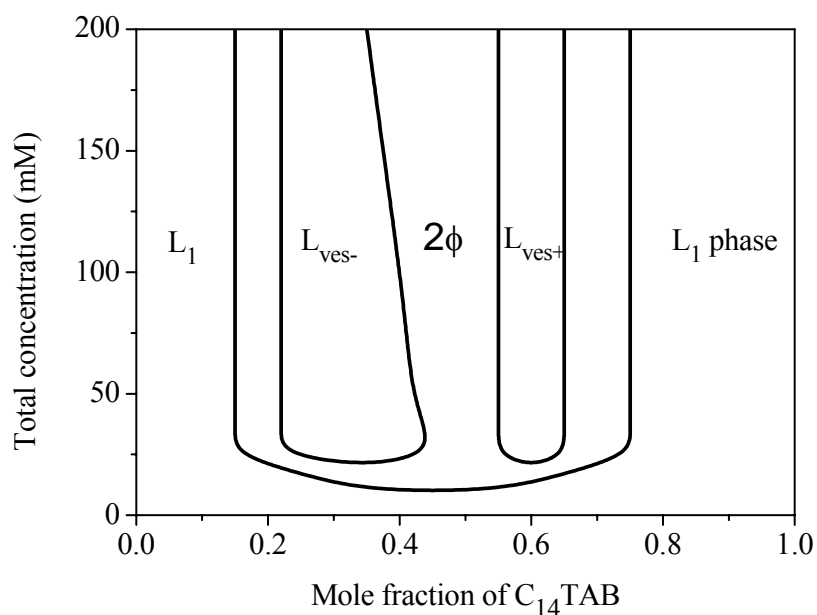


Figure 4.4.3: Phase diagram for the ternary system of Na-oleate/ C₁₄TAB/ water at 25°C.

Phase behaviour for the ternary system with C₁₄TAB has also been investigated at 25°C and the resulted phase diagram is plotted in figure 4.4.3. The phase diagram clearly illustrates that the aqueous Na-oleate shows completely different phase behaviour with aqueous C₁₄TAB than its homolog with shorter alkyl chain like C₁₀TAB and C₁₂TAB. In this case two L_{ves} phases were observed which were also separated by a two-phase region. The composition of one L_{ves} phase was with anionic rich and the other was with cationic rich, while the equimolar composition forms a two-phase region after exceeding certain concentration (10 mM). This is a typical phase diagram of catanionic system where equimolar composition forms precipitate or phase separate by the interaction of anionic components with an equal amount of oppositely charged cationic components^{15, 229, 230}. This indicates that equimolar mixing composition of oppositely charged surfactants with longer alkyl chain enhances the system to be crystallised via the charge neutralization of aggregate surface and consequently the system becomes phase separated. But moving towards a little more anionic or cationic direction from the equimolar composition, depending on the bilayer composition the surface of aggregates attains partial charge either negative or positive respectively which gives stability of the dispersion by forming an electrical double layer. The empirical phase diagram exposed in the figure illustrates that L_{ves} phase is not symmetrical about the equimolar composition; this asymmetry might be appeared because of the difference in chain-length of two surfactants. It

is clear from the phase diagram that by gradual addition of increasing amount of one component to another one can transform from L_1 phase to L_{ves} phase via a two-phase region and the two L_{ves} phases are also separated from each other by a two-phase border. This indicates that similar to other systems described above, all the phase transitions in the $C_{14}TAB$ system are also following the first-order phase transition rule. The phase diagram reveals that the two-phase region at equimolar composition becomes wider towards more anionic rich area at higher concentration, indicating the less stability of vesicles with low surface charge in L_{ves-} phase at higher ionic strength which is by virtue of released counter ions.

4.4.2 Conductivity Measurements

In order to monitor the composition of vesicular aggregation of Na-oleate systems with different cationic surfactants, the conductivity of a series of samples for every system was measured at 25°C after one week equilibration of the samples in a thermostat at 25°C. During the measurements the solutions were in the rest. The results of conductivity measurements at 100 mM total concentration but in different compositions were displayed in figure 4.4.4.

It is clear from the figure 4.4.4 that the conductivity of pure cationic solution depends significantly on the chain length of alkyl group. Higher conductivity is observed for the surfactant with shorter chain length. Probably, this is the reason of lower conductivity of pure anionic surfactant solution, since it has even longer alkyl hydrocarbon chain ($C_{17}COO-Na$). Another noticeable point for high conductivity of C_8TAB is that 100 mM concentration is below the cmc of C_8TAB while for other surfactants it has already been exceeded the cmc. The figure clearly reveals that there is no suppression in conductivity after adding and increasing the mole fraction of C_8TAB to the pure anionic solution. This observation indicates that C_8TAB does not interact with Na-oleate to form any vesicular aggregation which can trap some counter ions to reduce the conductivity. This result is in good agreement with the finding in phase behaviour. Likely for other surfactants, on addition of small quantity of cationic solutions to the pure anionic solution, conductivity increases steadily for all the surfactants studied here till $X_{NaOA} = 0.8$. Within this L_1 phase (see phase diagram) all the counter ions are free to take part in ionic conductance. This could be the plausible reason of increasing conductivity with increasing the ratio of cationic surfactants in the mixture.

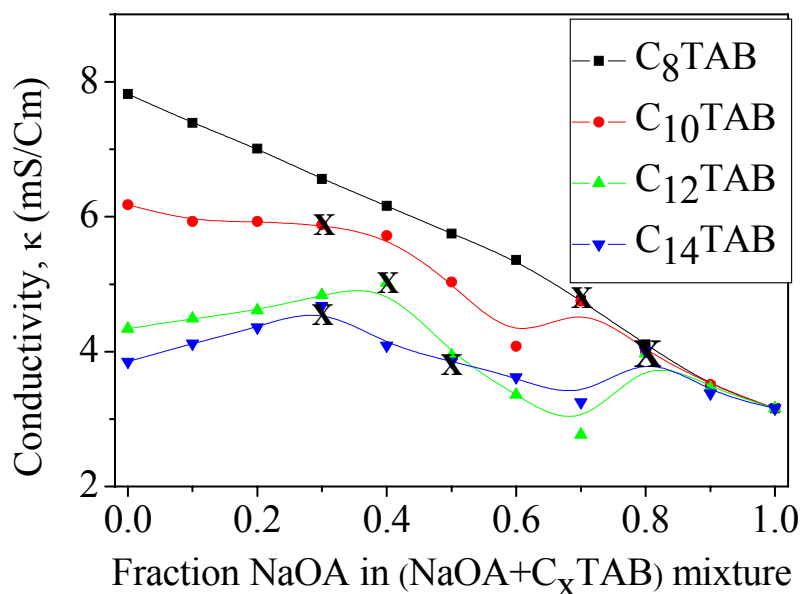


Figure 4.4.4: Experimentally measured conductance as a function of mole fraction of anionic solution in the mixture at 100 mM total concentration and at the temperature of 25°C. All x denoted points are the conductivity of two-phase regions.

Further increase in the mole fraction of cationic surfactants brings the composition at $X_{\text{NaOA}} = 0.7$ and at this composition conductivity decreases for both C_{12}TAB and C_{14}TAB ; but for C_{10}TAB conductivity still increases (see figure 4.4.4) and the decrease in conductivity for the system with C_{10}TAB was observed when the composition was $X_{\text{NaOA}} = 0.6$. The composition $X_{\text{NaOA}} = 0.8$ was the phase separated region for both C_{12}TAB and C_{14}TAB surfactant systems, while it was the L_1 phase for the system with C_{10}TAB . The phase separated region for the system with C_{10}TAB was $X_{\text{NaOA}} = 0.7$. It can be mentioned here that the trend of two extreme parts of the conductivity curves indicates that conductivity would be the maximum when the composition would be equimolar. But the empirical results show opposite nature of the curve – instead of getting summit they produced suppression. This implies that a significant amount of counter ions are trapped inside of vesicular structure. Conductivity curve for the catanionic vesicular system with C_{12}TAB shows the minimum conductance at the composition of $X_{\text{NaOA}} = 0.7$. This lowest conductivity indicates that the produced vesicles have a high trapping efficiency for water soluble ionic species. One can easily see from the figure (4.4.4) that the region of suppressed-conductivity becomes broader as the chain length of alkyl group in cationic surfactants becomes longer. This indicates that the formation efficiency of catanionic

vesicles for the surfactants with longer alkyl chain is higher and wider in composition, since surfactants with longer chain length can produce two different types (positively and negatively charged) of vesicles, as can be seen in phase diagram.

4.4.3 Rheological Measurements

Rheological behaviour of all the catanionic systems was demonstrated at different concentrations and compositions. After preparation and equilibration of the samples in a thermostat for one week at 25°C, it was observed that the samples were not very viscous. So, the double gap method was used to measure the viscosity of the samples with single phase. The measured viscosity at different compositions is summarized in figure 4.4.5.

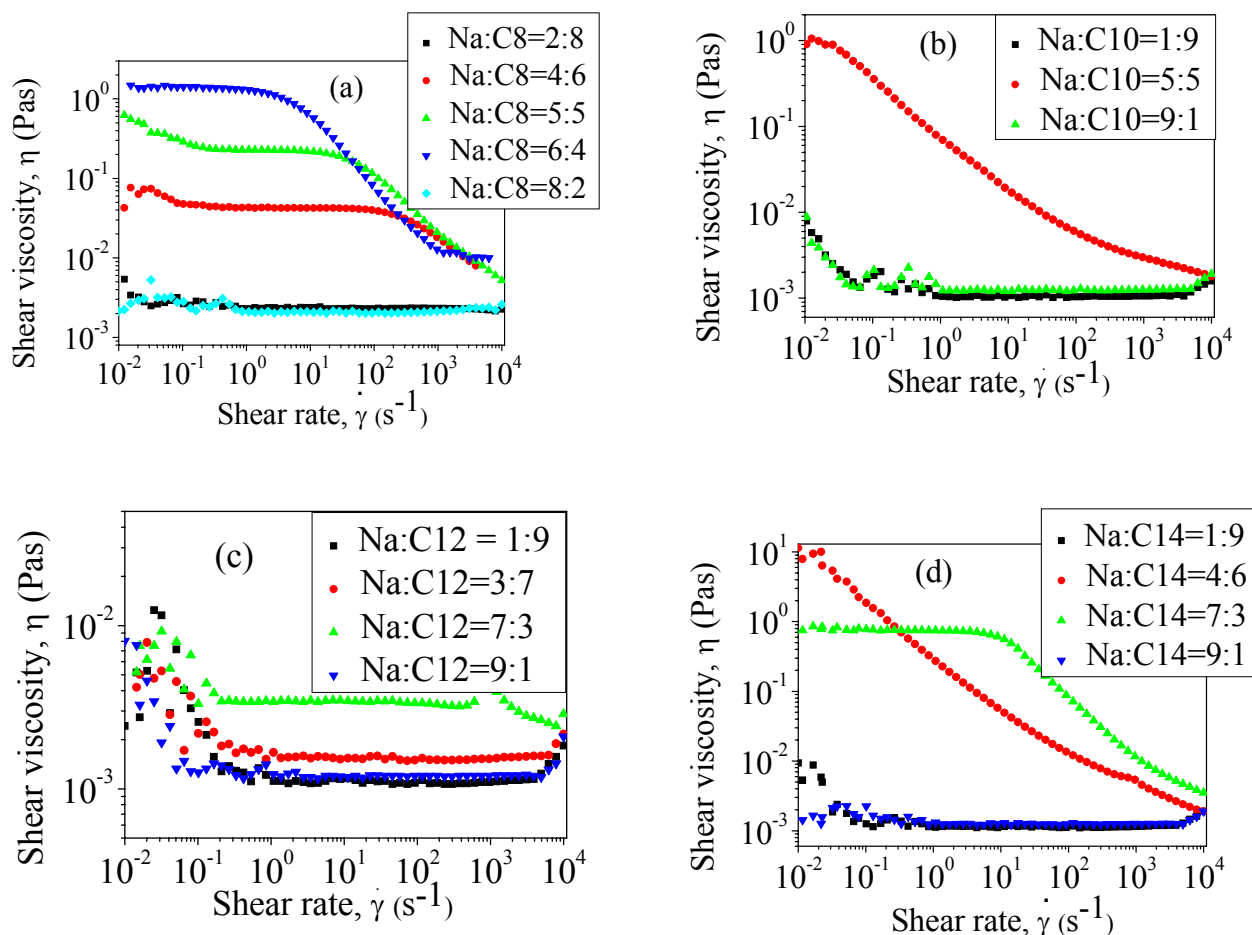


Figure 4.4.5: Double logarithmic plot of shear viscosity as a function of shear rate at the total concentration of 100 mM and at 25°C. Figures a, b, c and d represent the viscosity profile of catanionic system with different cationic surfactants C₈TAB, C₁₀TAB, C₁₂TAB and C₁₄TAB respectively. The Na in the inset indicates Na-oleate and C_x stands for C_xTAB.

All the figures presented above (4.4.5) show the viscosity of catanionic system at 100 mM total concentration with different compositions. The figure clearly reveals that the viscosity with rich composition of either cationic or anionic component ($X_{\text{NaOA}} = 0.1$ or 0.9) is very low, slightly higher than the dispersion medium and remains constant in entire shear rate region under investigation. The viscosity curves at very low shear rates are scattered, probably it is the limitation of the instrument. This Newtonian behaviour indicates that the solutions with such compositions have the micellar structure (L_1 phase). The viscosity of all the systems with low concentration ≤ 50 mM and almost all compositions (since only single phase samples have been studied) of catanionic mixture show such Newtonian behaviour (rheograms are not shown here). Although at 50 mM total concentration most of the systems studied here, except with $C_8\text{TAB}$, show vesicular phase at equimolar or around equimolar compositions, but the solutions are Newtonian and very low viscous. This low viscosity with Newtonian behaviour indicates that the vesicular dispersion in this concentration is very dilute. One can find such type of low viscosity with Newtonian behaviour for dilute system when vesicles are not interacting with each other¹⁹¹.

The viscosity profile of vesicular composition at 100 mM total concentration shows different nature for different catanionic systems. In most of the cases, rheogram shows shear thinning behaviour in entire shear rate (figure 4.4.5 b, d) or at higher shear rate (figure 4.4.5 d). Such type of low shear viscosity and partial shear thinning behaviour is also observed for other dilute vesicular system¹⁹¹. To analyse the shear thinning behaviour of steady-shear viscosity one can use power law (equation 4.3). The exponent term k determines the shear thinning rate of viscosity. The slope of the shear thinning, k has been calculated for catanionic vesicular system with $C_{10}\text{TAB}$ and the value is 0.63. On the other hand it was observed from the phase diagram that the catanionic system with $C_{14}\text{TAB}$ forms vesicles at two different compositions and both of them were showing shear thinning in steady shear viscosity. One is with anion rich and was termed as $L_{\text{ves-}}$ and other is with cation rich and was denoted as $L_{\text{ves+}}$ depending on the resultant charge on the vesicular bilayers. The slope of shear thinning, k has been calculated for both positively and negatively charged catanionic vesicular system and the values are 0.73 and 0.81 respectively. The values of high shear thinning rate again indicate that the samples have vesicular structure, since similar values for vesicular structure have been reported for other system¹⁹⁸. This high shear thinning rate can be explained on the basis of vesicular deformation and structural rearrangement. Vesicular structure can be deformed during shearing or randomly distributed vesicles can come into alignment or both can happen simultaneously¹⁵. The shear thinning behaviour of multilamellar vesicles is also similar to

this and its value of k is about 0.7⁴³. The estimated values from this investigation stand around this value which indicates that the present systems may have multilamellar vesicles. This pronounced shear thinning can be explained on the basis of reduction of vesicular size by successive removal off bilayer shells with increasing the shear rate. Microscopic analysis by cryo-TEM for the vesicular composition with C₁₀TAB clearly reveals that the system has multilamellar vesicles (see figure 4.4.6).

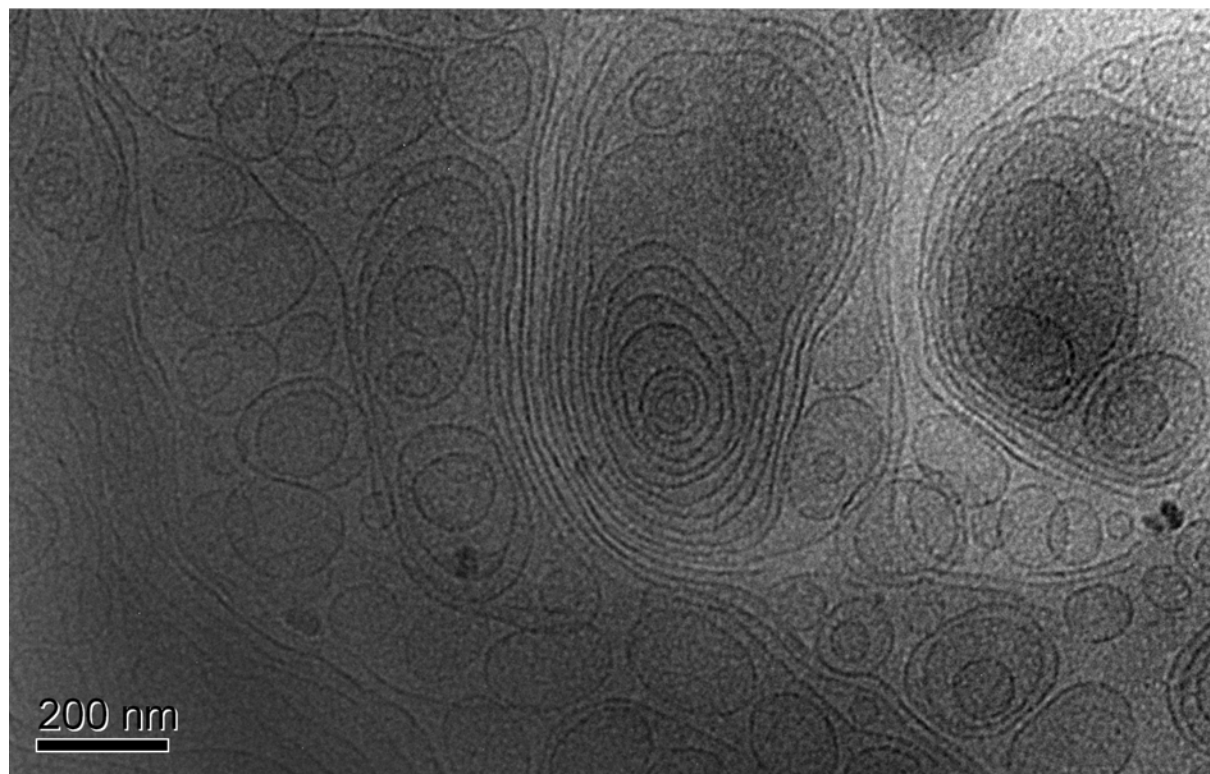


Figure 4.4.6: Cryo-TEM micrograph of vitrified specimen of catanionic system at the composition of NaOA: C₁₀TAB = 1:1 at 100 mM total concentration. This micrograph clearly reveals that equimolar mixing composition of these two surfactants produces a mixture of uni- and multilamellar vesicles.

One can see from figure the 4.4.5 that the zero-shear viscosity increases as the mixing composition of two components approaches to equimolar composition and this is more clear in the figure 4.4.7. For the systems with C₁₀TAB, C₁₂TAB and C₁₄TAB, substantially increased viscosity was observed when the systems transformed from micellar phase to vesicular phase, since vesicles are bigger aggregates compared to micelles. For the system with C₁₂TAB zero shear viscosity with vesicular composition increased a little, but compared to C₁₀TAB or C₁₄TAB this increase is very small. Moreover, the system was showing

Newtonian flow behaviour. Dilute vesicular dispersion could be the plausible reason for this individual behaviour.

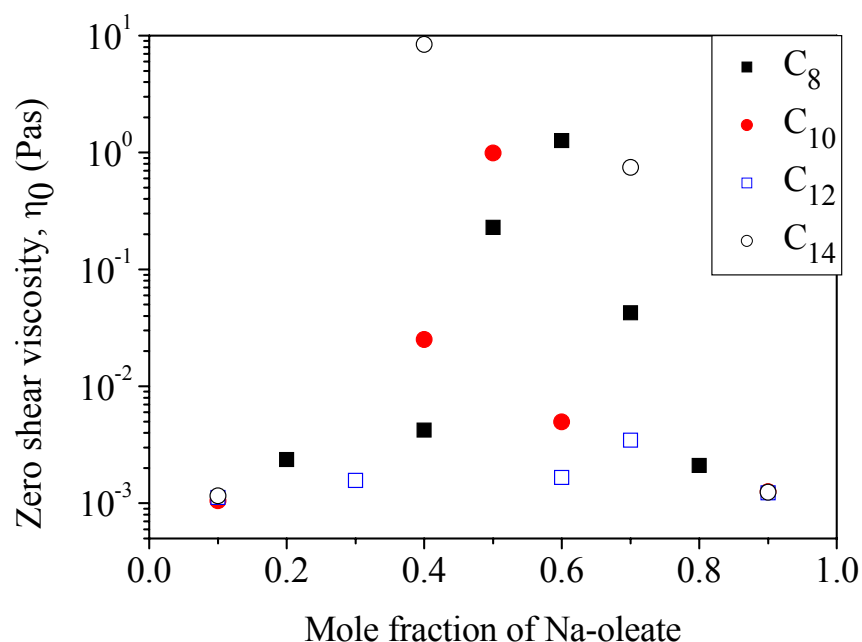


Figure 4.4.7: Zero shear viscosity as a function of mole fraction of Na-oleate in the mixture of catanionic solution at 100 mM total concentration and 25°C. The inset C_X values indicate the corresponding cationic surfactants with aqueous Na-oleate.

From the phase diagram and other instrumental measurements it was observed that C_8 TAB does not form vesicles with aqueous Na-oleate in the concentration window studied here. But it shows a pronounced high zero-shear viscosity at about equimolar mixing composition of two surfactant components. This high shear viscosity can be explained on the basis of formation and growth of rod-like micelle, since entangled rod-like micelle can show high viscosity and viscoelastic behaviour²⁰².

4.4.4 Dynamic Light Scattering

From the phase behaviour and other instrumental measurements it was observed that two oppositely charged surfactant solutions can interact with each other and form bigger aggregates, like vesicles. This finding leads to examine the result by DLS measurement. To

check the interaction of anionic and cationic solutions DLS measurements were performed for the solutions with single phase. The time dependent correlation function of the scattered light intensity was measured at a scattering angle of 90° . The normalized intensity correlation functions at different concentration and compositions at 25°C are shown in figure 4.4.8.

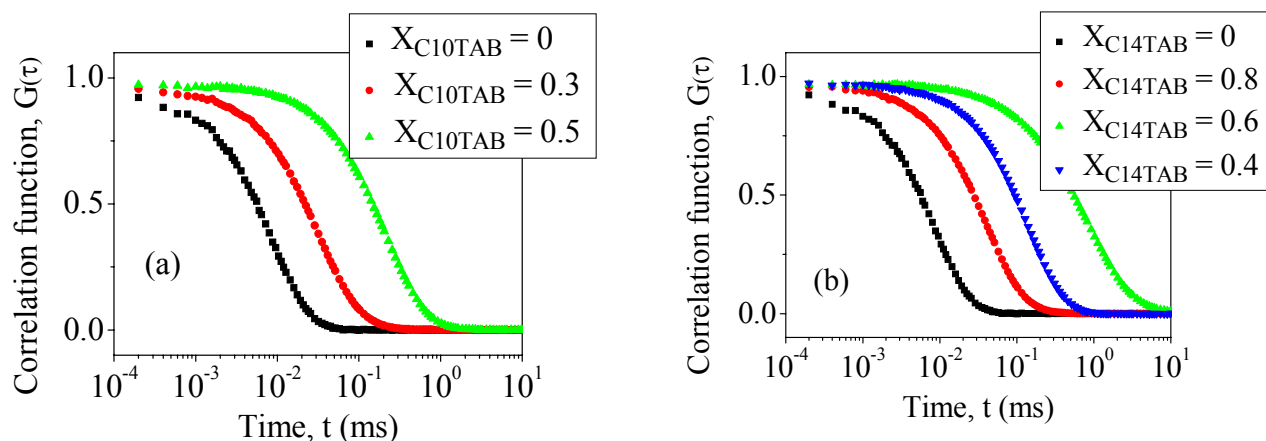


Figure 4.4.8: Normalized intensity correlation function against time at different composition of two oppositely charged surfactant mixtures at 25°C and at a scattering angle of 90° . Figure (a) is the scattering intensity curve for Na-oleate with C_{10}TAB while (b) is that of Na-oleate with C_{14}TAB at the total concentration of 50 mM and different compositions.

The DLS measurements were performed after one week of sample preparation and equilibration at 25°C in a thermostat. Figure 4.4.8(a) clearly shows that the decay time increases with increasing the mole fraction of C_{10}TAB in the solution and it becomes maximum when the composition is $X_{\text{C}_{10}\text{TAB}} = 0.5$ and according to phase diagram, it is a composition of vesicle phase. The decay time of scattering intensity and further calculation (results are tabulated in Table 4.4.1) clearly reveal that 1:1 ($X_{\text{C}_{10}\text{TAB}} = 0.5$) composition of investigated solution formed vesicles. Pure Na-oleate solution forms smaller micelles; the scattering intensity decays very fast; but after admixing the cationic solution it forms bigger micelles and hence the decay time increases a little. On the other hand, figure 4.4.8(b) clearly reveals that the samples at $X_{\text{C}_{14}\text{TAB}} = 0.4$ and 0.6 compositions have bigger aggregate structure, since scattering intensity decays quite slowly which indicates that the diffusion is very slow. The composition $X_{\text{C}_{14}\text{TAB}} = 0.8$ shows decay of the scattering intensity in L_1 phase which indicates that micelles become bigger after addition of oppositely charged surfactant.

From the phase diagram it was observed that the anionic solutions with aqueous C₁₄TAB formed two vesicular compositions, one is with anionic rich (L_{ves-} phase) and second one is with cationic rich (L_{ves+} phase). DLS measurements show that the hydrodynamic radius in L_{ves-} is about 25 nm and that in L_{ves+} is about 103 nm (see table 4.4.1).

It is clearly exposed from the table 4.4.1 that the size of the aggregation significantly depends on the composition of solutions. Pure Na-oleate forms micellar aggregation with particle size (radius) of about 1.5 nm which was increased to 6.1 nm after admixing C₁₀TAB at the composition X_{C₁₀TAB} = 0.3 and then the system transformed into vesicular phase where the radius became even bigger 38.3 nm. Similar effect was observed for both the cases of C₁₂TAB and C₁₄TAB. Vesicle size also depends on the alkyl chain length of cationic surfactants. It was observed that the particle size with C₁₀TAB at 1:1 composition is 38.3 nm, while the value for the same composition is 54.9 nm for the surfactant C₁₂TAB. In case of C₁₄TAB, the composition 1:1 formed two-phase region and the system forms two vesicular compositions. The most noticeable point is that each of these vesicular compositions form vesicles with significantly different in size.

Table 4.4.1: Diffusion coefficients, hydrodynamic radii and polydispersity index of aqueous catanionic mixed system with Na-oleate and C_XTAB (where X = 10, 12 and 14) at the total concentration of 50 mM and different compositions.

Composition	Decay time (ms)	Diffusion coeff. (m ² s ⁻¹)	Hydrodynamic radii (nm)	Polydispersity index
X _{C₁₀TAB} = 0		1.59E-10	1.54	
X _{C₁₀TAB} = 0.3	0.1	4.40E-11	6.1	0.27
X _{C₁₀TAB} = 0.5	0.5	6.40E-12	38.3	0.23
X _{C₁₂TAB} = 0.7	0.1	3.55E-12	6.9	0.24
X _{C₁₂TAB} = 0.5	0.8	4.46E-12	54.9	0.21
X _{C₁₄TAB} = 0.8	0.1	3.28E-11	7.5	0.22
X _{C₁₄TAB} = 0.6	2.34	2.39E-12	102.5	0.45
X _{C₁₄TAB} = 0.4	0.3	1.01E-11	24.3	0.15

From the table 4.4.1 one can see that the hydrodynamic radii of vesicles with C₁₄TAB in cationic rich composition are about four times bigger than the vesicles in anionic rich composition. With cationic rich composition two monolayers of vesicular bilayers are more balanced than with anionic rich composition and therefore a flatter bilayer is favoured.

4.5 Thermodynamic Behaviour of Mixed Vesicular System

4.5.1 Phase Behaviour

Figure 4.5.1 describes the phase behaviour for the mixed system of anionic and cationic aggregation. The samples were prepared by mixing of two component-solutions and homogenized them by a mechanical vibrator. After preparation samples were kept in a thermostat under complete rest for a week at 25°C. The phase diagram presented in the figure was drawn by visual observation of the physical state of the samples.

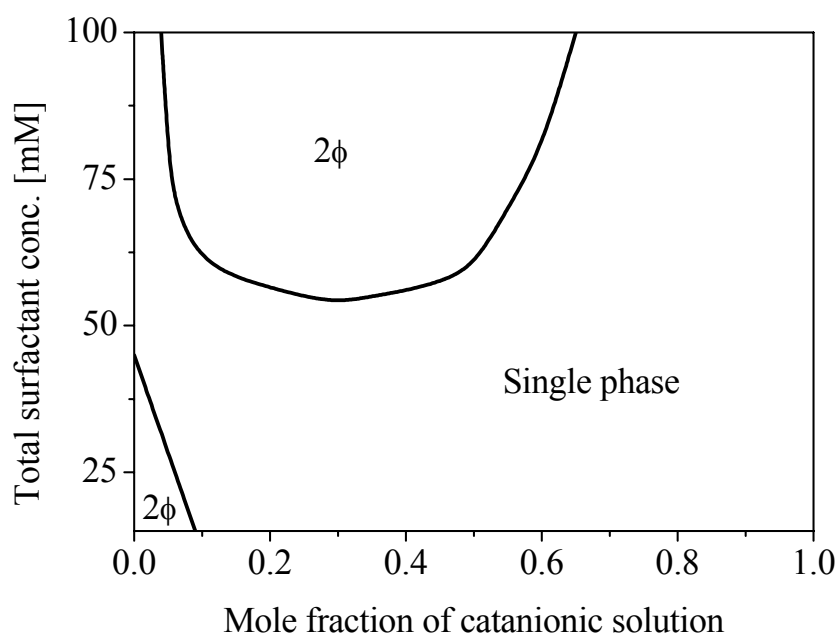


Figure 4.5.1: Phase diagram for the mixed vesicular system of anionic (Na-oleate with octanol) and cationic (1:1 mixing composition of Na-oleate and C₁₀TAB) aggregation at 25°C.

Before going to describe the phase diagram, it is necessary to introduce the components which are involved in this mixed aggregation system. In the previous analysis it was observed that Na-oleate forms anionic vesicular aggregation with octanol as co-surfactant when it exceeds certain octanol concentration (see section 4.1). This component of anionic vesicular solution was prepared maintaining the solution composition of 100 mM Na-oleate with 300 mM

octanol, which means, co-surfactant concentration was maintained three times more than surfactant concentration. Similarly it was found that decyltrimethyl ammonium bromide ($C_{10}TAB$) forms catanionic vesicles when the organic quaternary ammonium salt solution was mixed with aqueous Na-oleate maintaining 1:1 mixing ratio (see section 4.4). This component of catanionic vesicular solution was prepared by mixing the same volume and concentration of aqueous Na-oleate with $C_{10}TAB$, for instance 100 mM catanionic solution was prepared by mixing of the same volume of 100 mM Na-oleate with 100 mM $C_{10}TAB$ solution. Although both the individual systems (anionic and catanionic) form vesicles, but they have different nature – the former one is anionic aggregation with net negative charge on the vesicle surface and the later one is catanionic.

To determine the phase diagram for this mixed vesicular system initially two components with the concentration of 25 mM, 50 mM, 75 mM and 100 mM were mixed maintaining different mixing ratios. A phase separation appears between the total concentration of 50 mM and 75 mM in the anionic rich composition. In this concentration range some more samples were prepared maintaining different mixing ratios in the concentration interval of every 5 mM to determine the phase boundary precisely.

Depending on the concentration, the physical state of the pure anionic solutions was either phase separated or isotropic bluish. At lower concentration (25 mM) the solution was phase separated keeping the large and isotropic transparent phase in lower layer and a very thin oily layer was floating on the top while at higher concentration (≥ 50 mM) it was a single, isotropic and pale bluish phase. This indicates that the system is transformed into vesicular phase when the concentration of surfactant was raised at 50 mM. The pure catanionic solution, on the other hand, was turbid and this turbidity became more intense as the total concentration was increased. When a small quantity of catanionic solution was mixed to the anionic solution ($X_{\text{anionic}} = 0.9$) at 25 mM total concentration, the resulting solution became single phased and turbid and this single phase continued till pure catanionic composition i.e. no phase separation was observed with changing the composition. This indicates that on addition of catanionic solution into anionic solution the thin oily layer (which was originally present in pure anionic solution) became accommodated into the aggregates. No phase separation was observed with changing composition when the total concentration was 50 mM. On the other hand, 75 mM pure anionic solution was isotropic and bluish. On addition of small quantity of catanionic ($X_{\text{anionic}} = 0.9$) solution into this anionic vesicular solution, system enters into a two-phase region.

In two phase region, the upper phase was clear and transparent while the lower phase was very turbid. The quantity of floating transparent phase became larger as the ratio of anionic solution in the mixture was increased. This indicates that system precipitated with adequate amount of cationic form and rest of the anionic form is floating on the top.

4.5.2 Electrical Conductivity

In order to monitor the electrical behaviour of mixed aggregation system the conductivity of the solutions was measured at different concentrations and compositions. Conductivity was measured after one week equilibration of the samples in a thermostat at 25°C and during this period of time samples were under complete rest. The conductivity of pure anionic and cationic solutions (figure 4.5.2) increases with increasing the concentration, since the number of counter ions are also increasing with concentration. The figure reveals that the conductivity of pure cationic vesicular solution is always higher than that of pure anionic solution. The presence of two different counter ions (Na^+ from Na-oleate and Br^- from C_{10}TAB) in the cationic solution is the plausible cause for this high conductivity, whereas only one type of counter ion (Na^+ from Na-oleate) is present in pure anionic solution.

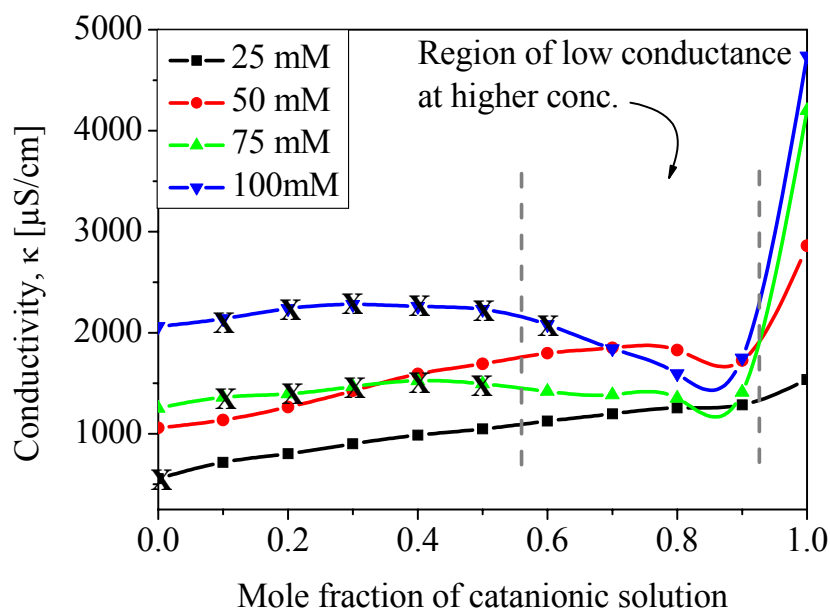


Figure 4.5.2: Conductivity for the mixed aggregation system as a function of mole fraction of cationic solution in the mixture at 25°C. All x denoted values are the conductivities of two-phase region.

For 25 mM total concentration, the conductivity increases steadily with increasing the mole fraction of cationic solution in the mixture. No suppression in conductivity was seen which indicates that anionic-cationic mixtures do not form a bigger aggregate that can entrap more counter ions to reduce the conductivity within this dilute concentration region.

On addition of small quantity of anionic solution ($X_{\text{anionic}} = 0.1$) to the highly conducting cationic solution the conductivity decreases sharply. This sharp decrease in conductivity can be explained on the basis of two phenomena: (1) as the fraction of high conducting cationic solution decreases ($X_{\text{cationic}} = 0.9$ and 0.8), the quantity of counter ions decreases simultaneously and (2) formation of bigger aggregates. These bigger aggregates can trap large number of counter ions and that influences the conductivity to be suppressed. Dynamic light scattering results and cryo-TEM measurements are also supporting this phenomenon that larger vesicles are formed in this composition range (see table 4.5.1 and figure 4.5.5b). Further increasing the mole fraction of anionic component in the mixture ($X_{\text{anionic}} \geq 0.3$) at the total concentration of 50 mM the conductivity decreases slowly. This could be the effect of low conducting anionic solution on total composition. On the other hand, for the same compositions but with total concentrations of 75 mM and 100 mM, the conductivity increases slowly till the system enters into the phase separated region. This indicates that after exceeding the composition $X_{\text{anionic}} = 0.2$, the formation tendency of bigger aggregates or water soluble ion trapping efficiency of vesicles decreases with increasing the X_{anionic} and finally the system enters into a two-phase region. The conductivity in this two phase region remains almost constant.

4.5.3 Dynamic Light Scattering

From the results of conductivity measurements it was assumed that admixing and equilibration of two different vesicular aggregations at proper concentration and composition may form bigger aggregates. This finding led to examine the results by DLS measurement and the measurements were performed for the samples in single phase region. The time-dependent autocorrelograms of the scattered light were measured at a scattering angle of 90° . The normalized intensity correlograms at different concentrations of a mixed aggregate system at 25°C are shown in figure 4.5.3.

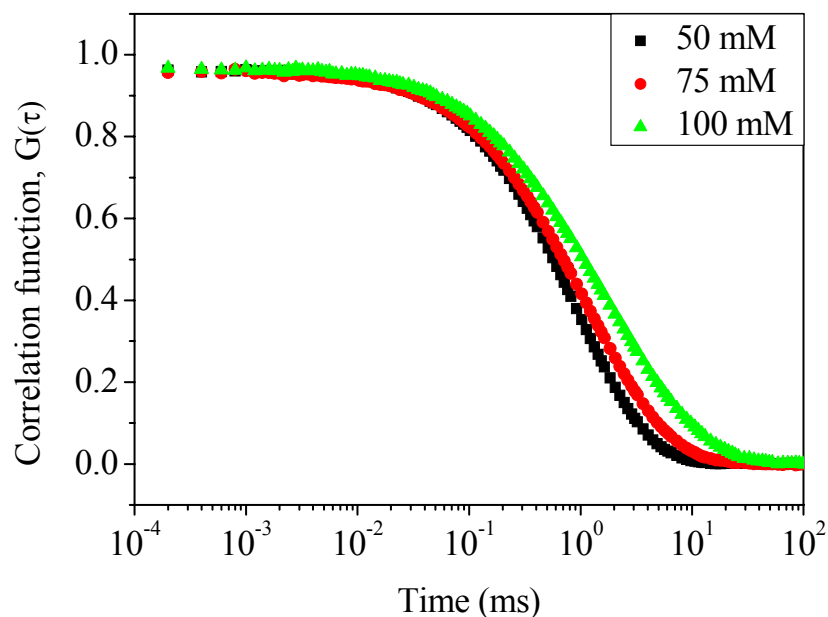


Figure 4.5.3: Normalized intensity correlation function is plotted against time for different concentration of mixed surfactant system at 25°C and at a scattering angle of 90° . The composition of mixed system was anionic: cationic = 1:9 and the inset values are indicating the total concentration of solutions.

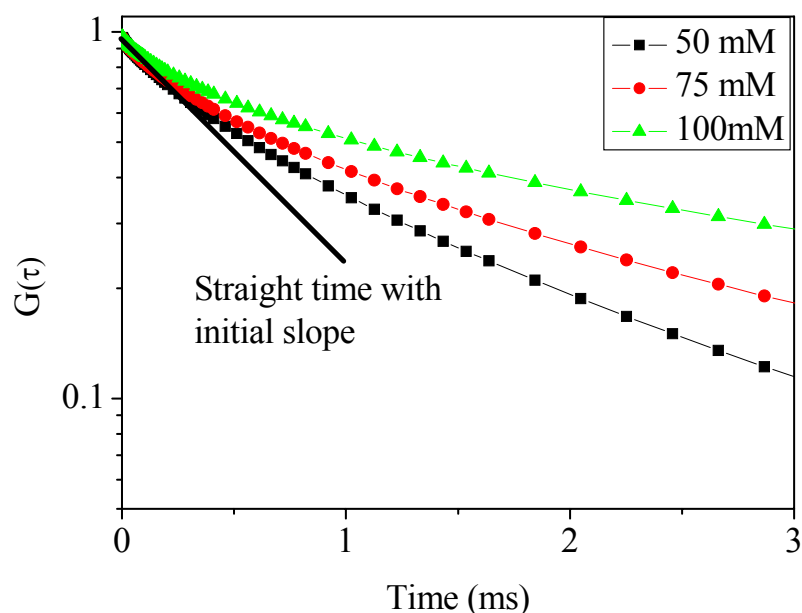


Figure 4.5.4: Correlation function $G(\tau)$ for the mixed vesicular system is plotted against time for different concentration of surfactants at 25°C and at a fixed scattering angle of 90° . The straight line in the figure represents the (almost) initial slope and clearly exposing that the decays are not linear. The inset values are indicating the total concentration of mixed aggregate system and the composition of the samples was $X_{\text{anionic}} = 0.1$.

The figure represents the intensity correlation function of mixed vesicular system at different concentration with a mixing composition of $X_{\text{catanionic}} = 0.9$. The decay time for the aggregated particles (vesicles) is quite large which implies that the samples have comparatively bigger aggregates. The picture emerges from this investigation is that the system has polydispersity which becomes clearer from the figure 4.5.4. This figure brought out the result that the correlation function does not decay linearly which is a sign of polydispersity. Indeed, a relatively high polydispersity index was recorded in these measurements (see table 4.5.1). The values of high polydispersity indicate that the size distribution range of vesicles is very wide. No systematic increase or decrease in polydispersity index was observed with changing the composition. Hydrodynamic radii and polydispersity index obtained from cumulant analysis of autocorrelation function are summarised in table 4.5.1.

Table 4.5.1: Diffusion coefficients, hydrodynamic radii and polydispersity index of mixed vesicular system at different concentration and composition.

Conc. (mM)	Composition	Decay time (ms)	Diffusion co- effic. (m^2s^{-1})	Hydrodynamic radii (nm)	Polydispersity index
50	$X_{\text{anionic}} = 1$	0.27	$1.92\text{e-}11$	13	0.49
	$X_{\text{anionic}} = 0.5$	0.88	$6.55\text{e-}12$	38	0.49
	$X_{\text{anionic}} = 0.1$	3.69	$2.57\text{e-}12$	95	0.49
	$X_{\text{anionic}} = 0$	18.1	$1.77\text{e-}12$	138	0.52
75	$X_{\text{anionic}} = 0.2$	4.45	$3.46\text{e-}12$	71	0.50
	$X_{\text{anionic}} = 0.1$	5.88	$2.46\text{e-}12$	100	0.52
	$X_{\text{anionic}} = 0$	4.89	$2.58\text{e-}12$	95	0.52
100	$X_{\text{anionic}} = 0.2$	4.53	$2.97\text{e-}12$	83	0.52
	$X_{\text{anionic}} = 0.1$	13.7	$1.85\text{e-}12$	132	0.51
	$X_{\text{anionic}} = 0$	4.79	$2.48\text{e-}12$	99	0.53

One can see from the table 4.5.1 that the formation of bigger aggregates largely depends on the concentration and composition of the solution. Admixing of two solutions (anionic and catanionic) does not influence the system to form a bigger aggregate at 50 mM total concentration. Pure anionic solution forms smaller vesicles (hydrodynamic radius 13 nm) at this concentration. On increasing the mole fraction of catanionic solution into the mixture, a

slow and systematic increase in hydrodynamic radii was observed, since pure catanionic solution forms bigger aggregates. This finding illustrates that after admixing the components, the system reforms new vesicles. A bigger aggregate which is the result of admixing of two component solutions was observed with the composition of $X_{\text{anionic}} = 0.1$ when the total concentration was ≥ 75 mM, since its surrounding compositions form relatively smaller vesicles. It was observed that the formation tendency of bigger vesicles by admixing of two component solutions is strongly concentration and composition dependent. A little effect was observed when the total concentration was 75 mM, but a pronounced effect was observed with 100 mM total concentration (see table 4.5.1). At 100 mM total concentration the calculated hydrodynamic radius of vesicles for pure catanionic solution was 99 nm, while the radius of vesicles increases to 132 nm when the composition of the solution is $X_{\text{anionic}} = 0.1$. Further increasing the mole fraction of anionic component to $X_{\text{anionic}} = 0.2$, the vesicular radius decreases to 83 nm. These results indicate that mixing composition of mixed-vesicular system plays an important role in forming bigger vesicles. Similar tendency for the formation of bigger vesicles at the same composition $X_{\text{anionic}} = 0.1$ was observed for the case of 75 mM solutions, but the effect is less pronounced (see table 4.5.1).

The results obtained from DLS analysis, revealed that mixing composition of $X_{\text{anionic}} = 0.1$ forms bigger vesicles at higher concentration. It can be mentioned here that a suppression in electrical conductivity was also observed when the composition of solution was $X_{\text{anionic}} = 0.1$. One can conclude from this comparative analysis that the reason for the suppression in electrical conductivity is the formation of bigger vesicles which encapsulate large number of water soluble counter ions. The figure 4.5.2 indicates that the interaction of two solutions is strongly concentration and composition dependent and the threshold concentration is 50 mM. Below this concentration (< 50 mM) no sign for the formation of bigger aggregates was observed. The composition of the solutions also plays a potential role in forming the bigger aggregates. No sign of bigger aggregates was observed in the region of anionic-rich composition in the single phase region. After exceeding the threshold concentration and with catanionic-rich composition especially the composition at $X_{\text{catanionic}} = 0.9$ the system forms bigger aggregates. At higher concentrations (≥ 75 mM) both the conductivity and DLS measurements indicate that bigger aggregation is possible when the composition of the solution is $X_{\text{catanionic}} = 0.9$.

4.5.4 Microscopic Observation

Cryogenic transmission electron microscopic (cryo-TEM) method was used to visualize the mixed vesicular product of anionic and cationic aggregation. The microscopic study reveals the pictorial view of aggregated morphology what is present in the sample. In cryo-TEM investigations of the mixed vesicular system, well defined unilamellar vesicles were observed and two micrographs are depicted in figure 4.5.5. They illustrate that the vesicles are spherical in shape and the diameter is ranging from 40 nm to 200 nm which indicates that the samples have a high polydispersity. This implies that the results from microscopic observation are in good agreement with those found in DLS analysis (see table 4.5.1).

From the microscopic images one can observe that only unilamellar vesicles are present in the system. An observation triggered extensive studies of the nature and occurrence of such vesicular structure in different parts of the vitrified specimen under the TEM and it was exposed that there are a few vesicles which have oligo-lamellar structures (figure 4.5.6). This indicates that mixing of two vesicular aggregations can combine together and can produce multilamellar vesicles with bigger size. Close observation of figure 4.5.6 it reveals that two oligo-lamellar vesicles are formed inside of a large bi-lamellar vesicle. Although a very few oligo- or bilamellar vesicles were observed, but the system forms mostly unilamellar vesicles. The interlamellar spacing was measured in these oligo-lamellar vesicles and it was observed that the value is about 30 nm.

In order to see the vesicular size distribution it is necessary to determine the classified vesicle sizes quantitatively that obtained from cryo-TEM. A histogram for the size distribution of vesicles is built up by measuring the size of about 1500 vesicles taken from different slides of micrograph of cryo-TEM images. Figure 4.5.7 shows the distribution of vesicular sizes at different concentration and composition of anionic and cationic mixed aggregation on the basis of outer vesicular diameter.

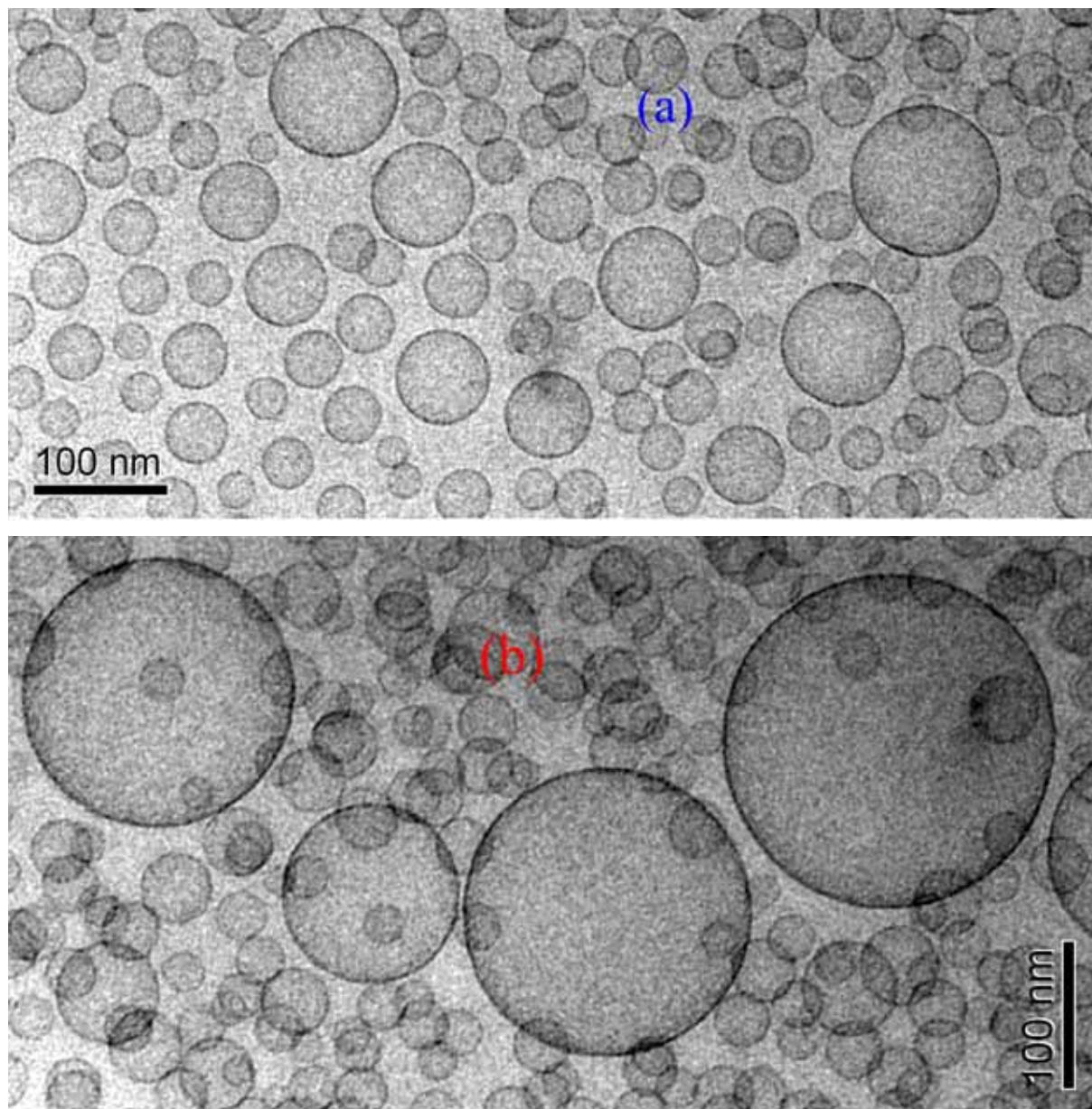


Figure 4.5.5: Cryo-TEM micrographs of mixed vesicular system. The micrograph (a) is of 50 mM solution with a composition of $X_{\text{anionic}} = 0.5$ while the micrograph (b) is chosen from the 75 mM solution with a composition of $X_{\text{catanionic}} = 0.9$. The bar length in each micrograph corresponds to 100 nm.

To determine the effective bilayer bending constant (K) and the radius of the vesicles with minimum curvature energy (R_0) it is necessary to apply a theoretical model proposed by Jung et al.¹⁸⁶ to the quantitative size distribution of vesicular aggregates. A best fit of equation (4.1) to the histogram built for the size distribution of classified vesicles at the total surfactant concentration of 50 mM and the composition $X_{\text{anionic}} = 0.5$ (figure 4.5.7a) results in $K = \kappa + \bar{\kappa}/2 = 0.21 \pm 0.01 k_p T$, the sum of Helfrich mean (κ) and Gaussian ($\bar{\kappa}$) curvature

moduli, and $R_0 = 39 \pm 1.6$ nm, the radii of vesicles with minimum curvature energy. But the fit for 75 mM solution with $X_{\text{catanionic}} = 0.9$ composition (figure 4.5.7b) reveals the results in $K = 0.22 \pm 0.01 k_B T$ and $R_0 = 69 \pm 2.6$ nm. Similar values of K have been reported for other surfactant systems which form vesicles^{186, 187, 232}. These results indicate that effective bilayer bending constant K remains almost the same with changing the concentration and composition. Since the bending constant K is significantly less than $k_B T$ in both cases, the vesicles are stabilized by fluctuations and the size distribution is wider.

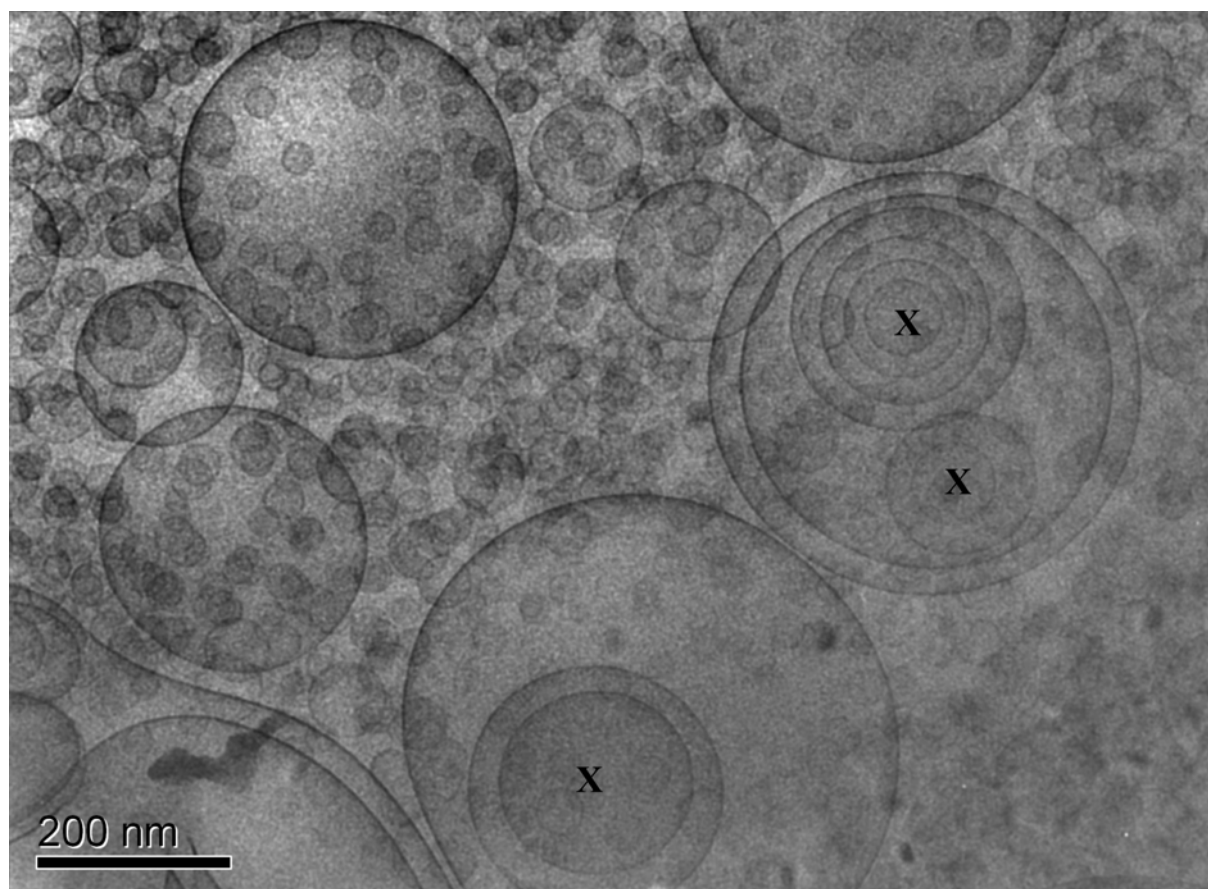


Figure 4.5.6: Cryo-TEM images of vitrified specimen of $X_{\text{catanionic}} = 0.9$ at 100 mM total concentration. In this micrograph one can see a few vesicles (X denoted) which are either bilamellar or oligo-lamellar. There are some vesicles which are very big with diameter more than 200 nm. The bar length corresponds to 200 nm.

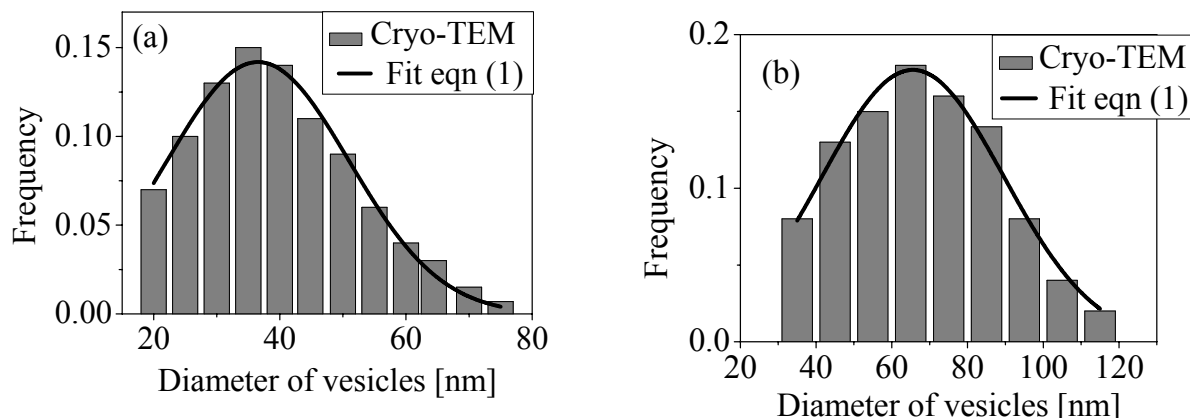


Figure 4.5.7: Number averaged vesicle size distribution histogram for the aggregation of anionic and cationic mixed system. Figure (a) expresses the histogram of 50 mM solution with a composition of anionic: cationic = 1:1 and (b) is that for 75 mM solution, but the composition was $X_{\text{cationic}} = 0.9$. For the case of (b) there were about 0.2% vesicles found with diameter larger than 200 nm and were not plotted in the histogram. The solid curve in each plot is the best fit of the bending rigidity model derived by Jung et al.¹⁸⁶

The figure 4.5.7 also illustrates that the radii of vesicles with minimum curvature energy, R_0 have been shifted towards larger diameter when the concentration was 75 mM and the composition was $X_{\text{cationic}} = 0.9$. The results are very good in agreement with the results obtained from DLS measurements which explored that hydrodynamic radii of vesicles (38 nm for 50 mM and 100 nm for 75 mM) are bigger for the concentration of 75 mM with composition $X_{\text{cationic}} = 0.9$ than that of 50 mM with composition $X_{\text{anionic}} = 0.5$.

4.5.5 Shear Viscosity

The rheological behaviour of mixed vesicular system at different concentrations and compositions was performed and some rheograms are depicted in figure 4.5.9. As it is shown in figure 4.5.9(a) that the pure anionic solutions behave like a Newtonian fluid. Viscosity does not depend on shear rate and it remains constant in entire shear rate under investigation. DLS measurements have already been revealed that the system has vesicular morphology when the total concentration is ≥ 50 mM. For a dilute dispersion of vesicular system one can find such type of Newtonian behaviour¹⁹¹. The viscosity of a dispersion of undeformed non-interacting vesicles resembles that of hard spheres.

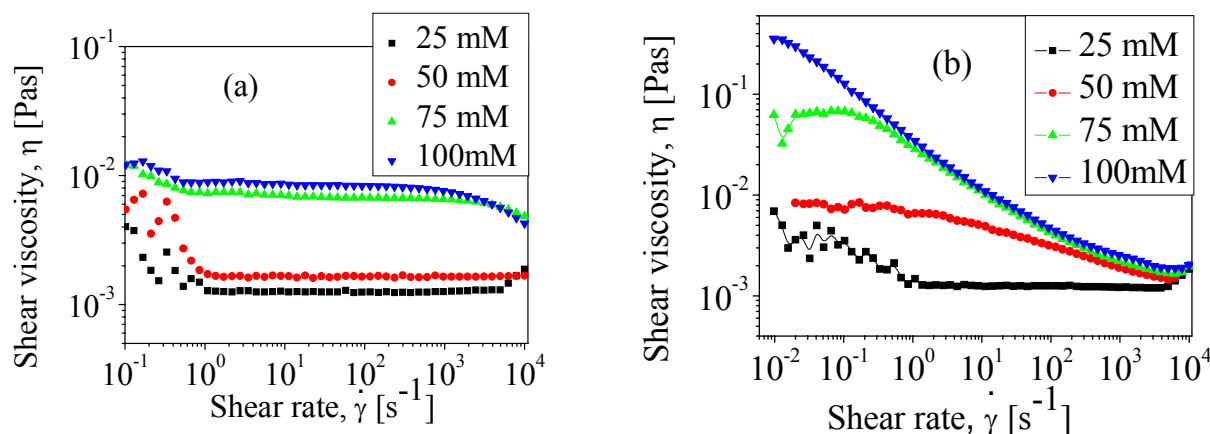


Figure 4.5.9: Shear viscosities for the system of mixed vesicles as a function of shear rate at different concentration and composition at 25°C. Figure (a) is with composition $X_{\text{anionic}} = 1.0$, i.e. pure anionic system at different concentrations, while figure (b) expresses the viscosity of pure cationic solution at different concentrations.

A deviation from such hard sphere behaviour is possible when the vesicles aggregate as a result of attractive interaction or, when the average intervesicle distance is so small that the static vesicle-interaction comes into play²³³. The figure 4.5.9(a) clearly reveals that, though the pattern of viscosity does not change with shear rate or with changing concentration, but the magnitude of viscosity increases with increasing the concentration, since the volume fraction is also increasing with concentration. The spherical micelles and dilute dispersion of vesicles have a weak effect on rheology – the solutions are Newtonian, and the viscosity rises with the volume fraction of the aggregates. The viscosity of 25 and 50 mM pure anionic solutions are 1.25 and 1.67 mPas respectively, slightly higher than that of dispersion medium indicating the presence of either micellar or dilute vesicular dispersions. A large and sharp increase in viscosity was observed when the concentration was jumped from 50 mM to 75 mM. The formation of relatively larger vesicle size could be the plausible cause for this sudden higher viscosity.

On the other hand, figure 4.5.9(b) illustrates the shear viscosity of a vesicular dispersion of pure cationic solution at different concentrations. This figure clearly reveals that the concentration has a significant effect on shear viscosity. At lower concentration (25 mM), the vesicular dispersion is very dilute and the vesicles probably have no interaction with their neighbouring one, as a consequence, according to hard sphere model the viscosity remains

constant in entire shear rate under investigation. The viscosity of this solution (25 mM) at low shear rate is scattered and non-reproducible. Probably this is the limitation of instrument. On increasing the concentration, a Newtonian plateau was still observed at low shear rate and a little shear thinning was observed at the intermediate shear rate, while at high shear rate again a Newtonian plateau was observed. The transition between the plateaus is the vanishing contribution of Brownian motion, due to a changing particle position distribution¹⁹¹. For such a system one can use Cross equation (equation 4.2) to determine the zero shear viscosity, η_0 , viscosity at very high shear rate, η_∞ , and two constant terms K and m . A best fit of Cross equation (4.2) to the shear viscosity of pure cationic solution at higher concentration (see figure 4.5.10) results in $K \approx 0.09$ s, 1.0 s and 147 s, and $m \approx 0.5$, 0.6 and 0.65 for 50, 75 and 100 mM respectively. Similar K and m values have been reported elsewhere for many other systems^{192, 234, 235}. All the K and m values including zero shear viscosity and other parameters are listed in table 4.5.2.

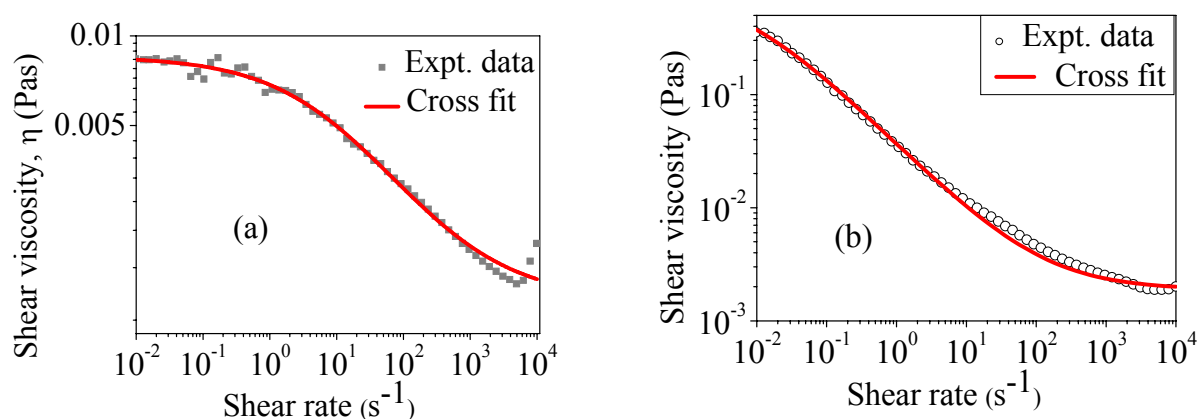


Figure 4.5.10: Fit of Cross equation (4.2) to the experimental shear viscosity data at the concentration of (a) 50 mM and (b) 100 mM cationic solution.

The results illustrate that K values are increasing with increasing the concentration of surfactant. This implies that the value of critical shear rate $\dot{\gamma}_c$ is decreasing with increasing the concentration that means samples start shear thinning at very low shear rate when the concentration of surfactants is higher, i.e. the relevant structural sizes increase. On the other hand m values are also increasing with increasing the surfactant concentration. This indicates that after crossing the critical shear rate samples show more pronounced shear thinning with higher surfactant concentration.

Table 4.5.2: Critical shear rate, zero shear viscosity, viscosity at very high shear rate including with other parameters came out from the Cross fitting for pure catanionic solution at different concentrations are displayed.

Conc. (mM)	Const. K (s)	Const. m	η_0 (Pas)	η_∞ (Pas)	Critical shear rate $\dot{\gamma}_c$
50	0.09	0.5	0.0085	0.0013	11.1
75	1.0	0.6	0.0611	0.0019	1.0
100	147	0.65	0.845	0.0019	0.007

For higher concentration (100 mM) the shear thinning region was broadened and the Newtonian plateau was no longer observed at low shear rates (see figure 4.5.9b). For such pronounced shear thinning behaviour of shear viscosity one can use the power law (equation 4.3) to evaluate the empirical results. The exponent term k in the power law determines the shear thinning rate of viscosity. The slope of shear thinning, k is 0.45 and 0.47 for 75 and 100 mM concentration, respectively. The values of high shear thinning rate indicate that the samples have vesicular structure, since similar values for vesicular structure have been reported for other system¹⁹⁸. This high shear thinning rate can be explained on the basis of vesicular deformation and structural rearrangement. Vesicular structure can be deformed during shearing or randomly distributed vesicles can come into alignment or both can happen simultaneously¹⁵. The shear thinning behaviour of multilamellar vesicles is also pronounced and in that case it has been reported that the size of vesicles was becoming smaller by successive removal off their bilayer shell with increasing the shearing rate⁴³. Microscopic analysis by cryo-TEM in previous analysis revealed that 100 mM catanionic solution has multilamellar vesicular structure.

Shear viscosity depends not only on the concentration of surfactant aggregates, but also on the composition of two components. Figure 4.5.11 reveals how the zero shear viscosity changes with composition. At 25 mM concentration, viscosity remains almost constant; no significant change was observed with changing the composition, since the solution is very dilute. At 50 mM total concentration shear viscosity changes a little with changing the composition especially in the catanionic rich compositions. The viscosity was increasing very slowly with increasing the mole fraction of catanionic component in the mixture, but a sudden increase in zero shear viscosity was observed when the composition changes $X_{\text{catanionic}} = 0.9$ to 1.0, although for rheological analysis this change is also very little.

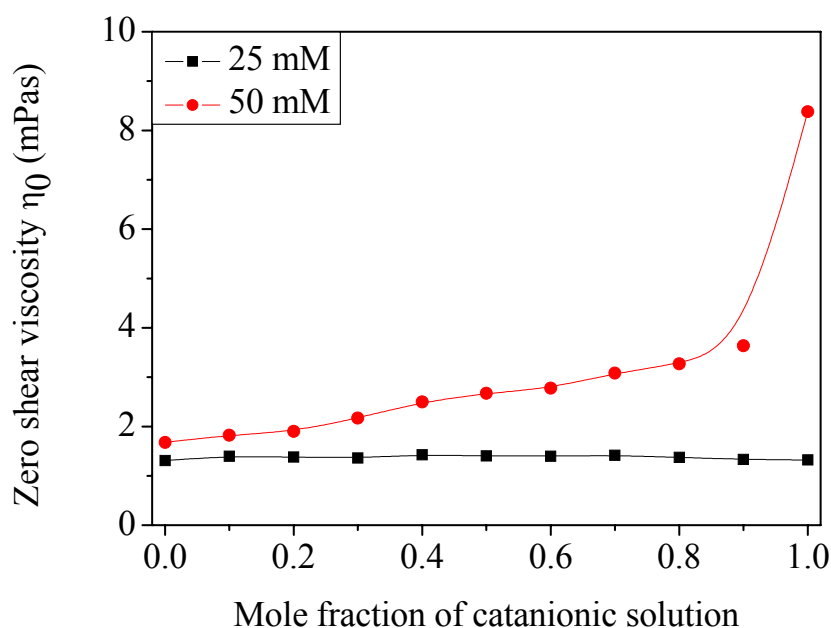


Figure 4.5.11: Zero shear viscosity as a function of the mole fraction of cationic solution in the mixture at two different concentrations. All the viscosities are measured by double gap method at 25°C.

4.5.6 Synergism

A surfactant solution may show synergism when another interacting surfactant solution is mixed with the first one, for instance an anionic surfactant solution may show synergism when an interacting cationic surfactant solution mixed with it ^{236, 237}. The effect can be observed in terms of viscosity ²³⁸, cmc ²³⁹ and surface tension ¹⁶⁴. The present study is the investigation of interaction between anionic aggregation and cationic aggregation. To verify the synergism, surface tension was measured for the series of samples and the results are displayed in figure 4.5.12. The figure shows that the surface tension in the range of anionic rich composition is almost constant. This indicates that mixing of cationic aggregation to anionic aggregation in anionic rich compositions has no effect under the consideration of surface tension profile. On the other hand, the picture is different when anionic aggregation is mixing with cationic aggregation i.e. in the range of cationic rich compositions. Surface tension decreases from 33 to 29 mNm⁻¹, about 4 units when the composition of solution was

changed from $X_{\text{catanionic}} = 1.0$ to 0.8. Similar to other methods described before, surface tension measurements are also indicating by showing synergism that thermodynamic behaviour of mixed vesicular system is strongly concentration and composition dependent.

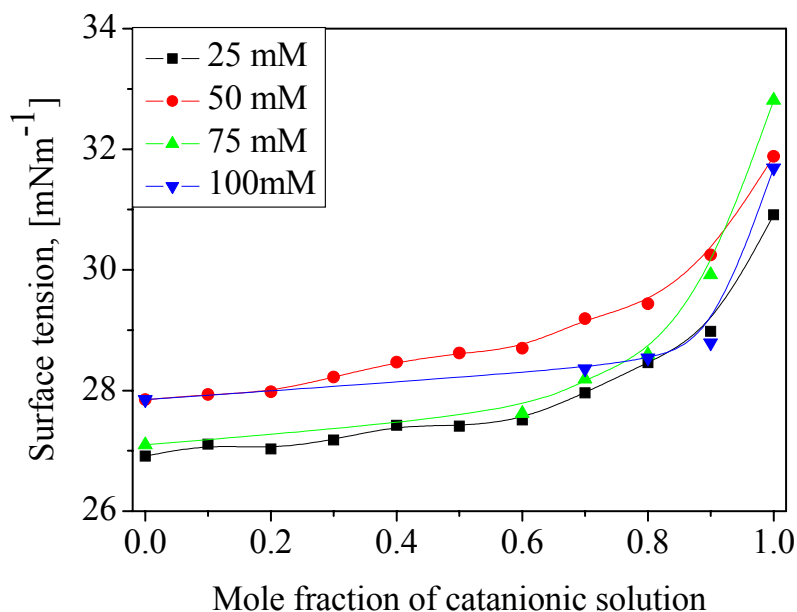


Figure 4.5.12: Surface tension of mixed aggregation system as a function of composition of solutions.

4.5.7 SANS Analysis

Figure 4.5.13 shows the scattering curves for anionic/catanionic mixed vesicular system in D_2O at the total concentration of 50 mM and at different compositions. One can see from the figure that the pure catanionic component (with mole fraction 0) does not show a minimum and the curve is characterised by a q^{-2} decay of the intensity at low and intermediate value of q , indicating the bilayer structure²²⁸. Upon increasing the mole fraction of anionic component in the solution a characteristic minimum was observed.

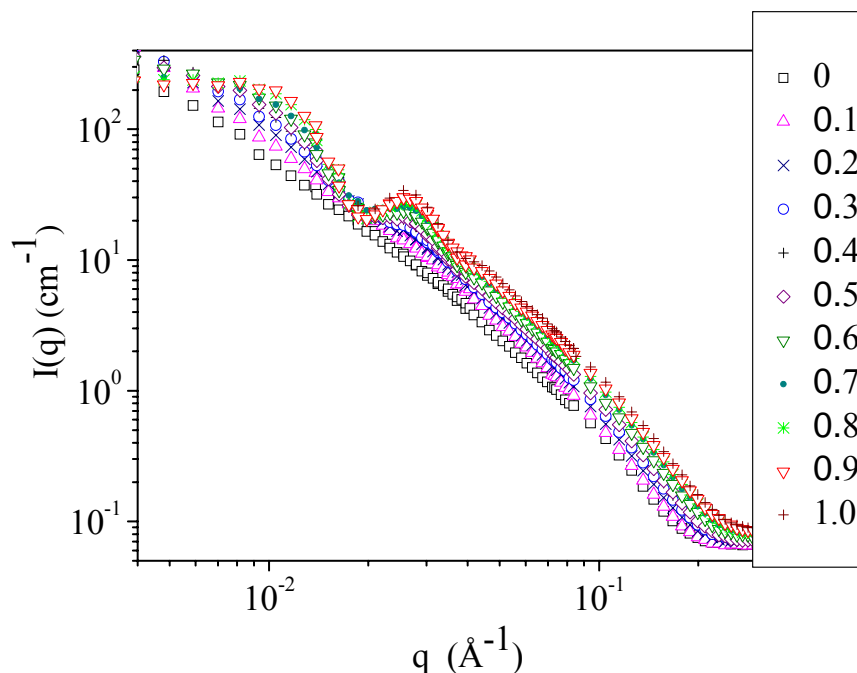


Figure 4.5.13: SANS spectra of anionic-cationic mixed vesicular system in D_2O at $25^\circ C$. The total concentration of samples was 50 mM. The inset values are indicating the mole fraction of anionic component in the samples.

The scattering intensity curve of pure cationic solution decays by q^{-2} , which is a signature of scattering from the bilayer structure²²⁸. Fitting of the empirical data with a model for planar lamellae resulted the bilayer thickness of about 2.5 nm. On the other hand spectra with higher mole fraction of anionic component show a well defined minimum indicating the presence of vesicles in the solution. Thus the spectra are qualitatively consistent with the DLS and cryo-TEM results for the presence of vesicles in the solution. Fitting the spectra to the core-shell model yields the radius of about 15 nm, a shell (bilayer) thickness of about 2.5 nm and polydispersity of about 0.25. Quantitatively the results are in good agreement with DLS observation (hydrodynamic radius 13 nm for pure anionic composition, see table 4.5.1), and both the methods revealed that the system has vesicular structure with high polydispersity.

Chapter 5: Summary

The present work is a study that concentrates on spontaneous or quasi-spontaneous formation of vesicles in the case of single chained oleate surfactant and mixed vesicles of catanionic aggregation of oleate with some cationic surfactants, with a focus on the phase behaviour. This work can be subdivided broadly into two main parts: the first part dealt with the influence of different co-surfactants on the formation of anionic vesicles from oleate and the effect of an organometallic on these vesicles. And the second part dealt with the formation of catanionic vesicles with oppositely charged surfactants.

Aqueous solution of 200 mM Na-oleate was isotropic micellar and was low viscous. Addition of octanol and geraniol as co-surfactants continuously lowered the mean spontaneous curvature on micellar interface, since they (co-surfactants) have a small head group area which increases the packing parameter. As a consequence of this continuous change in the curvature, the systems undergo a phase transition with increasing the concentration of co-surfactants from micellar L_1 phase to vesicular L_{ves} phase via a two-phase region. This indicates that the systems are spontaneously transforming from micellar to vesicular morphology following the first order phase transition rule. Aqueous Na-oleate with octanol followed this rule in the entire concentration range studied in this work (20 mM to 200 mM for surfactant and 0 to 600 mM co-surfactant). For the system with geraniol, on the other hand, it was observed that at higher concentration (150 mM to 200 mM) of surfactant, the system behaves as in the case of octanol; but when the concentration was lower than 100 mM, the system was transforming from L_1 phase to vesicular phase without forming any biphasic region. This individual phase behaviour can be interpreted by the $\pi - \pi$ stacking interaction between oleate and geraniol.

Dynamic light scattering (DLS) measurements and microscopic observations (cryo-TEM) clearly revealed that both the co-surfactants form spherical vesicles with Na-oleate. Cryo-TEM observations for the systems with both co-surfactants showed that the vesicles are unilamellar and spherical. From the comparative calculation of total surface area of all the

vesicles present in the same area of cryo-TEM micrograph it was evident that the same concentration and composition of system with geraniol produces about 18% less surface area than that of with octanol which reveals the efficiency of formation of vesicles by octanol. The rheological measurements show that the shear viscosity increases with increasing the concentration of co-surfactants in L_1 phase which indicates that the micelles are growing with increasing the co-surfactant concentration. In L_{ves} phase the viscosity increases very rapidly with co-surfactant concentration and rises approximately up to four orders of magnitude and finally at higher co-surfactant concentration the systems transformed into a stiff gel showing distinct yield stress values. This vesicular phase exhibited high viscoelasticity keeping the elastic modulus about one order of magnitude higher than the viscous modulus. It has also been observed that addition of electrolyte to the stiff gel composition reduces the viscoelastic properties of vesicular gel with a systematic decrease of storage modulus and yield stress with increasing the concentration of electrolyte. Five different electrolytes classified into two groups, mineral and organic salts, were used for the analysis and it has been observed that the effect is qualitatively similar for both mineral and organic salts. Screening of vesicular charge by the presence of electrolyte is responsible for such reduction of viscoelastic property.

The effects of an organometallic [$Ti(OBu)_4$, titanium tetra-butoxide (TTB)] have been studied on the vesiculation of surfactant and co-surfactant system. The kinetic measurements by monitoring the turbidity (originate from the emulsification of organic TTB solution into aqueous Na-oleate solution) it has been revealed that the time for the reduction of turbidity increases with increasing the metal precursor in the composition. Two simultaneous counter-acting mechanisms of dissolution of originally present emulsion droplets into the micellar aggregates and the slow production of TiO_2 network by the hydrolysis product of TTB leads to this slow decrease in turbidity. Addition of TTB on vesicular gel composition does not change the vesicle size. SAXS measurements revealed that size and ordering of the vesicles remain almost the same with increasing the TTB concentration. Rheological measurements illustrate that viscoelastic property decreases with increasing the concentration of TTB and the system transforms from stiff gel state to liquid state with higher TTB concentration. The local phase separation by the hydrolysis product of TTB, TiO_2 and the formation of a new network by TiO_2 is, maybe, a plausible explanation for this observation.

Catanionic interaction between two oppositely charged parent-surfactants oleic acid and decyltrimethyl ammonium hydroxide ($C_{10}TAOH$) is like an acid-base interaction. Phase behaviour of their interaction revealed that a narrow region with equimolar mixing

composition of two components form an isotropic partially bluish vesicular phase in the lower concentration range (≤ 50 mM total concentration). But at higher concentration (75 mM), the composition of L_{ves} phase moves towards anionic rich composition $X_{C_{10}TAB} = 0.4$ and the equimolar composition has phase separated because of crystallisation. Surprisingly no vesicular phase was observed when the total concentration was raised to 100 mM.

DLS measurements and microscopic observation by cryo-TEM indicate that equimolar composition (up to 50 mM) and $X_{C_{10}TAB} = 0.4$ at 75 mM have the vesicular morphology. Pictorial micrographs from cryo-TEM clearly revealed that the system has spherical and unilamellar vesicular structure. Sizes obtained by DLS and cryo-TEM are in good agreement and in addition it was observed that there is substantial polydispersity in the samples. In addition to the regular shaped vesicles some perforated vesicles have also been observed in cryo-TEM images which indicate the local instability of the bilayers.

In order to see an alternate way of unilamellar vesicle formation catanionic systems have been investigated. For this study four different cationic surfactants (C_8TAB , $C_{10}TAB$, $C_{12}TAB$ and $C_{14}TAB$) were selected to interact with an anionic surfactant, Na-oleate. Phase diagram and measurements of electrical conductivity clearly revealed that admixing of C_8TAB with Na-oleate does not form any phase separation and L_{ves} phase at any concentration and composition within this study range of 10 – 200 mM total concentration. Other three cationic surfactants, on the other hand, form L_{ves} phase which is separated from L_1 phase by a two-phase region which indicates that all the phase transformations are following the first order phase transition rule. In the cases of $C_{10}TAB$ and $C_{12}TAB$, only one vesicular phase has been observed; but the compositions of L_{ves} phase were a little different for different systems. For $C_{10}TAB$ the mixing composition of L_{ves} phase was always equimolar and it occurs after exceeding the concentration of 20 mM. But for $C_{12}TAB$, the vesicular phase was observed in anionic rich region including equimolar composition at low concentration, for instance at 50 mM. At higher concentration (≥ 100 mM) system was phase separated at equimolar composition. This indicates that vesicles become stabilised with long alkyl chained surfactant when it is partially charged. The ternary system of $C_{14}TAB$ shows completely different phase behaviour with aqueous Na-oleate. In this case two L_{ves} phases have been observed which have been separated by a two-phase region at equimolar composition. One L_{ves} phase is anionic rich with composition around $X_{C_{14}TAB} = 0.3$ and other L_{ves} is cationic rich with composition around $X_{C_{14}TAB} = 0.6$. These systems show a significant suppression in

conductivity by forming vesicles. Calculations revealed that maximum 18%, 30% and 22% conductivity was suppressed for the systems with C₁₀TAB, C₁₂TAB and C₁₄TAB respectively, because of the encapsulation of counter ions by the formation of vesicles.

The rheological measurements showed Newtonian behaviour for the dilute dispersion of vesicles at ≤ 50 mM total concentration. At the total concentration of 100 mM, vesicular compositions with C₁₀TAB and C₁₄TAB systems show a pronounced shear thinning behaviour, while the system with C₁₂TAB shows Newtonian behaviour; dilute vesicular dispersion is, probably, the reason for this Newtonian behaviour. The zero shear viscosities of L_{ves} phase are three to four orders of magnitude higher than the viscosity of L₁ phase with the same concentration. The results of DLS measurements further reveal that all catanionic systems with C₁₀TAB, C₁₂TAB and C₁₄TAB form vesicles at the compositions described above. The hydrodynamic radii of vesicles increases with increasing the alkyl chain length of cationic surfactants. It has been exposed from the results that cationic rich vesicles with composition $X_{C_{14}TAB} = 0.6$ is about four times bigger than the anionic rich vesicles with composition $X_{C_{14}TAB} = 0.4$.

Finally the mixed vesicular system composed with anionic aggregation and catanionic aggregation was studied – a bridge between two standard way of vesicle formation: catanionic vesiculation and co-surfactant stabilised vesiculation. Here anionic aggregation was Na-oleate with octanol as co-surfactant and catanionic aggregation was 1:1 mixing composition of aqueous Na-oleate with C₁₀TAB. The mixed vesicular system was analysed by electrical conductivity, surface tension, DLS, rheology and cryo-TEM methods. Thermodynamic behaviour of mixed aggregation system revealed that they did not form bigger aggregates at any composition when the concentration was 25 mM. The bigger aggregates (vesicles) were observed in catanionic rich compositions $X_{catanionic} = 0.8 - 0.9$ at higher concentrations, > 50 mM. The surface tension measurements also showed the synergism in the catanionic rich compositions. The surface tension reduced about 4 units when the composition is changed from $X_{catanionic} = 1.0$ to 0.8.

Chapter 6: Zusammenfassung

In der vorliegenden Arbeit wurde die spontane oder quasi-spontane Bildung von Vesikeln im Fall von als Einzelketten vorliegenden Oleat-Tensid und gemischten Vesikeln kationischer Aggregate von Oleat mit kationischen Tensiden untersucht. Hauptaugenmerk wurde dabei auf das Phasenverhalten gelegt. Diese Arbeit kann in zwei Teilabschnitte unterteilt werden: der erste Teil behandelt den Einfluss verschiedener Kotenside auf die Bildung anionischer Vesikel aus Oleat und den Effekt von organometallischen Verbindungen auf diese Vesikel. Der zweite Teil behandelt die Bildung von kationischen Vesikeln mit entgegengesetzt geladenen Tensiden.

Eine wässrige Lösung mit 200 mM Na-Oleat ist isotrop mizellar und niedrigviskos. Zugabe von Oktanol und Geraniol als Kotenside verringerten kontinuierlich die durchschnittliche spontane Krümmung der Mizellgrenzfläche, da sie durch ihre kleineren Kopfgruppen das System hin zu größeren Packungsparametern beeinflussen. Auf diese kontinuierliche Veränderung der Krümmung lässt sich der Phasenübergang von L_1 Phase zu vesikulärer L_{ves} Phase über ein Zweiphasengebiet mit steigender Kotensidkonzentration zurückführen. Das zeigt, dass die Systeme sich spontan von Mizell- in Vesikelmorphologie überführen lassen, indem sie der Phasenübergangsregel erster Ordnung folgen. Dieses Verhalten konnte bei wässrigem Na-Oleat mit Oktanol über den gesamten, in dieser Arbeit untersuchten Konzentrationsbereich (20 mM bis 200 mM für Tensid und 0 bis 600 mM Kotensid) beobachtet werden. Für das System mit Geraniol wurde bei höherer Tensidkonzentration (150 mM bis 200 mM) das selbe Verhalten wie bei Oktanol beobachtet; hingegen bei Konzentrationen niedriger als beispielsweise 100 mM geht das System von einer L_1 Phase in eine vesikuläre Phase über, ohne ein Zweiphasengebiet zu durchschreiten. Dieses individuelle Phasenverhalten kann durch $\pi - \pi$ Stacking Wechselwirkungen zwischen Oleat und Geraniol erklärt werden.

Dynamische Lichtstreuexperimente (DLS) und mikroskopische Untersuchungen (cryo-TEM) zeigten deutlich, dass beide Kotenside kugelförmige Vesikel mit Na-Oleat bilden. Winkelabhängige DLS-Messungen zeigten keine signifikante Veränderung des

hydrodynamischen Radius. Diese Beobachtung geht gut konform mit den cryo-TEM Ergebnissen, bei denen unilamellare, sphärische Vesikel beobachtet werden konnten. Von vergleichenden Berechnungen der Gesamtoberfläche aller vorhandener Vesikel, die im gleichen Bereich des cryo-TEM-Bildes vorhanden waren, zeigte sich, dass bei gleicher Konzentration und Zusammensetzung das System mit Geraniol ca. 18% weniger Oberfläche als das mit Oktanol aufweist, was die Effizienz der Vesikelbildung durch Oktanol zeigt. Rheologische Untersuchungen zeigten, dass die Scherviskosität mit steigender Konzentration an Kotensid in der L_1 Phase zunahm, was mit dem Wachstum der Mizellen erklärt werden kann. In der L_{ves} Phase stieg die Viskosität schnell mit der Kotensidkonzentration um bis zu vier Größenordnungen an. Letztlich ging das System bei höheren Kotensidgehalt in ein festes Gel über, welches deutliche Fließgrenzen aufweist. Diese Vesikelphase zeigte Viskoelastizität mit einem Elastizitätsmodul, welches um eine Größenordnung über dem viskosen Modul lag. Es wurde ebenfalls beobachtet, dass die Zugabe von Elektrolyt zum Gel die viskoelastischen Eigenschaften des Vesikelgels verringerte, was in einem fast systematischen Abfall von Speichermodul und Fließgrenze mit steigender Elektrolytkonzentration zu sehen war. Fünf unterschiedliche Elektrolyte, die sich in zwei Klassen (mineralische und organische Salze) einteilen lassen, wurden für die Analyse verwendet und es wurde beobachtet, dass der Effekt qualitativ vergleichbar für beide ist. Das Abschirmen der Vesikelladung in Gegenwart von Elektrolyt ist für eine solche Verminderung der viskoelastischen Eigenschaften verantwortlich.

Der Effekt einer organometallischen Verbindung [$Ti(OBu)_4$, titanium tetra-butoxide (TTB)] auf die Vesikelbildung von Tensid und Kotensid wurde ebenfalls untersucht. Kinetische Messungen der Veränderung der Trübung, die von der Emulsionsbildung der organischen TTB-Lösung in der wässrigen Na-Oleat-Lösung herrühren, zeigten, dass die Zeit für die Abnahme der Trübung mit zunehmendem Metallprecursor in der Zusammensetzung zunimmt.

Zwei entgegenwirkende Mechanismen - Lösung der anfänglich vorhandenen Emulsionströpfchen in den mizellaren Aggregaten und die langsame TiO_2 -Netzwerkbildung durch Hydrolyse von TTB mit Wasser - führen zu dieser langsamen Abnahme der Trübung. Zugabe von TTB zu Vesikelgelzusammensetzungen ändert die Vesikelgröße hingegen nicht. SAXS-Messungen haben gezeigt, dass die Größe und die Orientierung der Vesikel mit zunehmender TTB-Konzentration im Gel nahezu unverändert bleiben. Rheologische Messungen zeigen, dass die viskoelastischen Eigenschaften mit steigender TTB-

Konzentration geringer werden und das System von einem festen Gel in einen flüssigen Zustand übergeht. Lokale Phasentrennung durch das Produkt der Hydrolyse von TTB, TiO_2 und Bildung eines neuen Netzwerks aus TiO_2 und gleichzeitiger Zerstörung des Vesikelgels sind die Gründe dafür.

Kationische Wechselwirkungen zwischen entgegengesetzt geladenen Tensiden, Ölsäure und Decyltrimethyl ammonium hydroxid (C_{10}TAOH) ist ähnlich einer Säure-Base Wechselwirkung. Das Phasenverhalten zeigt, dass in einem kleinen Bereich mit äquimolarer Mischungszusammensetzung eine isotrope, teilweise bläuliche Vesikelphase im unteren Konzentrationsbereich (≤ 50 mM Gesamtkonzentration) gebildet wird. Hingegen wurde bei höheren Konzentrationen (75 mM) die Zusammensetzung der L_{ves} Phase zur anionenreichen Zusammensetzung $X_{\text{C}_{10}\text{TAB}} = 0.4$ hin verschoben und eine äquimolare Zusammensetzung wurde aufgrund von Kristallisation phasensepariert. Überraschenderweise wurde keine Vesikelphase beobachtet, wenn die Konzentration auf 100 mM erhöht wurde.

DLS-Messungen und cryo-TEM zeigten, dass äquimolare Zusammensetzungen (bis zu 50 mM) und $X_{\text{C}_{10}\text{TAB}} = 0.4$ bei 75 mM Vesikelmorphologie besitzen. cryo-TEM-Bilder zeigen deutlich, dass das System sphärische unilamellare Struktur aufweist. DLS und cryo-TEM zeigen übereinstimmende Größen und beide Methoden bestätigen die Polydispersität der Probe deutlich. Zusätzlich zu den regelmäßig geformten Vesikeln wurden ebenfalls einige perforierte Vesikel im cryo-TEM beobachtet.

Ein Alternativweg zur Bildung unilamellarer Vesikel sind kationische Tensidsysteme. Für diese Versuche wurden vier verschiedene kationische Tenside (C_8TAB , C_{10}TAB , C_{12}TAB and C_{14}TAB) ausgesucht, die mit einem anionischen Tensid, Na-Oleat, gemischt wurden. Phasendiagramm und elektrische Leitfähigkeit zeigen deutlich, dass Zumischung von C_8TAB zu Na-Oleat bei kleiner Konzentration und Zusammensetzung innerhalb des untersuchten Bereichs von 10 – 200 mM Gesamtkonzentration weder Phasentrennung noch L_{ves} Phasen zur Folge hat. Die anderen drei kationischen Tenside andererseits bilden L_{ves} Phasen, welche durch ein Zweiphasengebiet von der L_1 Phase getrennt sind. Das zeigt, dass es sich um Phasenübergänge erster Ordnung handelt. Im Fall von C_{10}TAB und C_{12}TAB wurden nur Vesikelphasen beobachtet. Aber die Zusammensetzung der L_{ves} Phase unterschied sich geringfügig bei unterschiedlichen Systemen. Für C_{10}TAB war die Mischungszusammensetzung immer äquimolar und die Vesikelphase tritt oberhalb von 20 mM auf.

Hingegen wurde bei $C_{12}TAB$ die Vesikelphase im anionisch angereicherten Bereich beobachtet, welcher die äquimolare Zusammensetzung bei geringen Konzentrationen bei beispielsweise 50 mM einschließt. Bei höheren Konzentrationen (≥ 100 mM) unterlief das System einer Phasentrennung bei äquimolarer Zusammensetzung. Das zeigt, dass die Vesikel durch Tenside mit langen Alkylketten stabilisiert werden, wenn sie teilweise geladen sind. Das ternäre System $C_{14}TAB$ zeigt unterschiedliches Phasenverhalten mit wässrigem Na-Oleat. In diesem Fall wurden zwei L_{ves} Phasen beobachtet, die durch ein Zweiphasengebiet bei äquimolarer Zusammensetzung getrennt sind. Eine L_{ves} Phase ist anionisch angereichert mit der ungefähren Zusammensetzung von $X_{C_{14}TAB} = 0.3$ und die andere L_{ves} ist kationisch angereichert mit $X_{C_{14}TAB} = 0.6$.

Die Systeme mit anderen kationischen Tensiden zeigen eine signifikante Unterdrückung der Leitfähigkeit durch Vesikelbildung. Berechnungen zeigen, dass maximal 18%, 30% und 22% Leitfähigkeit in den Systemen mit $C_{10}TAB$, $C_{12}TAB$ und $C_{14}TAB$ aufgrund von Einschluss von Gegenionen während der Vesikelbildung unterdrückt wurden.

In rheologische Messungen wurde Newtonsches Verhalten für verdünnte Dispersionen der Vesikel bei Gesamtkonzentrationen ≤ 50 mM beobachtet. Bei Gesamtkonzentrationen von 100 mM zeigen Zusammensetzungen mit $C_{10}TAB$ und $C_{14}TAB$ ein ausgeprägtes scherverdünnendes Verhalten, während das System mit $C_{12}TAB$ sich newtonsch verhält. Die Nullscherviskositäten der L_{ves} Phase sind drei bis vier Größenordnungen höher als die Viskosität der L_1 Phase mit gleicher Konzentration. DLS Messungen zeigen weiterhin, dass alle kationischen Systeme mit $C_{10}TAB$, $C_{12}TAB$ und $C_{14}TAB$ bei allen oben beschriebenen Zusammensetzungen Vesikel ausbilden. Der hydrodynamische Radius der Vesikel steigt mit zunehmender Alkylkettenlänge des kationischen Tensids. Den Ergebnissen ist zu entnehmen, dass kationisch angereicherte Vesikel der Zusammensetzung $X_{C_{14}TAB} = 0.6$ etwa viermal größer als die anionisch angereicherten Vesikel der Zusammensetzung $X_{C_{14}TAB} = 0.4$ sind.

Zuletzt wurden die gemischten vesikulären Systeme, die aus anionischer und kationischer Aggregation entstehen, untersucht. Dies stellt eine Brücke zwischen zwei Standardprozeduren zur Bildung von Vesikeln dar: Kationische Vesikelbildung und kotensidstabilisierte Vesikelbildung. Hier stellte Na-Oleat das anionische Aggregat mit Oktanol als Kotensid. Das kationische Aggregat war eine 1:1 Mischung aus wässrigem Na-Oleat mit $C_{10}TAB$. Das gemischt-vesikuläre System wurde mittels elektrischer Leitfähigkeit, Oberflächenspannung,

DLS, Rheologie, SANS und cryo-TEM untersucht. Thermodynamisches Verhalten der gemischt aggregierten Systeme zeigte, dass sie bei keiner Zusammensetzung größere Aggregate bilden, wenn die Konzentration 25 mM beträgt. Größere Aggregate (Vesikel) wurden in kationisch angereicherten Zusammensetzungen $X_{\text{catanionic}} = 0.6 - 0.9$ bei höheren Konzentrationen > 50 mM beobachtet. Die Oberflächenspannung zeigte ebenfalls Synergismen in den kationisch angereicherten Zusammensetzungen. Die Oberflächenspannung sank um vier Einheiten, wenn die Zusammensetzung von $X_{\text{catanionic}} = 1.0$ hin zu 0.8 verändert wird.

Chapter 7: References

1. Ekwall, P., and Mandell, L., Fontell, K.; *Mol. Cryst. Liq. Cryst.*; **1969**, 8, 157.
2. Wennerström, H., and Lindman, B.; *Phys. Rep.*; **1979**, 52, 1.
3. Tiddy, G. J. T.; *Phys. Rep.*; **1980**, 57, 1.
4. Chevalier, Y., and Zemb, T.; *Rep. Prog. Phys.*; **1990**, 53, 279.
5. Laughlin, R. G.; *The Aqueous phase behaviour of surfactant* (London, academis); **1994**.
6. Tanford, C.; *The Hydrophobic Effect: Formation of Micelles and Biological Membranes*, Second Edition, (New York, John Wiley); **1980**.
7. Jirgensons, B., and Straumanis, M. E.; *Kurzer Lehrbuch der Kolloidchemie*; Bergman und Springer, Berlin, Heidelberg, New York; **1949**.
8. Staudinger, H.; *Organische Kolloidchemie, 3^{te} Ausgabe*, Vieweg Verlag, Braunschweig; **1950**.
9. Wedler, G.; *Lehrbuch der Physikalischen Chemie*, Verlag Chemie VCH, Weinheim; **1987**.
10. Beck, J. S., Vertuli, J. C., Roth, W. J., Leonowicz, M. E., Kresge, C. T., Schmitt, K. D., Chu, C. T. W., Olson, D. H., and Sheppard, E. W.; *J. Am. Chem. Soc.*; **1992**, 114, 10834.
11. Smith, W. V., and Ewart, R. H.; *J. Chem. Phys.*; **1948**, 16, 592.
12. Tsujii, K.; *Surface Activity: Principles, Phenomena and Application*; Academy press; **1998**, p-196.
13. Derjaguin, B., and Landau, L.; *Acta Physicochim*; **1941**, 14, 633.
14. Verwey, E., and Overbreek, J. Th. G.; *Theory of the Stability of Lyophobic Colloids*, Elsevier, Amsterdam; **1948**.
15. Gradzielski, M.; *J. Physics: Condens. Matter*; **2003**, 15, R655.
16. Israelachvili J. N., Mitchell, D. J., and Ninham, B. W.; *J. Chem. Soc. Faraday Trans. II*; **1976**, 72, 1525.
17. Balmbra, R. R., Clunie, J. S., and Goodman, J. F.; *Nature*, **1969**, 222, 1159.
18. Hoffmann, H., Platz, G., Rehage, H., Reizlein, K., and Ulbricht, W.; *Makromol. Chem.*; **1981**, 182, 451.
19. Schneider, M. B., and Webb, W. W.; In Safran, S. A., and Clark, N. A. (Ed.) *Physics of Complex and super molecular Fluids*, J. Wiley and Sons, New York; **1987**, p-179.
20. Papahadjopoulos, D; *Ann. New York Acad. Sci.*; **1978**, 308, 371.

21. Bangham, A. D., and Horne, R. W.; *J. Mol. Biol.*; **1964**, 8, 660.
22. Bangham, A. D., Standish, M. M., and Watkins, J. C.; *J. Mol. Biol.*; **1965**, 13, 239.
23. Pinazza, P., Roux, D., Vuillaume, V., Lu, C. Y. D., and Cates, M. E.; *Langmuir*; **1996**, 12, 248.
24. Regev, O., and Guillemet, F.; *Langmuir*, **1999**, 15, 4357.
25. Israelachvili J. N., Mitchell, D. J., and Ninham, B. W.; *Biochim. Biophys. Acta*; **1977**, 470, 185.
26. Schomäcker, R., and Strey R.; *J. Phys. Chem.*; **1994**, 98, 3908.
27. Benton, W. J., and Miller, C. A.; *J. Chem. Phys.*; **1983**, 87, 4981.
28. Lang, J., and Morgan, R. D.; *J. Phys. Chem.*; **1980**, 73, 5849.
29. Gazeau, D., Bellocq A. M., Roux, D., and Zemb, T.; *Europhys. Lett.*; **1989**, 9, 447.
30. Strey, R., Jahn, W., Porte, G., and Bassereau, P.; *Langmuir*; **1990**, 6, 1635.
31. Miller, C. A., Gradzielski, M., Hoffmann, H., Krämer, U, and Thunig, C.; *Prog. Colloid Polym. Sci.*; **1991**, 84, 243.
32. Roux, D., Coulon, C., and Cate, M. E.; *J. Phys. Chem.*; **1992**, 96, 4174.
33. Mitchell, D. J., and Ninham, B. W.; *J. Chem. Soc. Faraday Trans. II*; **1981**, 77, 601.
34. Helfrich, W.; *Z. Naturforsch.*; **1973**, 28c, 693.
35. Helfrich, W.; *J. Phys.: Condens. Matter*; **1994**, 6, A79.
36. Bangham, A. D.; *Annu. Rev. Biochem.*; **1972**, 41, 753.
37. Lipowski, R., and Sackmann, E. (ed); *Structure and Dynamics of Membrane*, (Amsterdam, Elsevier), **1995**.
38. Mc Calden, T. A.; *Adv. Drug Deliv. Rev.*; **1990**, 5, 253.
39. Lasic, D. D., and Losoff, M. (Ed.); *Vesicles* (Surface Science Series, Vol. 62) (New York: Dekker), **1996**, p-447.
40. Felgner, P. L.; *Adv. Drug Deliv. Rev.*; **1990**, 5, 163.
41. Szoka, F., and Papahadjopoulos, D.; *Annu. Rev. Biophys. Bioeng.*; **1980**, 9, 467.
42. Tadros, T. F.; *Adv. Colloid. Interface Sci.*; **1993**, 46, 1.
43. Gradzielski, M., Müller, M., Bergmeier, M., Hoffmann, H., and Hoinkis, E.; *J. Phys. Chem. B*; **1999**, 103, 1416.
44. Söderman, O., Herrington, K. L., Kaler, E. W., and Miller, D. D.; *Langmuir*; **1997**, 13, 5531.
45. Tanford, C.; *The Hydrophobic Effect*, John Wiley, New York, **1980**.
46. Israelachvili, J. N.; *Intermolecular and Surface Forces*, 2nd Edition; Academy Press, London, **1992**.

47. Everett, D. H.; *Pure Appl. Chem.*; **1972**, 31, 579.
48. Information Bulletin from Int. Union of Pure and Applied Chemistry “*Reporting Experimental Data Dealing with Critical Micellization Concentrations*”; Sept., **1976**.
49. Shaw, D. J.; *Introduction to Colloid and Surface Chemistry*; (Butterworths, London, **1970**).
50. Murray, R. C., and Hartley, G. S.; *Trans. Faraday Soc.*; **1935**, 31, 183.
51. Moroi, Y., and Matuura, R.; *Bull Chem. Soc. Jpn.*; **1988**, 61, 333.
52. Shinoda, K., and Becher, P.; *Principles of Solution and Solubility*; Marcel Dekker: New York, **1978**, p-159.
53. Yu, Z. J., Zhang, X., Xu, G., and Zhao, G. X.; *J. Phys. Chem.*; **1990**, 94, 3675.
54. Shinoda, K., Minegishi, Y. and Arai, H.; *J. Phys. Chem.*; **1976**, 18, 1987.
55. Shinoda, K., Hato, M., and Hayashi, T.; *J. Phys. Chem.*; **1972**, 76, 909.
56. Tartar, H. V., and Cadle, R. D.; *J. Phys. Chem.*; **1939**, 43, 1173.
57. Tsujii, K., and Mino, J.; *J. Phys. Chem.*; **1978**, 82, 1610.
58. Nilsson, F., Söderman, O., and Johansson, I.; *Langmuir*, **1997**, 13, 3349.
59. Kunieda, H., Shigeta, K., Ozawa, K., and Suzuki, M. ; *J. Phys. Chem. B.*; **1997**, 101, 7952.
60. Kunieda, H., Uddin, Md. H., Horii, M., Furukawa, H., and Harashima, A.; *J. Phys. Chem. B.*; **2001**, 105, 5419.
61. London, F.; *Trans. Faraday Soc.*; **1937**, 33, 19.
62. Hamaker, H. C.; *Physica IV*, **1937**, 10, 1058.
63. Lifshitz, E. M.; *Soviet Physics*; **1956**, 2(1), 73.
64. Hough, D. B., and Lee, R. W.; *Adv. Colloid Interface Sci.*; **1980**, 14, 3.
65. Prieve, D. C., and William, B. R.; *J. Colloid Interface Sci.*; **1981**, 81(1), 285.
66. Israelachvili, J.; *Intermolecular and Surface Forces*; Academic Press, San Diego, **1991**, p-169.
67. Muller, D. J. and Engel, A.; *J. Structural Biol.*; **1997**, 119(2), 149.
68. Sogami, I.; *Physics Letter A*; **1983**, 96A (4), 199.
69. Langmuir, I.; *J. Chem. Phys.*; **1938**, 6, 873.
70. Israelachvili, J. N., and Wennerström, H.; *Nature*; **1996**, 379, 219.
71. Parsegian, V. A., and Rand, R. P.; *Langmuir*; **1991**, 7, 1299.
72. Binder, H., Dietrich, U., Schalke, M., and Pfeiffer, H.; *Langmuir*; **1999**, 15, 4857.
73. Pfeiffer, H., Binder, H., Klose, G., and Heremans, K.; *Biochim. Biophys. Acta*, **2003**, 1609, 144.

74. Leneveu, D. M., Rand, R. P., and Parsegian, V. A.; *Nature*; **1976**, 259, 601.
75. Leneveu, D. M., Rand, R. P., Parsegian, V. A., and Gingell, D.; *Biophys. J.*; **1977**, 18, 209.
76. Clunie, J. S., Goodman, J. F. and Symons, P. C.; *Nature*; **1967**, 216, 1203.
77. Marsh, D.; *Biophys. J.*; **1989**, 55, 1093.
78. Rand, R. P., and Parsegian, V. A.; *Biochim. Biophys. Acta*; **1989**, 988, 351.
79. Pfeiffer, H., Binder, H., Klose, G., and Heremans, K.; *Phys. Chem. Chem. Phys.*; **2004**, 6, 614.
80. Rand, R. P., Fuller, N. L., Gruner, S. M., and Parsegian, V. A.; *Biochem.*; **1990**, 29, 76.
81. Pavelic, Z., Skalko-Basnet, N., and Schubert, R.; *Intl. J. Pharm.*; **2001**, 219, 139.
82. Papahadjopoulos, D., and Watkins, J. C.; *Biochim, Biophys. Acta*; **1967**, 135, 639.
83. Johnson, S. M., Bangham, A. D., Hill, M. W., and Korn, E. D.; *Biochim. Biophys. Acta*; **1971**, 233, 820.
84. Huang, C. H.; *Biochemistry*; **1969**, 8, 344.
85. Butler, P.; *Current Opinion Colloid Interface Sci.*; **1999**, 4, 214.
86. Wiesner, U.; *Macromol. Chem. Phys.*; **1997**, 198, 3319.
87. Diat, O., and Roux, D.; *J. Phys. II*; **1993**, 3, 9.
88. Diat, O., Nallet, F., and Roux, D.; *J. Phys. II*; **1993**, 3, 1427.
89. Montalvo, G., Rodenas, E., and Valiente, M.; *J. Colloid Interface Sci.*; **1998**, 202, 232.
90. Bergmeier, M., Gradzielski, M., Hoffmann, H., and Mortensen, K.; *J. Phys. Chem. B*; **1999**, 103, 1605.
91. Gradzielski, M., Bergmeier, M., Hoffmann, H., Müller, M., and Grillo, I.; *J. Phys. Chem. B*; **2000**, 104, 11594.
92. Bergenholtz, J., and Wagner, N. J.; *Langmuir*; **1996**, 12, 3122.
93. Herve, P., Roux, D., Bellocq, A. M., Nallet, F., and Gulik-Krzywicki, T.; *J. Phys. II*; **1993**, 3, 1255.
94. Van der Werff, J. C., and de Kruif, C. G.; *J. Rheol.*; **1989**, 33, 421.
95. Escalante, J. I., Gradzielski, M., Hoffmann, H., and Mortensen, K.; *Langmuir*; **2000**, 16, 8653.
96. Mendes, E., Narayanan, J., Oda, R., Kern, F., Candau, S. J., and Manohar, C.; *J. Phys. Chem. B*; **1997**, 101, 2256.
97. Mendes, E., Oda, R., Manohar, C., and Narayanan, J.; *J. Phys. Chem. B*; **1998**, 102, 338.
98. Ninham, B. W., Evans, D. F., and Wei, G. J.; *J Phys. Chem.*; **1983**, 87, 5020.

99. Brady, J. E., Evans, D. F., Kachar, B., and Ninham, B. W.; *J. Am. Chem. Soc.*; **1984**, 106, 4279.
100. Hoffmann, H., Gräbner, D., Hornfeck, U., and Platz, G.; *J. Phys. Chem. B*; **1999**, 103, 611.
101. Kamenka, N., Chorro, M., Talmon, Y., and Zana, R.; *Colloid Surf.*; **1992**, 67, 213.
102. Kaler, E. W., Murthy, A. K., Rodriguez, B. E., and Zasadzinski, J. A. N.; *Science*; **1989**, 245, 1371.
103. Kaler, E. W., Herrington, K. L., Murthy, A. K., and Zasadzinski, J. A. N.; *J. Phys. Chem.*; **1992**, 96, 6698.
104. Seddon, J. M.; *Biochim. Biophys. Acta*; **1990**, 1, 1031.
105. Lindblomand, G., and Rilfors, L.; *Biochim. Biophys. Acta*; **1989**, 221, 988.
106. Oetter, G., and Hoffmann, H.; *J. Disp. Sci. Tech.*; **1988-89**, 9, 459.
107. Leung, R., and Shah, D. O.; *J. Colloid Interface Sci.*; **1987**, 120, 320.
108. Gradzielski, M.; *Langmuir*; **1998**, 14, 6037.
109. Hofmeister, F.; *Arch. Exp. Pathol. Pharmacol.*; **1888**, 24, 247.
110. Schott, H.; *Collids Surf.*; **1984**, 11, 51.
111. Atherton, A. D., and Barry, B. W.; *J. Colloid Interface Sci.*; **1985**, 106, 479.
112. Iwanaga, T., Suzuki, M., and Kunieda, H.; *Langmuir*; **1998**, 14, 5775.
113. Grossfield, A., Ren, P., and Ponder, J. W.; *J. Am. Chem. Soc.*; **2003**, 125, 15671.
114. Kropman, M. F., and Bakker, H. J.; *Science*; **2001**, 291, 2118.
115. Corti, M., and Degiorgio, V.; *J. Phys. Cham.*; **1981**, 85, 1442.
116. Blankstein, D., Thurston, G. M., and Benedek, G. B.; *J. Chem. Phys.*; **1986**, 85, 7268.
117. Mitchell, D. J., Tiddy, G. J. T., Waring, L., Bostok, T., and McDonald, M. P.; *J. Chem. Soc. Faraday Trans. I*; **1983**, 79, 975.
118. Warr, G. G., Zemb, T. N., and Drifford, M.; *J. Phys. Chem.*; **1990**, 94, 3086.
119. Buckingham, S. A., Garvey, C. J., and Warr, G. G.; *J. Phys. Chem.*; **1993**, 97, 10236.
120. Cohen, I., Hiskey, C. F., and Oster G.; *J. Colloid Sci.*; **1954**, 9, 243.
121. Cates, M. E., and Milner, S. T.; *Phys. Rev. Lett.*; **1989**, 62, 1856.
122. Helfrich, W.Z.; *Naturforsch.*; **1978**, a33, 305.
123. Diat, O., and Roux, D.; *J. Phys. II*; **1993**, 3, 9.
124. Roux, D., Nallet, F., and Diat, O.; *Europhys. Lett.*; **1993**, 24, 53.
125. Van der Linden, E., Hogervorst, W. T., and Lekkerkerker, H. N. W.; *Langmuir*; **1996**, 12, 3127.
126. Evans, D. J.; *Phys. Rev. A*; **1982**, 25(5), 2788.

127. Clark, N.A., and Ackerson, B. J.; *Phys. Rev. Lett.*; **1980**, 44, 1005 and **1981**, 46, 1123.
128. Cates, M. E., and Milner, S. T.; *Phys. Rev. Letter*; **1987**, 87, 697.
129. Rehage, H, and Hoffmann, H.; *Rheol. Acta*; **1982**, 21, 561.
130. Hoffmann, H., Hofmann, S., Rauscher, A., and Klaus, J.; *Prog. Colloid Polym. Sci.*; **1991**, 84, 24.
131. Diat, O., and Roux, D.; *Langmuir*; **1995**, 11, 1392.
132. Yamamoto, J., and Tanaka, H.; *Phys. Rev. Letter*; **1996**, 77, 4390.
133. Berghausen, J., Zipfel, J., Lindner, P., and Richtering, W.; *Europhys. Lett.*; **1998**, 43(6), 683.
134. Mukerjee, P., and Mysels, K. J.; *Critical Micelle Concentration of aqueous Surfactant Systems*; US Government Printing office, Washington DC, **1971**.
135. Flockhart, B. D., and Graham, H.; *J. Colloid Sci.*; **1953**, 8, 105.
136. Seddon, J. M.; *Biochim. Biophys. Acta*; **1990**, 1031, 1.
137. Seddon, J. M., and Templer, R. H.; *Philos. Trans. R. Soc. Lond. A*; **1993**, 344, 377.
138. Lindblom, G., and Rilfors, L.; *Biochim. Biophys. Acta*; **1989**, 988, 221.
139. Kunieda, H., Kanei, N., Uemoto, A., and Tobita, I.; *Langmuir*; **1994**, 10, 4006.
140. Barnes, H. A., Hutton, J. F., and Walters, K.; *An Introduction to Rheology*; Elsevier, Amsterdam, **1989**.
141. Cross, M. M.; *J. Colloid Sci.*; **1965**, 20, 417.
142. Cox, W. P., and Merz, E. H.; *J. Polym. Sci.*; **1958**, 28, 619.
143. Ferry, J. D.; *Viscoelastic Properties of Polymers*; John Wiley, New York, **1980**.
144. Pflaumbaum, M., Rehange, H., and Talmon, Y.; *Tenside, Surf. Det.*; **2002**, 39, 212.
145. Hoffmann, H., Thunig, C., Schmiedel, P., and Munkert, U.; *Langmuir*, **1994**, 10, 3972.
146. Saltero, J. F. A., Bautista, F., Puig, J. E., and Manero, O.; *Langmuir*; **1999**, 15, 1604.
147. Saltero, J. F. A., Puig, J. E., and Manero, O.; *Langmuir*; **1996**, 12, 2654.
148. Manero, O., Bautista, F., Saltero, J. F. A., and Puig, J. E.; *J. Non-Newt. Fluid Mech.*; **2002**, 106, 1.
149. de Gennes, P. G.; *J. Chem. Phys.*; **1971**, 55, 572.
150. Doi, M., and Kuzuu, N. Y.; *J. Polym. Sci. Polym. Lett. Ed.*; **1980**, 18, 775.
151. Graessley, W. W.; *Adv. Polym. Sci.*; **1982**, 47, 68.
152. Berne, B. J. and Pecora, R.; *Dynamic Light Scattering* (Krieger, Malabar, Fla.); **1990**.
153. Schätzel, K.; “Single Photon Correlation Techniques” in *Dynamic Light Scattering*, Brown, W. Ed., (Oxford University, Oxford, UK); **1993**.
154. Frisken, B. J.; *Applied Optics*; **2001**, 40(24), 4087.

155. Ford, N. C. Jr., and Pecora, R. Ed.; *Dynamic Light Scattering*; Plenum Press, New York, **1985**, p-18.
156. Koppel, D. E.; *J. Chem. Phys.*; **1972**, 57(11), 4814.
157. Stepanek, P.; *Data Analysis in Dynamic Light Scattering*; Brown, W. Ed. (Oxford University, Oxford, UK), **1993**, pp 177-240.
158. Chu, B.; *Laser Light Scattering: Basic Principles and Practice*, Academic Press, Boston, **1991**.
159. Guinier, A., Fournet, G.; *Small Angle Scattering of X-ray*; John Wiley, New York, **1955**.
160. Porod, G.; *Kolloid-Z*; **1951**, 124, 83.
161. Hashimoto, T., Fujimura, M., and Kawai, H.; *Macromolecules*; **1980**, 13, 1660.
162. Hiemenz, P. C.; *Principles of Colloid and Surface Chemistry*; Marcel Dekker, New York, **1986**.
163. Bockris, J. O.; and Reddy, A. K. N.; *Modern Electrochemistry, Vol. I*; Plenum Press, New York, **1970**.
164. Hoffmann, H.; *Progr. Colloid Polym. Sci.*, **1990**, 83, 16.
165. Platz, G., Thunig, C., and Hoffmann, H.; *Ber. Bunsen-Ges. Phys. Chem*; **1992**, 96, 667.
166. Gradzielski, M., Bergmeier, M., Müller, M., and Hoffmann, H.; *J. Phys. Chem. B*; **1997**, 101, 1719.
167. Zimmels, Y., and Lin, I.; *J. Colloid Polym Sci.*; **1974**, 252, 594.
168. Edwards, K., Silvander, M., and Karlsson, G.; *Langmuir*; **1995**, 11, 2429.
169. Laura, L. B., Kathleen, L. H., and Kaler E. W.; *Langmuir*; **1995**, 11, 4267.
170. Song, B., Wang, Z., Chen, S., Zhang, X., Fu, Y., Smet, M., and Dehaen, W.; *Angew. Chem.*; **2005**, 117, 4809.
171. Hargreaves, W. R., and Deamer, D. W.; *Biochemistry*; **1978**, 17, 3759.
172. Talmon, Y., Evans, D. F., and Ninham, B. W.; *Science*; **1983**, 221, 1047.
173. Hoffmann, H., Thunig, C., Munkert, U., Meyer, H. W., and Richter, W.; *Langmuir*; **1992**, 8, 2629.
174. Ambuhl, M., Bangerter, F., Luisi, P. L., Skrabal, P., and Watzke, H. J.; *Langmuir*; **1993**, 9, 36.
175. Chiruvolu, S., Warriner, H. E., Naranjo, E., Idziak, S., Radler, J. O., Plano, R. J., Zasadzinski, J. A., and Safinya, C. R.; *Science*; **1994**, 266, 1222.
176. Ristori, S., Appell, J., and Porte, G.; *Langmuir*; 1996, 12, 686.
177. Martinez, J. S., Zhang, G. P., Holt, P. D., Jung, H. T., Carrano, C. J., Haygood, M. G., and Butler, A.; *Science*; **2000**, 287, 1245.

178. Viseu, M. I., Edwards, K., Campos, C. S., and Costa, S. M. B.; *Langmuir*; **2000**, 16, 2105.
179. Helfrich, W.; *Z. Naturforsch*; **1973**, A 33, 305.
180. Safran, S. A., Pincus, P., and Andelman, D.; *Science*; **1990**, 248, 354.
181. Safran, S. A., Pincus, P. A., Andelman, D., and McKintosh, F. C.; *Phys. Rev. A At. Mol. Opt. Phys.*; **1991**, 43, 1071.
182. Herve, P., Roux, D., Bellocq, A. M., Nallet, F., and Gulik-Krzywicki, T.; *J. Phys. II*; **1993**, 3, 1255.
183. Szleifer, I., Ben-Shaul, A., and Gelbart, W. M.; *J. Phys. Chem.*; **1990**, 94, 5081.
184. Szleifer, I., Kramer, D., Ben-Shaul, A., Gelbart, W. M., and Safran, S. A.; *J. Chem. Phys.*; **1990**, 92, 5081.
185. Doebereiner, H. G., Selchow, O., and Lipowski, R.; *Eur. Biophys. J.*; **1999**, 28, 174.
186. Jung, H. T., Coldren, B., Zasadzinski, J. A., Iampietro, D. J., and Kaler, E. W.; *Proceedings of the National Academy of Sciences of the United States of America*; **2001**, 98(4), 1353.
187. Coldren, B., van Zanten, R., Mackel, K. J., Zasadzinski, J. A., and Jung, H. T.; *Langmuir*; **2003**, 19, 5632.
188. Valiente, M., Thunig, C., Munkert, U., Lenz, U., and Hoffmann, H.; *J. Colloid Interface Sci.*; **1993**, 160, 39.
189. Penfold, J., Staples, E., Tucker, I., Hubbard, J., Soubiran, L., and Creeth, A.; *Fibre Diffraction Rev.*; **2003**, 11, 68.
190. Mean-Jeng, H., and Shah, D. O.; *Langmuir*; **1987**, 3, 1086.
191. de Haas, K. H., Blom, C., van den Ende, D., Duits, M. H. G., Haveman, B., and Mellema, J.; *Langmuir*; **1997**, 13, 6658.
192. Quemada, D.; *Rheol. Acta*; **1978**, 17, 643.
193. Hill, A., Candau, F. and Selb, J.; *Macromolecules*; **1993**, 26, 4521.
194. Glass, J. E., Schulz, D., and Zukoski, C. F.; In *Polymers as Rheology Modifiers*; Schulz, D., Glass, J. E., Eds; American Chemical society, Washington DC, **1991**, Vol. 462, pp 1-15.
195. Volpart, E., Selb, J. and Candau, F.; *Macromolecules*; **1996**, 29, 1452.
196. Volpart, E.; *Polymer*; **1998**, 39, 1025.
197. Hill, A., Candau, F. and Selb, J.; *Prog. Colloid. Polym. Sci.*; **1991**, 84, 61
198. van der Werff, J. C., de Kruif, C. G., and Dhont, J. K.G.; *Physica A*; **1989**, 160, 205.

199. Bergmeyer, M., Gradzielski, M., Hoffmann, H., and Mortensen, K.; *J. Phys. Chem. B*; **1998**, 102, 2837.
200. Hao, J., Hoffmann, H., And Horbaschek, K.; *Langmuir*; **2001**, 17, 4151.
201. Laughlin, R.G., Munyon, R. L., Burns, J. L., Coffindaffer, T. W. and Talmon, Y.; *J. Phys. Chem.*; **1992**, 96, 374.
202. Abdel-Rahem, R; *PhD thesis, Physical Chemistry I*; Bayreuth University, **2003**.
203. Leng, J., Egelhaaf, S. U., and Cates, M. E.; *Biophys. J.*; **2003**, 85, 1624.
204. Fromherz, P.; *Chem. Phys. Lett*; **1983**, 94, 259.
205. Hoffmann, H., Thunig, C., Schmiedel, P., and Ulbricht, W.; *Langmuir*; **1994**, 10, 2594.
206. Wierenga, A., Philipse, A. P., Lekkerkerker, H. N. W., and Boger, D. V.; *Langmuir*; **1998**, 14, 55.
207. Hoffmann, H., and Ulbricht, W.; *Recent Res. Devel. Phys. Chem.*; **1998**, 2, 113.
208. Hoffmann, H., Thunig, C., Schmiedel, P., and Munkert, U.; *Langmuir*; **1994**, 10, 3972.
209. Rehage, H., and Hoffmann, H.; *Mol. Phys.*; **1991**, 74, 933.
210. Yamashita, Y.; *PhD Dissertation, Phys. Chem. I*, Bayreuth University; **2004**, p-54.
211. Apel, C. L., Deamer, D. W., and Mautner, M. N.; *Biochim. Biophys. Acta*; **2002**, 1559, 1.
212. Cistola, D. P., Hamilton, J. A., Jackson, D., and Small, D. M.; *Biochemistry*; **1988**, 27, 1881.
213. Morigaki, K., Walde, P., Misran, M., and Robinson, B. H.; *Colloids Surf. A*; **2003**, 213, 37.
214. Borne, J., Nylander, T., and Khan, A.; *J. Colloid Interface Sci.*; **2003**, 257, 310.
215. Rosen, M. J.; *Surfactant and Interfacial Phenomena*, Second edition, John Wiley and Sons, New York; **1989**, p-67.
216. Won, Y. Y., Brannan, A. K., Davis, H. T., and Bates, F. S.; *J. Phys. Chem. B*; **2002**, 106, 3354.
217. Putlitz, B. Z., Hertz, H. P., Landfester, K., and Antonietti, M.; *Langmuir*; **2000**, 16, 3003.
218. Manasa, V. G., Sum, P. L., Dganit, D., and Steven, P. W.; *Biochemistry*; **2005**, 44, 7294.
219. Walter, A., Vinson, P.K., Kaplun, A., and Talmon, Y.; *Biophys. J.*; **1991**, 60, 1315.
220. Thomas, H. C., and Talmon, Y.; *Biochemistry*; **1998**, 37, 10987.
221. Mui, B. L. S., Cullis, P. R., Evans, E. A., and Madden, T. D.; *Biophys. J.*; **1993**, 64, 443.
222. Almgren, M.; *Aust. J. Chem.*; **2003**, 56, 959.

223. Denkov, N. D., Yoshimura, H., Kouyama, T., Walz, J., and Nagayama, K.; *Biophys. J.*; **1998**, 74, 1409.
224. Morse, D. C., and Milner, S. T.; *Phys. Rev. E*; **1995**, 52, 5918.
225. Simons, B. D., and Cates, M. E.; *J. Phys. II (France)*; **1992**, 2, 1439.
226. Berne, B. J., and Pecora, R.; *Dynamic Light Scattering*, Wiley Interscience, New York, **1976**.
227. Hassan, P. A., Raghavan, S. R., and Kaler, E. W.; *Langmuir*; **2002**, 18, 2543.
228. Iampietro, D. J. and Kaler, E. W.; *Langmuir*; **1999**, 15, 8590.
229. Hentze, H. P., Raghavan, S. R., McKelvey, C. A., and Kaler, E. W.; *Langmuir*; **2003**, 19, 1069.
230. Koehler, R. D., Raghavan, S. R., and Kaler, E. W.; *J. Phys. Chem. B*; **2000**, 104, 11035.
231. Chen, L., Xiao, J. X., Ruan, K., and Ma, J.; *Langmuir*; **2002**, 18, 7250.
232. Gonzalez, Y. I.; Stjerndahl, M., Danino, D., and Kaler, E. W.; *Langmuir*; **2004**, 20, 7053.
233. Russel, W. B., Saville, D. A., and Schowalter, W. R.; *Colloidal Dispersion*; Cambridge University Press: Cambridge, **1989**.
234. Boger, D. V.; *Nature*; **1977**, 265, 126.
235. Whitcomb, P. J., and Macosko, C. W.; *J. Rheology*; **1978**, 22, 493.
236. Bakshi, M. S., Crisantino, R., de Lisi, R., and Milioto, S.; *J. Phys. Chem.*; **1993**, 97, 6914.
237. Maeda, H., Yamamoto, A., Souda, M., Kawasaki, H., Hossain, K. S., Nemoto, N., and Almgren, M.; *J. Phys. Chem. B*; **2001**, 105, 5411.
238. Weers, J. G.; Rathman, J. F., and Scheuing, D. R.; *Colloid Polym. Sci.*; **1990**, 268, 832.
239. Shiloach, A., and Blankschtein, D.; *Langmuir*; **1997**, 13, 3968.

Hiermit erkläre ich, dass ich die Arbeit selbständig verfasst und keine anderen als die angegebenen Quellen und Hilfsmittel benutzt habe.

Ferner erkläre ich, dass ich nicht andersweitig mit oder ohne Erfolg versucht habe, eine Dissertation zu diesem oder gleichartigem Thema einzureichen oder mich der Doktorprüfung zu unterziehen.

Bayreuth, den 27. Oktober 2005

Md. Ekramun Nabi